

NUMERALS IN THE VENTRAL STREAM: BRAIN ARCHITECTURE AND  
DEVELOPMENT

By

Benjamin Neal Conrad

Dissertation

Submitted to the Faculty of the  
Graduate School of Vanderbilt University  
in partial fulfillment of the requirements  
for the degree of

DOCTOR OF PHILOSOPHY

in

NEUROSCIENCE

August 31<sup>st</sup>, 2021

Nashville, Tennessee

Approved:

James R. Booth, Ph.D.

Gavin R. Price, Ph.D.

Laurie E. Cutting, Ph.D.

Mikhail Rubinov, Ph.D.

## ACKNOWLEDGEMENTS

I first would like to acknowledge the unwavering support I have received from my family over the last five years, including my wife, Brooke, my daughters, Savanna and Ivy, and my parents, Kathy and Bill. They have always encouraged me to follow my intellectual curiosities and push forward in my endeavor to become a scientist. Their presence through this journey has helped keep me motivated and grounded, and their love has truly kept me afloat through it all.

I would also like express my gratitude for my advisor, Dr. Gavin Price, who has been instrumental in my development as a researcher and critical thinker. From day one, he has embraced my strengths and pushed me to improve on my weaknesses. Gavin's compassion for his mentees has been especially remarkable, not only for our professional development, but also for our personal well-being. His support has helped me through many difficult periods, and I will carry his example forward in my future roles as a mentor.

For my committee members, I am also sincerely grateful. Dr. James Booth, Dr. Laurie Cutting, and Dr. Mikail Rubinov have helped guide me from my nervous qualifying exam through to this day. Over multiple iterations of my proposal, they have been there to provide sometimes critical, but always necessary and constructive, feedback. I deeply respect their commitment to scientific training and willingness to share their time and expertise over these years.

Along the same vein, I would like to thank my mentors from the Vanderbilt University Institute of Imaging Science, including Drs. John Gore, Seth Smith, Victoria Morgan, and Robert Barry. They took a chance on me as a young research assistant nearly eight years ago and ushered me into the world of neuroimaging. In working with these professors and their labs, I learned many foundational lessons in how to conduct rigorous science. Their mentorship was fundamental to my later success as a graduate student.

Finally, I would like to thank the members of the Numerical Brain Lab. I joined the lab in 2017, completely naïve to the field. Dr. Eric Wilkey showed me the ropes and set an impressive example of how to be successful as a graduate student. Other members have been critical to the success of our projects, including Dr. Courtney Pollack, Lisa Venanzi, Adam Kaminski, Amanda Goodwin, Sharo Costa, Charles Neal, and Sarah Wiesen. I have thoroughly enjoyed my time with each of them. It has also been a pleasure to work alongside our newest member, Dr. Andrew Lynn, over the past year. He has helped pushed me to the finish line as my final projects came together. Last but not least, I have to acknowledge Dr. Darren Yeo, who was in my cohort and has become a dear friend. Darren possesses a quiet brilliance and sharp intellect, but at the same time is extraordinarily generous and patient. Our many long hours of discussion have been integral in my development as a scientist.

## TABLE OF CONTENTS

<b>ACKNOWLEDGEMENTS .....</b>	<b>ii</b>
<b>LIST OF TABLES .....</b>	<b>vi</b>
<b>LIST OF FIGURES .....</b>	<b>vii</b>
<b>INTRODUCTION .....</b>	<b>1</b>
<b>1.1 Category Selectivity in the Ventral Stream .....</b>	<b>2</b>
<b>1.2 An Occipitotemporal Area for Numbers? .....</b>	<b>7</b>
<b>1.3 Explaining Symbol Category Preference in the OTC: Mechanisms and         Developmental Models.....</b>	<b>11</b>
1.3.1 Proto-maps and the shape hypothesis .....	11
1.3.2 The biased connectivity hypothesis .....	12
1.3.3 Interactive specialization.....	15
1.3.4 The interactive account of OTC function.....	17
<b>1.4 Recent Insights into the “Inferior Temporal Numeral Area” and         Outstanding Questions .....</b>	<b>18</b>
1.4.1 Beyond the “visual number form” .....	18
1.4.2 Task demands matter for ITNA engagement .....	20
1.4.3 Bilateral, but functionally asymmetric ITNAs.....	21
1.4.4 The uncharted development of the ITNAs.....	23
<b>1.5 Overview of Current Studies .....</b>	<b>25</b>
<b>CONNECTIVITY CONSTRAINTS ON SYMBOL AREAS IN THE OCCIPITOTEMPORAL CORTEX .....</b>	<b>29</b>
<b>2.1 Introduction.....</b>	<b>29</b>
<b>2.2 Methods.....</b>	<b>33</b>
2.2.1 Participants.....	33
2.2.2 fMRI task .....	34
2.2.3 MRI Acquisition parameters .....	35
2.2.4 Anatomical processing .....	35
2.2.5 Seed fROI Definition .....	37
2.2.6 DWI Preprocessing .....	39
2.2.7 Streamline tractography pipeline .....	40
2.2.8 Seed to whole-brain connectivity and consistency-based thresholding .....	42
2.2.9 Fiber Density & Length and Bundle Overlap Analyses.....	44
2.2.10 fMRI Preprocessing .....	45
2.2.11 Beta-series connectivity .....	45
2.2.12 Landmark-Based Homotopic Mapping.....	48
2.2.13 Statistical Analysis and Threshold-Free Cluster Enhancement .....	49
<b>2.3 Results .....</b>	<b>51</b>
2.3.1 Structural connectivity of Digit versus Letter area .....	51

2.3.2	Functional connectivity of Digit versus Letter area .....	52
2.3.3	Structural connectivity of the left versus right Digit area .....	55
2.3.4	Functional connectivity of the left versus right Digit area.....	56
<b>2.4</b>	<b>Discussion: ITNA Localization and Connectivity .....</b>	<b>59</b>
2.4.1	The ITNA is functionally and structurally connected to intraparietal sulcus .....	60
2.4.2	The ITNA is more structurally connected to language areas .....	62
2.4.3	The Letter area is functionally and structurally connected to the fusiform gyrus.....	64
<b>2.5</b>	<b>Discussion: Lateralization of ITNA Connectivity .....</b>	<b>64</b>
2.5.1	Left ITNA has greater anatomical connectivity with inferior frontal gyrus .....	65
2.5.2	Both ITNAs are connected to the frontoparietal control network.....	68
2.5.3	Right ITNA is more structurally and functionally connected to the intraparietal sulcus .....	69
2.5.4	Distinct connectivity of the ITNA with anterior and posterior IPS .....	70
2.5.5	Double dissociation in ITNA connectivity with the angular gyrus.....	71
<b>2.6</b>	<b>Limitations.....</b>	<b>72</b>
<b>2.7</b>	<b>Conclusions.....</b>	<b>74</b>
<b>FUNCTIONAL DEVELOPMENT OF INFERIOR TEMPORAL NUMERAL AREAS FROM KINDERGARTEN THROUGH 2<sup>ND</sup> GRADE.....</b>		<b>75</b>
<b>3.1</b>	<b>Introduction.....</b>	<b>75</b>
<b>3.2</b>	<b>The present study.....</b>	<b>79</b>
<b>3.3</b>	<b>Methods.....</b>	<b>83</b>
3.3.1	Participants .....	83
3.3.2	fMRI Tasks.....	85
3.3.3	MRI Acquisition parameters .....	87
3.3.4	Motion reduction strategy .....	88
3.3.5	Anatomical processing .....	90
3.3.6	fMRI preprocessing.....	91
3.3.7	Motion Censoring and Nuisance Regressors .....	91
3.3.8	General Linear Models.....	93
3.3.9	Category-level Representational Similarity Analysis .....	94
3.3.10	Exemplar Discriminability – SVM Classification .....	96
3.3.11	Task-Evoked and Background Functional Connectivity .....	97
3.3.12	Definition of Occipitotemporal ROIs.....	99
3.3.13	Definition of Target fROIs for Connectivity Analyses.....	102
3.3.14	Linear Mixed-Effects Models .....	104
<b>3.4</b>	<b>Results .....</b>	<b>105</b>
3.4.1	Longitudinal changes in behavioral performance .....	105
3.4.2	Longitudinal changes in signal quality and motion .....	107
3.4.3	Task Performance by Symbol Category .....	107
3.4.4	Longitudinal changes in occipitotemporal ROI activation versus baseline .....	109
3.4.5	Longitudinal changes in relative activation between conditions .....	111
3.4.6	Longitudinal changes in category-level representational geometry.....	112
3.4.7	Longitudinal changes in exemplar decodability.....	114

3.4.8	Longitudinal changes in “background” functional connectivity.....	116
3.4.9	Longitudinal changes in task-evoked functional connectivity .....	118
3.4.10	Relations between connectivity and local functional metrics .....	120
<b>3.5</b>	<b>Discussion.....</b>	<b>126</b>
3.5.1	Novel symbols elicit strong responses in digit and letter areas .....	126
3.5.2	An increasing preference for digits in the right ITNA .....	128
3.5.3	Increasing digit-biased categorical representations in left ITNA.....	130
3.5.4	No evidence for symbol identity representations in symbol-preferring ROIs ....	135
3.5.5	The ITNAs are functionally connected to number-sensitive IPS by kindergarten 135	
3.5.6	No parietal bias in left ITNA versus OTLA connectivity .....	137
3.5.7	No digit-selective coupling of the ITNAs with IPS and no change over schooling 139	
<b>3.6</b>	<b>Limitations.....</b>	<b>140</b>
3.6.1	COVID-19.....	140
3.6.2	Assumption of normality and individual differences in trajectories .....	141
3.6.3	Group-level ROI Definition .....	142
<b>3.7</b>	<b>Conclusions.....</b>	<b>142</b>
<b>GENERAL DISCUSSION .....</b>		<b>144</b>
<b>4.1</b>	<b>Digit versus letter area connectivity .....</b>	<b>144</b>
<b>4.2</b>	<b>Hemispheric asymmetries in ITNA connectivity .....</b>	<b>149</b>
<b>4.3</b>	<b>The functional development of symbol areas .....</b>	<b>153</b>
4.3.1	The shape hypothesis .....	153
4.3.2	The interactive account .....	155
4.3.3	The biased connectivity hypothesis .....	157
4.3.4	Interactive specialization.....	158
4.3.5	Representational similarity.....	161
<b>4.4</b>	<b>Final Remarks .....</b>	<b>162</b>
<b>REFERENCES.....</b>		<b>163</b>

## LIST OF TABLES

Table	Page
Table 1. Linear mixed-effects model parameters for all longitudinal analyses of imaging-derived metrics.....	123
Table 2. One-sample t-test results for activation vs. baseline levels, by grade level.....	124
Table 3. One-sample t-test results for activation differences, by grade level. ....	124
Table 4. One-sample t-test results for category-level representational geometry, by grade level. .....	125
Table 5. One-sample t-test results for exemplar decodability, by grade level.....	125
Table 6. One-sample t-test results for background functional connectivity, by grade level. ....	125
Table 7. One-sample t-test results for task-evoked connectivity with $IPS_{Ratio}$ ROIS, by grade level.....	126

## LIST OF FIGURES

Figure	Page
Figure 1. Numeral processing in the inferior temporal gyrus.....	9
Figure 2.1 fMRI task paradigm.....	34
Figure 3. Digit and Letter seed areas in relation to reported literature coordinates.....	37
Figure 4. Schematic of the homotopic mapping procedure. ....	47
Figure 5. Structural Connectivity of Digit and Letter areas.....	52
Figure 6.1 Functional Connectivity of Digit and Letter areas .....	54
Figure 7. White Matter Bundle Overlap .....	57
Figure 8. Digit-selective Coupling from Left versus Right Digit Area – Bayes Factor and T-maps .....	58
Figure 9. Stimulus-selective Coupling from left Digit versus Letter Area – Bayes Factor and T- maps .....	59
Figure 10. Longitudinal sample and usable data. ....	85
Figure 11. All stimuli used in the symbol classification task .....	86
Figure 12. Example of symbolic digit comparison stimuli.....	87
Figure 13. Benchmarking censor fraction thresholds across software. ....	92
Figure 14. Outline of ROI definition for developmental analyses.....	102
Figure 15. Longitudinal change in task performance, signal quality, and motion over academic months.....	106
Figure 16. Symbol classification task performance by grade and longitudinal effects .....	109
Figure 17. Longitudinal change in activation level versus baseline .....	110
Figure 18. Longitudinal change in activation differences between conditions .....	112
Figure 19. Longitudinal change in category-level representational geometry.....	114
Figure 20. Longitudinal change in exemplar decodability .....	116
Figure 21. Longitudinal change in background functional connectivity with IPS <sub>Ratio</sub> ROIs .....	118
Figure 22. Longitudinal change in task-evoked connectivity with IPS <sub>Ratio</sub> ROIs .....	120
Figure 23. Relations between ITNA-IPS <sub>Ratio</sub> connectivity and local functional metrics .....	122

# CHAPTER 1

## INTRODUCTION

Written symbols are ubiquitous in our everyday lives and integral to the functioning of modern societies. Mastering symbolic notations for numbers (e.g., Arabic numerals) and one's native language (e.g., Roman letters) are critical developmental milestones which lay a foundation for both academic success and personal well-being (G. J. Duncan et al., 2007; Geary, 2011; OECD, 2016; Parsons & Bynner, 2005; Undheim, 2003). The neurobiological basis of symbol use, and particularly the development of these mechanisms, however, remains poorly understood. The capacities for quantity perception and vocal communication are shared across many species (Hauser, Chomsky, & Fitch, 2010; Nieder, 2016), but the use of arbitrary signs to denote numerical quantities and speech sounds is an evolutionarily recent human invention (Dehaene & Cohen, 2007; Hannagan, Amedi, Cohen, Dehaene-Lambertz, & Dehaene, 2015; Nissen, 1986). Remarkably, the brain areas that come to support numeral and letter recognition are spatially segregated and consistently localized in the adult occipitotemporal cortex (L. Cohen & Dehaene, 2004; Shum et al., 2013). Symbol processing provides a model system for investigating the plasticity and innateness of brain function. How do novel and necessarily *learned* abilities come to engage different areas of the brain? What *constrains* the localization of these areas? These questions, along with the practical importance of symbol use, provide an overarching context and motivation for the present work.

In this dissertation, I explore the neurobiological bases and development of symbol processing in the occipitotemporal cortex, with a particular focus on recently identified “numeral” areas in the left and right hemisphere and how they compare to a left hemisphere



“letter” area. In the remaining sections of this introductory chapter: 1) outline the extant literature on functional selectivity and its origins in the occipitotemporal cortex, 2) review evidence for the existence of numeral areas, 3) describe several theories of functional specificity and development, 4) discuss outstanding questions concerning numeral areas, and 5) provide an overview of the present studies and their findings. Subsequently, in my first empirical chapter (Chapter 2), I characterize how symbol areas are wired to and communicate with the rest of the brain, exploring the idea that connectivity may constrain a brain region’s functional role. In my second empirical chapter (Chapter 3), I assess the functional development of symbol areas over Kindergarten through 2<sup>nd</sup> grade, exploring how early symbol learning shapes brain function.

### **1.1 Category Selectivity in the Ventral Stream**

A longstanding agenda in cognitive neuroscience has been to characterize the functional localization of particular processes in the brain (Kanwisher, 2010). Studies of the human occipitotemporal cortex (OTC) have provided some of the most impressive evidence to date that focal areas in the brain can become selectively tuned for certain operations (Op de Beeck, Pillot, & Ritchie, 2019). At the transition between the occipital and temporal lobes, the OTC falls along the ventral visual stream – often referred to as the “what” pathway due to its involvement in object perception and identification (Milner & Goodale, 2008; Mishkin, Ungerleider, & Macko, 1983). Starting with retinal inputs to primary visual cortex, information is thought to undergo a series of hierarchical transformations along the ventral pathway, leading to increasingly abstract representations supported by OTC areas (Grill-Spector & Weiner, 2014). In the adult human brain, the spatial layout of OTC areas appears to be coarsely organized around different object *categories*. For instance, specific areas associated with processing faces, scenes, animals, tools, and body parts can be reliably identified in adult OTC using functional magnetic resonance

imaging (fMRI), as defined by greater neural activity in response to the preferred category relative to others (Downing, Chan, Peelen, Dodds, & Kanwisher, 2006; Kanwisher, 2010; Martin, 2007). Despite decades of investigation, outstanding questions remain regarding why OTC areas are consistently localized across individuals and how these areas come to develop their selectivity for a given category (Op de Beeck et al., 2019; Peelen & Downing, 2017).

Faces, scenes, animals, tools, and body parts, are all *evolutionarily relevant* domains, in that they were likely important to early hominids going back several million years (Harmand et al., 2015; Mahon & Caramazza, 2009). Over this timescale, it is plausible that evolutionary pressures were enough drive the development of a genetic predisposition for the cortical architecture observed in OTC. Category selectivity for certain domains may thus be *innate* – arising directly from a programmed sequence of gene expression patterns. Supporting this view, face and scene-preferring areas of OTC are already adult-like by 4-6 months (Deen et al., 2017). Also, individual differences in the fine scale arrangement of selective areas are highly heritable, as recently demonstrated in a large comparison of monozygotic and dizygotic twins (Abbasi, Duncan, & Rajimehr, 2020). Furthermore, macaques develop distinct face, scene, and body “patches” in inferotemporal cortex (Tsao, Freiwald, Knutsen, Mandeville, & Tootell, 2003), and, their spatial layout and response properties are highly similar to those in human OTC (Kriegeskorte, Mur, Ruff, et al., 2008; Rajimehr, Young, & Tootell, 2009; Tsao et al., 2003). The consistency in which OTC selectivity is observed within and across species suggests it is an ancient feature of the primate brain.

While some genetic contribution to OTC organization may be indisputable, a number of observations indicate that *experience* is also a critical driver of selectivity. An impressive demonstration came from a study by Arcaro and colleagues who raised a group of macaques that

were deprived of all exposure to faces from birth. Compared to control monkeys, the face-deprived group developed scene, body, and hand areas in stereotypical locations, but *did not* develop face patches (Arcaro, Schade, Vincent, Ponce, & Livingstone, 2017), indicating that early visual experience is necessary for the formation of domain-selective regions regardless of a domain's biological relevance. The authors acknowledged, however, that experience is not sufficient on its own. They instead argue for an innate "proto-map" in which the processing of low-level visual properties is at least initially coarsely segregated across OTC. For instance, in newborn macaques, gradients of activity across OTC have been observed for foveal-to-peripheral and curvilinear-to-rectilinear shape processing (Arcaro & Livingstone, 2017). This innate organization may then *scaffold* the experience-driven formation of domain-selective areas. For example, faces are typically foveated on and contain curvilinear features, while scenes are encountered in the periphery and contain more rectilinear features, leading to their functional segregation along the preexisting proto-map.

In humans, fMRI studies also indicate that OTC responses are dependent on experience. Cross-sectional studies comparing children, adolescents, and adults have reported that the preferential activity and volume of the fusiform face area (FFA) are increasing until at least early adulthood, suggesting a protracted developmental process potentially shaped by experience (Cantlon, Pinel, Dehaene, & Pelphrey, 2011; Golarai et al., 2007; Golarai, Liberman, Yoon, & Grill-Spector, 2010; Scherf, Behrmann, Humphreys, & Luna, 2007). Recent longitudinal studies support these early findings, demonstrating that category selective areas for faces, houses, bodies, and tools are already identifiable by 6 years of age, but show a steady increase in selectivity through late childhood (Dehaene-Lambertz, Monzalvo, & Dehaene, 2018; Nordt et al., 2020; Saygin et al., 2016). Another study, which included participants from 7-40 years old,

found that the FFA is most responsive to faces of one's own age (Golarai, Liberman, & Grill-Spector, 2017). This argues against a unidirectional acquisition of function in FFA and instead implies this tuning is malleable over the lifespan and may adapt to experiential context. Further evidence comes from a large body of work on visual expertise, which has demonstrated that individual differences in OTC responses are associated with increased exposure to and practice within a particular domain (Gauthier, Tarr, Anderson, Skudlarski, & Gore, 1999; Harel, 2016; McGugin, Gatenby, Gore, & Gauthier, 2012). Taken together with the work in non-human primates, the prolonged elaboration of category selectivity in human OTC is consistent with an experience-dependent developmental process.

We have heretofore focused on evolutionarily *relevant* domains like faces, places, and bodies, which are shared across species and undoubtedly remain integral parts of human life. However, perhaps the most remarkable case for experience-dependent plasticity in the human OTC involves the evolutionary *recent* domain of symbolic notation. Written symbols, including the most ubiquitous symbol sets used in the modern world, the Roman alphabet and Arabic numerals, are *recent* inventions in the history of our species. In particular, the earliest characterized use of abstract symbols, or those which do not physically resemble their referent, comes from the pre-cuneiform writing system of ancient Mesopotamian societies 5100-5400 years ago (Dehaene & Cohen, 2007; Hannagan et al., 2015; Nissen, 1986; note that pictographic or mnemonic markings predate abstract symbol use, such as tally marks found on bones dating back as far as 43,000 years, D'Errico et al., 2012). These early ideographic (referring to an abstract idea such as a quantity) and logographic symbols (referring to a unit of speech) were used for economic purposes, e.g., to keep track of commodities, count livestock, or refer to different professions (Nissen, 1986), and served as precursors to numerals and letters – marking

the advent of human writing systems. At only several thousand years ago, this was far too short a period for the emergence of *dedicated* brain areas for written symbol processing – genetic evolution operates on a scale of millions of years (Rakic, 2009; Uyeda, Hansen, Arnold, & Pienaar, 2011). Fascinatingly, however, separate areas selective for letters (or words) and numerals have been observed in human OTC, namely, the “visual word form area” (VWFA) and the “number form area” (NFA) (L. Cohen & Dehaene, 2004; Pollack & Price, 2019; Shum et al., 2013; D. J. Yeo, Wilkey, & Price, 2017).

Letter and number symbol knowledge is culturally transmitted and so is necessarily acquired through *learning*. Yet the consistent localization of the VWFA and NFA across individuals suggests some *biological constraints* on their ontogenetic emergence. Symbol processing in the OTC thus provides a model system for investigating both innateness and functional plasticity in the brain. Given the ubiquity and critical importance of symbols in modern societies, understanding the neural mechanisms supporting symbol use may also have practical implications for education, such as to inform remediation strategies for those with learning disabilities (Geary, 2011; Norton, Beach, & Gabrieli, 2015; OECD, 2016; Parsons & Bynner, 2005; Pollack, Luk, & Christodoulou, 2015; Shaywitz et al., 2004).

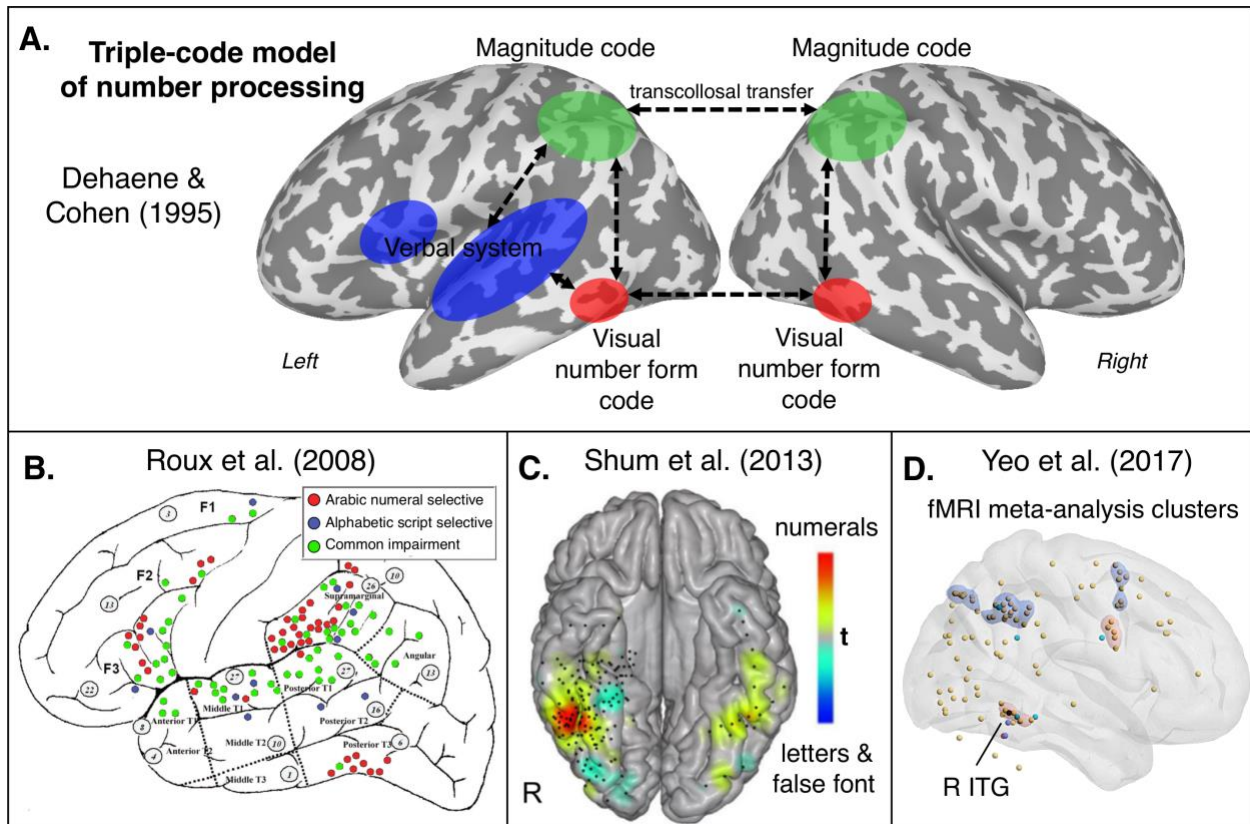
The goal of the present thesis is to probe the underlying constraints and functional development of symbol processing in the OTC. In the remaining introductory chapters I first describe the current state of the literature regarding the VWFA and the more recently discovered NFA, with the latter being the primary focus of the studies herein. I then discuss several theoretical accounts that motivate the present work and outline several puzzling observations and outstanding questions regarding numeral processing in the OTC. Finally, I conclude with a brief overview of the empirical studies contained within this thesis.

## 1.2 An Occipitotemporal Area for Numbers?

Investigations into the brain mechanisms supporting word reading have revealed an OTC area critical to this process within the left fusiform gyrus, dubbed the “visual word form area” (VWFA) (Allison, McCarthy, Nobre, Puce, & Belger, 1994; McCandliss, Cohen, & Dehaene, 2003). The VWFA is preferentially engaged by written words compared to other objects, and even compared to closely matched stimuli such as consonant, false font, or numeral strings (Dehaene & Cohen, 2011). While the constituent parts of words are processed in prior (more posterior) stages of the ventral hierarchy, evidence suggests that the representations in VWFA are high-level, in that they are tuned to whole words and also invariant to low-level features like letter size, case, and font (Glezer, Jiang, & Riesenhuber, 2009; Vinckier et al., 2007). Functional selectivity to words in the VWFA is also closely related to familiarity with a script, reading speed, and the acquisition of reading in both children and illiterate adults (Baker et al., 2007; Dehaene & Cohen, 2011; Dehaene et al., 2010), providing empirical validation that experience drives the functional emergence of the VWFA. However, the consistent localization and leftward asymmetry of the VWFA across cultures and alphabet systems suggests that this area of left OTC is particularly well suited to take on the task of word processing, implying that word processing is, at least to some extent, biologically constrained within the human brain (Dehaene, Cohen, Morais, & Kolinsky, 2015).

In contrast to word reading and the VWFA, evidence for an OTC region selectively involved in *number* processing is scarce. Before the advent of modern neuroimaging, the component mechanisms of symbolic number processing were already being laid out based on observations of patients with brain lesions (Dehaene, 1992; McCloskey, 1992). For instance, in particular cases, damage to OTC resulted in deficits to Arabic numeral transcoding (e.g., multi-

digit reading), while sparing a patient's ability to perform verbal calculation and other approximate numerical operations. Though certain details were disputed, the proposed models commonly implicated a *modular* architecture supported by functionally segregated operations in the brain. Stanislas Dehaene hypothesized the existence of "visual Arabic number form" representations as part of his highly-influential "triple-code model" of number processing (Figure 1A) (Dehaene, 1992; Dehaene & Cohen, 1995). Dehaene postulated that three neuroanatomically distinct systems subserve number processing in humans: 1) the aforementioned *visual code* for processing Arabic numerals housed in bilateral OTC regions of the visual ventral pathway, 2) a *verbal code* for auditory/linguistic representations of number and operands and utilization of verbal working memory/articulatory loops, housed in the left-lateralized language areas such as superior/middle temporal gyrus and inferior frontal gyrus, and 3) a *quantity code* for analog magnitude representation involving the bilateral intraparietal sulci (Dehaene & Cohen, 1995; Dehaene, Piazza, Pinel, & Cohen, 2003).



**Figure 1.** Numerical processing in the inferior temporal gyrus.

Highlighted history of numeral processing areas in the inferior temporal gyri, starting with A) the conjecture of a visual number form area in the triple-code model of Dehaene and Cohen (1995). B) Reprinted from <https://doi.org/10.1212/01.wnl.0000297194.14452.a0>, Copyright (2008), with permission from Wolters Kluwer Health, Inc.; C) Reprinted from <https://doi.org/10.1523/JNEUROSCI.4558-12.2013>; D) Reprinted from <https://doi.org/10.1016/j.neubiorev.2017.04.027>, Copyright (2017), with permission from Elsevier.

The first empirical evidence for numeral-selective processing in the OTC came from a cortical electrostimulation mapping study in patients undergoing neurosurgery (Roux, Lubrano, Lauwers-Cances, Giussani, & Démonet, 2008). Roux and colleagues stimulated sites spanning across frontal, parietal, and temporal areas in 53 patients over six years. During stimulation periods, patients performed sentence, number word, and Arabic numeral reading, as well as picture naming. Selective impairments to numeral reading (e.g., speech arrest) versus the other



tasks were observed during stimulation of the left posterior inferior temporal gyrus (ITG) (Figure 1B, red circles), located laterally and anteriorly within OTC. Other numeral-selective sites were observed in the frontal lobe and supramarginal gyrus, indicating a numeral-preferring network that extended beyond OTC. Notably, Roux et al.'s work provided *causal* evidence for posterior ITG's role in visual numeral reading. This initial report was corroborated in a study by Shum and colleagues, who analyzed intracranial recordings in epilepsy patients performing symbol and word recognition tasks (Shum et al., 2013). They found that a focal region in right posterior ITG (Figure 1C, red cluster), responded preferentially to Arabic numerals compared to *perceptually* similar letters, false font stimuli, and foreign symbols (e.g., 1 vs. T), *semantically* related number words (e.g., 1 vs. one), and *phonologically* similar non-number words (e.g., 1 vs. won). The majority of cortical sites included in this study were in the right hemisphere, while the opposite was true of Roux et al.'s study. Taken together, these reports indicated that numeral recognition involves a focal area in the bilateral posterior ITG, precisely as predicted by the triple-code model.

Despite evidence from direct cortical recording and stimulation, the search for “number-form” areas in OTC using fMRI had largely gone empty handed. For instance, several prior fMRI studies that had included numeral stimuli did not find numeral-selectivity in the OTC (Baker et al., 2007; Cantlon et al., 2011; James, James, Jobard, Wong, & Gauthier, 2005; Polk et al., 2002; G. R. Price & Ansari, 2011). Given the reliable localization of VWFA using letter and word stimuli (even within the same studies), the extant fMRI literature suggested that numeral-selectivity in OTC was *less robust*, potentially due to variability in location across individuals, poor fMRI signal quality due to proximity to the ear canals, and/or differing task demands across studies (D. J. Yeo et al., 2017). Nevertheless, beginning with a report by Abboud and colleagues

in 2015, subsequent studies successfully identified numeral-selective regions in the posterior ITG (Abboud, Maidenbaum, Dehaene, & Amedi, 2015; Amalric & Dehaene, 2016; Grotheer, Herrmann, & Kovacs, 2016; Grotheer, Jeska, & Grill-Spector, 2018; Pollack & Price, 2019), possibly through the use of more advanced acquisition and post-processing techniques (though such claims have yet to be directly tested). To consolidate this literature, Yeo and colleagues performed a quantitative meta-analysis of fMRI studies that reported numeral preference *anywhere* in the brain (D. J. Yeo et al., 2017). They found converging evidence for Arabic numeral processing (compared to appropriate non-numeric control tasks) in the right posterior ITG (Figure 1D), as well as in bilateral parietal cortex and right frontal areas. Along with additional reports of numeral-selectivity in posterior ITG from intracranial recordings (Daitch et al., 2016; Hermes et al., 2017; Pinheiro-Chagas, Daitch, Parvizi, & Dehaene, 2018), the accumulated evidence to date supports the existence of so-called “number form areas” in the bilateral adult OTC. There are a number of theoretical models of brain function and development that may help explain the existence and segregation of alphanumeric symbol processing in the OTC. In the following section, we discuss several non-mutually exclusive ideas that inform the present work.

### **1.3 Explaining Symbol Category Preference in the OTC: Mechanisms and Developmental Models**

#### **1.3.1 Proto-maps and the shape hypothesis**

We previously discussed the idea of an innate *proto-map* in primate OTC that guides the localization of category selectivity based on common visual features across category members and their related computational requirements (Arcaro & Livingstone, 2017). For instance, numerals and letter are relatively simple shapes, contain similar curvilinear features, and are

processed foveally rather than peripherally. Representations for single characters should also be invariant to transformations of size and font and instead tuned to the configural arrangements of lines and edges (Brincat & Connor, 2006). In their “shape hypothesis,” Hannagan and colleagues (2015) adopt the proto-map framework and posit that the shared processing requirements across symbol categories leads to a rough confinement of symbol-selectivity in the lateral OTC. The most direct support for this hypothesis came from a series of training studies in macaques who learned to associate different types of object sets with juice rewards, including Helvetica characters (numbers and letters), Tetris block patterns, and faces (Srihasam, Mandeville, Morocz, Sullivan, & Livingstone, 2012; Srihasam, Vincent, & Livingstone, 2014). Though the object sets were all mapped to the same referents (i.e., 27 exemplars in a set associated with 0-26 drops of juice), they came to engage distinct areas of inferotemporal cortex over training. Remarkably, the areas were consistently localized across monkeys according to object category, regardless of training order. In all 10 individuals, Helvetica symbols activated nearly the same focal area of lateral inferotemporal cortex. This implies that low-level visual and/or shape characteristics may be more consequential in determining high-level OTC organization than has been appreciated. Establishing direct homology between humans and macaques is difficult, so it remains unclear whether such a proto-symbol area exists in humans (Hannagan et al., 2015). The shape hypothesis predicts that the *general* location of symbol processing is constrained within the OTC, implying that the sites of the NFA and VWFA are (at least initially) equally suited to processing alphanumeric forms. To explain the ultimate *segregation* of numeral and letter processing, however, some additional mechanism is required.

### **1.3.2 The biased connectivity hypothesis**

Hannagan and colleagues propose the “biased connectivity hypothesis” as a necessary

additional constraint to explain the locations of the NFA and VWFA (Hannagan et al., 2015). This theory instantiates a prominent view in the field that functional preferences of OTC areas are driven in part by each area's differential pattern of anatomical and functional *connectivity* to the rest of the brain (Mahon & Caramazza, 2011; Op de Beeck et al., 2019). Building on earlier work, e.g., the “distributed domain-specific hypothesis” (Mahon & Caramazza, 2009), the biased connectivity hypothesis posits that the functional potential of a given area in OTC is constrained by the relative strength of its connectivity with other regions engaged by a particular *conceptual domain*.

This idea is in part motivated by the observation that objects with similar features may be processed in *separate* areas (e.g., numerals and letters), but also, that objects with differing features may be processed in the *same* area. Such dissociations indicate that OTC preferences could not *solely* be a product of image statistics (Bracci, Ritchie, & de Beeck, 2017). For example, tools (e.g., scissors, hammer, stapler) have been shown to engage an area in lateral OTC that is also selective for hands, but not other body parts (Bracci, Cavina-Pratesi, Ietswaart, Caramazza, & Peelen, 2012). The tools in this study were all hand-manipulable objects, suggesting an *action*-related rather than *visual feature*-related organization in OTC. Interestingly, the tool area was shown to be selectively functionally connected to a parietal region involved in hand action execution, as predicted by connectivity-based accounts of OTC function.

To further make this case, many studies have shown that categorical organization in OTC is largely preserved in blind subjects (Hurka, Baelena, & Beecka, 2017; Mahon, Anzellotti, Schwarzbach, Zampini, & Caramazza, 2009; Reich, Szwed, Cohen, & Amedi, 2011). Such findings indicate that OTC representations are not fundamentally *visual*, but instead may be sensitive to the cognitive and/or perceptual contexts in which an object is used or experienced.

Although blind subjects lack visual inputs, distributed connectivity with other sensory and/or associative regions may support some degree of reverse mapping across brain areas, allowing for the development of a grossly normal OTC. The biased connectivity hypothesis thus suggests that *white matter architecture* provides a scaffold on which domain-selective functional networks emerge. Evidence for a direct relationship between structural connectivity and OTC organization has started accumulating, including observations of selective connectivity of face, place, and body areas with other regions that are functionally involved in these domains (Gomez et al., 2015; Grimaldi, Saleem, & Tsao, 2016; Osher et al., 2016; Saygin et al., 2012).

In this case of number and letter areas, the biased connectivity hypothesis predicts their connectivity patterns should reflect differing associations with numerical quantity and speech sounds, respectively. For instance, compared to the more medial fusiform face area, the VWFA is preferentially connected to language areas (F. Bouhali et al., 2014). On the other hand, the VWFA is also structurally and functionally connected with dorsal parietal areas, including the intraparietal sulcus (IPS), a region more putatively involved in number processing (L. Chen et al., 2019; A. C. Vogel, Miezin, Petersen, & Schlaggar, 2012). A recent study found distinct patterns of resting-state functional connectivity of the putative NFA and VWFA with the rest of the brain (Nemmi, Schel, & Klingberg, 2018). However, a direct comparison of how the numeral and letter-preferring areas are structurally connected to the rest of the brain has not yet been made.

Supporting the idea that domain-specific axonal pathways *precede* the development of symbol areas, it has been demonstrated that structural connectivity (particularly with language areas) in pre-reading children can predict the future location of the VWFA (Saygin et al., 2016). The VWFA is also already functionally connected to language areas at birth, suggesting the

affiliation of the VWFA with the language network may indeed be *innate* (J. Li, Osher, Hansen, & Saygin, 2020). However, in another study of newborn functional connectivity, the expected dissociation in connectivity between the future locations of the VWFA and NFA was not observed (Barttfeld et al., 2018). Thus, the extent to which functional and/or structural connectivity contributes to the development of symbol areas in OTC remains an open area of investigation.

### **1.3.3 Interactive specialization**

Whether local circuitry or distributed connectivity constrain OTC development, these accounts do not describe the mechanistic *process* by which neural populations acquire their tuning. According to the theory of “interactive specialization” put forward by Mark Johnson, the development of selectivity is thought, through mechanisms of Hebbian-like plasticity, to be driven by repeated co-activation of a region with functional networks engaged by a particular behavior or task context (Johnson, 2001, 2011). Brain areas in the OTC (and elsewhere) are thought to start out *broadly* tuned, responding equally to non-preferred stimuli. Over experience, responses to a stimulus category become both more *focal* and, within an area, more *selective*. At the local level this process is thought to occur via synaptic *pruning* and/or increasing lateral inhibition. In regards to numeral and letter processing, support for a pruning-based account was provided in a study by Cantlon and colleagues (2011). They showed that a region defined by its letter-selectivity in adults was equally responsive to letters and numerals in 4-year old children. The selectivity in adults was characterized by a *decreased* response to numerals, rather than an increased response to letters. Within the child sample, behavioral performance on both face and symbol identification tasks was specifically related to decreased responses to non-preferred stimuli, further suggesting a local pruning effect related to experience and/or learning, consistent

with the prediction of interactive specialization (Cantlon et al., 2011).

Interactive specialization is additionally a theory about the development of domain-specific *networks*. Repeated co-activity among sets of regions is hypothesized to mutually constrain their stimulus preferences. Consequently, the acquisition of selectivity in one region is should (almost) always be accompanied by increasing selectivity in other regions. Johnson speculates that both intrinsic (e.g., spontaneous coupling present already at birth) and context-dependent (i.e., task-evoked) functional interactions are causally involved in shaping a region's response profile. Note that domain-specific interactions may occur across *polysynaptic* pathways, and so may go undetected if one focuses solely on biases in structural connectivity (which is intended to measure direct axonal projections). This suggests that structural and functional connectivity measures may both be valuable, and likely complementary, in understanding OTC selectivity and development.

In focusing on functional networks, interactive specialization also adopts a contemporary view of regional “specialization.” Contrary to what is often implied in the OTC literature (including our treatment of the topic thus far), many brain regions, including in particular lateral OTC, appear to be involved in multiple contexts and task settings (Anderson, Kinnison, & Pessoa, 2013; A. C. Vogel, Petersen, & Schlaggar, 2014). The role of a brain region may be more appropriately conceptualized by considering its diverse set of interactions and patterns of co-activity across different cognitive states (C. J. Price & Friston, 2005). According to this view, a region is best thought of as a computational unit performing an operation that contributes to a given experience or behavioral outcome (Genon, Reid, Langner, Amunts, & Eickhoff, 2018). Its “operation-function” is therefore *situated* and necessarily a product of *context*, i.e., relative to the inputs and outputs to/from the region as defined by the dynamic and distributed state of the

system. This indicates that the functional connectivity of OTC areas may be relevant for understanding not only the development of category selectivity, but also the nature of selectivity in the mature state.

#### **1.3.4 The interactive account of OTC function**

To further elaborate on how OTC responses may be influenced by functional interactions with other regions, we can turn to the “interactive account” put forward by Price & Devlin (2011). Upon encountering a stimulus, it is proposed that bottom-up information from primary visual cortex is accumulated in OTC and momentarily broadcast to other areas. This evokes top-down *prediction* signals from higher-order areas (e.g., phonological and semantic), which attempt to “make sense” of the stimulus according to prior experiences (K. Friston, 2010). The interplay of these two information streams provides constraints on the maintained representation and/or computations occurring in OTC areas (C. J. Price & Devlin, 2011). Exchange across this hierarchy appears to occur *automatically*, outside of conscious awareness, implying that both bottom-up and top-down influences can spontaneously affect OTC activity. For example, it has been shown in priming experiments (e.g., a picture of lion is briefly flashed on a screen followed by the word “LION”) that a semantic association between the unconscious prime and target is enough to elicit reduced responses in the OTC (Kherif, Josse, & Price, 2011). The idea is that a distributed representation is engaged by the prime image and so, upon viewing the word, top-down predictions are already in effect. This leads to more efficient processing in OTC, or reduced *prediction error*, and results in a net reduction of neural activity. Price & Devlin’s framework helps to explain observations of heightened activity for pseudowords compared to real words, low compared to high frequency words, and false font compared to letter strings – in each case the former condition elicits higher prediction error (Graves, Desai, Humphries,



Seidenberg, & Binder, 2010; Kronbichler et al., 2004; Vinckier et al., 2007). One implication of this account for development is that in the early stages of acquiring object knowledge (e.g., children learning to map symbols to their referents) there is reduced top-down “support” and so relatively *heightened* activity in OTC. After sufficient learning responses should *decrease*, as the stimulus-specific network is more well established.

Price & Devlin recognize that top-down signals also arise from conscious, goal-oriented processing. For instance, it has been well documented that task demands *alone* can modulate OTC responses (e.g., Song et al., 2010; Twomey et al., 2011). This was elegantly demonstrated in a recent study where stimulus presentation was held constant but cognitive task was varied (Kay & Yeatman, 2017). The VWFA and FFA reliably responded to their preferred category during passive fixation but, responses increased when performing a categorization task, and increased further during a one-back task. We can conclude that a combination of bottom-up and top-down sources drive OTC responses, and these signals are likely dependent on both the degree of familiarity with an object category and ongoing task demands. It is thus critical to keep these study and stimulus-specific factors in mind when interpreting OTC activity and its change over time.

## **1.4 Recent Insights into the “Inferior Temporal Numeral Area” and Outstanding Questions**

### **1.4.1 Beyond the “visual number form”**

The study by Abboud et al., which was the first identify putative NFAs using fMRI, found these areas in *congenitally blind* subjects who were trained to associate auditory sequences with (roman) numerals and letters. This suggests that 1) NFAs can emerge in the *absence* of visual experience and 2) the NFAs are not necessarily involved in representing the visual *forms*

of Arabic numerals (Abboud et al., 2015). Their result is consistent with aforementioned evidence that blind individuals show typical category-selective organization in the OTC (Hurka et al., 2017; Mahon et al., 2009), and in particular, that the VWFA is engaged during Braille reading (Reich et al., 2011). Whether or not auditory/tactile stimuli commonly activate OTC areas in sighted individuals, the data from blind subjects indicate that OTC operations are not tied to vision *per se*, but instead to the more abstract computational requirements of a given domain (Mahon et al., 2009). In the case of the NFA, it has been shown that the same area can be similarly engaged by numerals, dice patterns, or finger representations during an addition task (Grotheer et al., 2018), suggesting that this region may be involved in representing numerical *objects* more abstractly and/or “ascribing numerical content” to inputs (p. 188). Relatedly, using intracranial recordings, an equivalent degree of NFA engagement by numerals *and* number words was also observed in patients performing addition (Hermes et al., 2017). Another study found that the bilateral NFAs are engaged by numerals *and* mathematical formulas (e.g.,  $A = \pi r^2$ ) in mathematicians and control subjects (Amalric & Dehaene, 2016). Fascinatingly, in mathematicians, even *auditorily* presented mathematical statements engaged the bilateral NFAs, further suggesting this region is not strictly tuned to the visual form of numerals.

In a direct test of this hypothesis, Yeo and colleagues recently used representational similarity analyses (RSA) to show that neither NFA carried information about the visual form of symbols (D. J. Yeo, Pollack, Merkley, Ansari, & Price, 2020). Instead, activity patterns in the right NFA distinguished between numerals and other symbols at a *categorical* level. Based on theirs and other’s findings, the authors proposed replacing “number form area” with a new label, the “Inferior Temporal Numeral Area” (ITNA), to emphasize its consistent anatomical location and deemphasize a functional association with visual forms. From this point forward, we thus

refer to the area as the “ITNA”. These observations leave us with the following questions. If the ITNAs are involved in the perception and/or manipulation of numerical “objects” more generally, what kind of computations would this entail? What about this area of OTC makes it particularly well-suited for handling numerical information? Does the NFA show biased connectivity with other regions involved in number processing?

#### **1.4.2 Task demands matter for ITNA engagement**

Another observation from the literature is that the ITNAs are particular sensitivity to task demands. It may be that some level of *active* engagement with numerals is necessary for a reliable ITNA response. For instance, the studies of Price & Ansari and Cantlon et al. used *passive* designs in which participants performed target or color detection tasks – neither study found numeral-selectivity in OTC. Such a design ensures participants view the stimuli, but the maintained task goal and button response is *unrelated* to the symbols themselves (Cantlon et al., 2011; G. R. Price & Ansari, 2011). To rule out the possibility that the study by Price & Ansari was underpowered and/or suffered from poor image quality, we recently replicated the study in a larger sample (n=37 vs. n=19) using a higher spatial and temporal resolution fMRI sequence (TR=1000ms, 2.5mm<sup>3</sup> vs. TR=2300ms, 3.3mm<sup>3</sup>) (Merkley, Conrad, Price, & Ansari, 2019). Confirming the previous result, we found no evidence for numeral-selectivity in either ITNA using the same passive viewing paradigm. This again suggests that the *bottom-up* response to numerals in ITNA is weak and that some degree of *top-down* modulation may be necessary, highlighting the utility of Price & Devlin’s interactive account for understanding ITNA function.

As we previously outlined, Kay & Yeatman (2017) reported increasing VWFA and FFA activation to words over passive, categorization, and one-back tasks. This study first highlights the fact that, in contrast to numerals, passive designs with faces and words or letters *do* activate

their respective OTC areas, as has been observed in previous work (Berman et al., 2010; Cantlon et al., 2011; Dehaene & Cohen, 2011; Polk et al., 2002). It also demonstrates a roughly linear increase in BOLD signal amplitude with increasing attentional demands (Kay & Yeatman, 2017). Compared to FFA and VWFA, successful localizations of numeral-selective ITNA responses have all involved some form of *active* design, e.g., symbol reading, categorization, or one-back tasks (Grotheer et al., 2016; Hermes et al., 2017; Roux et al., 2008; Shum et al., 2013). Responses in the ITNA are further strengthened when numerals are processed in a mathematical context, such as simple addition (Grotheer et al., 2018; Hermes et al., 2017), perhaps due to increased attentional “scaling” of OTC representations as reported in Kay & Yeatman (2017). A caveat to note is that a recent RSA study by Yeo et al. (2020) analyzed passive task data, and reported numeral-biased categorical information in the right ITNA. This indicates that automatic (i.e., bottom-up) engagement of numeral-selective populations in the ITNAs occurs to some extent, but detecting this activity with fMRI may require the increased sensitivity afforded by multivariate techniques (Kriegeskorte, Goebel, & Bandettini, 2006; D. J. Yeo et al., 2020).

It remains an open question whether bottom-up numeral processing in ITNA is *quantitatively* weaker than (e.g., subthreshold during passive fMRI paradigms) or *qualitatively* different from (e.g., computationally distinct) word and letter processing in VWFA. Does the ITNA receive different sources of top-down input? Are they differentially connected during task states?

### **1.4.3 Bilateral, but functionally asymmetric ITNAs**

The VWFA is consistently observed in the left hemisphere and is presumed to be related to leftward lateralization of language processing (Dehaene & Cohen, 2007). The ITNA is more consistently observed in the right hemisphere, as demonstrated in the meta-analysis by Yeo et al.

(2017), but reports of numeral processing in the same area of left OTC are not uncommon (Amalric & Dehaene, 2016; Bugden, Woldorff, & Brannon, 2019; Grotheer et al., 2016; Pollack & Price, 2019; Roux et al., 2008). Indeed, neuropsychological studies of lesion and split brain patients suggest either hemisphere may support the recognition of numerals, but subtle differences in their capacities appear to exist (Dehaene & Cohen, 1995). For instance, verbal-based operations with numbers, such as the reading of multi-digit strings, were found to be particularly impaired with lesions to left OTC (L. Cohen & Dehaene, 1995), perhaps related more generally to a left-hemispheric dominance for language processing. It possible that the tasks employed in previous fMRI studies favored right ITNA engagement and that, in natural contexts, the left and right ITNA may be equally important (D. J. Yeo et al., 2020). Whatever the case, the literature suggests that the left and right ITNAs are not simply *copies* of each other, but instead differentially support numeral processing.

Some insight into the lateralization of ITNA function may come from a long history of work showing asymmetric processing of numerical stimuli in parietal areas (Chochon, Cohen, Moortele, & Dehaene, 1999). Research in human infants, for instance, has found early numerical processing to be lateralized to the right parietal cortex (Hyde, Boas, Blair, & Carey, 2010; Izard, Dehaene-Lambertz, & Dehaene, 2008). fMRI studies have corroborated these findings showing that the right IPS is reliably and stably engaged by number tasks from early childhood onward, but that the left IPS undergoes a more protracted development (Cantlon, Brannon, Carter, & Pelphrey, 2006; Rivera, Reiss, Eckert, & Menon, 2005; S. E. Vogel, Goffin, & Ansari, 2015) (for a review and meta-analysis, see Kersey & Cantlon, 2017). For instance, it has recently been demonstrated that the right IPS in 3-4 year old children is already *adult-like* in its perceptual tuning to numerosity, while the effect is absent in left IPS (Kersey & Cantlon, 2017a).

Fascinatingly, a twin study found a strong genetic contribution to number-related activity in the right IPS, but not the left (Pinel & Dehaene, 2013). These results point to an early-developing, and possibly *innate*, right-hemispheric bias for number processing.

Connectivity-based accounts suggest that the same mechanisms driving the localization of category selectivity are also likely to drive the lateralization of function within the OTC (Behrmann & Plaut, 2015, 2020). Returning to the ITNA, it has been observed that individual differences in the rightward asymmetry of digit-related responses in OTC are associated with rightward asymmetry for numerical processing in the parietal cortex, suggesting the functional lateralization of these areas is somehow *linked* (Park, Hebrank, Polk, & Park, 2012). These findings lead us to ask, do pre-existing biases for number and language processing in the right and left hemispheres constrain the functions of the ITNAs? Do the connectivity of the ITNAs with these respective systems differ between hemispheres?

#### **1.4.4 The uncharted development of the ITNAs**

Only a few prior studies have investigated the *development* of numeral processing in the OTC. Notably, *none* have detected the emergence of numeral selectivity, leaving a significant gap in our understanding of ITNA development. Firstly, Libertus and colleagues had participants perform a 2-back working memory task with numerals, letters, and faces separately (Libertus, Brannon, & Pelphrey, 2009). In children (8 years old), neither numeral nor letter-specific activity was observed in the OTC. In adults, only *letter-specific* activity was found in OTC. As the study did not detect an ITNA in adults, the task paradigm may not have been optimal, making it consequently difficult to draw conclusions about ITNA development from this early study. Their result did, however, suggest some difference in the development letter and numeral processing in OTC. In a later study by Cantlon et al. (2011), voxels were detected in lateral OTC that

responded more to symbols than faces in 4-year old children but, activity levels were equivalent between numerals and letters. In an adult sample, selectivity for letters, but not numerals, was observed. A color change detection task was used in this case, making it a *passive* design with respect to the symbol stimuli. As we discussed in the prior section 1.4.2, passive designs appear to be insufficient in selectively activating the ITNAs adults, again making it difficult to draw conclusions about the development of numeral processing from this result.

A more recent study, also employing a passive design (phase-scrambled background detection), focused on the representational patterns of activity in OTC, including responses to pseudowords and multi-digit numerals, and several other categories including faces, bodies, places, and objects (Nordt et al., 2018). They found that categorical patterns for numerals and pseudowords were generally more similar to each other than to other categories, but only patterns for pseudowords showed increasing distinctiveness across age bins (5-9, 10-12, 22-28 years old). Though the triple-code model implicates the ITNA in multi-digit reading, multi-digit stimuli may be less likely to engage discrete representations of numerical quantity, and particularly so in a passive viewing task. Using the same paradigm (and presumably an overlapping sample), Nordt and colleagues recently reported that selective responses to words in the left OTC significantly increased over time in a longitudinal analysis of children from 5-12 years old (Nordt et al., 2020). Critically, however, no detectable change in numeral-related activity was observed in either left or right OTC.

Another recent longitudinal study followed 5-7 year old children from the end of kindergarten through the end of 1<sup>st</sup> grade, employing a similar passive fMRI paradigm (i.e., target detection with multiple visual categories including multi-digit numerals) (Dehaene-Lambertz et al., 2018). Consistent with previous work, there was no evidence of an emerging

ITNA and, the few voxels that were sensitive to numerals were *equally* responsive to words. Word-selective activity in the VWFA, however, reliably increased over the study.

At present, we are aware of only one study that reported a neural distinction between digits and letters in early school-age children. Using electroencephalography (EEG), Lochy and Schiltz found a rightward-lateralized OTC responses to digits versus letters in 1<sup>st</sup> graders (Lochy & Schiltz, 2019). This study suggests an early-developing distinction in the brain, but due to the poor spatial resolution of EEG, it is far from clear whether this activity is specifically tied to ITNA function. Furthermore, Lochy and Shiltz's result stands in conflict with another recent EEG study that found no distinction between digit and letter responses in groups of 7 year-olds and 10 year-olds (Park, van den Berg, Chiang, Woldorff, & Brannon, 2018). In sum, to our knowledge, there exists no convincing evidence of a developmental increase in the ITNA's selectivity for numerals, in stark contrast to studies of the VWFA. Thus, investigations into the developmental *origins* of ITNA specialization are critically needed to address *how* and *when* the ITNA acquires a preference for numerals.

## 1.5 Overview of Current Studies

In the present thesis, I build on the current state of knowledge of numeral processing in the ventral stream to provide insights into our understanding of OTC organization and development. The primary questions I address are as follows:

- 1) How is the ITNA structurally and functionally connected to the rest of the brain?
- 2) Are there hemispheric differences in ITNA connectivity?
- 3) When does the ITNA's selectivity for numerals develop?

As we have discussed, the biased connectivity and interactive specialization hypotheses provide appealing frameworks for explaining the segregation and development of symbol-



preferring areas in the OTC. The interactive account of OTC function further informs us on how differential contributions of bottom-up and top-down inputs may affect ITNA responses depending on task context. To address questions 1 and 2, in Chapter 2 we build on these connectivity-focused perspective to characterize the structural and functional connectivity profiles of the left and right ITNA, as well as a letter-sensitive area in the left hemisphere (proximal to the putative VWFA), in the adult brain. We compared these profiles between areas to test predictions regarding domain-specific connectivity patterns and hemispheric asymmetries in ITNA function.

In particular, we hypothesized that the ITNA's involvement in numeral processing is related to increased axonal connectivity and functional interactions with the intraparietal sulcus, as opposed to the letter area, which should be more connected to language areas supporting phonology and speech production. Note that such findings in adults would not directly support the developmental claims that domain-specific connectivity *precedes* and/or *drives* the specialization of OTC areas. However, if connectivity does impose an early bias on OTC preferences, biased connectivity patterns should *persist* into adulthood and potentially even be strengthened, e.g., through increased myelination of repeatedly used white matter tracts and/or network-level tuning mechanisms proposed in interactive specialization. If we do not see the expected patterns of differential connectivity, it may suggest that either 1) connectivity is not consequential in determining categorical preferences for symbols in the OTC or that 2) the dichotomy we have laid out, numerals-to-magnitude versus letters-to-phonemes, is not the organizing dimension along which these symbol categories differ, at least at the neural level.

We further hypothesized that an *automatic* mapping process occurs within these circuits, which should be robust in adult subjects given their extensive experience using numerals and

letters in separate contexts. As proposed in the interactive account, such a pattern may reflect the engagement of distributed representations for numerals and letters that occur regardless of task goals. If differences in category-specific coupling are not observed, it may suggest that 1) distributed representations for numerals and letters are not automatically activated in the employed task context, that 2) distributed representation of numerals and letters are sufficiently similar, or 3) the distributed activity is too subtle or transient to be detectable in the fMRI signal.

In regards to question 2, we hypothesized that the same connectivity-based principles of OTC organization should govern the laterality of functions supported by the left and right ITNA. We predicted that the left ITNA, given its privileged access to the left-hemispheric language system outlined in the triple-code model and reported role in verbal-based operations with numbers, should demonstrate stronger structural and functional connectivity with language areas compared to the homologous circuits in the right hemispheres. We also predicted the right ITNA would show stronger within-hemisphere connectivity with the IPS, given the general right-parietal bias for number processing and more robust engagement of the right ITNA in prior work. It is alternatively possible that these circuits are in fact symmetric, and that differential roles of the ITNAs are more simply due to their *proximity* to asymmetric functional networks. Further, given evidence that the left IPS is increasingly tuned for processing symbolic numbers over development, it may be that connectivity in the left ITNA-IPS circuit “catches up” with the right hemisphere, and so may be similar by adulthood. Whatever the case, this comparison is a necessary first step in addressing how connectivity-based constraints may impact the bilateral processing of numerals in the OTC.

To address question 3, in Chapter 3, we conducted a longitudinal analysis of children in kindergarten through 2<sup>nd</sup> grade who performed a symbol classification task during fMRI. We

characterized the functional development of symbol areas in terms of their sensitivity and selectivity to numbers and letters, the representational content within these areas, and their functional connectivity with intraparietal regions involved in number processing. We hypothesized that symbol learning is enhanced in the early years of formal schooling and so should represent a critical period of OTC development. We predicted the ITNAs would demonstrate increasingly “digit-biased” functional properties over the study. On one level, our inclusion of multiple functional measures (i.e., activity, representational patterns, and connectivity) serves an exploratory purpose, asking whether the ITNAs become functionally differentiated *in any sense* over this time window. However, specific findings would have implications for current models of OTC development. For instance, if the ITNA similarly (and positively) responds to all symbols at baseline, this would support the shape hypothesis’s prediction of shared processing of symbols in the initial state. If such an observation is then followed by both a *declining* response to non-preferred symbols and a *maintained* response to numerals, this would provide evidence for a pruning-based account such as proposed in interactive specialization. Alternatively, if the ITNA’s response to numerals is at its peak early on and then declines over the study, it may support the interactive account’s proposal of decreasing prediction error with learning. Furthermore, based on the biased connectivity hypothesis, we may expect stronger functional connectivity between the ITNA and IPS compared to the letter area already at baseline, indicating that a domain-specific circuit is established prior to learning and is possibly innate. Functional connectivity in this circuit may also increase over the study, supporting the notion of increasing network-level selectivity put forth in theory of interactive specialization.

In the subsequent empirical chapters (Chapters 2 & 3), I introduce each study, describe their

methods, and then present and discuss the results. In the General Discussion (Chapter 4), I emphasize the most important findings and reflect more generally on the implications of my work, as well as how it speaks to theoretical frameworks I have outlined in this introduction.

## **CHAPTER 2**

### **CONNECTIVITY CONSTRAINTS ON SYMBOL AREAS IN THE OCCIPITOTEMPORAL CORTEX**

#### **2.1 Introduction**

To explain the spatial segregation of number versus letter processing in OTC, the biased-connectivity hypothesis predicts that the “inferior temporal numeral area” (ITNA; Yeo et al., 2020) emerges due to increased structural connectivity with areas involved in magnitude processing, such as the intraparietal sulcus (Nieder & Dehaene, 2009). On the other hand, letters may be processed near the more medial “visual word form area” (VWFA) due to this area’s increased connectivity to perisylvian language regions (Hannagan et al., 2015). Indeed, a “letter form area” has been observed in the fusiform gyrus, immediately posterior to the VWFA (Thesen et al., 2012).

In addition to an area’s distinct profile of axonal projections, the set of regions which an area communicates may also drive its preference for certain object categories (Johnson, 2011; Mahon & Caramazza, 2011). These interactions could occur through a direct axonal pathway, but also indirectly, through polysynaptic functional networks. The ITNA, compared to the VWFA, is more strongly coupled to parietal areas during rest (Abboud et al., 2015; Nemmi et al., 2018), while the VWFA exhibits “privileged” functional connectivity with the language system (Stevens, Kravitz, Peng, Tessler, & Martin, 2017). Note that these studies characterized intrinsic

functional connectivity (i.e., correlations in spontaneous activity occurring in a resting state), so do not directly demonstrate the *context-dependent* pattern of communication between symbol areas and domain-specific networks, as predicted by an interactive specialization account. A recent electrophysiological-recording study found that functional interactions of the pITG and parietal cortex are selectively increased in the context of an arithmetic compared to reading task (Daitch et al., 2016). However, multiple demands differ between arithmetic and reading so, we cannot infer this communication was related to digit processing *per se*. Furthermore, given the aforementioned studies have only characterized functional connectivity, they do not provide direct support for the biased (structural) connectivity account and additionally provide no information about the relations between, or relative importance of, structural and functional connectivity.

Outside of the number domain, structural connectivity patterns have been shown to reliably predict the location of OTC areas involved in processing faces, objects, scenes, and bodies (Mahon & Caramazza, 2011; Osher et al., 2016; Saygin et al., 2012). Similarly, compared to the adjacent fusiform face area (FFA), the VWFA is more structurally connected to areas involved in language (F. Bouhali et al., 2014). Structural connectivity patterns in pre-reading children can even predict the *future* location of the VWFA (Saygin et al., 2016), providing perhaps the strongest evidence to date for the primacy of white-matter projections in driving OTC organization in humans. The extent to which white-matter projections underlie anatomically distinct locations for digit and letter processing, however, is unknown. Of note, a recent tractography study by Grotheer and colleagues contrasted structural connectivity among networks of regions involved in reading and adding (which included distinct areas of the OTC) (Grotheer, Zhen, Lerma-Usabiaga, & Grill-Spector, 2019). They found that while many

projections between regions of the “reading” and “math” networks ran in parallel, along the arcuate and superior longitudinal fasciculi, they occupied distinct sub-bundles and could be reliably distinguished in individuals. This study thus provides convincing evidence that domain-specific networks for reading and math are structurally differentiable. However, the regions analyzed in this study were defined based their engagement in two qualitatively different task contexts, i.e., reading or adding, and so cannot specifically address *digit* versus *letter* processing. Critically, the biased connectivity hypothesis provides causal explanations for why digits and letters would be processed in *different* cortical locations under the *same* task conditions.

Connectivity-based constraints on OTC organization are thought to influence not only the *localization* of selectivity within a hemisphere, but also the *lateralization* of function between hemispheres (Behrmann & Plaut, 2015, 2020). In the Introduction section 1.4.3, I reviewed findings that both a left and right ITNA may support digit recognition, but functional asymmetries in their roles have been observed. In particular, the right ITNA appears to be more reliably be engaged by numbers compared to other symbols (D. J. Yeo et al., 2020, 2017), possibly related to a right-hemispheric dominance for number processing more generally. The right IPS in particular appears to be innately predisposed to magnitude processing, compared to a more protracted and experientially-driven development of numerical tuning in the left IPS (Chochon, Cohen, Van De Moortele, et al., 1999; Kersey & Cantlon, 2017a; Pinel & Dehaene, 2013; Rivera et al., 2005; S. E. Vogel et al., 2015). Based on neuropsychological evidence, the left ITNA appears more important for verbally-mediated number operations, such as arithmetic fact retrieval and multi-digit reading (L. Cohen & Dehaene, 1995; Dehaene & Cohen, 1995), presumably due to privileged access to the left-hemisphere language system. The triple-code model describes within-hemisphere pathways linking the “visual” and “quantity” codes of ITNA

and IPS bilaterally, and the “visual” and “verbal” codes specifically within the left hemisphere (Figure 1A). However, the model does not explicitly address how connectional architectures may differ between hemispheres (Dehaene & Cohen, 1995). Here, we hypothesized that hemispheric asymmetries in ITNA connectivity with right parietal areas and left language areas may underlie their functional differentiation.

In the present study, we set out to examine, for the first time, both the structural and functional connectivity of digit- and letter-sensitive areas in OTC. We reanalyzed fMRI data from Pollack and Price (2019) and computed measures of structural connectivity via diffusion-weighted imaging in the same sample of individuals. Functionally defined seed regions were derived from a previously published group-level analysis of this dataset, including left and right hemisphere Digit areas, anatomically consistent with the putative ITNAs, and a left hemisphere Letter area, slightly posterior to the VWFA and consistent with other studies of letter processing (Rothlein & Rapp, 2014; Thesen et al., 2012). We examined whether different symbol areas demonstrate differential white-matter projections and/or task-evoked functional connectivity to *any* area of the brain. Based on connectivity-based accounts of OTC function, we made the following predictions:

1. Localization: The left Digit area will be more structurally and functionally connected than the Letter area to the intraparietal cortex due to its domain-specific involvement in magnitude processing and math, while the Letter area will be more connected to language areas involved in reading.
2. Lateralization: The left hemisphere Digit area will be more connected to left hemisphere language network (compared to the homologous pathways in the right hemisphere), while

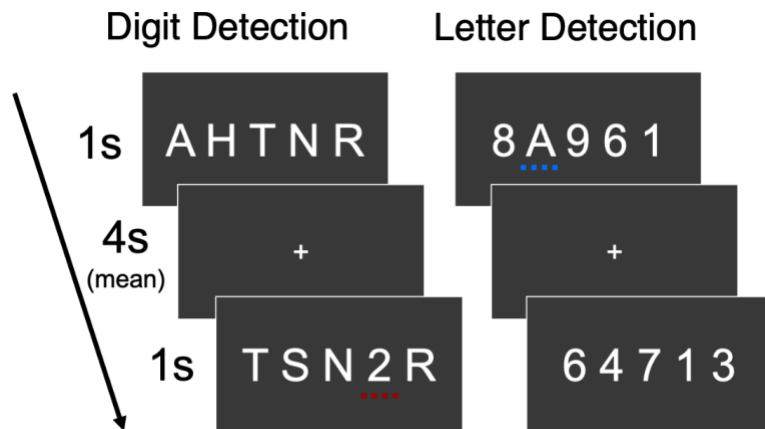
right Digit to right IPS connectivity will be stronger than the homologous pathway in the left hemisphere.

## **2.2 Methods**

### **2.2.1 Participants**

Participants who completed the fMRI tasks were 33 neurologically healthy, right-handed, English speaking 18-23 year old adults from our university and the surrounding community ( $M = 19.42$ ,  $SD = 1.50$ , 22 females). Of these, 29 also underwent diffusion weighted imaging. Participants were recruited from our university and the surrounding community via postings to the psychology study pool and local research listservs. Participants received either course credit (1 credit for each half-hour of time) or monetary compensation of \$20 (if not an eligible student) for participating. All participants gave written consent and the study was approved by the Vanderbilt University Institutional Review Board. We included only normal healthy, right-handed, English speaking adults between the ages of 18 and 35. No gender or ethnic group was targeted or excluded. To determine a participant's eligibility for MRI, screening questions were asked that determined if there was metal in the participant's body (including non-ferrous metal such as braces), claustrophobia, vision or hearing problems, conduct disorder or the inability to hold still for 3 minutes at a time. Participants were excluded if there was a diagnosis of any psychiatric disorder, including ADD/ADHD, history of head injury, perinatal complications, poor hearing or vision, current pregnancy, a history of claustrophobia or the presence of metal in the body. MRI exclusionary criteria were determined via self-report on an MRI screening form, which was further reviewed by an MRI technologist before allowing any subject to enter the MRI magnet room.





**Figure 2.1** fMRI task paradigm

Figure adapted from Pollack & Price (2019). Dotted lines under the target stimuli are included here for presentation purposes only. Detection tasks were performed separately, and counterbalanced across participants.

### 2.2.2 fMRI task

As reported in Pollack & Price (2019), during the digit detection task, participants viewed a string of 5 symbols (either 5 letters or 4 letters + 1 digit) and determined whether a digit was present (Yes or No), responding via button press of either the right index or middle finger. The letter detection task was the same, except a letter was to be detected among digits. The digits 1-9 and letters T, S, N, R, H, E, D, C, and A in Arial font were used as stimuli. On target present trials, the target appeared at either the 2nd, 3rd, or 4th positions in the string. Each task had 54 distinct trials grouped into 27 pairs, involving a target present and target absent version. Strings were random subsets of the selected stimuli but excluded letter strings that formed words or pseudowords and digit strings that contained a strictly increasing or decreasing number sequence. Trials lasted 1000ms each and inter-trial intervals (ITI) were either 2000, 4000, or 6000ms (average of 4000ms), during which a fixation cross was present on the screen. Each digit/letter was matched once with each ITI and ITIs were counterbalanced across target string positions. Stimuli were presented with PsychoPy 1.84 (Peirce, 2007). Runs began and ended

with 16 seconds of fixation, totaling 5m2s each. Each run consisted of the same 54 trials in a different pseudorandom order. No ITI was repeated more than twice and no correct response repeated more than three times. Four sequential runs of each task were completed, with the order of digit and letter task counterbalanced across participants.

### **2.2.3 MRI Acquisition parameters**

All images were acquired using a 3T Philips Achieva (Philips Medical Systems, Best, The Netherlands) and 32-channel head coil. T2\*-weighted, single shot echo-planar imaging (EPI) was used for functional scans, with the following parameters: TR/TE = 2000/25 ms, FA = 90°, FOV = 240 x 240 x 130 mm, voxel size = 3 mm<sup>3</sup> (with 0.25 mm gap), SENSE = 2.5. Each run lasted approximately 5m 16s in which 151 volumes were acquired (8 runs total = 4 runs digit task, 4 runs of letter task).

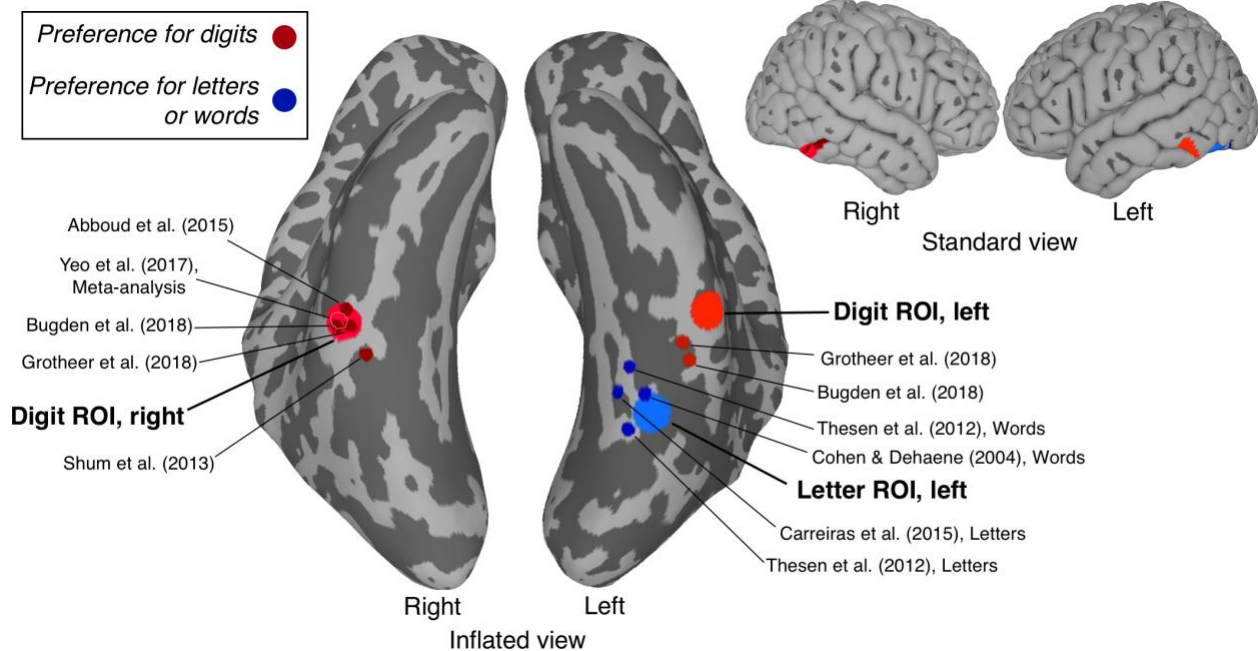
Diffusion MRI was performed using a pulsed gradient spin-echo (PGSE-EPI) sequence with the following parameters: 60 diffusion-weighted directions, b-value = 2000, TR/TE = 8600/66ms, FA = 90°, FOV = 240 x 240 x 125 mm, voxel size = 2.5 mm<sup>3</sup>, partial-fourier = 0.6, SENSE = 2, fat shift direction = P, acquisition time = 9m 36s. A non-diffusion weighted (b0) volume preceded the diffusion-weighted volumes. DWI was acquired immediately after the final fMRI run.

A T1-weighted anatomical scan was acquired between tasks, with the following parameters: TR/TE = 8.1/3.8ms, FA = 5°, FOV = 256 x 256 x 170 mm, inversion time = 936 ms, SENSE = 2, acquisition time = 6m 26s. This scan was segmented with FreeSurfer and used for anatomical reference.

### **2.2.4 Anatomical processing**

T1-weighted anatomical images were processed using FreeSurfer (v6.0.1,

<http://surfer.nmr.mgh.harvard.edu>), via the Vanderbilt University XNAT platform (Harrigan et al., 2016). The default “recon-all” pipeline was run along with inclusion of the extra “-3T” flag (which optimizes bias correction parameters and the target atlas for data acquired at 3T). All cortical surfaces and subcortical parcellations were visually inspected and manually edited where necessary using FreeView, according to FreeSurfer guidelines (<https://surfer.nmr.mgh.harvard.edu/fswiki/Edits>). FreeSurfer outputs were further processed for use in AFNI/SUMA using AFNI’s *@SUMA\_Make\_Spec\_FS* program (Cox, 1996; Saad & Reynolds, 2012). As part of this process, standard surface meshes were generated which preserve the overall geometry of subjects’ original meshes, but provide node-to-node correspondence across subjects based on alignment of sulcal and gyral landmarks. To take advantage of the sub-voxel resolution provided by streamline tractography, high-density “ld141” meshes were used, while the lower-density “ld60” meshes were used for fMRI analyses.



**Figure 3.** Digit and Letter seed areas in relation to reported literature coordinates.

Depicted coordinates represent a non-comprehensive subset of studies employing digit, letter, and word stimuli. One can appreciate that our functionally defined seed ROIs are approximately consistent with prior reports. For a more comprehensive set of coordinates from studies using letter stimuli, see Figure 14.

### 2.2.5 Seed fROI Definition

The seed regions of interest for the present study were functionally defined (fROIs) based on three results from the Pollack & Price (2019) group-level analyses. The digit fROI in the left hemisphere was derived from the contrast of Digit Present > Digit Absent and we focus specifically on the peak in the inferior temporal gyrus in Brodmann area 37 (MNI: -57,-52,-11). We can say that, based on the contrast, this region demonstrated digit selectivity, i.e., its activity was increased significantly when a digit was present and detected in the string of symbols compared to when the string contained only letters. Similarly, the letter fROI in the left hemisphere was derived from the contrast of Letter Present > Letter Absent and we focus on the peak in the left inferior occipital gyrus in Brodmann area 19 (MNI: -42,-64,-11). In the right

hemisphere, we focus on the peak of the cluster in the inferior temporal gyrus (MNI: 54,-52,-14) which showed a positive brain-behavior correlation between digit selective activity (Digit Present > Digit Absent) and mathematics competence (residualized Calculation Skills). Though this region did not show an overall group-level effect of digit selectivity, we were motivated to include it in the present due to 1) the behavioral relevance of its selectivity, 2) it is a nearby homolog of the left hemisphere digit region, facilitating our laterality analyses, and 3) a right-hemispheric ITNA has been more consistently identified in the literature (G. R. Price, Yeo, Wilkey, & Cutting, 2017).

To facilitate our cortical surface-based connectivity analyses, a series of steps was conducted to generate subject-specific surface ROIs. Using the MNI152-2009 template and the associated FreeSurfer surfaces distributed with AFNI ([https://afni.nimh.nih.gov/pub/dist/tgz/suma\\_MNI152\\_2009.tgz](https://afni.nimh.nih.gov/pub/dist/tgz/suma_MNI152_2009.tgz)), we first mapped each volumetric peak coordinate to its closest node on the MNI template surface (using AFNI's *3dVol2Surf* command). We then created circular ROIs around these nodes on each subject's inflated standard surface, dilating to a radius of 7mm. By using the standardized subject-space surfaces, we ensured that 1) the ROIs were centered on the same cortical location across subjects (based on gyral/sulcal anatomy), but also that 2) each ROI occupied the same total area of cortical tissue. The latter feature was particularly important for our quantitative tractography analyses to eliminate a potential confounding of ROI size with streamline count (and subsequently the sum of streamline weights, see tractography pipeline below). The ROI size (7mm radius) was chosen to be consistent with several other analyses of OTC connectivity (Grotheer et al., 2019; Gschwind, Pourtois, Schwartz, Van De Ville, & Vuilleumier, 2012; Klein, Moeller, Glauche, Weiller, & Willmes, 2013; Yeatman, Rauschecker, & Wandell, 2013).

To situate our findings within the broader literature on the ITNA, we qualitatively evaluated the relative proximity of our functionally defined ROIs to prior reports. Critically, there is not a one-to-one correspondence between the Euclidean distance of volumetric coordinates and their distance along the cortical sheet. We therefore used the same volume-to-surface mapping approach for a number of reported coordinates from studies looking at either digit, letter, or word selectivity. In Figure 3 we plot these coordinates on the MNI cortical surface along with the ROIs used in the present study. We can appreciate the consistency of findings for digit selectivity in both hemispheres, but particularly in the right. Furthermore, the Letter area used in the present study is comparatively much closer than the left Digit area to locations of letter and word selectivity (e.g., the VWFA). This provides confidence that the localization of digit and letter selectivity in the ventral stream is relatively task-invariant. Importantly, the study-specific seeds used herein are consistent with prior reports, making the present results more broadly relevant for the field.

### **2.2.6 DWI Preprocessing**

The DWI data were processed in MATLAB using tools from FSL (v6.0), ANTs, AFNI, and MRtrix3 (Cox, 1996; S. M. Smith et al., 2004; J-Donald Tournier et al., 2019; Tustison, Avants, Cook, & Gee, 2010). First, the raw diffusion data was first converted from DICOM to NIfTI format using `dicm2nii` (X. Li, Morgan, Ashburner, Smith, & Rorden, 2016). Next, the DWIs were denoised using MRtrix3's `dwidenoise` program, which has been shown to improve the subsequent estimation of diffusion parameters and fiber orientation distributions (Cordero-Grande, Christiaens, Hutter, Price, & Hajnal, 2019; Veraart et al., 2016). To correct for distortion (which is critical for anatomically accurate tractography), we employed a recently published method (Synb0-DisCo) which uses deep learning to generate a synthetic, undistorted  $b_0$  volume

using a subject's T1-w anatomical image (Schilling et al., 2020, 2019). The synthetic volume was then passed to FSL's TOPUP program to correct distortions in the acquired DWI images (Andersson, Skare, & Ashburner, 2003). A publicly-available MATLAB pipeline ([https://github.com/justinblaber/topup\\_eddy\\_preprocess](https://github.com/justinblaber/topup_eddy_preprocess)) was used to implement TOPUP and FSL's eddy tool, which corrects for motion and eddy current artifacts including outlier replacement (Andersson, Graham, Zsoldos, & Sotiropoulos, 2016; Andersson & Sotiropoulos, 2016). The T1-w anatomical image was affine registered to the distortion-corrected b0 image via AFNI's align\_epi\_anat.py script. With this transformation, the surface ROIs and FreeSurfer-derived tissue masks were sampled to a subject's native DWI-space for use within the tractography pipeline. While the primary analyses were carried out in native DWI-space followed by sampling to subjects' standardized cortical surfaces, we further assessed the volumetric overlap of our tracts of interests with canonical white matter bundles. For this analysis, a nonlinear registration of the T1-w anatomical images to the MNI152-2009 template was achieved using AFNI's auto\_warp.py script, and the transformation subsequently applied to the DWI-space streamline density images (see below).

### **2.2.7 Streamline tractography pipeline**

Streamline tractography was carried out using MRtrix3 (J-Donald Tournier et al., 2019). From the preprocessed DWI volumes, we first implemented an unsupervised method for estimating single-fiber response functions for white matter (WM), gray matter (GM), and cerebrospinal fluid (CSF), via dwi2response with the "dhollander" algorithm (Dhollander, Mito, Raffelt, & Connelly, 2019). To facilitate later group-level comparisons, the group average response function for each tissue type was used for subsequent estimation of fiber orientation distributions (FODs) (R. E. Smith, Raffelt, Tournier, & Connelly, 2020). Single-Shell 3-Tissue

constrained spherical deconvolution (SS3T-CSD) was performed to obtain WM-like FODs as well as GM-like and CSF-like compartments in all voxels (Dhollander & Connelly, 2016), using MRtrix3Tissue (<https://3Tissue.github.io>), a fork of MRtrix3. SS3T-CSD takes advantage of multi-tissue CSD, a framework which more faithfully resolves FODs in areas of partial voluming between tissues and ultimately improves tractography (Jeurissen, Tournier, Dhollander, Connelly, & Sijbers, 2014), while uniquely requiring only single-shell data. Prior to streamline generation, the FOD maps were corrected for bias fields and intensity inhomogeneities via mtnormalise (Raffelt et al., 2017). Probabilistic tracking was then performed to construct a whole-brain structural connectome (i.e., “tractogram”) via tckgen with the “iFOD2” algorithm (J-D. Tournier & , F. Calamante, 2010). The tractogram was created by generating 50 million streamlines which were randomly seeded and terminated (including “back-tracking”) at the GM/WM interface (GMWMI) as delineated by FreeSurfer. This method, called Anatomically-Constrained Tractography (ACT), improves the biological accuracy of the reconstructed streamlines by ensuring that, like the underlying axons, all streamlines begin and end (i.e., “synapse”) at some GM structure (R. E. Smith, Tournier, Calamante, & Connelly, 2012). Following tractogram construction, we used the successor to the “spherical-deconvolution informed filtering of tractograms” method (SIFT2, via tcksift2) to assign a weight (i.e., a cross-sectional area multiplier) to each streamline (R. E. Smith, Tournier, Calamante, & Connelly, 2013, 2015a). This process corrects for biases in tractography associated with the fact that streamlines are volume-less entities, which, for instance, can result in overrepresentation of certain tracts. Specifically, SIFT2 ensures that the (weighted) streamline reconstruction is an adequate fit of the diffusion signal (i.e., the CSD model) at each voxel, which is itself proportional to the volume of tissue aligned in each orientation. This effectively guarantees that



the summed weight of streamlines connecting any two brain regions is proportional to the total cross-sectional area of WM fibers connecting these regions, providing a physically interpretable, quantitative measure of structural connectivity (R. E. Smith et al., 2020). Overall, the tractography pipeline implemented here capitalizes on recent advancements in the field and has been shown to: 1) significantly improve the biological validity of structural connectivity metrics derived from streamlines (R. E. Smith, Tournier, Calamante, & Connelly, 2015b), 2) reduce inter-subject variability introduced by fiber-tracking biases (Yeh, Smith, Liang, Calamante, & Connelly, 2016), and 3) improve the reproducibility of tractography results compared to other pipelines (Nath et al., 2019).

### **2.2.8 Seed to whole-brain connectivity and consistency-based thresholding**

To facilitate correspondence with the tractography data, the cortical surface ROIs were first sampled to subjects' DWI-space. The weighted streamlines intersecting each ROI were extracted and served as a volumetric representation of the ROI's white-matter projections. Connectivity was assessed by mapping the streamline endpoints to the cortical surface and summing the streamline weights at each surface node. The node-level values were then multiplied by the subject-specific proportionality coefficient generated by SIFT2 ( $\mu$ ) (R. E. Smith et al., 2015a). Along with our previous steps that implemented group-average response functions and intensity normalization, multiplication by  $\mu$  yields maps containing theoretically *absolute* measures of fiber cross-sectional area, making them finally comparable across subjects (R. E. Smith et al., 2020). The maps were then smoothed to a FWHM of 6mm (using SUMA's SurfSmooth program).

Prior literature suggests that probabilistic tractography methods produce a high rate of spurious connections. In the present case, due to the large number of streamlines and SIFT2

weighting procedure, the seed-to-whole-brain connectivity maps generated were nearly fully connected. That is, while the connectivity of the seed to a target area may have been vanishingly small, it was almost never zero. We thus sought to threshold these maps before statistical testing to account for potential false positive connections. We implemented a recently proposed consistency-based thresholding approach which, compared to traditional weight-based approaches, was shown to yield structural connectivity results that more faithfully represent empirical estimates from tracer data (Roberts, Perry, Roberts, Mitchell, & Breakspear, 2017). For each surface node, the coefficient of variation (standard deviation/mean weight across subjects) was computed and served as a measure of connection consistency. The values for all surface nodes of the analyzed hemisphere (excluding the seed areas) were then ranked by their consistency. The logic goes that, regardless of its overall strength, as long as a connection is highly consistent across subjects it can be considered a true positive. This approach helps account for distance-dependent biases such that weak but consistent long-range connections may be retained while inconsistent short-range connections, e.g., due to overrepresented propagation errors, are removed. We principally chose a cutoff for masking based on reports of approximately 30% connection density in the mammalian brain (Buchanan et al., 2020; Oh et al., 2014; Roberts et al., 2017; van den Heuvel, Scholtens, & de Reus, 2016). Specifically, a binary mask was created from the top 30% most consistent nodes connected to each ROI, and a union of these served as a combined inclusion mask for subsequent analyses. Prior to statistical testing, the structural connectivity weights were log<sub>10</sub> transformed, due to prior demonstrations that errors in streamline-based connectivity are multiplicative rather than additive (R. E. Smith et al., 2015b). A benefit of this transformation is that the residuals from the linear contrasts should be more normally distributed. Note as well, given the exponential decline in axonal connectivity

with distance, logarithmic transformation of axonal connection densities is common practice in the literature (Oh et al., 2014).

### **2.2.9 Fiber Density & Length and Bundle Overlap Analyses**

To supplement our tractography results, we performed several additional analyses involving assessments of 1) average length and total cross-sectional area (“density”) of white-matter fibers innervating each of the seed areas, and 2) the overlap of each area’s projections with canonical white-matter tracts. Whole-brain length and density images were created using Mrtrix3’s *tckmap* tool and were derived from the full set of streamlines. SIFT2 weights were incorporated into this calculation to down-weight spurious fibers’ contributions to the average estimate at each voxel. The density images were multiplied by the subject-specific proportionality coefficient as in our seed-based connectivity estimates, to allow for valid group-level comparisons of these values (R. E. Smith et al., 2020). Length and density images were then sampled to the surface, where average values were extracted from each subject’s seed ROIs.

We then calculated the degree of overlap of the each seed ROI projection map with canonical white-matter bundles from the Xtract subset of the Pandora 4D atlas (Hansen et al., 2021; Warrington et al., 2020). The MNI-normalized track-density images were used to represent a subject’s weighted, volumetric map of projections from each seed ROI through the white matter. Bundle images and density images were thresholded at levels of 0.6 and 3, respectively, and then binarized. Overlap between the binarized 3D images was assessed using the Dice coefficient. The threshold settings were arbitrary, but led to the highest overall Dice coefficients and seemed reasonable upon visual inspection. We found that the results were consistent across a range of thresholds.

### **2.2.10 fMRI Preprocessing**

Surface-based analyses respect subject-specific gyral and sulcal anatomy and have been shown to improve cortical area localization as well as increase statistical power (Anticevic et al., 2008; Coalson, Van Essen, & Glasser, 2018). Given these potential benefits, and to facilitate comparisons with our structural connectivity results, the fMRI data from Pollack and Price (2019) were reanalyzed in the present study using a surface-based pipeline. The raw imaging files were first converted from Philips PARREC format to NIfTI format using the *dicm2nii* MATLAB toolbox (X. Li et al., 2016). The fMRI data was then preprocessed in MATLAB using AFNI and SUMA tools (Cox, 1996; Saad & Reynolds, 2012; Saad, Reynolds, Argall, Japee, & Cox, 2005). Trial onset timestamps were extracted from the PsychoPy output files for each condition separately (i.e., Digit Present, Digit Absent, Letter Present, Letter Absent, Errors, and Omissions) and onset files were created for use in AFNI. The *afni\_proc.py* program was used to build a preprocessing pipeline that included the following steps: despiking, slice-time correction, EPI-anatomical alignment, motion correction, sampling EPI data to subjects' standardized cortical surface, smoothing on the surface with a 6mm FWHM filter, and scaling to percent signal change.

### **2.2.11 Beta-series connectivity**

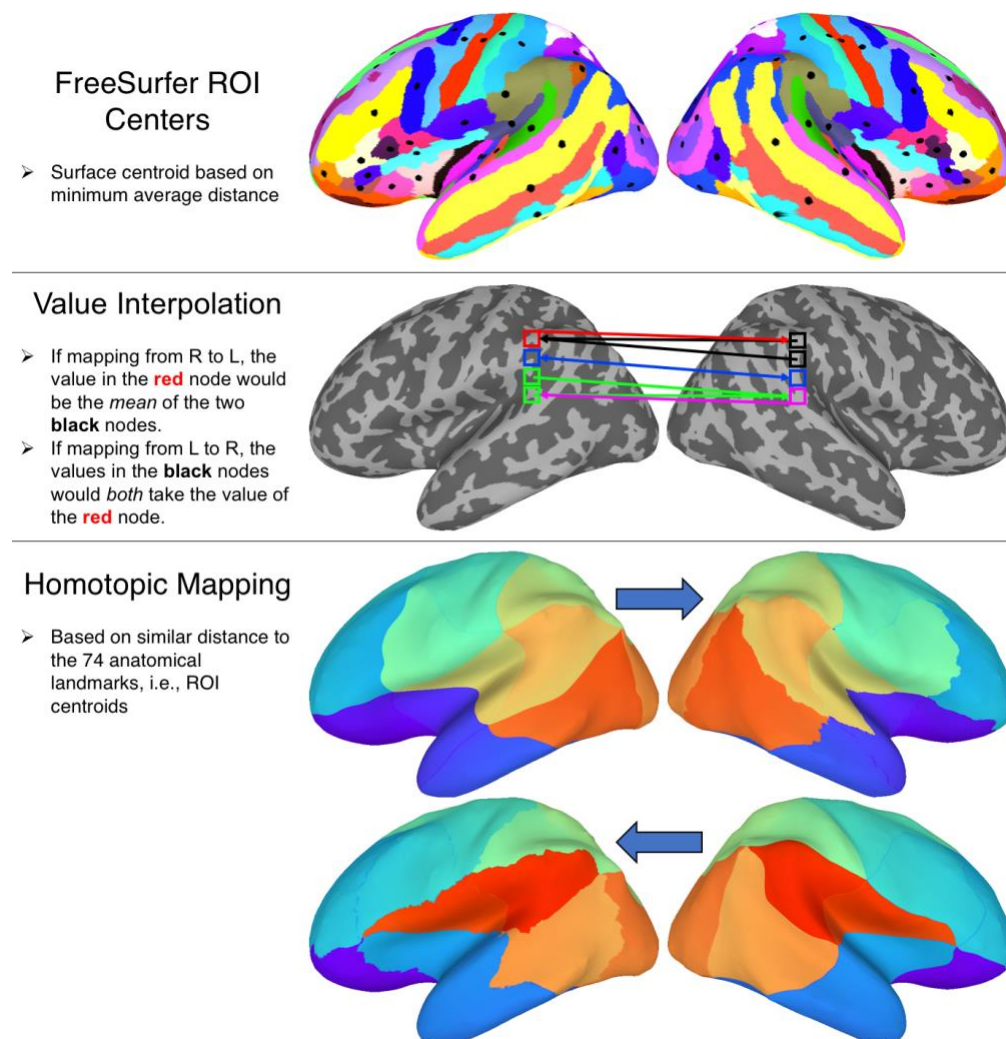
To assess task-evoked functional connectivity, we performed beta-series correlation (BSC) (Rissman, Gazzaley, & D'Esposito, 2004), which has been shown to be more powerful than psychophysiological interaction (PPI) analysis for assessing task-modulated connectivity in event-related paradigms, and is more robust to variability in the hemodynamic response across subjects (Cisler, Bush, & Steele, 2014). The independent BOLD response was estimated for each trial, generating a series of beta maps, and this series was then used to assess condition-specific

coupling of our ROIs with the rest of the brain. We used the computationally efficient “least-squares-separate” estimation method via AFNI’s *3dLSS* function (Mumford, Turner, Ashby, & Poldrack, 2012).

Specifically, AFNI’s *3dDeconvolve* function was first used to generate a general linear model (GLM) that combined all data from both the digit and letter tasks, containing nuisance parameters and an separate regressor for every trial. Trial-level regressors were defined by convolving the onset time with a gamma function modelling the hemodynamic response (i.e., AFNI’s default basis function, specifying an event duration of 1 second, “GAM(8.6,0.547,1”). Head-motion and outlier censoring was performed by removing volumes from the GLM which demonstrated between-volume movement of  $> 0.3\text{mm}$  Euclidean norm distance or if  $> 5\%$  of voxels within a brain mask were determined to be outliers. Nuisance parameters were defined for each run separately, including 6 motion parameters, 6 motion derivatives, and 0-3rd order Legendre polynomials to model low-frequency drifts. The GLMs additionally included the first three principal components in both white matter and lateral ventricles, as defined by a subject’s FreeSurfer segmentation. These additional regressors helped to mitigate the impact of non-neural physiological fluctuations and unmodeled motion effects in the beta series, which can artificially inflate connectivity values (Caballero-Gaudes & Reynolds, 2017; Ciric et al., 2017; Muschelli et al., 2014). The full GLM was then passed to the *3dLSS* function, which constructed and fit the reduced model for each trial separately.

Due to the censoring approach, we implemented a “beta-scrubbing” procedure where we excluded from BSCs those betas which had more than one volume censored over the span of the associated ( $\sim 14\text{s}$ ) HRF, with the assumption that these trials were contaminated by motion artifacts (Conrad, Wilkey, Yeo, & Price, 2020; Ray et al., 2017). This serves as a principled

strategy to eliminate outlier beta estimates resulting from an insufficient number of observations (volumes). Finally, the mean beta series for each condition was computed from the digit and Letter areas and correlated with the beta series of each node on the cortical surface, resulting in condition-specific seed-to-whole-brain functional connectivity maps. The Pearson correlation coefficients were transformed to Fisher Z estimates to allow for quantitative comparisons (Fisher, 1915).



**Figure 4.** Schematic of the homotopic mapping procedure.

This process was used to estimate an anatomically-informed transformation of data between

surfaces of each hemisphere. This allowed for direct, whole-surface comparisons of the within-hemisphere connectivity profiles of the left and right Digit areas. Images in the bottom panel demonstrate the mapping result with indexed data, validating that the transformation in either direction performed as expected.

### 2.2.12 Landmark-Based Homotopic Mapping

To facilitate direct comparisons of the left and right Digit area connectivity to their ipsilateral targets, we implemented an anatomical landmark-based mapping procedure adopted from Jo et al. (Jo, Saad, Gotts, Martin, & Cox, 2012). The procedure is outlined in **Error! Reference source not found.** First, we determined the centroid of each FreeSurfer ROI on the left and right cortical surfaces, using the 74-region Destrieux parcellation of the MNI152\_2009 template surfaces (Destrieux, Fischl, Dale, & Halgren, 2010). We calculated all pairwise distances among the nodes of each ROI and then defined the centroid as the node with the shortest average distance to all others (via AFNI's *SurfDist* function). Next, we calculated the distance of every surface node to the 74 ROI centroids, producing a vector of within-hemisphere distances for each node. We then assessed, for each node in a hemisphere, what node in the opposite hemisphere had the most similar distance profile using Pearson correlation. This process yielded a complete set of node-level correspondences between hemispheres, representing a fine-grained mapping each node's homotopic location with respect to gyral and sulcal landmarks. Correspondences were determined for both the high and low density meshes to facilitate comparisons of structural and functional connectivity patterns, respectively. Prior to statistical contrasts, subject-level connectivity maps for the right Digit area were sampled to the left hemisphere. To ensure our results were robust to the particular direction of mapping, we performed the same contrasts using left Digit connectivity maps sampled to the right hemisphere. The results were effectively identical, including all significant clusters reported herein.

### 2.2.13 Statistical Analysis and Threshold-Free Cluster Enhancement

The goal of this study was to assess similarities and differences in the structural (SC) and functional connectivity (FC) profiles of digit and letter-sensitive areas in the OTC. We focus only on connections to the ipsilateral cortical surface, due to the relatively sparse degree of axonal projections between hemispheres involving non-homologous areas. This approach is consistent with other studies in the field (F. Bouhali et al., 2014; Grotheer et al., 2019). While FC is much more bilateral in nature, we chose to also restrict these analyses to the ipsilateral hemisphere to facilitate comparisons with the structural results. “Task-general” functional connectivity was defined based on BSCs over *all trials* combined (ALL). Recent work has shown baseline BSC connectivity patterns are highly similar to those observed in a resting-state (Di, Reynolds, & Biswal, 2017), due to the fact that task-evoked activity accounts for only a small portion of the variance in the BOLD signal (Cole, Bassett, Power, Braver, & Petersen, 2014). Thus, we expected our task-general connectivity measure to reflect a mixture of both spontaneous and stimulus-evoked coupling (see Limitations for further discussion). We also assessed condition-specific coupling by contrasting the BSCs derived from trials of one condition versus others.

Using the subject-level, seed-to-whole-brain connectivity maps, we carried out a series of paired t-tests involving the following contrasts:

- I. **SC** – Digit area L > Letter Area
- II. **SC** – Digit area L > Digit area R (sampled to the left hemisphere)
- III. **Task-general FC** – Digit area L, ALL > Letter area, ALL
- IV. **Task-general FC** – Digit area L, ALL > Digit area R, ALL (sampled to the left hemisphere)
- V. **Digit-selective FC** – Digit area L, Dp > Da



- VI. **Letter-selective FC** – Letter area,  $L_p > L_a$
- VII. **Digit-selective FC** – Digit area R,  $D_p > D_a$
- VIII. **Difference in Digit-selective vs Letter-selective FC** –  
 [Digit area L,  $D_p - D_a$ ] > [Letter area,  $L_p - L_a$ ]
- IX. **Difference in Digit-selective FC** –  
 [Digit area L,  $D_p - D_a$ ] > [Digit area R,  $D_p - D_a$ ] (sampled to the left hemisphere)

For each contrast, the paired test was carried out simultaneously with a multiple comparison correction procedure, using a surface-based implementation of threshold free cluster enhancement (TFCE) from the CoSMoMVPA toolbox, with default null settings and 100k permutations (Oosterhof, Connolly, & Haxby, 2016; S. M. Smith & Nichols, 2009). A final corrected threshold of  $p < 0.05$  was used to indicate significance. Uncorrected t-statistic and the associated Bayes factor maps (Bayesian prior: Cauchy distribution, scale = 0.707) were created in the case of null results, in order to assess the level of evidence in support of the null hypothesis. To assess areas of shared connectivity between seeds, conjunction analyses were carried out for each of the contrasts. The group-level conjunction maps were computed by thresholding each subject-level connectivity map, creating a binary map of their overlap for each subject, and then computing a percentage map that indicated the proportion of subjects demonstrating an overlap at each node. SC maps were thresholded at  $\log_{10}(\text{mm}^2) = -6$ , and further masked by the previously defined group-level consistency mask. FC maps were thresholded at an uncorrected  $p < 0.005$  level.

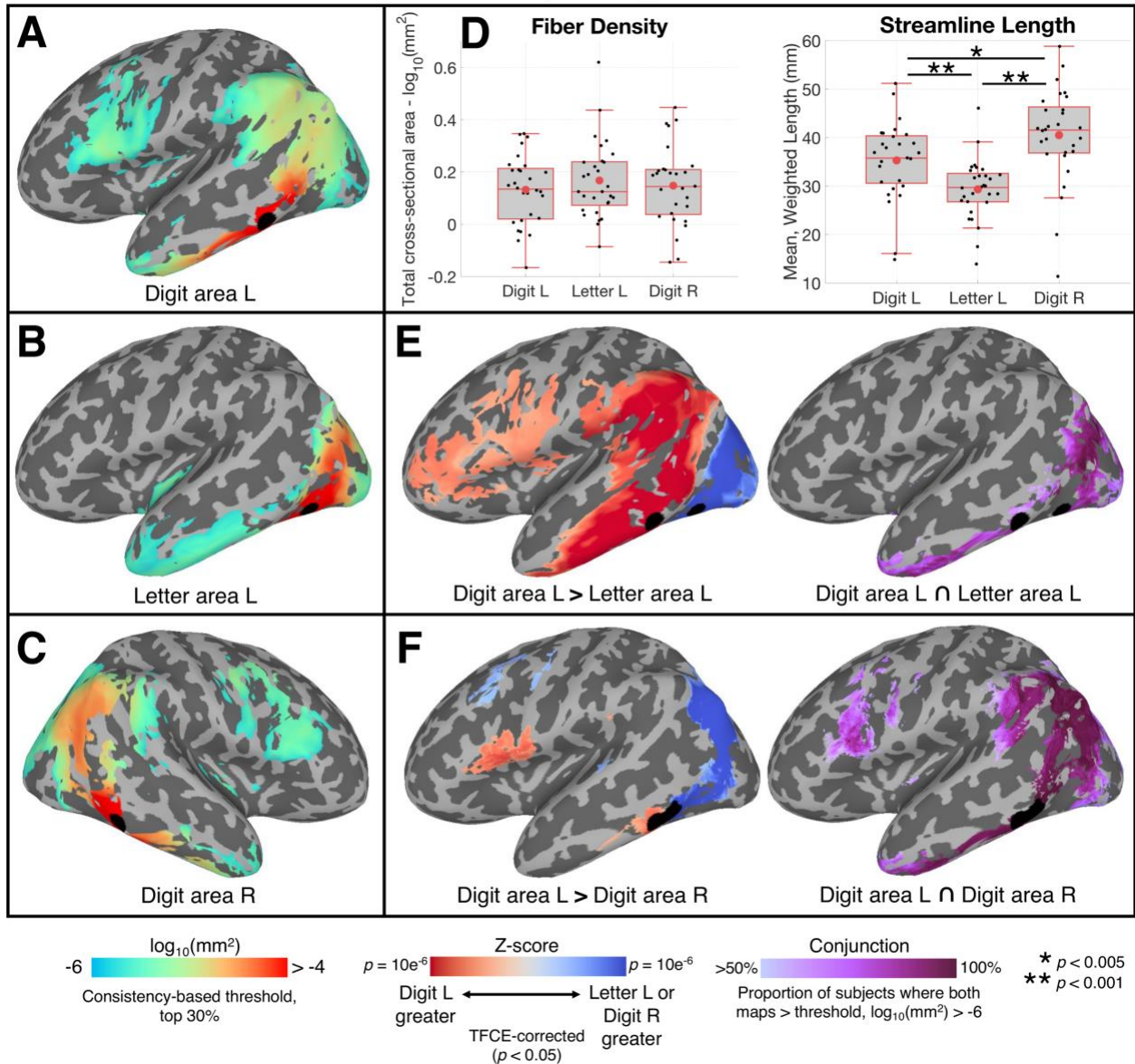
## 2.3 Results

### 2.3.1 Structural connectivity of Digit versus Letter area

We hypothesized that distinct connectivity patterns may underlie the localization of digit and letter processing in the ventral visual stream. In our first set of analyses we asked whether our functionally-defined Digit and Letter area in the left hemisphere were differentially connected, both in terms of their 1) white matter projections and 2) functional coupling during symbol detection. Specifically, we predicted the Digit area would show stronger connections to the intraparietal sulcus (IPS), known to be involved in magnitude processing and domain-specific numerical operations, while the Letter area would be more strongly connected to perisylvian and inferior frontal language areas involved in reading.

Our results demonstrated that the Digit area was more structurally connected to large swaths of parietal, lateral temporal, and lateral prefrontal cortex (red) (Figure 5E). The Letter area was more structurally connected to occipital areas and the fusiform gyrus. Our prediction of greater connectivity between the Digit area and the IPS was supported. These projections included most of the inferior parietal lobule but did not extend to the superior parietal lobule (Figure 5E). The Letter area, however, *was not* found to have stronger connectivity with putative language areas of the perisylvian fissure and inferior frontal gyrus. We instead observed that the Digit area was more connected to these areas. In a conjunction analysis (Figure 5E), we observed that both areas were similarly connected to the lateral/superior occipital and inferior/anterior temporal areas.

## Structural Connectivity of Digit and Letter Areas



**Figure 5.** Structural Connectivity of Digit and Letter areas

A-C) Group-average connectivity to ipsilateral cortical surface of each seed ROI, measured in units of fiber cross-section area ( $\text{mm}^2$ ), and masked according to the consistency-based thresholding procedure. D) Average fiber density and streamline length for each seed ROI. E) Contrast and conjunction statistical maps involving the left Digit and Letter area connectivity profiles. Contrast Z-scores derived from the TFCE-correction procedure. F) Contrast and conjunction maps involving the left and right Digit area.

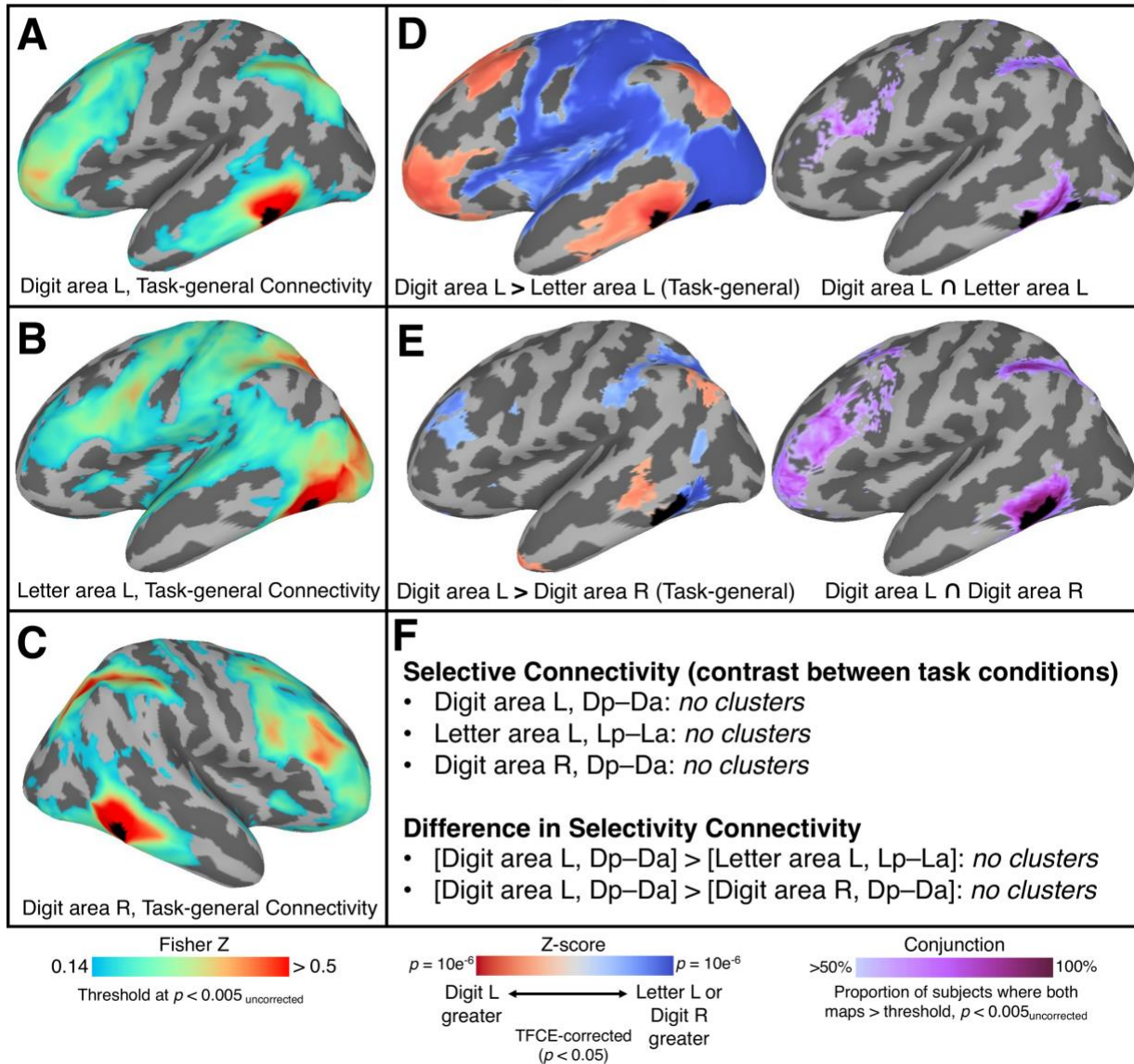
### 2.3.2 Functional connectivity of Digit versus Letter area

We next compared the functional connectivity profiles of the Digit and Letter areas. In the

first contrast, we compared their task-general connectivity patterns, defined as the BSC across all trials combined. We found the Digit and Letter area participated in largely distinct, whole-brain functional networks (Figure 6A-D). The Digit area was more strongly coupled with the IPS, the angular gyrus, the middle frontal and orbital gyri, and proximal areas in inferior temporal and middle temporal gyrus. The Letter area was more coupled with many areas spanning across occipital, superior temporal, superior parietal, pre/postcentral, insula, and inferior frontal gyrus. In the conjunction analysis (Figure 6D), we observed both areas were coupled to portions of the IPS, lateral prefrontal, and proximal OTC areas.

We next asked whether the Digit area's connectivity pattern was sensitive to digit detection, contrasting the Digit Present and Digit Absent maps. No significant clusters were observed, indicating a similar pattern of connectivity regardless of the stimulus condition (Figure 6F). Upon inspection of the Bayes Factor maps for this contrast (Figure 8; Figure 9), there existed some evidence of an effect in the IPS, such that the detection of a digit was associated with increased Digit area to IPS coupling. However, given it did not survive multiple comparison correction, we consider this an inconclusive result. We furthermore observed no letter-selective coupling from the Letter area. Finally, we observed no reliable difference between the Digit and Letter areas in terms of their stimulus-selective coupling.

## Functional Connectivity of Digit and Letter Areas



**Figure 6.1** Functional Connectivity of Digit and Letter areas

A-C) Group-average task-general functional connectivity to ipsilateral cortical surface from each seed ROI. Task-general connectivity referred to the correlation in the beta-series across all task events, regardless of condition. Pearson R values were then converted to Fisher Z. D) Contrast and conjunction statistical maps involving the left Digit and Letter area connectivity profiles (task-general connectivity). Contrast Z-scores derived from the TFCE-correction procedure. E) Contrast and conjunction maps involving the left and right Digit area. F) Description of condition-specific connectivity analyses, where the beta-series correlation across trials of one or more conditions was contrasted with another. No clusters survived TFCE-correction for any contrast.

### **2.3.3 Structural connectivity of the left versus right Digit area**




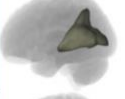
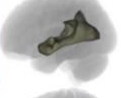


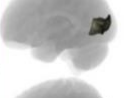

In our second set of analyses we asked whether our functionally defined Digit areas in the left and right hemisphere were differentially connected, both in terms of their 1) white matter projections and 2) functional coupling during symbol detection. Specifically, we predicted the left Digit area would show stronger connections to ipsilateral language regions, due to the known hemispheric asymmetry of language processing. We predicted the right Digit area would be more connected to the ipsilateral IPS, due to prior neuropsychological and neuroimaging evidence suggesting that a right hemispheric bias for numerical magnitude processing and a more consistent rightward lateralization for numeral processing in the OTC. Note, to test these predictions, the data from the right hemisphere was first sampled onto the left hemisphere surface, using a homotopic mapping procedure (see Methods).

In general, the left and right Digit areas showed a similar pattern of structural connectivity (Figure 5A,C), with the conjunction analysis demonstrating projections from both areas to the lateral occipital, inferior parietal, and lateral prefrontal cortices. However, the structural connectivity contrast highlighted significant differences in the total density of connections with several regions (Figure 5F). Among posterior areas, the right Digit area was more connected to lateral occipital cortex, angular gyrus, and portions of the intraparietal and parieto-occipital sulci. The right ROI was also more strongly connected to portions of the middle frontal and precentral gyri. The left Digit area was more strongly connected to the opercular inferior frontal and inferior precentral gyri, as well as a small section of the supramarginal gyrus (Figure 5F). We attribute the significant positive cluster at the anterior border of the left Digit area to the slight discrepancy in homotopic location, as it may be an artifact of local smoothing.

### **2.3.4 Functional connectivity of the left versus right Digit area**

We next compared the functional connectivity profiles of the left and right Digit areas. In the first contrast, we compared their task-general connectivity patterns. We found the left Digit area was more functionally coupled with the angular and middle temporal gyri, as well as the temporal pole (Figure 6E). The right Digit area was more coupled with the IPS, a posterior portion of the middle temporal gyrus, and antero-lateral prefrontal areas. The conjunction of their task-general connectivity patterns revealed both were strongly of coupled to a frontoparietal network including IPS and lateral prefrontal cortex (Figure 6E).

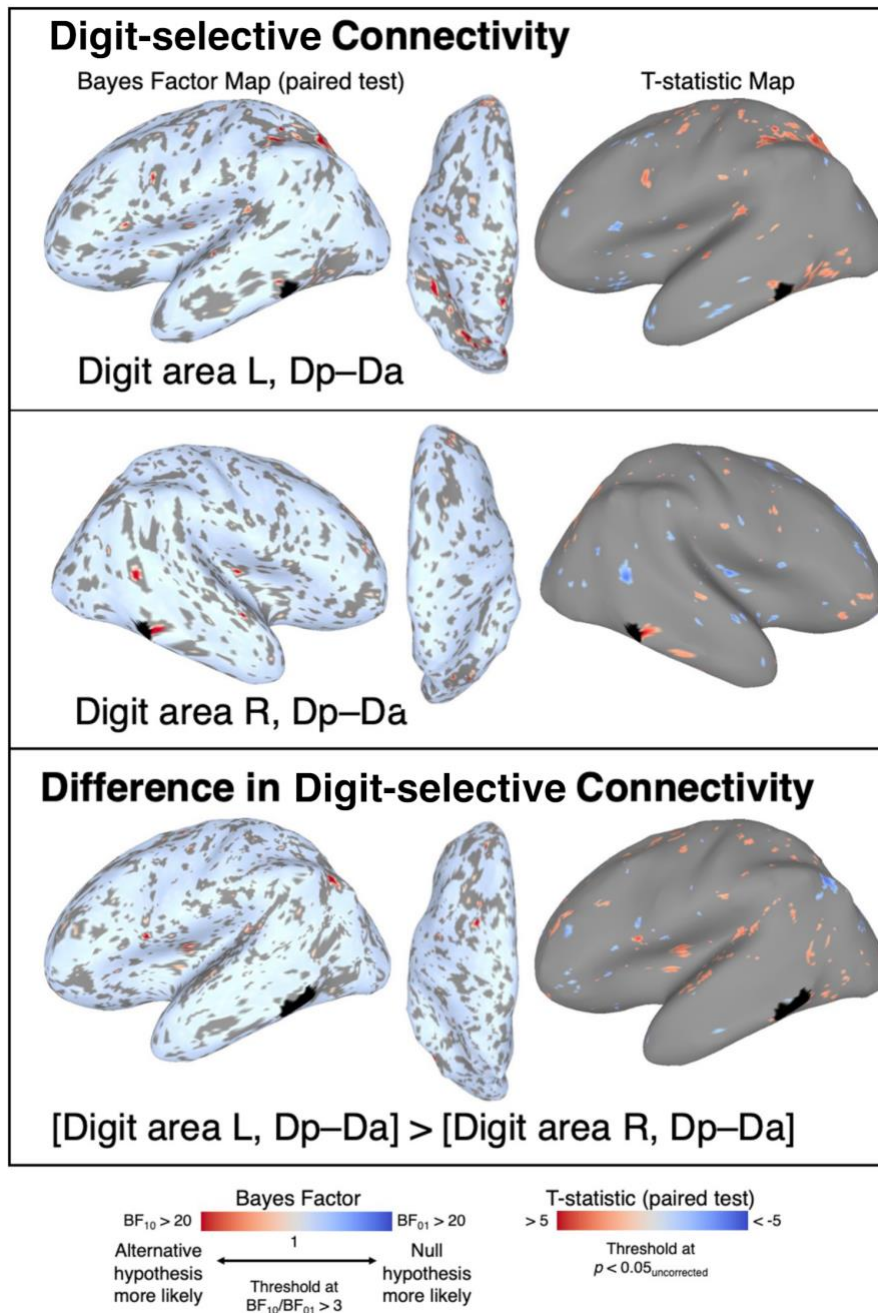
We observed no evidence of digit-selective coupling for either region separately (Figure 6F), other than the previously mentioned subthreshold effect between the left Digit area and IPS (Figure 8). Furthermore, we observed no difference between the left and right Digit area in terms of digit-selective coupling (Figure 6E).

Bundle Name	Digit area L	Letter area L	Digit area R	
Inferior Longitudinal Fasciculus	0.355	0.269	0.287	
Inferior Fronto-occipital Fasciculus	0.300	0.340	0.277	
Arcuate Fascicle	0.293	0.090	0.256	
Optic Radiation	0.270	0.316	0.252	
Medio-Dorsal Longitudinal Fasciculus	0.267	0.225	0.244	
Superior Longitudinal Fasciculus 3	0.164	0.018	0.120	
Superior Longitudinal Fasciculus 2	0.132	0.038	0.171	
Forceps Major	0.103	0.207	0.150	
Vertical Occipital Fasciculus	0.091	0.226	0.084	

**Figure 7.** White Matter Bundle Overlap

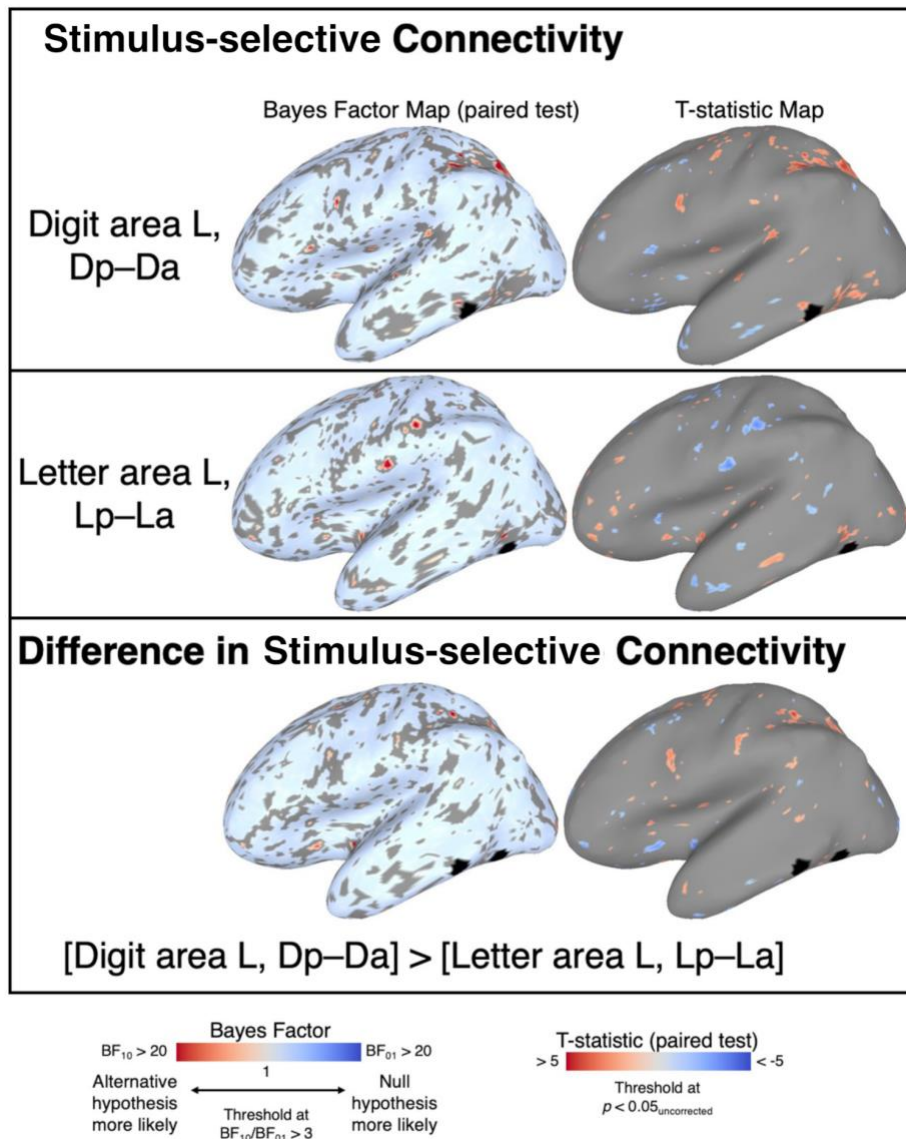
Mean volumetric overlap (Dice coefficient) of bundle and track-density images (TDI), across subjects. MNI-space bundles taken from the XTract subset of the Pandora 4D population atlas (Hansen et al., 2021; Warrington et al., 2020).





**Figure 8.** Digit-selective Coupling from Left versus Right Digit Area – Bayes Factor and T-maps

Due to the null results from TFCE-corrected contrasts (Figure 6E) we performed exploratory Bayesian analyses to test for strong evidence for the null hypothesis. In general, there was a lack of evidence for the null, indicating that the contrast was inconclusive in either direction. A positive cluster in favor of the alternative hypothesis (digit-selective coupling) was observed in IPS for the left Digit area, providing moderate evidence for increased coupling with this area during digit detection.



**Figure 9.** Stimulus-selective Coupling from left Digit versus Letter Area – Bayes Factor and T-maps

Due to the null results from TFCE-corrected contrasts (Figure 6E) we performed exploratory Bayesian analyses to test for strong evidence for the null hypothesis. In general, there was a lack of evidence for the null, indicating that the contrast was inconclusive in either direction. A positive cluster in favor of the alternative hypothesis (digit-selective coupling) was observed in IPS for the left Digit area, providing moderate evidence for increased coupling with this area during digit detection (note the Digit area L panel is the same data as the top panel in Figure 8).

## 2.4 Discussion: ITNA Localization and Connectivity

Based on the biased connectivity hypothesis, we predicted that an OTC area sensitive to

digits, given the association of digits with numerical magnitudes and their contextualized use in the domain of arithmetic and mathematics, would be preferentially connected to other regions reliably engaged by numerical processes, such as the intraparietal sulcus (IPS) (Nieder & Dehaene, 2009). We further predicted that an OTC area sensitive to letters, given the association of letters with written language and reading, would be preferentially connected to left-hemispheric language regions, such as inferior frontal and poster perisylvian cortex (Binder, 2015). In the following sections, I refer to the “Digit area” and “ITNA” interchangeably.

#### **2.4.1 The ITNA is functionally and structurally connected to intraparietal sulcus**

In a whole-brain contrast, we found that the Digit and Letter areas were highly distinct in terms of their anatomical connectivity. As predicted, across our sample, the Digit area reliably projected to the IPS and was more connected than the Letter area to the IPS, including most of the inferior parietal lobe (Figure 5E). These projections provide a plausible candidate pathway through which number symbols could be mapped to their magnitude referents. It is furthermore consistent with the idea that the localization of the ITNA could be driven by direct axonal connectivity of ITNA with other regions involved in representing numbers (see General Discussion section 4.1 for more on this finding).

Similarly, in contrasts of functional connectivity (FC), though both areas showed strong task-general coupling with the IPS (Figure 6A,B), the digit area was more strongly coupled to the IPS than the Letter area (Figure 6D). The pattern of differences in task-general FC was highly consistent with that from a recent analysis which compared the intrinsic connectivity of the “number form area” (i.e., ITNA) with the VWFA in a large sample of individuals ranging from 3-21 years of age (Nemmi et al., 2018). The authors showed the FC of the ITNA to the left IPS increased with age, suggesting this circuit is increasingly refined over experience. A similar

pattern was reported in early work by Abboud and colleagues (Abboud et al., 2015). In both studies, however, the observed ITNA-IPS coupling was *intrinsic*, i.e., without reference to a specific stimulus or task-context. Our findings build on this work, showing that when one is engaged in an active cognitive task, though both symbol areas interact with the IPS, the ITNA's interaction is stronger, presumably supporting a higher degree of information exchange between areas.

If this circuit supports the *domain-specific* process of digit-magnitude mapping, we should expect these areas to interact more so when processing their preferred stimulus category. Although the present task did not require actively processing magnitude information, behavioral studies have shown that digits are implicitly mapped to their magnitude referents, even when magnitude information is irrelevant to the task (Dehaene & Akhavein, 1995; Henik & Tzelgov, 1982; Rubinsten, Henik, Berger, & Shahar-Shalev, 2002), and further, the interactive account of Price & Devlin predicts the *automatic* engagement of distributed representations once a stimulus is processed in the OTC (C. J. Price & Devlin, 2011). Thus, in the present study, we expected to see evidence of this mapping in terms of stronger coupling during digit detection (i.e., Digit present > Digit absent). While there were indications that ITNA-IPS FC increased during the digit present versus absent condition (see Bayes Maps, Figure 8/Figure 9, top panel), this finding did not survive TFCE-correction (Figure 6F). We further found no evidence that the ITNA was selectively coupled to any region during digit versus letter detection. If digits were mapped to magnitudes during the task, it is possible that the signal from these events was too weak and/or transient to detect with fMRI, or that ITNA connectivity was anatomically variable across our sample. Despite the present results, other studies have demonstrated some domain-specificity to ITNA-IPS interactions. For instance, using intracranial electrocorticography, Daitch et al. have

shown that pITG and IPS sites were intrinsically coupled at baseline, but that this coherence was even more pronounced during an arithmetic task, as well as in comparison to a control task involving sentence reading (Daitch et al., 2016). Similarly, a longitudinal fMRI study in 8-14 year-olds demonstrated task-evoked coupling between IPS and a left OTC areas during arithmetic compared to a control task (Battista et al., 2018). This interaction increased with age, presumably due to a history of repeated co-activation of these areas over schooling (Johnson, 2011). Furthermore, the aforementioned study of Nemmi et al. found that ITNA-IPS FC related positively to arithmetic ability (Nemmi et al., 2018). This evidence all suggests the ITNA-IPS circuit is an integral component of the domain-specific network involved in number processing and mathematics. Our study provides new evidence that this reported functional circuit is not only distinct from the that of the Letter area during task performance, but is also supported by a larger degree of axonal connectivity between the ITNA and IPS, as predicted by the biased connectivity hypothesis.

#### **2.4.2 The ITNA is more structurally connected to language areas**

A curious aspect to our structural connectivity results was that it was not the Letter area, but the Digit area that demonstrated more projections to putative language areas, a finding that potentially provides evidence against the biased connectivity hypothesis. The Digit area was in fact more connected to large swaths of temporal, parietal and prefrontal cortex. Compared to the Letter area, the Digit area's axonal projections also had more distant targets on average (Figure 5D) and overlapped more prominently with the arcuate fasciculus (Figure 7), a white matter tract that has been heavily implicated in language and reading (Wandell, Rauschecker, & Yeatman, 2012). If structural connectivity drives categorical preference in the OTC, the present results suggest that the ITNA's position in the ventral stream may be a product of more than just the

association of digits with magnitudes. One possibility that single digits have higher-order semantic referents while letters, on the other hand, have no intrinsic meaning on their own. It could be that the distributed representation of a digit is simply more *distributed*, in that it taps into a wider range of cortical regions. In other words, the association of a single character (or object) to a wider conceptual network may be supported by a more broad axonal network. Such an interpretation is consistent with the largescale pattern of differential connectivity from the ITNA we observed here, as well as its significantly longer projections (Figure 5D). One interesting implication for this finding may be in the explanation for the so-called “digit-advantage,” whereby behavioral studies have reported a slight but consistent increase in processing speed for single digits over letters (for a review see T. M. Schubert, 2017). Interestingly, a digit advantage was reported in the present dataset in Pollack & Price (2019), in which digit detection took less time on average than letter detection, tying this idea more closely to the functional ROIs we analyzed here. A number of hypotheses have been proposed, but perhaps the most promising suggests that, due to their association with a conceptual representation, digits are afforded higher top-down support compared to single letters. Such an idea is in line with the interactive account, which outlines the effect of top-down prediction signals on processing efficiency in the OTC (C. J. Price & Devlin, 2011). The structural connectivity of the Digit area we observed here may underlie increased top-down support, and may further explain increased processing speed for digits compared to letters. This suggestion remains speculative, but is a fascinating avenue for future research.

As a final comment on this finding, we note that the Letter area was more *functionally coupled* to language areas in terms of its task-general connectivity (Figure 6D). This highlights a significant discrepancy between functional and structural connectivity patterns and suggests that

these two metrics should not be conflated in theories of OTC organization and development (see General Discussion section 4.1 for more on this topic).

### **2.4.3 The Letter area is functionally and structurally connected to the fusiform gyrus**

In the above sections, we have focused on why the ITNA may be situated where it is, and how its location is potentially supported by unique connectivity patterns. Note, however, that the Letter area was more strongly connected to fusiform gyrus, including to the classical location of the VWFA (Figure 5E, Figure 6D). The Letter area's projections also showed greater overlap with the vertical occipital fasciculus (Figure 7), a primary white matter tract associated with the VWFA which connects ventral and dorsal aspects of the occipital cortex (Yeatman et al., 2013, 2014). This fusiform-centered pathway involving the Letter area likely underlies the posterior-to-anterior hierarchy of ventral stream stages critical to reading, involving the processing of shapes, letters, bigrams, and finally a binding of these representations into whole words (Vinckier et al., 2007). The repeated involvement of letters (and not digits) in this computational hierarchy may itself lead to selectivity of this area for letters over digits. Note that although multi-digit numbers have their own syntactic structure involving place values, this process may not rely on the fusiform system (or if so is less frequently engaged than word reading) and so this area of cortex is not involved in single digit processing (see Dotan & Friedmann, 2019, for distinct cognitive models for multi-digit versus word reading). From this perspective, *biased connectivity* of the Letter area with this computational system may indeed play a consequential role in driving the selectivity of this area for single letters.

## **2.5 Discussion: Lateralization of ITNA Connectivity**

The distribution of functions among the left and right hemispheres of the brain has long

been a topic of investigation and debate, but yet remains an open area of research in which many outstanding questions remain. Despite a remarkable degree of symmetry in their anatomy, it is well appreciated that the two hemispheres consistently take on distinct and often complementary roles in service of behavior. The hemispheric asymmetry of visual object processing in the occipitotemporal cortex (OTC) is no exception and has received a great deal of attention in the literature (Behrmann & Plaut, 2020). As with functional localization among OTC areas *within* a hemisphere, the functional roles taken on by each hemisphere are thought to be constrained by dissociations in their connectional architectures. In the present study, we compared the structural and functional connectivity profiles of the inferior temporal numeral area (ITNA) in the left and right hemisphere. Prior neuropsychological and neuroimaging evidence has highlighted distinctions in their functional contributions, but no study has directly contrasted their connectivity profiles. Based on the prior evidence, and in particular drawing on the triple-code model of Dehaene and colleagues (Figure 1A), we predicted that the left and right ITNA would show distinct patterns of connectivity to domain-specific regions involved in language and numerical magnitude processing.

### **2.5.1 Left ITNA has greater anatomical connectivity with inferior frontal gyrus**

First, in accordance with our prediction, we found that the left ITNA was more structurally connected to the opercular inferior frontal gyrus (IFGop), also known as pars opercularis or Brodmann area 44, as well as the neighboring sulcus that separates the opercular and triangular IFG (the vertical ramus of the anterior lateral sulcus) (Destrieux et al., 2010). The IFGop in the left hemisphere is a core component of the language network and has been described as a cortical “convergence zone” involved in the perception and production of speech (Fedorenko & Blank, 2020; Keller, Crow, Foundas, Amunts, & Roberts, 2009; C. J. Price, 2012).



For instance, evidence from studies using direct cortical stimulation and recording have demonstrated that the left IFGop is engaged when processing both phonologic and semantic aspects of language (Tate, Herbet, Moritz-Gasser, Tate, & Duffau, 2014), and involved in transforming representations from temporal areas into an articulatory code that can be implemented in motor cortex (Flinker et al., 2015). In terms of its anatomical projections, tractography studies have found the IFG to be anatomically connected via the arcuate fasciculus (AF) to Brodmann area 37, which includes posterior aspects of the middle and inferior temporal gyrus (Friederici, 2009; Glasser & Rilling, 2008; Grotheer et al., 2019). In our tract overlap analysis (Figure 7), we found that a portion of projections from the both the left and right ITNA overlapped with the AF, but that the overlap was greater in the left hemisphere ( $t(28) = 3.16$ ,  $p = 0.004$ ,  $BF_{10} = 10.56$ ), suggesting asymmetric ITNA-IFGop connectivity involves a difference in the AF pathway. Our result is consistent with a well-established finding of greater fiber density within the left AF compared to its right homolog (Allendorfer et al., 2016; Barrick, Lawes, Mackay, & Clark, 2007; Glasser & Rilling, 2008; Hagmann et al., 2006; Nucifora, Verma, Melhem, Gur, & Gur, 2005; Powell et al., 2006; Vernooij et al., 2007). Asymmetry in the AF is present even in infants, suggesting this architecture may serve as an early and long-lasting constraint on hemispheric organization (Dubois et al., 2009). In a study similar to our own which focused on the lateralization of AF connectivity, it was shown that the left lateral temporal cortex is more structurally connected than its right homolog to the IFG (Takaya et al., 2015). The authors also found that the intrinsic coupling of the temporal and IFG regions was greater in left hemisphere and that their level of activation was closely related during a semantic word classification task, suggesting that the higher density of AF fibers supports increased functional interactions within the left hemisphere. The lateral temporal ROI used in that study only

bordered the ITG, however, and instead included aspects of the STG, STS, and MTG, leaving open the question of whether asymmetry in the AF included projections to the lateral ITG. Our results indicate that the left ITNA is not simply proximal to the language network, but that it is directly connected to this network via the AF and shares a similar profile of hemispheric asymmetry in its projections. These projections provide a plausible substrate through which both feedforward and feedback interactions could occur, such that number symbols could be efficiently linked to left hemisphere-based verbal representations and language areas could in turn provide top-down prediction signals to the left ITNA (C. J. Price & Devlin, 2011). As a consequence, the existence of this asymmetric white matter architecture may result in differential tuning of the left and right ITNA over enculturation.

It should be noted, however, that we found no evidence of a leftward asymmetry in the *functional* connectivity of the ITNA and IFGop. In fact, neither ITNA was strongly coupled with IFGop. Instead, both were engaged with a frontoparietal system that included IPS and orbital/middle frontal areas (see Figure 6E, FC conjunction). Relatedly, it has been shown that the VWFA is intrinsically connected to the dorsal attention network, including the superior aspect of the IPS, SPL, and frontal eye fields, while only weakly connected to language regions (A. C. Vogel et al., 2012). During language processing, however, VWFA connectivity with the language system significantly increases compared to baseline (L. Chen et al., 2019). It is possible that the left ITNA and IFGop only interact strongly in particular contexts when verbal representations are engaged, such as during digit identification or retrieval-based arithmetic operations, as opposed to the task employed here which involved a category-level decision (i.e., *is a digit present or not?*). Thus, although the underlying channel for communication between the ITNA and language system exists in the left hemisphere, this circuit may only be tapped

when needed. For instance, we would expect the functional coupling patterns of the left and right ITNA to be more clearly differentiated in tasks that place a greater emphasis on verbal mechanisms.

### **2.5.2 Both ITNAs are connected to the frontoparietal control network**

The functional connectivity of a region is thought to in part reflect a region's history of coactivation (Lewis, Baldassarre, Committeri, Romani, & Corbetta, 2009), and so the pattern of coupling observed at “rest” is likely to reflect the most consistent coalition in which a region participates (Anderson, 2015; Johnson, 2011). Given we did not observe strong functional connectivity of the left ITNA with the IFGop (or other language areas) (Figure 6A,D,E), a further implication of our results is that the primary functional role of the left ITNA is *likely not* to connect symbols with verbal representations. As mentioned, both ITNAs were primarily connected to what is often referred to as the frontoparietal “control” network or FPN (Vincent, Kahn, Snyder, Raichle, & Buckner, 2008; B. T. Yeo et al., 2011). Their shared structural projections also included parts of this network (see Figure 5F, conjunction results). The FPN has been described as a global “hub” network that supports cognition by flexibly connecting with other networks and coordinating their activity (Cole, Repovš, & Anticevic, 2014). A bilateral ventral ITG area, precisely at the location of the ITNAs studied here, is consistently assigned to the frontoparietal network (FPN) across studies (Marek & Dosenbach, 2018). Furthermore, studies specifically looking at intrinsic connectivity of the ITNAs have found strong coupling with the FPN (Nemmi et al., 2018), including in blind subjects (Abboud et al., 2015). Remarkably, however, the ITG's contribution to the FPN has rarely been discussed in the large body of recent literature on this network and, consequently, remains poorly understood. While we proceed to discuss additional distinctions in the left and right ITNA connectivity patterns, we

pause to note that an understanding the ITG's general computational contributions to the FPN will likely be key to a more complete characterization of the ITNA's specific role in numerical cognition.

### **2.5.3 Right ITNA is more structurally and functionally connected to the intraparietal sulcus**

In the present study, we found the ITNAs were both structurally and functionally connected to portions of the ipsilateral IPS (Figure 5F; Figure 6E), indicating that direct axonal projections exist between these areas and suggesting that their functional roles are tightly linked. This finding supports the triple-code model's postulation that a "visual-to-quantity code" pathway exists in both hemispheres. However, on each measure, the right ITNA demonstrated a greater degree of connectivity, structurally to the posterior IPS (26.0% of FreeSurfer's IPS ROI (Destrieux et al., 2010)) and functionally along the entire length of the IPS (79.9%), supporting the prediction of rightward asymmetry in this pathway. In the context of the present dataset, Pollack & Price (2019) found that the left ITNA was sensitive to digits (i.e., Digit present > Digit absent) at the group-level, but the same effect was not observed in the right ITNA. In contrast, individual differences in digit-sensitivity of the right, but not the left, ITNA positively related to math achievement. The task employed here involved a simple categorical decision, "Is a digit present among a string of letters?", and so required no explicit mapping of digits to their magnitude referents in the IPS. This task may be more efficiently achieved via activation of the left hemisphere verbal pathway. In contrast, individual differences in the *spontaneous* engagement of the quantity-biased right hemisphere circuit may be related to mathematical competence.

#### 2.5.4 Distinct connectivity of the ITNA with anterior and posterior IPS

An interesting structure/function distinction we observed in both hemispheres was that the ITNA was functionally coupled with IPS along its entire length, but was only consistently structurally connected to the posterior IPS (pIPS) (e.g., the raw connectivity and conjunction figures; Figure 5A,C,F; Figure 6A,C,E). Our results are consistent with prior tractography studies in humans which show stronger OTC projections to pIPS compared to anterior IPS (aIPS; Bouhali et al., 2014; Bray, Arnold, Iaria, & MacQueen, 2013; Grotheer et al., 2019; Uddin et al., 2010), and a similar pattern has also been observed in macaque tracer data (Seltzer & Pandya, 1984). This suggests that interactions between the ITNA and the aIPS are supported by a *polysynaptic*, rather than direct, pathway. Consequently, it is plausible that information flow in this circuit follows an ITNA ↔ pIPS ↔ aIPS (bidirectional) chain of processing. Some empirical support for this model may be found in a recent study by Daitch et al. (2016) who directly measured cortical responses in the pITG, pIPS, and aIPS during numeral viewing and arithmetic tasks (Daitch et al., 2016). The authors found that both tasks activated sites in the pITG and pIPS, and that the pIPS responses were equally engaged by non-numeric control conditions. The aIPS, on the other hand, was engaged only in the arithmetic task, significantly more so than during a reading-based memory control task. These findings are consistent with prior work showing domain-specific involvement of the aIPS in higher-order arithmetic and numerical magnitude representation, whereas the pIPS is involved more generally in visuospatial attention (Dehaene et al., 2003; Piazza, Izard, Pinel, Le Bihan, & Dehaene, 2004; Pinel, Piazza, Le Bihan, & Dehaene, 2004). Daitch and colleagues further demonstrate that the pITG and aIPS were functionally connected at rest and that their coupling was selectively amplified during arithmetic. Intriguingly, the authors acknowledge that this interaction may be direct *or* indirect,

potentially mediated by a thalamo-cortical pathway (Saalman & Kastner, 2011). As discussed, our structural connectivity results suggest the ITNA to aIPS pathway may indeed be indirect but could *plausibly* be mediated by the pIPS. Though this hypothesis is admittedly speculative, it demonstrates the potential for tractography to constrain computational models of number processing. The results of this study, however, do contribute to a recent emphasis on understanding how IPS subdivisions differentially contribute to numerical cognition (Castaldi, Vignaud, & Eger, 2020; Harvey, Ferri, & Orban, 2017).

### **2.5.5 Double dissociation in ITNA connectivity with the angular gyrus**

We observed a dissociation in regard to how the ITNAs were structurally and functionally connected to the angular gyrus (AG), such that the left ITNA, compared to the right, showed *reduced* structural connectivity but *greater* functional coupling with AG (Figure 5F; Figure 6E). A large body evidence suggests that, in general, structural and functional connectivity are well aligned across the brain. This particular observation involving the AG thus serves as a fascinating counter-example and poses a puzzling interpretive challenge. In the Three Parietal Circuits model, Dehaene and colleagues postulated that the left AG supports verbal-based number processing, such as retrieval of multiplication facts, while also acknowledging its involvement in reading and verbal short-term memory (Dehaene et al., 2003). Though some work suggests the right AG plays an important role in number processing (Arsalidou & Taylor, 2011; Göbel, Walsh, & Rushworth, 2001), the preponderance of evidence points to the left AG as more critical for specifically symbolic numerical abilities (Faye et al., 2019). AG activity has been demonstrated across many task contexts, including when passively viewing numerals compared to other symbols (G. R. Price & Ansari, 2011), when actively accessing the magnitude of symbolic compared to non-symbolic stimuli (e.g., dot sets) (Castaldi et al., 2020; Holloway,

Price, & Ansari, 2010), and during retrieval-based arithmetic (Grabner et al., 2009). More generally, the left AG is thought to support symbol-referent mapping (Ansari, 2008), and outside of numerical cognition, it has been described as a global hub that integrates conceptual knowledge across multiple semantic and perceptual domains (Seghier, 2013). The left ITNA-AG circuit may support the mapping of lexicalized numerical “objects” to a language-based semantic network in the left hemisphere. We speculate that the increased axonal projections in the right hemisphere may predate the presumably experience-driven formation of this structural circuit in the left hemisphere, and that this rightward-lateralized structural connectivity persists into adulthood. The discrepancy between structure and function in this case requires further investigation, to address, for instance, what is the functional role of the right ITNA-AG circuit, given the strong(er) axonal connectivity between these areas?

## **2.6 Limitations**

Our functionally defined ROIs were defined at the group level, based on previously published contrasts in Pollack et al. (2019). It has been argued that subject-level ROIs are more sensitive to individual differences in the functional localization of visual object processing areas in occipitotemporal areas (Nieto-Castañón & Fedorenko, 2012). Despite this potential limitation, we note that our method does represent an improvement over traditional volumetric ROI approaches, in that it accounted for individual variation in cortical geometry. We first mapped the peak coordinate of each cluster to its closest location (node) on the MNI-template cortical surface. Rather than an absolute geometrical position in volumetric space, the surface-space node indexes a location relative to gyral and sulcal boundaries. We then took advantage of the aligned surfaces which preserved an individual’s native cortical geometry while also providing node-level correspondence across individuals. The circular ROIs used herein were generated by

“growing” a circle (14mm diameter) around the defined surface location. This process ensured that the ROI was centered on approximately the same cortical location and encompassed an absolute surface area of  $\sim 154\text{mm}^2$  for every subject.

Our study included more females than males (20F/9M) and therefore may have been skewed in relation to the general population. Previous studies have found that AF white matter demonstrates stronger leftward asymmetry in right-handed males compared to women and left-handed males (Catani et al., 2007; Hagmann et al., 2006) and that activation levels are more symmetric in females in the language network during language processing (Shaywitz et al., 1995). This suggests our findings may be conservative with respect to the asymmetries we observed in structural and functional connectivity, particularly involving language regions such as the IFGop. Our study was not designed to detect sex differences, so future work in larger samples will be necessary to examine the potential relation between sex and ITNA connectivity.

In the present study, we defined “task-general” connectivity as the correlation in response patterns across all trials of the task. Connectivity results derived from such baseline beta-series correlations (i.e., where no contrasts is made between conditions) have been shown to be highly similar those observed in traditional resting-state time series correlations (Di, Zhang, & Biswal, 2020), indicating that a large portion of variance in the BOLD signal is attributable to intrinsic fluctuations. However, in principle, since our results are based on coupling over *trials of a task*, they will be somewhat biased towards general task engagement. For instance, the BOLD signal assessed here included visual processing and motor responses that are unrequired in typical resting-state scans. Given we know the ITNAs are engaged by the task, we would expect that any effect of task performance on our measure functional connectivity to be amplified. Resting-state data was not collected in this study, so comparison to a true “resting” state was not possible. To



understand the generalizability of our functional connectivity findings, it will be important in future work to assess how similar our task-general connectivity patterns are to those in the absence of a task context, as well as to those in other task contexts such as arithmetic.

## **2.7 Conclusions**

Alphanumeric symbol processing in the OTC provides a useful model system for understanding both the localization and lateralization of functionally distinct areas in the brain. It has been proposed that areal patterns of structural and functional connectivity provide constraints on the topographic layout of categorical selectivity in the OTC. We tested these ideas by comparing the connectivity profiles of segregated digit and letter-sensitive areas in young adults. The left Digit area showed stronger connectivity than the Letter area to inferior parietal cortex and IPS, revealing a pathway that may support the mapping of digits to their magnitude referents and bias the posterior section of the ITG towards digit sensitivity. The left, compared to the right, Digit area was more connected to language areas, while the right Digit area was more connected to the IPS. These results are in line with the triple-code model of number processing and provide the first empirical evidence of architectural asymmetries between homologous digit-preferring areas of the OTC, potentially supporting their differential functional roles in particular task contexts. Understanding the causal role of connectivity in driving areal selectivity will require further work involving longitudinal data in young children.

## CHAPTER 3

### FUNCTIONAL DEVELOPMENT OF INFERIOR TEMPORAL NUMERAL AREAS FROM KINDERGARTEN THROUGH 2<sup>ND</sup> GRADE

#### 3.1 Introduction

The human occipitotemporal cortex (OTC) contains a patchwork of category-selective areas that respond preferentially to particular classes of objects (Grill-Spector & Weiner, 2014; Kanwisher, 2010). Despite decades of work characterizing the functional profile of the OTC in adults, understanding how these areas come to develop their selectivity is a comparatively open frontier. A number of theories make predictions about the origins and developmental trajectories of OTC function (Arcaro & Livingstone, 2017; Behrmann & Plaut, 2020; Cantlon et al., 2011; Hannagan et al., 2015; Johnson, 2011; Op de Beeck et al., 2019; C. J. Price & Devlin, 2011). Testing these predictions, however, requires measurements prior to and/or concurrent with the process of interest. OTC responses to common visual domains like faces and places occur in stereotypical locations at birth and are further refined within the first few years of life (Arcaro & Livingstone, 2017; Cantlon et al., 2011; Deen et al., 2017), resulting in a critical window of growth that is difficult to capture with current neuroimaging methods. *Alphanumeric symbols*, on the other hand, are particularly appealing class of objects for investigating OTC development for a number of reasons.

Firstly, with writing systems coming into existence over just the past 5000 years, alphanumeric symbols are an *evolutionarily recent* invention. This is far too short a time period for the human brain to have acquired *dedicated* brain systems for processing symbols. Instead, the brain must adapt or “recycle” preexisting architecture to fluently use symbols (Dehaene &

Cohen, 2007). The *arbitrary* association of symbols with their referents further necessitates that this class of objects is *learned* through experience. These features make symbol learning a perfect model system for understanding not only plasticity in the brain's capacity for object recognition, but also how ventral stream areas *interface* with distributed circuits involved in language, magnitude, and attentional processes.

Secondly, symbol learning occurs over a protracted developmental window extending into at least the early years of formal schooling. For instance, the U.S. Common Core Standards specify that students should be able to write the numbers 0-20 by the end of kindergarten and all upper and lower case letters by the end of 1<sup>st</sup> grade (Practices & Officers, 2010). The use of symbols in foundational skills, such as adding and subtracting numbers up to 100 and reading common two-syllable words, is not expected until the end of 2<sup>nd</sup> grade. The repeated and contextualized experience with alphanumeric symbols over this window provides an extensive and (relatively) controlled case of visual object learning in children. Critically, over this period children also acquire the ability to actively engage in novel cognitive tasks and simultaneously remain still in a scanner, making this window particularly suitable for studying the emergence of brain function with fMRI.

Finally, in human adults, the neural populations most sensitive to digits and letters are reliably *segregated* in the OTC. Given these symbol sets are effectively identical in terms of their low-level visual properties, functional segregation suggests that OTC activity is not solely a product of visual perception but is related to the higher-order associations and/or the contextualized use of objects in different domains. Studies in blind subjects further demonstrate this point, revealing that the same areas are engaged when numerical or phonological concepts are associated with auditory or tactile inputs. Investigating *how* and *when* responses to digits and

letters diverge in the OTC should help to clarify the fundamental mechanisms governing the development of human brain function.

Prior work on early symbol processing in the brain has largely focused on the development of the “visual word form area” (VWFA), a region in the left OTC that is preferentially engaged by letter and words. Responses in the VWFA track closely with literacy acquisition, whether that occurs with early reading instruction in school *or* later in life in illiterate-to-literate adults (Dehaene et al., 2015, 2010), suggesting that tuning of the VWFA is indeed a product of reading experience. Studies in children indicate that a preference for letters and words emerges in the left occipitotemporal sulcus (OTS; the site of the mature VWFA) from approximately 5 to 8 years of age, corresponding to the kindergarten through 2<sup>nd</sup> grade period (Ben-Shachar, Dougherty, Deutsch, & Wandell, 2011; Brem et al., 2010; Dehaene-Lambertz et al., 2018; Nordt et al., 2020; Saygin et al., 2016). In particular, it is the functional *specificity* for letters in the left OTS that appears to be changing over this period, i.e., greater response to letters relative to other symbols (Cantlon et al., 2011; Tracy M. Centanni, King, Eddy, Whitfield-Gabrieli, & Gabrieli, 2017). Already by kindergarten, individual differences in letter specificity are positively related to word reading, suggesting that early symbol processing in OTC is not only a product of symbol learning but is behaviorally relevant in children (Tracy M. Centanni et al., 2018).

In contrast to developmental studies of the VWFA, only a few studies have looked at digit processing in early school-age children. Of the existing fMRI studies that included number stimuli, none have found evidence for the emergence of digit specificity in the OTC (Cantlon et al., 2011; Dehaene-Lambertz et al., 2018; Libertus et al., 2009; Nordt et al., 2018, 2020). As we reviewed in Chapter 1 section 1.4.4, these results may be due to: 1) the use of passive task

designs which do not reliably engage the ITNA in adults (see also Chapter 1 section 1.4.2), 2) the use of multi-digit stimuli which may be less engaging in young children (e.g., understanding of place value beyond two-digit numbers is not taught until 2<sup>nd</sup> grade or later), 3) the inclusion of small sample sizes (20 or fewer participants studied under the age of 9 in all studies), and 4) a focus on univariate measures of the fMRI signal. Despite their potential limitations, it is important to recall that several of these studies found letter-specific activation in OTC within the same paradigms and also detected developmental increases in letter specificity (Cantlon et al., 2011; Dehaene-Lambertz et al., 2018; Nordt et al., 2018, 2020). This suggests that the development of digit specificity in OTC may be less robust or reliable and/or qualitatively different from the development of letter specificity.

Outside of the fMRI work, one recent study acquired electroencephalography (EEG) recordings in 20 first graders who viewed sequences of either single digits or letters while performing a color-change detection task (Lochy & Schiltz, 2019). The authors observed lateralized responses in occipitotemporal electrodes, with stronger rightward activity for digits and stronger leftward activity for letters, indicating that children's brains already distinguish between symbols categories *at some level* (note that given the limited spatial resolution of EEG, the precise localization of activity in OTC remains unclear). This result stands in contrast to another recent EEG study that found *no difference* in responses to letter strings and multi-digit numbers in 7 year-olds ( $n = 27$ ) or 10 year-olds ( $n = 29$ ) performing an oddball detection task (Park et al., 2018). Park and colleagues did, however, observe lateralized responses similar to Lochy & Schiltz in a group of 15 year-olds and a group of adults, suggesting a more protracted development of symbol-related processing in OTC. Whatever the case, given the current state of evidence, it is unclear *when* and *in what manner* the ITNA acquires its functional specificity for

digits.

### 3.2 The present study

In the present study, we address these questions using an approach that improves upon prior work in a number of ways. We collected fMRI in children who performed an active classification task on single digits, letters, and scrambled versions of digits and letters. Longitudinal measurements were collected in a comparatively large sample of children over kindergarten through 2<sup>nd</sup> grade. A total of 86 children had usable imaging data over 145 scans and a majority contributed two or more timepoints, more than doubling the sample size of previous studies. Using mixed-effect models, we assessed how functional responses to symbols in the bilateral ITNAs and a proximal letter area changed over children's time in school. We predicted the following:

- 1) Both ITNAs would show an increase over time in their *sensitivity* to digits (digit response vs. baseline).
- 2) Both ITNAs would show an increase over time in their *selectivity* to digits (digit vs. other symbol responses).

Furthermore, we analyzed not only univariate measures of activity and specificity, but also multivariate patterns (MVPA) including representational similarity analysis (RSA) and decoding (Kriegeskorte, Mur, & Bandettini, 2008; Norman, Polyn, Detre, & Haxby, 2006). MVPA-based approaches abstract away from response amplitudes at specific locations and instead look for information contained in the *spatial pattern* of activity elicited by different stimuli. Digits and letters may engage distinct arrangements of neural populations across an area, even if the overall mean response of the area is similar (e.g., Cantlon et al., 2011). Importantly,

with MVPA there is no requirement for activity patterns to spatially overlap *across individuals* – an inherent assumption of univariate analyses which may be invalid due to differences in cortical geometry, inadequate alignment, or idiosyncratic neural tuning. These features make MVPA-based measures complementary to, and potentially more powerful than, univariate analyses (Kriegeskorte et al., 2006).

RSA uses pattern information to examine the second-order representational “geometry” across stimuli/categories, i.e., the extent to which the similarity matrix itself follows a particular hierarchical structure. Employing RSA, Yeo and colleagues recently detected *digit-biased* category-level representations in the right ITNA when adult participants passively viewed single digits, letters, and scrambled symbols, despite similar univariate engagement across categories (D. J. Yeo et al., 2020). Representational patterns have also been shown to *precede* the development of category selectivity in the OTC for common visual domains, including faces, bodies, scenes, and objects (M. A. Cohen et al., 2019). Similarly, the distinctiveness of activation patterns for words, but not other categories, has been shown to increase over development in a cross-sectional study of children, adolescents, and adults (Nordt et al., 2018). Interestingly, a recent longitudinal study found that within-category representational similarity in OTC was already stable for multiple visual domains in 6 year-old children, but for words, representational similarity increased over early schooling (Dehaene-Lambertz et al., 2018). Taken together, these studies suggest that RSA may be a more sensitive marker of categorical preference in early developmental windows, especially for alphanumeric symbols, and thus motivate its inclusion in the present work. We hypothesized that the ITNAs may demonstrate increasing digit-biased representational geometries over early schooling, even if a univariate preference for digits is not yet established. We predict the following:

- 1) In both ITNAs, representational differences will increase between response patterns for digits and other symbols. (i.e., digit-biased representational geometry)
- 2) In both ITNAs, representational differences will increase between response patterns for digits and letters. (i.e., categorical distinction between digits and letters)

MVPA-based decoding involves training a classifier to distinguish between labelled activity patterns and then predicting the label of an untrained pattern. If one can successfully “decode” a stimulus from an area’s activity patterns alone, one can infer neural populations in this area encode information about stimulus identity. Our lab has recently demonstrated discriminability between digits in the left ITNA in tasks requiring explicit access to digit identity and magnitude (Wilkey, Conrad, Yeo, & Price, 2020). During simple digit detection, however, exemplar-level discriminability was not significant at the group level in either ITNA but did positively relate to math ability in the left ITNA (Yeo et al., *in prep*). These results together suggest that the left ITNA is “capable” of representing digit identity but it depends on task demands and potentially mathematical competence. Other work indicates that, in a delayed matched-to-sample task, digits are distinguishable in the right OTC, and that representational geometry there is related to the frequency of environmental co-occurrence, implying that digit-specific tuning is sensitive to experience (Lyons & Beilock, 2018). Though there is clearly more work required to understand how digits are represented in the ITNAs in the adult state, we hypothesized that digit-specific representations in the ITNA would strengthen over kindergarten through 2<sup>nd</sup> grade and therefore become more *decodable*. We predicted the following:

- 1) In both ITNAs, exemplar-level decoding of digits, but not letters, would increase.



Our univariate and multivariate measures focused on response levels and representational patterns *within* symbol areas of the OTC. As we have discussed, however, these regions do not act alone. It is important to consider local response properties within a broader context of distributed processing to understand the functional role of any brain region (Karl J. Friston & Price, 2011; Genon et al., 2018). And furthermore, connectivity-based accounts of OTC function posit that domain-specific connectivity profiles help to constrain and/or determine an area's functional selectivity. The interactive specialization (IS) hypothesis postulates that local processing is refined over development through repeated co-activation and interaction among interregional networks (Johnson, 2001, 2011). IS provides an explanatory framework for how functional connectivity causally drives, and potentially *precedes*, regional specialization. In our analyses of symbol area connectivity in adults (Chapter 2), we found that digit areas were more functionally connected than a letter area to parietal regions putatively involved in magnitude representation. We further found stronger functional coupling in the ITNA-parietal circuit of the right hemisphere. Finding these patterns in adults, however, does not address the developmental predictions put forward by the IS hypothesis. In the present sample, we more directly tested these predictions, assessing both the background and stimulus-specific coupling of the ITNAs to number-sensitive parietal regions and whether connectivity in these circuits changed over schooling. We hypothesized that if connectivity drives the development of category-selectivity in the ventral stream, domain-specific connectivity may be observable *before* changes in the local response profiles. Furthermore, as IS addresses both functional specialization and *localization*, the initial presence of and/or developmental change in ITNA-parietal coupling should be specific to the ITNAs, and not characteristic of the letter area. We predicted the following:

- 1) Both ITNAs would be functionally connected to a number-sensitive parietal regions in the earliest timepoint, but this connectivity would be greater in the right hemisphere due to an early-developing hemispheric asymmetry.
- 2) Spontaneous coupling of the ITNAs with number-sensitive parietal areas would increase over schooling, possibly reflecting repeated co-activation through math instruction.
- 3) Digit-specific, task-evoked coupling in this circuit should also increase over schooling as these areas are mutually tuned towards their preferred stimulus domain.

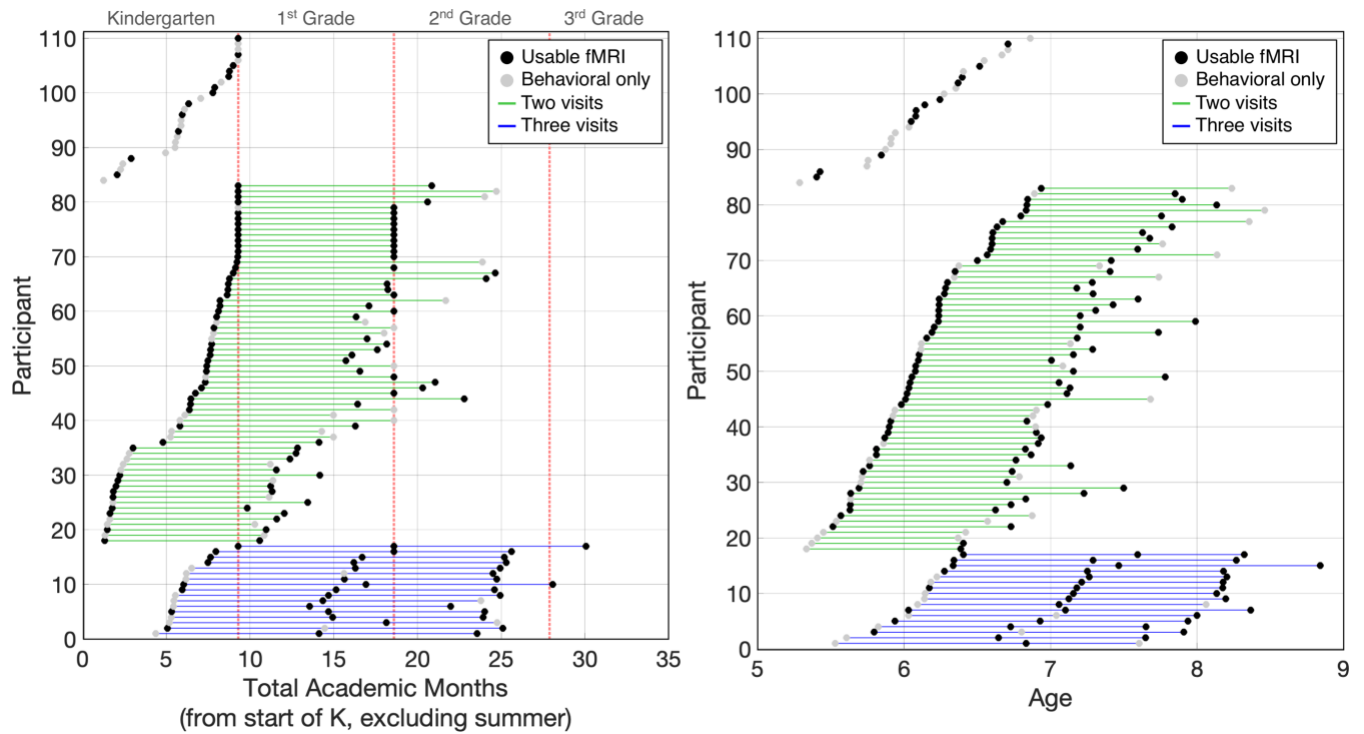
### **3.3 Methods**

#### **3.3.1 Participants**

The children included in the present analysis were participants in a longitudinal study of symbolic number processing in neuro-typical children from K-2<sup>nd</sup> grade, which began data collection in January of 2018. The study involved a behavioral and an imaging visit (median = 2.3 weeks apart) each year for three years. Families were recruited via several mechanisms including through announcements on relevant email list-serves and Vanderbilt research participant databases, Facebook advertisements, flyers at local schools, and word-of-mouth. Participants had to be enrolled in a school that follows Tennessee's academic curriculum and in kindergarten or the summer between kindergarten and 1<sup>st</sup> grade. Exclusion criteria included homeschooling, pre-term birth, diagnosis of any psychiatric or neurological disorder (including ADHD and/or other learning disability), history of neurological injury, or any MRI contraindication. All participants and their parents gave written consent and the study was approved by the Vanderbilt University Institutional Review Board.

A total of 110 children completed baseline behavioral testing ( $M \pm SD = 6.1 \pm 0.4$  years old, 47 female, 92 right-handed). The racial composition of this initial cohort was 74.5% White, 10.9% multiracial, 9.1% Black, 1.8% Hispanic, and the remaining 3.6% unreported. Self-reported family income was distributed as follows: \$0–\$24,999 (0%), \$25,000–\$49,999 (6.4%), \$50,000–\$74,999 (14.6%), \$75,000–\$99,999 (14.6%), \$100,000–\$124,999 (11.8%), and \$125,000–\$149,999 (10.0%), \$150,000+ (33.6%), and the remaining 11.8% unreported. The mean IQ across the group was  $109.0 \pm 14.4$ , as measured by the KBIT-2 (Kaufman Brief Intelligence Test 2).

As of the current date, the study is in its final phase of data collection and only a portion of the final visits have been completed. The study was significantly disrupted by the COVID-19 pandemic that halted research activities for most of 2020 (see Limitations section 3.6.1 for further discussion).



**Figure 10.** Longitudinal sample and usable data.

Sample plotted based on academic months (left) and age (right). Black dots refer to a visit with usable fMRI data. Gray dots refer to visit where behavioral data was collected, but fMRI was either not collected or was unusable (e.g., due to motion or below chance accuracy). Blue lines indicate individuals with three visits. Green lines indicate individuals with two visits. Red dotted lines indicate the transition between grade levels, where a full academic year = 9.29 months.

### 3.3.2 fMRI Tasks

#### *Symbolic Classification Task (“SYM”)*

Participants viewed a series of centrally located stimuli involving either a single digit, letter, or unfamiliar symbol. Using either their left and right thumbs, participants indicated via button press whether they “knew the name” of the stimulus (i.e. is a digit or letter; press left) or not (i.e. an unfamiliar symbol; press right). Digits from 2 - 8 were used as well as the capitalized letters A, E, H, N, R, S, T, which are highly common in the English alphabet and excluded those that look visually similar to a digit (e.g. O or I) (Jones & Mewhort, 2004). The unfamiliar symbols were adapted from a previous study of symbol processing in adults (G. R. Price & Ansari, 2011)

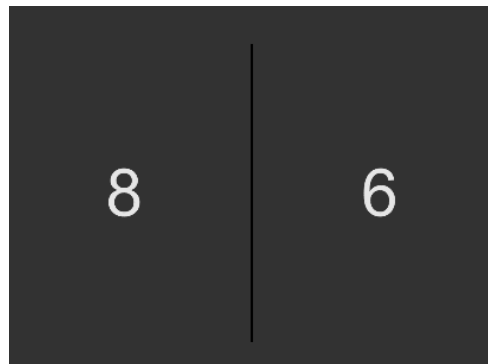
and, were originally created by segmenting and rearranging the intact letters and digits into unified but entirely novel shapes. Thus, each letter and each digit had an unrecognizable scrambled counterpart with equivalent number of pixels and approximately similar numbers of angles and curves. Each digit and letter appeared twice per run and each scrambled symbol appeared once per run (i.e., 14 digit, 14 letter, and 14 scrambled trials per run). Stimuli remained on the screen for 2000ms and inter-trial intervals (ITIs) range from 2000-5100ms with an average of 3000ms. Stimulus and ITI randomization was performed using the NeuroDesign toolbox which uses a genetic algorithm to optimize the presentation sequence for increased detection power and BOLD response estimation efficiency (Durnez, Blair, & Poldrack, 2017). Three runs are administered in succession, including a total of 126 trials (42 digit, 42 letter, and 42 scrambled) over approximately 11.5 minutes of scan time. The SYM task was acquired first in every MRI session, in part to minimize explicit processing of magnitude that may be induced by the number comparison tasks. This paradigm was modelled after an ECoG study in adults by Shum et al., which demonstrated preferential processing of numerals in the ITG (Shum et al., 2013). For all tasks, stimulus presentation and response recording was performed using E-Prime 3.0. Upon completion of the SYM task, a T1-weighted anatomical image was acquired.



**Figure 11.** All stimuli used in the symbol classification task

### *Symbolic Comparison Task (“NUM”)*

Following the T1-weighted acquisition symbolic and nonsymbolic comparison tasks were performed. The order of these tasks were reversed in approximately half of the sample, then reversed at each timepoint within an individual, to minimize task-order effects. In the symbolic comparison task (“NUM”), participants viewed two Arabic numerals on either side of the screen, separated by a vertical bar. With responses boxes in each hand, participants indicated with either the right or left thumb button the stimulus that was greater in magnitude for each trial. The range of stimuli was 1-9 and involved small (0.167-0.375) and large (0.667-0.778) ratio conditions. Numeral pairs remained on the screen for 2000ms and ITIs ranged from 2300-8500ms with a mean of 4000ms. Stimulus randomization and ITI optimization were again performed using the NeuroDesign toolbox. Two runs were administered in succession, involving a total of 64 trials over approximately 7 minutes of scan time.



**Figure 12.** Example of symbolic digit comparison stimuli

### **3.3.3 MRI Acquisition parameters**

All images were acquired using a Philips Achieva dStream 3T scanner (Philips Medical Systems, Best, The Netherlands) and 32-channel head coil. T2\*-weighted, single shot echo-

planar imaging (EPI) was used for functional scans, with the following parameters: TR/TE = 1110/28 ms, FA = 62°, FOV = 240 x 240 x 129.75 mm, voxel size = 2.5 x 2.5 x 3 mm (with 0.25 mm gap), SENSE = 2, multi-band factor = 2. For the symbol classification task, each run lasted approximately 3m51s in which 198 volumes were acquired, with an additional 8 dummy volumes acquired at the beginning of the sequence to allow for steady-state magnetization to be reached. In cases where significant motion and/or below chance accuracy was observed for a given run, a re-run was attempted when possible. During approximately the mid-point of every scan session, a small set of reverse phase-encoded EPI volumes were acquired with the same parameters as the primary fMRI sequence (i.e., with the fat shift direction set to A instead of P), to be used for EPI distortion correction.

A T1-weighted turbo field echo anatomical scan was acquired immediately following the final run of the symbolic classification task with the following parameters: TR/TE = 8.3/3.9 ms, inversion time = 1060 ms, shot interval time = 2400 ms, FA = 8°, FOV = 256 x 240 x 184 mm, SENSE = 2 AP / 1.5 RL, acquisition time = 4m 19s. This scan was segmented with FreeSurfer and used for anatomical reference. Diffusion-weighted imaging (DWI) was acquired during the final 15 minutes of each session and was not analyzed here.

### **3.3.4 Motion reduction strategy**

Given the pediatric population of interest, the reduction of motion-related artifacts and MR signal degradation was of paramount concern for us (Satterthwaite et al., 2012). Recent work suggests that shorter fMRI run lengths with fast-paced stimuli are associated with less head movement in both children and adults (Engelhardt et al., 2017; Meissner, Walbrin, Nordt, Koldewyn, & Weigelt, 2020), motivating in part our use of fast event-related designs broken into short runs (i.e., 3m51s x 3 runs for symbol classification and 3m33s x 4 runs for

symbolic/nonsymbolic comparison). To prepare children for the scan experience, our lab developed a mock-scanner training protocol in which children became progressively more familiar with the scanning environment, including multiple visits to the mock-scanner suite over the behavioral visit. Participants completed at least one full fMRI training run during this visit, involving the same style of button boxes, a similar head coil, and MRI scanner sounds played over speakers. This training additionally allowed us to ensure each participant was capable of remaining still while performing the tasks and also to screen for children who may be scared of the scanning environment.

On the day of the MRI, participants completed a short training session within the mock scanner suite, including example trials from each task and a final review of the scan instructions. Once a participant was situated on the real MRI table, Micropore paper tape was placed gently across the forehead and attached to each side of the head coil. The tape provided tactile feedback to the participant in cases of head motion, without compromising comfort, and served as a minimally invasive strategy for motion reduction. We have found tape to be effective in prior studies in our lab and this method was recently shown to quantitatively improve fMRI measures (Krause et al., 2019). A “scanner buddy”, typically a research assistant from the lab, accompanied each child in the scanner room and sat at the end of the scanner bore. The buddy provided a sense of security for the child but also closely monitored for motion throughout the scan. In cases where motion was detected, the buddy tapped the child’s foot twice as a reminder to hold still. Following each run, the experimenter reviewed the fMRI series to qualitatively assess the degree the motion and decide whether a re-run was necessary.

To improve anatomical image and DWI quality, participants watched clips of an animated movie (Disney’s WALL-E), following previous demonstrations that movie viewing is an



effective motion reduction strategy in children (Cantlon & Li, 2013; Greene et al., 2018). We also developed our own animation slides themed around the story of WALL-E. After each run, WALL-E collected a trash block and added it to his trash tower. At each step, he made his way further down a path, ultimately arriving at his friend Eve upon completion of the scan. In an effort to improve participant compliance, these animations provided a visual indication of progress over the session and a fun, motivating aspect to the fMRI tasks. Additionally, a scan slot of 1.5 hours was reserved which afforded a short break during which participants could stand up to stretch or use the restroom. Incorporating such a break into fMRI sessions has recently been shown to relate to reduced head motion in children (Meissner et al., 2020). Similarly, we found the break to be beneficial on many occasions and allowed for a lower-stress experience for our participants. Despite these extensive efforts, participants inevitably moved during MRI. Thus, further analytical strategies were employed during data processing to mitigate the effect of motion on our data and are described in subsequent sections.

### **3.3.5 Anatomical processing**

Similarly to the adult study, T1-weighted anatomical images were processed using FreeSurfer (v6.0.1, <http://surfer.nmr.mgh.harvard.edu>), via the Vanderbilt University XNAT platform (Harrigan et al., 2016), involving the default “recon-all” with the “-3T” flag. The segmentations were carefully inspected and manually edited when necessary using FreeView. FreeSurfer outputs were further processed for use in AFNI/SUMA using AFNI’s @SUMA\_Make\_Spec\_FS program (Cox, 1996; Saad & Reynolds, 2012). As part of this process, standard surface meshes were generated and the low density “ld60” meshes (36,002 nodes per hemisphere) were used for subsequent fMRI analyses.

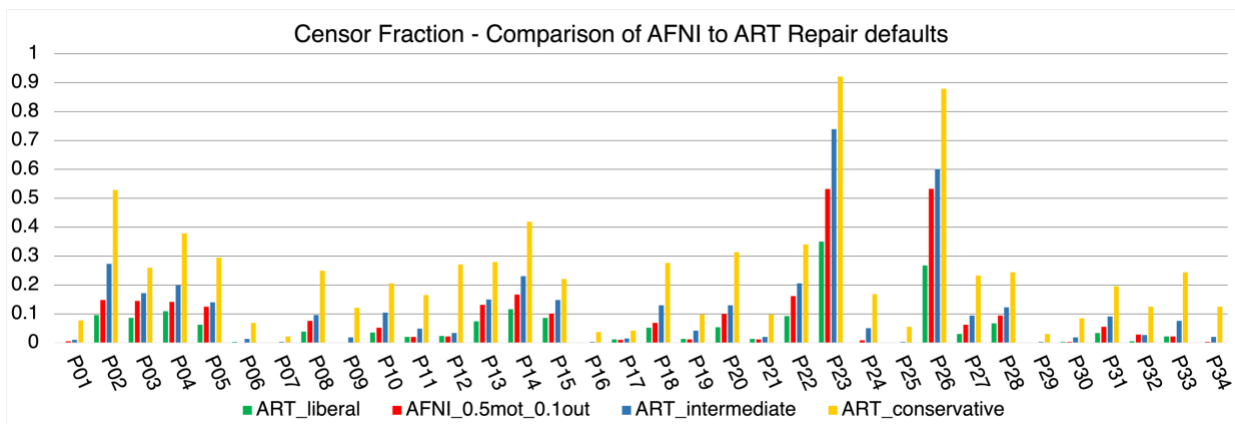
### 3.3.6 fMRI preprocessing

The raw imaging files were first converted from DICOM to NIfTI format using *dcm2nii* (X. Li et al., 2016). The fMRI data was then preprocessed in MATLAB using AFNI and SUMA tools (Cox, 1996; Saad & Reynolds, 2012; Saad et al., 2005). Trial onset timestamps were extracted from the E-Prime tab-delimited output files for each condition, exemplar, and/or trial and timing files were created for use in AFNI. Onset times for errors (of commission) and omissions were specified separately within the output files. The *afni\_proc.py* program was used to build a preprocessing pipeline that included the following steps: despiking, slice-time correction, dewarping of fMRI volumes via reverse phase-encoded volumes, EPI-anatomical alignment, motion correction, sampling of EPI data to subjects' standardized cortical surface, smoothing on the surface with a 6mm FWHM filter, and scaling to percent signal change.

### 3.3.7 Motion Censoring and Nuisance Regressors

Prior to fitting first-level models to the preprocessed data, we performed volume censoring (or “scrubbing”) based on estimates of volume-to-volume motion and outlier signal values. Specifically, this involved the flagging of timepoints in which the Euclidean norm of the motion derivative exceeded 0.5mm as well as timepoints in which 10% of voxels were flagged as outliers. Note that the particular thresholds used in the child analysis were relaxed compared our adult study. This decision represented a compromise between adequately controlling for motion and retaining more data in the child sample. As there is no agreed-upon “correct” setting for these thresholds, we quantitatively compared them with those of another popular processing package, the CONN Toolbox (Whitfield-Gabrieli & Nieto-Castanon, 2012), which implements an analogous motion scrubbing procedure called ART Repair. Importantly, though both AFNI and ART refer to their thresholds in terms of millimeters, the calculation of volume-to-volume

motion is different between the packages. We ran a subset of the data through these programs and found that, in terms of the final fraction of volumes censored, the AFNI thresholds chosen here fell between CONN’s “intermediate” (the default) and “liberal” setting (Figure 13), providing a point of comparison for future studies. For all subsequent analyses, a participant’s data for a given task was determined to be *unusable* when greater than 25% of the volumes across all runs were flagged for censoring.



**Figure 13.** Benchmarking censor fraction thresholds across software.

The motion thresholds used in the present study are depicted in red. In test data from a preliminary group of participants, these settings resulted in a total censor fraction that fell within the “intermediate” and “liberal” default settings of the ART Repair module included in the CONN toolbox (Whitfield-Gabrieli & Nieto-Castanon, 2012).

Nuisance regressors, or “signals of no interest”, were defined within a task including 6 motion parameters, 6 motion derivatives, and 0-2<sup>nd</sup> order Legendre polynomials to model low-frequency drifts (all defined for each run separately). We defined 6 additional nuisance regressors which spanned across runs involving the first 3 principal components of signals in the white matter and in the lateral ventricles, as defined by a subject’s FreeSurfer segmentation, in approach analogous to the “aCompCor” method (Behzadi, Restom, Liau, & Liu, 2007). These tissue-based regressors helped to mitigate the impact of non-neural physiological fluctuations

and unmodeled motion effects in BOLD signal, which can contaminate task-related responses in the gray matter and artificially inflate connectivity values (Caballero-Gaudes & Reynolds, 2017; Muschelli et al., 2014; Satterthwaite et al., 2012). The full set of nuisance regressors was included in each of first-level models described below. These denoising and censoring procedures are in line with recommendations put forward by recent studies that assessed many different pipelines for handling motion artifacts in fMRI data (Ciric et al., 2017).

### 3.3.8 General Linear Models

General linear model (GLMs) were fit which captured the mean BOLD response to each condition. In the SYM task, this involved the Digit, Letter, and Scrambled conditions. *Condition-level* regressors were defined by convolving the trial onset times with a gamma function modelling the hemodynamic response (HRF), using AFNI's default basis function, "GAM(8.6,0.547,2)", specifying an event duration of 2 seconds. Errors of commission and omission were modelled as two separate conditions. Prior to fitting the GLMs, volumes (i.e., observations) flagged for censoring were removed from the design matrix. Models were fit using AFNI's *3dREMLfit* program and outputs included coefficients and t-statistics for condition versus baseline responses as well as for contrasts between conditions (e.g., Digit > Letter, Digit > Letter + Scrambled, etc.). The coefficients represented the mean percent signal change (PSC) in response to a condition or, the relative difference in PSC between conditions. The GLMs were run on both unsmoothed and smoothed. For analyses in which the mean response was extracted from an ITNA ROI, unsmoothed data was used to avoid the mixing of signal from voxels outside the ROI, as category-selective ventral stream areas are often located in close proximity.

Using the same process as above, GLMs were fit to capture the mean BOLD response to each of the 28 unique symbols ("exemplars") presented in the SYM task. In this case, *exemplar-*

*level* regressors were created which modelled the HRF for all 6 instances of a symbol across runs. Depending on trial accuracy and censoring, the number of usable trials for a given exemplar varied from subject to subject (any sig diff among exemplars?). The exemplar-level response maps were derived from unsmoothed data and used in for representational similarity analyses.

Finally, *trial-level* GLMs were fit to model the response to each trial separately. We used the computationally efficient “least-squares-separate” estimation method via AFNI’s *3dLSS* function (Mumford et al., 2012). This method fits a separate GLM for each trial, including a regressor for the single trial response, a regressor of no-interest derived from the sum of all other trial responses, and the other nuisance regressors. These models generated a series of response maps which we refer to as a “beta-series.” The beta-series data was used for beta-series correlation (BSC) analyses and for classification-based multi-voxel pattern analyses (MVPA). Compared to a traditional approach where all trial regressors are included in a single GLM, the LSS approach not only preserves degrees of freedom, but has been shown to improve trial-specific activation estimates which benefit MVPA analysis (and presumably BSC as well) (Mumford et al., 2012).

### **3.3.9 Category-level Representational Similarity Analysis**

To perform RSA, for each participant and ITNA, activation patterns were characterized by the spatial distribution of *t*-values determined from the exemplar-level GLMs. As opposed to the univariate activation analysis where change in the mean response level (PSC) was of interest, *t*-values were used in this case because they take into account the noise level in each node and have been shown to be advantageous for multivariate analysis (Misaki, Kim, Bandettini, & Kriegeskorte, 2010). There were a total of 57 surface nodes in the left ITNA and 60 in right ITNA. Subsequent analyses were carried out using in-house MATLAB scripts. Activation

patterns were first scaled by subtracting from each node its mean activation level across all considered exemplars. This normalization step removes the common response pattern shared across exemplars, which can artificially increase the correlations among exemplars and obscure the underlying representational distance (Diedrichsen & Kriegeskorte, 2017; Walther et al., 2016). From the 60 (or 57) node x 28 exemplar activation patterns, a 28 x 28 representational dissimilarity matrix (RDM) was computed using a correlational distance of  $1 - \text{Pearson's } r$ .

Each neural RDM was then compared to hypothetical model RDMs that captured several the representational geometries of interest. We first considered a Digit versus Other model (DvO), which tests the hypothesis that Digits are represented in a manner similar to each other and different to that of letters and scrambled symbols. In the DvO model letters and scrambled symbols are indistinguishable categories, making it the strongest case for a “digit-biased” representational geometry (D. J. Yeo et al., 2020). Model RDMs were constructed to be the same dimensions as the neural RDM (e.g., 28 x 28) but with values of 1 or 0, indicating dissimilar or perfectly similar activation patterns, respectively. As a control analysis, we considered a Letter versus Other model (LvO), which is constructed the same as DvO but with Letters as the preferred category. Though the DvO model suggests a digit-biased geometry, it may be driven by a particular distinction between Digits and Scrambled symbols. We thus also considered a Digit versus Letter model (DvL). On its own, evidence for DvL would indicate that the two (familiar) categories are distinguishable but would not imply a digit-bias. In tandem with evidence for DvO, however, this would suggest a specificity for digits beyond simply their familiarity. To compare the neural and model RDMs, a Spearman correlation was computed on the upper triangular portion of each matrix and transformed to a Fisher  $Z$  value for use in statistical models.

### 3.3.10 Exemplar Discriminability – SVM Classification

In addition to category-level representations in the ITNAs, we were also interested in exemplar discriminability *within* a category, i.e., the extent to which individual digits can be distinguished from one another. While the previous analysis asked whether Digit patterns are more similar to each other than to Letters and Scrambled symbols, exemplar discriminability *within* a category could simultaneously exist along one or more orthogonal dimensions. The RSA framework was appropriate for assessing category-level representational geometry, where comparisons to categorical model RDMs could be drawn. For the present analysis, however, we were not interested in a particular geometry *per se*, but instead on whether a presented digit could be *decoded* from the spatial pattern of responses in the ITNA. That is, do responses in the ITNA carry information about the *identity* of the presented digit? This question naturally lent itself to classification-based MVPA (Mur, Bandettini, & Kriegeskorte, 2009; Norman et al., 2006). To implement this approach, from each participant and ITNA, we extracted the unsmoothed trial-level response estimates (*t*-values) from the LSS GLMs. We used the CoSMoMVPA toolbox to perform a leave-one-out cross validation procedure where a single trial was held out and a model (linear support vector machine) was trained to predict digit identity from the remaining trials (Oosterhof et al., 2016). The identity of the left-out trial was predicted from the model and the accuracy recorded, with chance accuracy in the case of 7 exemplars = 14.29%. Overall accuracy was computed for each exemplar separately, then the mean of these averages was used as the final index of exemplar discriminability. Incorrect trials (i.e., error or omitted response) were excluded from modeling, leading to unbalanced numbers of trials across exemplars. To circumvent potential algorithmic biases, we randomly excluded trials such that every training partition contained a balanced set of response patterns. In cases where an

exemplar had fewer than 3 usable trials, the exemplar was excluded and decoding was performed on the remaining set. To standardize classifier performance across participants and timepoints, we z-scored the accuracies by comparing to a null distribution. Specifically, for each dataset, the classifier target labels were randomly shuffled and decoding was performed for 1000 iterations. A z-score was then computed as  $[\text{AccTrue} - \text{mean}(\text{AccNull})] / \text{std}(\text{AccNull})$ .

### **3.3.11 Task-Evoked and Background Functional Connectivity**

To assess task-evoked functional connectivity (FC), we used the BSC method (Rissman et al., 2004). This method extracts trial-level response values and then correlates over trials of the same condition, across voxels, vertices, or regions of interests (Florence Bouhali, Bézagu, Dehaene, & Cohen, 2019; Conrad et al., 2020; Fornito, Yoon, Zalesky, Bullmore, & Carter, 2011; Geib, Stanley, Dennis, Woldorff, & Cabeza, 2017; Göttlich, Beyer, & Krämer, 2015; Monge et al., 2017; Ray et al., 2017; Schedlbauer, Copara, Watrous, & Ekstrom, 2014). We used Pearson correlation and converted the values to Fisher  $Z$  estimates prior to further statistical testing (Fisher, 1915). The BSC  $Z$  value represented the degree to which two areas respond in unison to a particular task condition (i.e., their task-evoked coupling or connectivity). Note that the first order BSC, involving coupling during a condition (versus baseline), indexed task-related connectivity involving information exchange between areas *but also* “simple” co-activations in which two regions are engaged in parallel but do not interact. Critically, the BSCs were compared between conditions to assess differential degrees of coupling when processing one type of stimuli versus another (e.g., Digit > Letter). With a proper control condition, a BSC contrast should “subtract out” shared co-activation patterns resulting from, for example, low-level visual processing, response selection, and motor output, and reveal stimulus-specific coupling. In principle, a BSC contrast should detect similar task-modulated connectivity as that



detected in the more common generalized psychophysiological interaction (gPPI) analysis, and this was recently demonstrated in empirical data (Di et al., 2020). Importantly, however, BSC has been shown to be more powerful than gPPI for assessing task-modulated connectivity in event-related paradigms, is more robust to variability in the hemodynamic response across subjects (Cisler et al., 2014), and is thought to be resistant to the artificial inflation of FC estimates due to task-related activity (Cole et al., 2019). These observations, along with the relative simplicity of the BSC framework, motivate our use in the present work.

Given the high levels of motion in the present sample, we opted to forego the explicit censoring of volumes within the LSS GLMs. This allowed for a consistent number of volumes to contribute to every trial-level response estimate. We did, however, implement a “beta-scrubbing” procedure where we excluded from BSCs those betas in which more than 1/3 of the volumes over the span of the associated (~14s) HRF were flagged for censoring, with the assumption that these trials were contaminated by motion artifacts (Conrad et al., 2020; Ray et al., 2017). This served as a principled strategy to eliminate outlier beta estimates resulting from an insufficient number of observations (volumes).

To assess “background” FC, the residuals of the condition-level GLMs were catenated across *all* tasks and used as the timeseries of interest. These signals contain the unexplained variance in the BOLD signal after accounting for task and nuisance effects, and thus in principle should reflect spontaneous brain activity occurring in the “background”. Again, Pearson correlation was used to derive region-to-region FC estimates. We intended this measure to serve as a proxy for “intrinsic” FC, as may be measured in a resting state, and such an approach has been used in previous work (Fair et al., 2007; Wendelken et al., 2017). We do acknowledge prior evidence that task states can alter spontaneous fluctuations (Norman-Haignere, McCarthy, Chun, & Turk-

Browne, 2012), and that, from a statistical perspective, the presence of task-induced activations may inflate FC and/or contaminate FC estimates through unmodeled nonlinear effects (Cole et al., 2019; Fair et al., 2007). However, the timeseries analyzed here spanned across all tasks, stimulus events, interstimulus intervals, and pre/post task baseline periods and so are unlikely to be related to any specific task state or stimulus type. The background FC metric is thus the closest we can get to intrinsic FC in the absence of a true resting-state acquisition. Importantly, it is distinct from the BSCs, which explicitly model task-evoked coupling and are used to contrast FC between conditions.

### **3.3.12 Definition of Occipitotemporal ROIs**

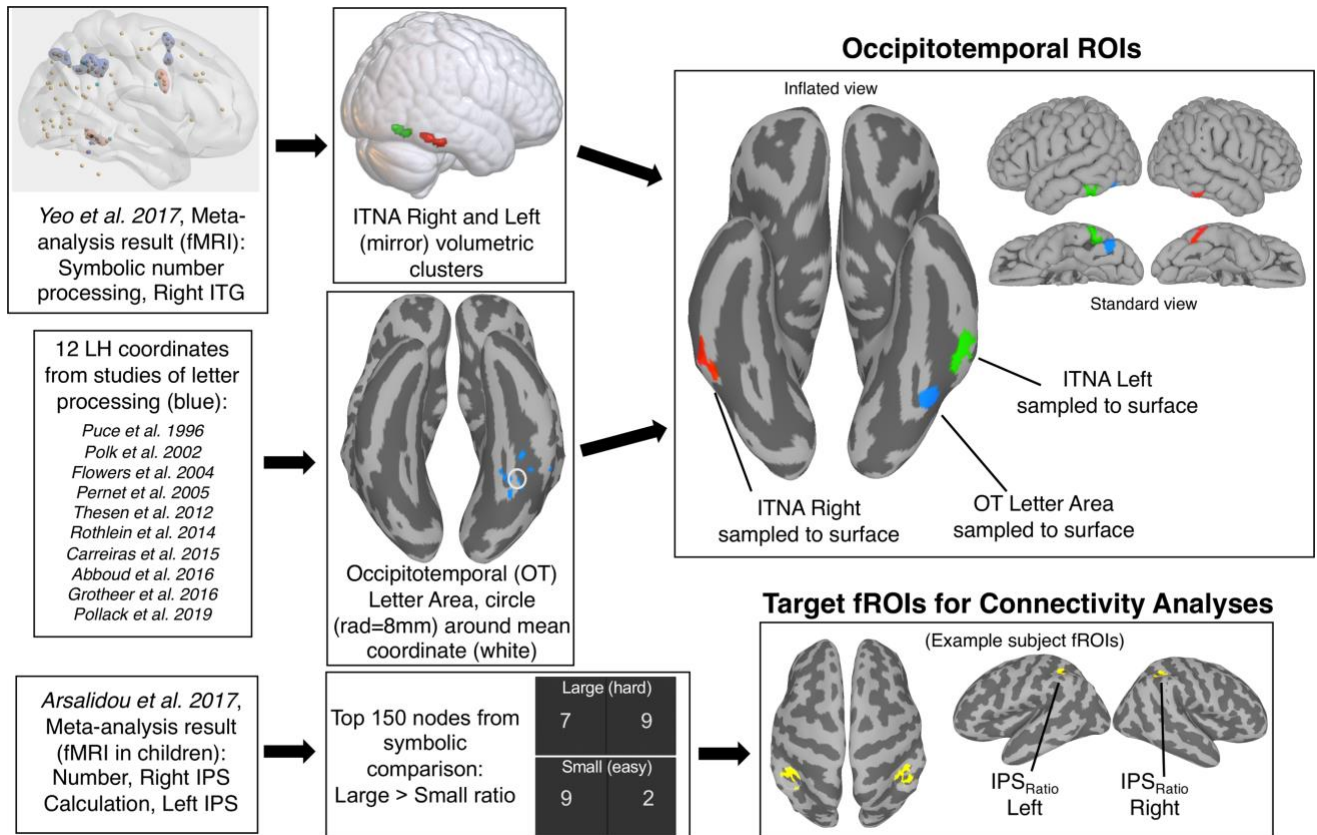
The ITNA seed ROIs were derived from an ITG cluster that showed selectivity to digits compared to other symbols in a recent meta-analysis (D. J. Yeo et al., 2017). The right hemisphere volumetric cluster in MNI was first binarized and then was sampled onto the standardized MNI cortical surface using AFNI's *3dVol2Surf* program. While subject-specific functionally defined ROIs (fROIs) have been shown to increase sensitivity in group-level analyses and are commonly used in studies of the OTC (Glezer & Riesenhuber, 2013; Nieto-Castañón & Fedorenko, 2012; Stigliani, Weiner, & Grill-Spector, 2015), our use of an *a priori* group-level ROI was motivated by several factors. Firstly, we would not expect the ITNA to be *selective* for digits, compared to other symbols, in 5-6 year old children. Previous work, for instance, has shown that word-selectivity in ventral cortex does not emerge until later in schooling (Dehaene-Lambertz et al., 2018; Saygin et al., 2016), and that this development extends through adolescence (Ben-Shachar et al., 2011; Tracy M. Centanni et al., 2017). From a practical perspective, even if digit-selectivity could be detected in the last timepoint of our sample (7-9yo), defining an fROI would require independent task data to avoid biasing our

longitudinal analyses towards detecting a change (i.e., circularity). Also, most subjects contributed only two timepoints, so defining a retrospective fROI and discarding the final timepoint, as in a recent study (Dehaene-Lambertz et al., 2018), was not an option for the present analyses.

While selectivity is likely not present, some *sensitivity* to digits compared to other (non-symbol) stimuli may have emerged in the OTC by school entry due to environmental exposure and/or preschool instruction involving numerals. For instance, greater responses to digits and letters compared to faces have been observed in lateral OTC areas in 4-6 year old children (Cantlon et al., 2011; T. M. Centanni et al., 2019; Tracy M. Centanni et al., 2018), suggesting that an “ITNA” may be definable in kindergarteners based on a criterion of *sensitivity*. Note that this approach would require a more diverse stimulus set than used here, where only digits, letters, or scrambled symbols were presented. Critically though, whether the neural populations initially *sensitive* to an object category are the same as those that later become *selective* for the category is an open area of investigation, and is outside the scope of the present work. Thus, we instead chose to focus our analysis on the mature (and remarkably consistent) location of the ITNA as observed in adults.

While our focus here was on developmental trajectories of ITNA function, representational content, and connectivity, we sought to compare these trajectories with a nearby region involved in letter processing. Our adult work showed distinct anatomical and functional connectivity profiles of proximal digit and letter areas. If connectivity drives categorical specialization in the OTC, we would expect “digit-biased” developmental trajectories in the ITNAs, whether or not a broader area of OTC is responsive to alphanumeric symbols (i.e., the shape hypothesis). Thus, the letter area would serve as a conservative control region that could be initially sensitive to but

ultimately not specialized for digit processing. To define this area, we conducted a (non-exhaustive) search for fMRI studies of letter processing that reported a coordinate in the fusiform gyrus, occipitotemporal sulcus, or inferior temporal gyrus. We identified twelve coordinates in the literature from ten studies that met our criteria (Abboud et al., 2015; Carreiras, Quiñones, Hernández-Cabrera, & Duñabeitia, 2015; Flowers et al., 2004; Grotheer et al., 2016; Pernet, Celsis, & Démonet, 2005; Polk et al., 2002; Pollack & Price, 2019; Puce, Allison, Asgari, Gore, & McCarthy, 1996; Rothlein & Rapp, 2014; Thesen et al., 2012). When necessary, coordinates were converted from Talairach to MNI space using the *tal2icbm\_other* Lancaster transform (Lancaster et al., 2007; <https://brainmap.org/icbm2tal/>). Consistent with findings of a strongly left-lateralized VWFA, of the included studies, there were no reports of letter-sensitivity in the right hemisphere within the aforementioned anatomical boundaries. We used the mean of the twelve reported coordinates (-42.7,-60.2,-13.2) to define an occipitotemporal letter area (OTLA). Interestingly, though none of the included coordinates pertained to word processing, our OTLA mapped to a location consistent with the classical VWFA (L. Chen et al., 2019; L. Cohen et al., 2002; Dehaene et al., 2010; Grotheer et al., 2016; A. C. Vogel et al., 2012), on the border of the posterior fusiform gyrus and occipitotemporal sulcus. A circle was dilated on the MNI surface to a radius of 8mm around this coordinate, resulting in an ROI that approximately matched the surface areas of the left and right ITNA ROIs.



**Figure 14.** Outline of ROI definition for developmental analyses

### 3.3.13 Definition of Target fROIs for Connectivity Analyses

In terms of ITNA functional connectivity, we predicted an increase in coupling with regions involved in magnitude processing over children’s time in school, which would indicate increased interactions across this domain-specific circuit over experience. While many regions have been implicated in numerical tasks, the intraparietal sulcus (IPS) is thought to house neural populations involved in processing and/or representing abstract numerical magnitude information (Dehaene et al., 2003; Nieder, 2016; Piazza, Pinel, Le Bihan, & Dehaene, 2007), and thus served as the primary target region of interest. However, the IPS is a large area of cortex involved in multitude of operations including visual attention and working memory (Corbetta & Shulman, 2002; Goltz et al., 2015; Molenberghs, Mesulam, Peeters, & Vandenberghe, 2007;

Owen, McMillan, Laird, & Bullmore, 2005; Vossel, Geng, & Fink, 2014). Thus, we first defined an anatomical constraint mask based on a recent meta-analysis of number processing in children (Arsalidou, Pawliw-Levac, Sadeghi, & Pascual-Leone, 2017). We chose coordinates in the right (38, -46, 42) and left (-42, -48, 42) inferior parietal lobes/sulci that showed convergence across fMRI studies for number and calculation tasks in children, respectively. Importantly, these areas were proposed to be involved in numerical quantity representation and are similarly involved in adults (Arsalidou & Taylor, 2011). A circular ROI with a radius of 14mm was generated on the MNI cortical surfaces around each coordinate, serving as group-level constraint masks. To further increase our sensitivity to areas involved in magnitude processing within individuals, we defined subject-specific fROIs within the anatomical masks, as detailed below.

In addition to the symbol classification task, children completed symbolic and nonsymbolic comparison tasks in the scanner in which two simultaneously presented quantities (digits or dots) were compared for each trial. A critical manipulation in these tasks involved varying the ratio of the two numbers being compared. In this case, trials were binned into small (easier; e.g., 3 vs. 9) and large (harder; e.g., 5 vs. 7) ratio conditions. Dominant theory suggests that larger ratios engage more overlapping quantity representations and thus lead to increased reaction times and decreased accuracy (Dehaene, 2007; Verguts & Fias, 2004). A “neural” ratio effect, i.e., greater activity during large vs. small ratio trials, is thought to index the locality of these representations and is typically found in the IPS, including in children (Bugden, Price, McLean, & Ansari, 2012; Gullick, Sprute, & Temple, 2011; Lussier & Cantlon, 2017; G. R. Price, Holloway, Räsänen, Vesterinen, & Ansari, 2007; S. E. Vogel et al., 2015; Wilkey, Barone, Mazzocco, Vogel, & Price, 2017). Though it is an area of contention (Wilkey & Ansari, 2020), evidence suggests that both symbolic and nonsymbolic formats tap into shared magnitude representations in the IPS

(Eger, Sterzer, Russ, Giraud, & Kleinschmidt, 2003; Wilkey et al., 2020). It has been postulated that symbolic and nonsymbolic magnitude representations are most “integrated” in children who are just learning symbolic notation (Lyons, Ansari, & Beilock, 2012; Matejko & Ansari, 2016; Piazza, 2011). To our knowledge, however, there exist no empirical evidence to support this “integration” hypothesis. Thus, to ensure that the final fROIs showed sensitivity to symbolic magnitude information, we restricted our neural ratio effect to only the symbolic comparison task. For each subject, the symbolic Large > Small ratio contrasts was computed using smoothed data. The top 150 nodes based on the contrast t-statistics within each of the left and right IPS were selected as the final fROIs. 150 nodes were chosen as this matched approximately the surface area of the occipitotemporal ROIs (on average across participants) and further ensured the fROI size was consistent across participants. In cases where the symbolic comparison task data was unusable, the dataset was excluded from connectivity analyses. fROIs were defined separately for each timepoint, allowing the location of maximal ratio-sensitivity to vary within an individual over time.

### **3.3.14 Linear Mixed-Effects Models**

To test for associations of each of our dependent measures of ITNA function with children’s time in school, we employed linear mixed-effect models (LMMs) with participants specified as random effects. We computed participant’s time in school as the total number of days between the beginning of kindergarten and the day of the MRI scan, excluding summer breaks. A standard summer break from May 20<sup>th</sup> to August 10<sup>th</sup> was used for this calculation. The total time in school was converted to academic months and served as a continuous independent variable in the LMMs. The fixed effect of academic months was the primary coefficient of interest.

Participants were modeled as random effects, including terms for random intercepts and slopes.

The inclusion of random slopes in the present models was theoretically motivated by the fact that, in addition to individual differences in entry levels (random intercepts), we expected children to undergo differential trajectories in the development of their ITNAs. Models were fit using MATLAB's *fitlme* function. It is important to note that given the number of timepoints (1-3, but 2 in most cases), the random slope estimates (i.e., participant-level trajectories) from these models are likely to be unreliable on their own (King et al., 2018; Wright, 2017). Instead, the goal here was to characterize the *fixed effect* of academic months, which represented the *average* change in the dependent variable over academic months. Estimating this group-level effect using LMMs allows for unequal intervals between scans and the inclusion of incomplete data (e.g., participants with only one timepoint). Furthermore, the use of mixed-effects models for studying brain development is now well established, and represents the gold standard in the literature (Haller, Mills, Hartwright, David, & Cohen Kadosh, 2018; Mills et al., 2016; Vijayakumar, Mills, Alexander-Bloch, Tamnes, & Whittle, 2018; Wendelken et al., 2017; Wierenga, Langen, Oranje, & Durston, 2014).

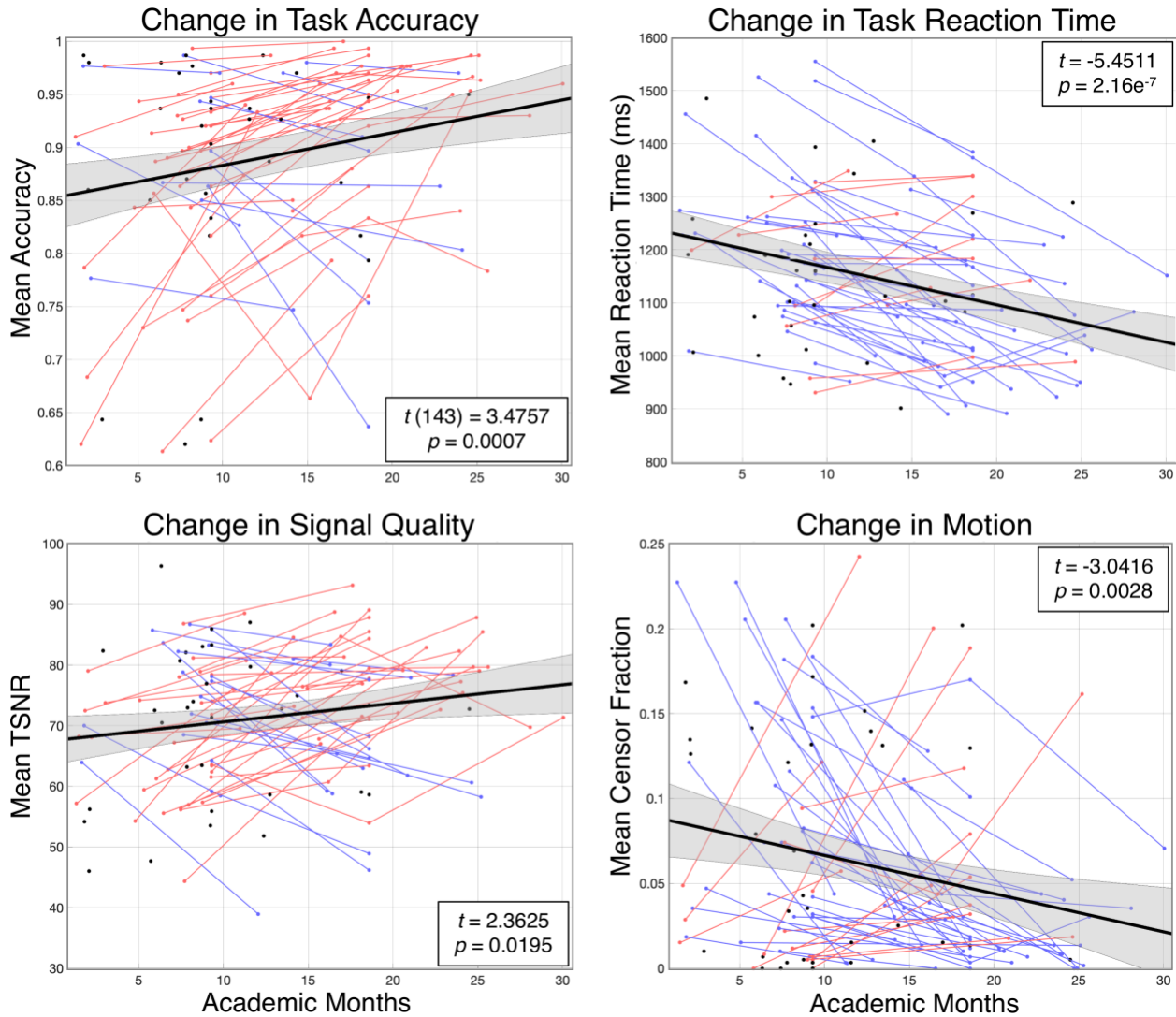
### 3.4 Results

#### 3.4.1 Longitudinal changes in behavioral performance

We first assessed whether performance on the symbol classification task was related to our continuous measure of months in school (academic months), using linear mixed-effects models with academic months modelled as a fixed and random effect. These analyses involved only those subjects with usable imaging data (i.e., significantly greater than chance accuracy across all trials and less than 25% censor fraction). Accuracy was computed as the number of trials with a correct response divided by the total number of trials across all available runs. Reaction time was computed from correct trials only and averaged across stimulus categories. A



significant fixed effect of academic months was observed in both models. Accuracy increased and reaction time decreased, indicating that task performance improved over schooling (Figure 15).



**Figure 15.** Longitudinal change in task performance, signal quality, and motion over academic months

Black lines depict the fixed effect of academic months with gray lines indicating 95% confidence interval bands. Single black dots represent subject data in which only one usable timepoint was acquired. Red dots/lines represent subjects where more than one timepoint was acquired and the subject-specific slope (change over months) was positive. Blue dots/lines indicate subjects where the slope was negative. The t-statistic ( $t$ ) and p-value ( $p$ ) refer to the significance of the fixed effect of academic months. TSNR = temporal signal to noise ratio.

### **3.4.2 Longitudinal changes in signal quality and motion**

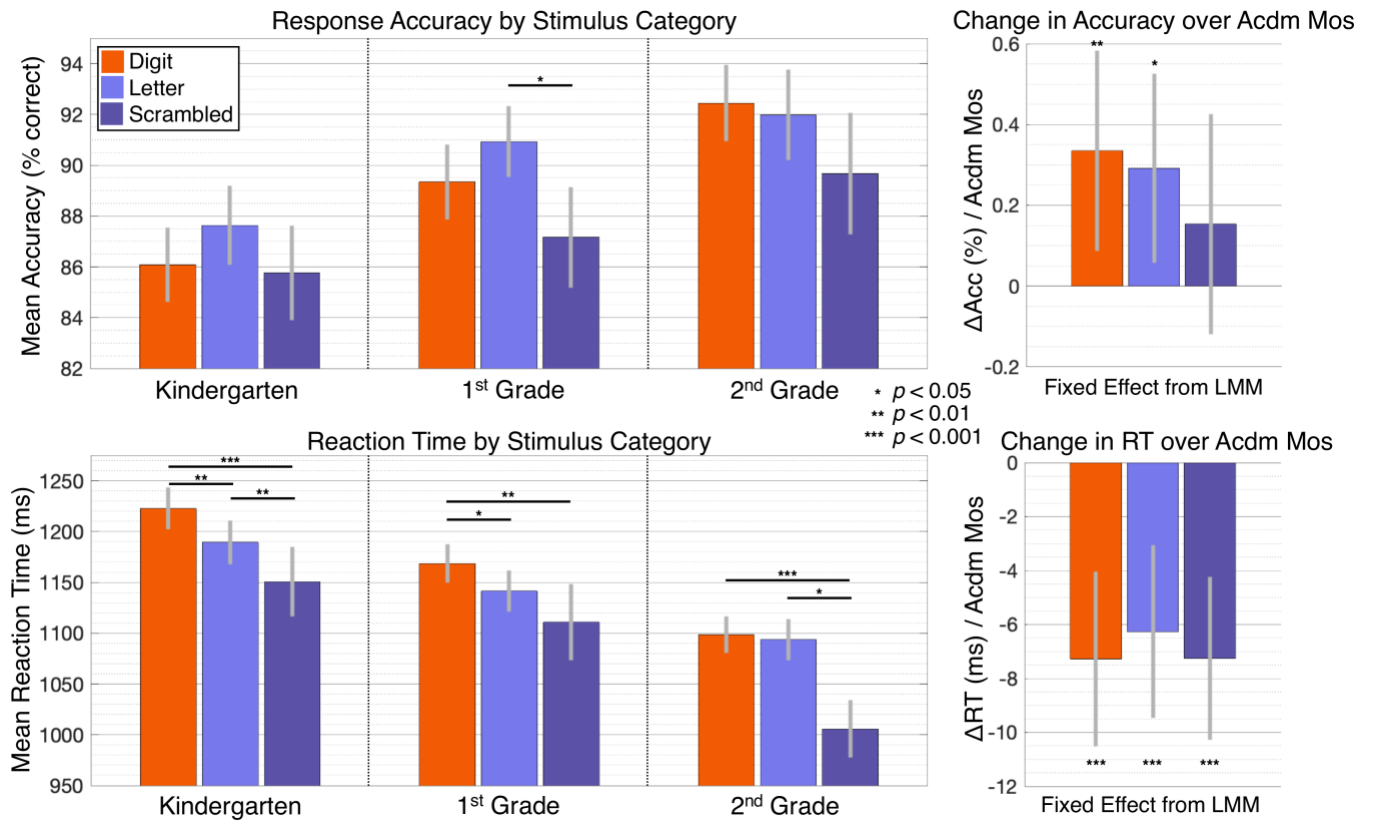
Next, using the same mixed-modelling procedure, we assessed whether signal quality and motion related to academic months. Temporal signal to noise ratio (TSNR), a metric commonly used to assess fMRI signal quality, was computed as the mean signal amplitude divided the standard deviation in amplitude across all (catenated) runs of the SYM task. TSNR was derived from the unsmoothed cortical surfaces, immediately following the motion correction and surface sampling procedures. For each subject, the average was taken across all nodes from both hemispheres. TSNR was significantly positively related to academic months, indicating image quality improved as children progressed in school (Figure 15).

Participant motion was measured in terms of the mean censor fraction across all runs, and was also significantly related to academic months (Figure 15). We previously discussed the potential for motion to confound longitudinal imaging analyses in children (see section 3.3.4). Though a number of analytical steps were taken to reduce the impact of motion on our imaging metrics, the significant effect observed here motivated us to include mean censor fraction as a nuisance covariate in subsequent LMMs looking at measures of brain function.

### **3.4.3 Task Performance by Symbol Category**

The previous analyses combined across all task conditions (i.e., symbol categories), giving a picture of overall task performance and change over schooling. However, as our primary analyses focused on relative differences in how the ITNAs functionally respond to each symbol category, we sought to also test whether task performance was similar across categories, and whether category-level performance similarly changed over academic months. We first looked at the mean accuracy and reaction time for each condition, binned by grade level. Within each grade, we conducted paired t-tests to look for differences between conditions (Figure 16). In

terms of accuracy, the only significant difference was observed in the 1<sup>st</sup> grade sample between Letters and Scrambled ( $t(54) = 2.29, p = 0.026$ ). LMMs were fit with condition-wise accuracy included as the dependent variable and indicated that accuracy significantly improved over academic months for only Digits ( $t(142) = 2.68, p = 0.008$ ) and Letters ( $t(142) = 2.46, p = 0.015$ ), but not for Scrambled ( $t(142) = 1.11, p = 0.267$ ). In terms of reaction times, a number of differences were observed between conditions within each grade (Figure 16). Reaction times to Digits were consistently slower than Scrambled (K,  $t(67) = 4.33, p = 0.00005$ ; 1<sup>st</sup>,  $t(54) = 3.34, p = 0.002$ ; 2<sup>nd</sup>,  $t(18) = 4.75, p = 0.0002$ ), and also slower than Letters in K and 1<sup>st</sup> grade (K,  $t(67) = 3.05, p = 0.003$ ; 1<sup>st</sup>,  $t(54) = 2.19, p = 0.03$ ). Reaction times to Letters were slower than Scrambled in K and 2<sup>nd</sup> grade (K,  $t(67) = 2.74, p = 0.008$ ; 2<sup>nd</sup>,  $t(18) = 2.84, p = 0.01$ ). LMMs showed that reaction times for all three conditions were strongly related to academic months (Digits,  $t(142) = -4.43, p = 2e^{-5}$ ; Letters,  $t(142) = -3.86, p = 2e^{-4}$ ; Scrambled,  $t(142) = -4.74, p = 5e^{-6}$ ).



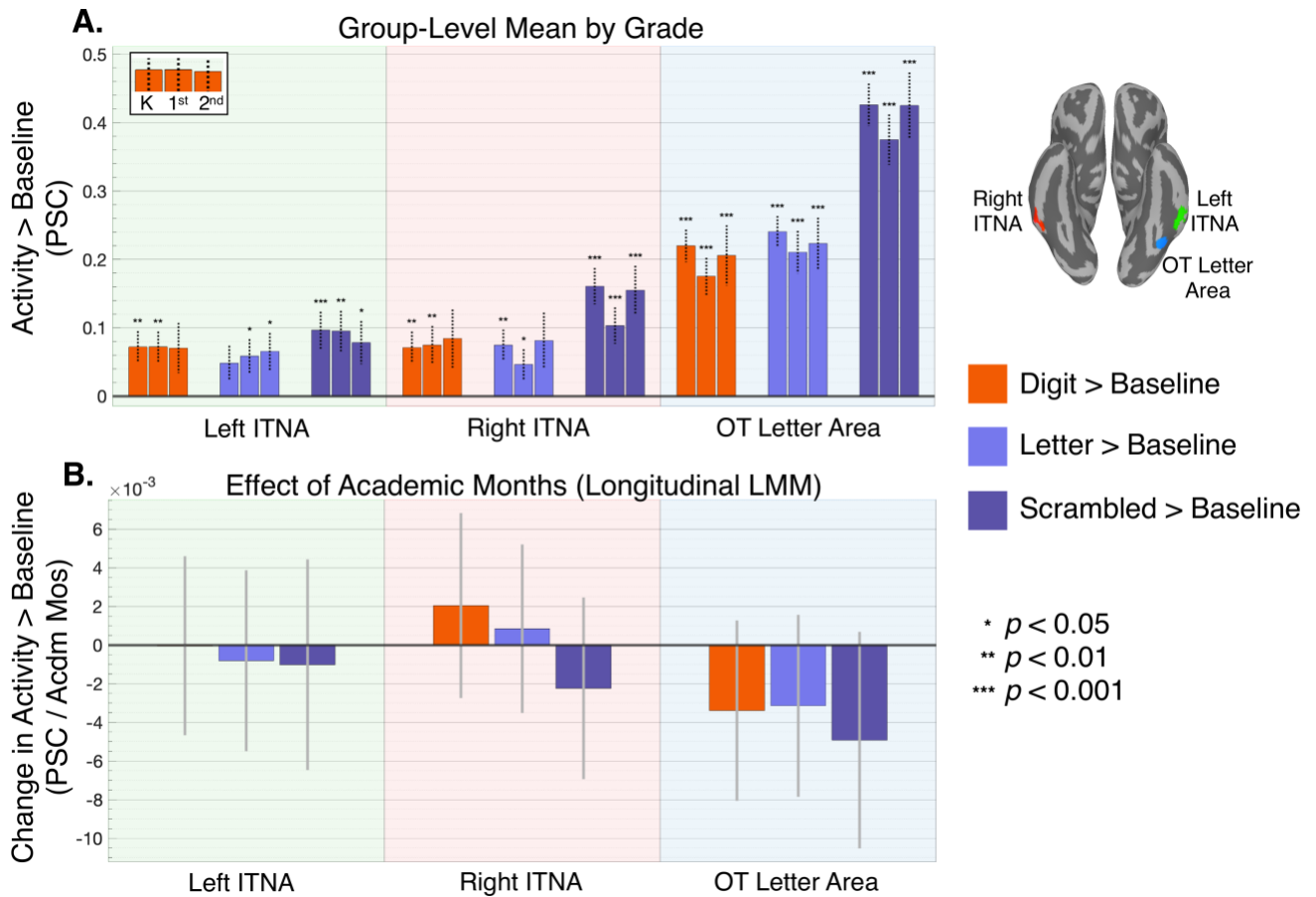
**Figure 16.** Symbol classification task performance by grade and longitudinal effects

Accuracy and reaction time measures are presented for each symbol category separately, and binned by grade level (left). LMM results for each metric/category looking at the fixed effect of academic months across the entire sample are also presented (right).

### 3.4.4 Longitudinal changes in occipitotemporal ROI activation versus baseline

In our first set of analyses looking at the functional properties of the ITNAs and OTLA control region, we focused on the mean response level for each condition. This metric indicates the sensitivity of the region to each stimulus category relative to baseline periods where a blank screen was presented and was measured as the BOLD percent signal change. We first plotted the raw group-level means in Figure 17A, binned by grade level. One sample t-tests were used to determine whether activity levels were significantly greater than zero at the group level (Table 2. One-sample t-test results for activation vs. baseline levels, by grade level. Table 2), which would

indicate some degree of sensitivity to the symbol category. In almost all cases, the responses versus baseline were above zero, indicating the three ROIs were engaged by each symbol category. Notably, however, the response levels in the OTLA were two times greater (or more) than in the ITNAs. We further used LMMs to characterize the relationship between activity levels and academic months (Figure 17B). Censor fraction (motion) was included as a covariate in these models. We observed no significant effects of academic months, suggesting that activity levels were relatively stable over K-2<sup>nd</sup> grade.



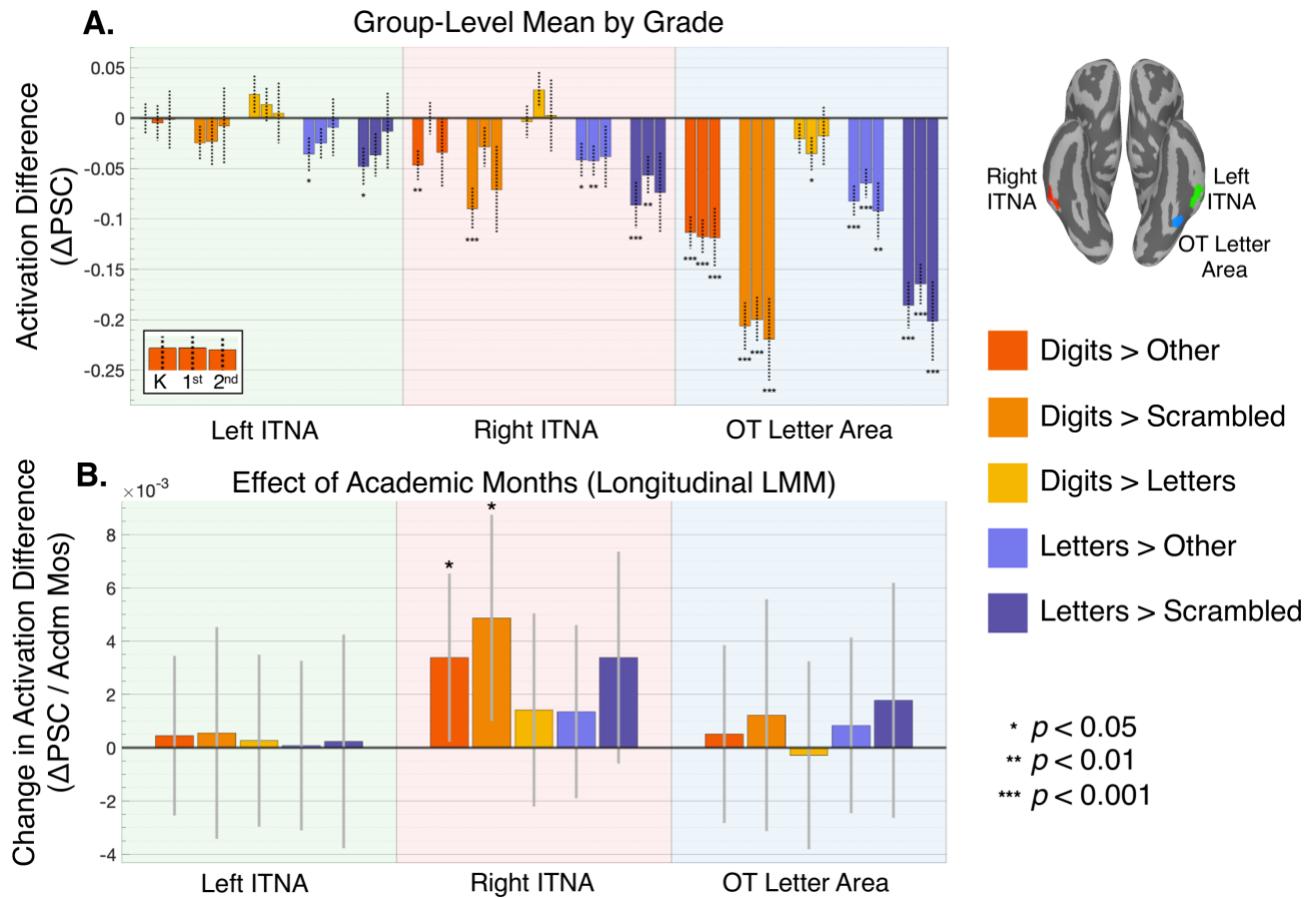
**Figure 17.** Longitudinal change in activation level versus baseline

A) Mean percent signal change (PSC) is plotted by grade level and ROI, with dotted lines indicating the standard error of the mean. Asterisks indicate the significance of one-sample t-tests. Shaded sections (green, red, blue) correspond to the ROI colors as depicted on the inferior

view of the inflated MNI surfaces (right). B) Fixed effect of academic months and 95% confidence intervals for each linear mixed-effect model, where the imaging metric was the dependent variable. LMMs included academic months as a fixed effect and subject as a random effect (slope + intercept), along with censor fraction as a time-varying covariate. Full statistical results are provide in Table 1 & 2. Acdm Mos = academic months; ITNA = inferior temporal numeral area; OT = occipitotemporal

### **3.4.5 Longitudinal changes in relative activation between conditions**

To assess the specificity of the ITNAs response to Digits relative to other symbols, we next looked at contrast between conditions, where values represent the relative difference in activation between symbol categories within each subject (i.e., difference in PSC). The Digits versus Other (average of Letters and Scrambled) response was computed, along with the pairwise difference compared to Letters and Scrambled separately. The Letters > Others and Letters > Scrambled contrasts were included for comparison. We again plotted the raw group-level means, binned by grade level, and tested whether these values were significantly different from zero, which would indicate a significant difference in response between conditions (Figure 18A/Table 3). Contrast values were mostly near zero in the left ITNA, indicating similar responses levels across symbol categories. Values in the right ITNA and OTLA were generally negative, indicating smaller responses to Digits/Letters relative to Scrambled stimuli. For the LMMs results, the right ITNA demonstrated a positive relation between academic months and the Digits > Other and Digits > Scrambled response (Figure 18B), suggesting the digit-specific activity in the right ITNA increased over schooling. No significant longitudinal changes were observed in the left ITNA or OTLA, suggesting category-specific activation levels were stable in these regions.



**Figure 18.** Longitudinal change in activation differences between conditions

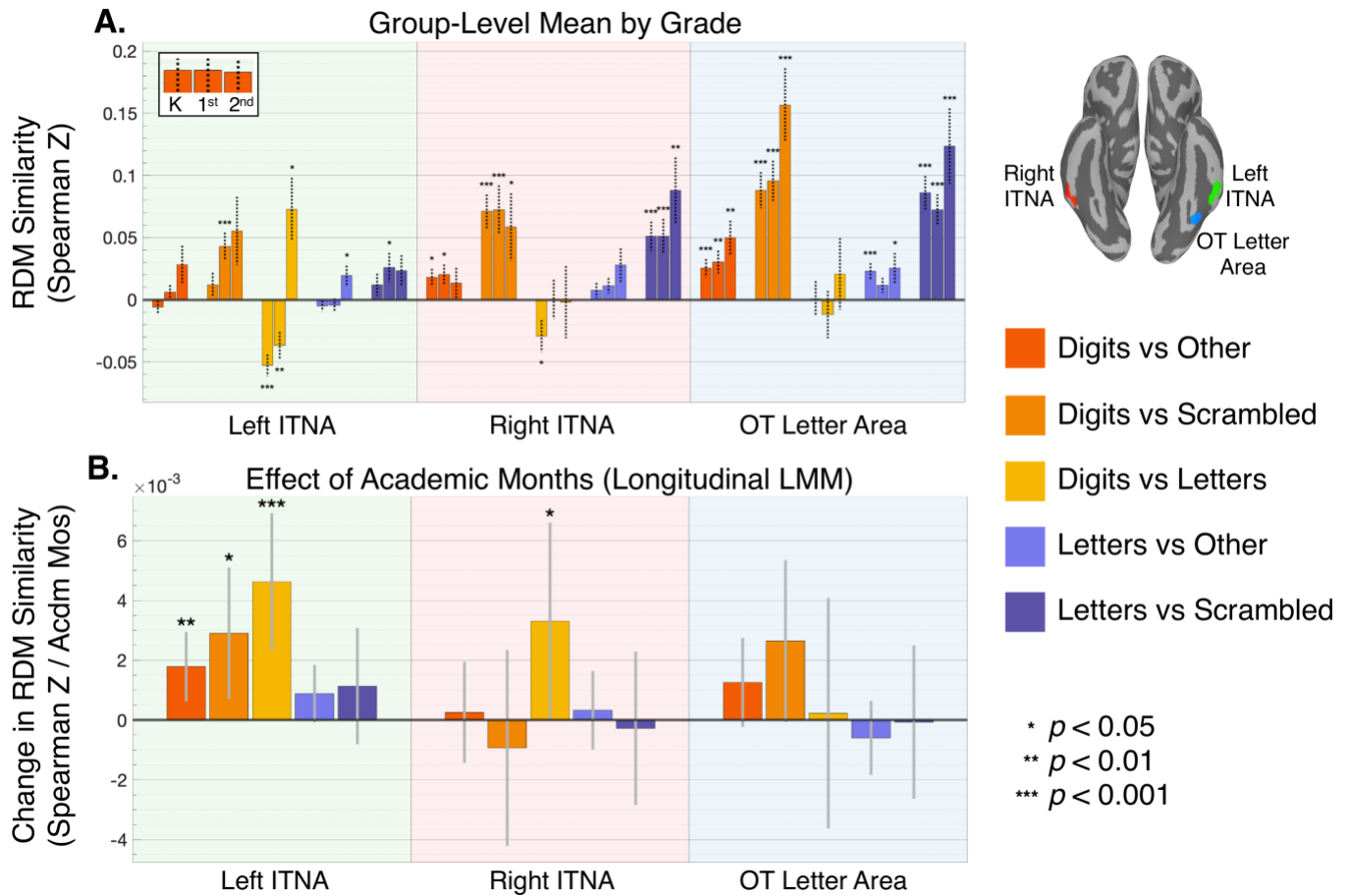
A) Mean activation contrast values for each subject were extracted from the ROIs. Group-level means and standard error of means (dotted line) by grade level are plotted. Asterisks indicate the significance of one-sample t-tests. Negative value indicates higher response level for the condition to the right of the > sign. B) Fixed effect of academic months and 95% confidence intervals for each linear mixed-effect model, where the imaging metric was the dependent variable. LMMs included academic months as a fixed effect and subject as a random effect (slope + intercept), along with censor fraction as a time-varying covariate. Full statistical results are provide in Table 1 & 3. Acdm Mos = academic months; PSC = percent signal change; ITNA = inferior temporal numeral area; OT = occipitotemporal

### 3.4.6 Longitudinal changes in category-level representational geometry

We next sought to determine whether spatial patterns of activity across each ROI carried information about symbol category. Exemplar-level response patterns were estimated and correlated, and the resulting representational (dis)similarity matrices (RDMs) were compared to

idealized candidate models. Group-level means by grade level are plotted in Figure 19A. Neural RDMs involving Digits or Letters and Scrambled separately showed generally higher fits, suggesting response patterns for familiar versus novel stimuli were the most distinct (Table 4). Digit vs. Letter model fits were relatively low, in comparison, albeit reaching a significant positive level in the left ITNA by 2<sup>nd</sup> grade. Turning to the LMM results, a significant relation between academic months and the Digit vs. Letter geometry was observed in both the left and right ITNAs (Figure 19A; full statistical results provided in Table 1). In the left ITNA, The Digits vs. Other and vs. Scrambled geometries also showed a longitudinal increase in fit. This was not the case for the Letter focused control models, suggesting a “digit-biased” change in the left ITNA’s representational geometry. Compared to the other indices of ITNA function studied here, category-level RSA metrics appeared to be most sensitive to changes over academic months based on the significance of the fixed effects.





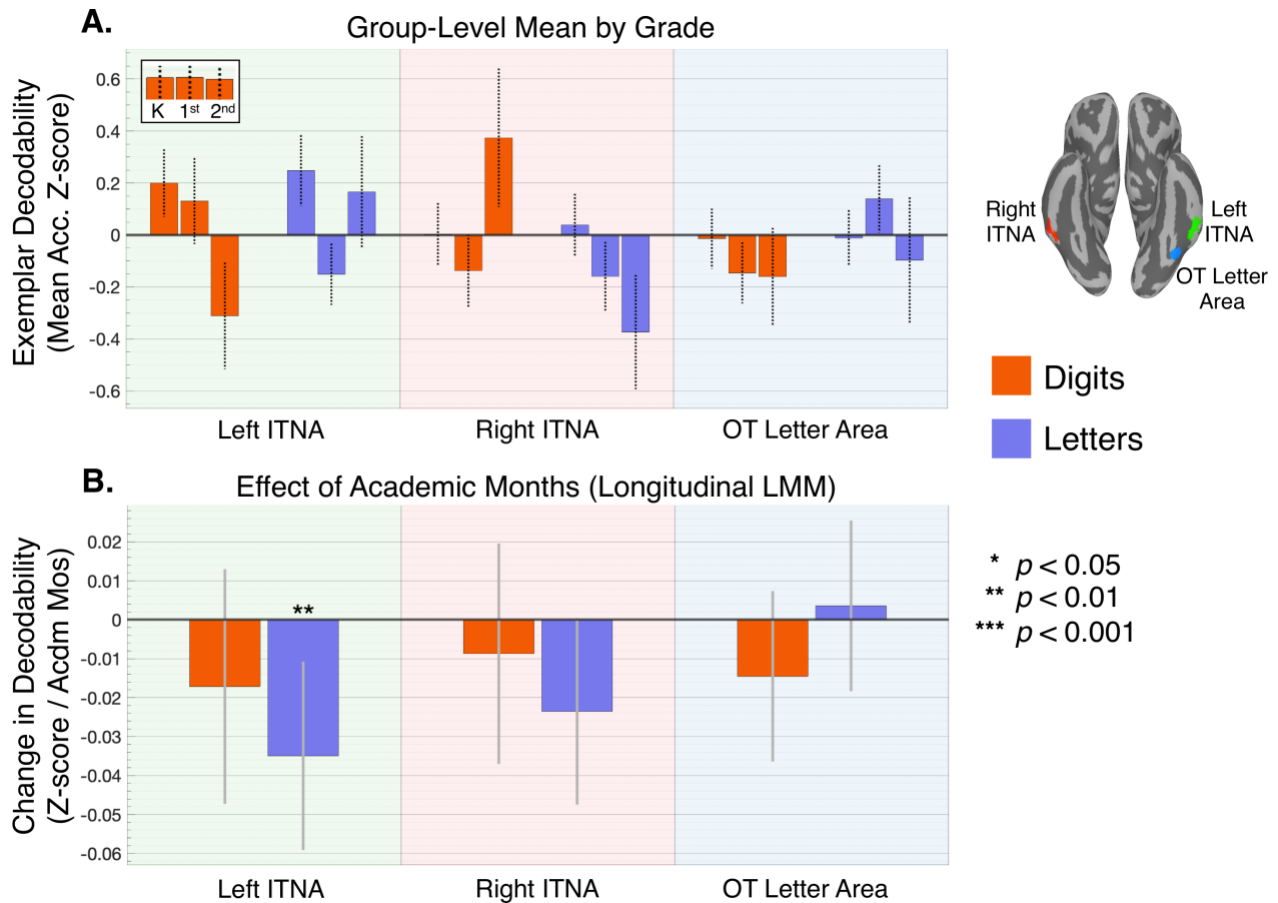
**Figure 19.** Longitudinal change in category-level representational geometry

A) Mean fits between neural and candidate model representational dissimilarity matrices (RDMs) are plotted, along with standard error of means (dotted line), by grade level. Asterisks indicate the significance of one-sample t-tests. Positive value indicates a neural representational geometry consistent with the candidate model. B) Fixed effect of academic months and 95% confidence intervals for each linear mixed-effect model, where the imaging metric was the dependent variable. LMMs included academic months as a fixed effect and subject as a random effect (slope + intercept), along with censor fraction as a time-varying covariate. Full statistical results are provide in Table 1 & 4. Acadm Mos = academic months; RDM = representational dissimilarity matrix; ITNA = inferior temporal numeral area; OT = occipitotemporal

### 3.4.7 Longitudinal changes in exemplar decodability

While the category-level representational similarity analyses focused on response pattern similarity within and between stimulus conditions, we were also interested in the extent to which the ITNAs carried distinct information about stimulus identity, i.e., unique patterns for each

symbol exemplar. MVPA decoding analyses were performed on Digit and Letter sets separately. Mean decodability (classification accuracy) levels were converted to Z-scores based on null-distributions created from shuffling exemplar labels. The group-level mean Z-scores by grade level are plotted in Figure 20A (with stats reported in Table 5). We observed no significantly above chance decoding for any grade level, for either Digits or Letters, suggesting response patterns within these ROIs did not contain reliable exemplar-level information. LMMs showed decreasing decodability for Letters in the left ITNA over academic months, but no other effects were significant (Figure 20B), suggesting that these regions are coding at the category level rather than the item level during this developmental time frame.



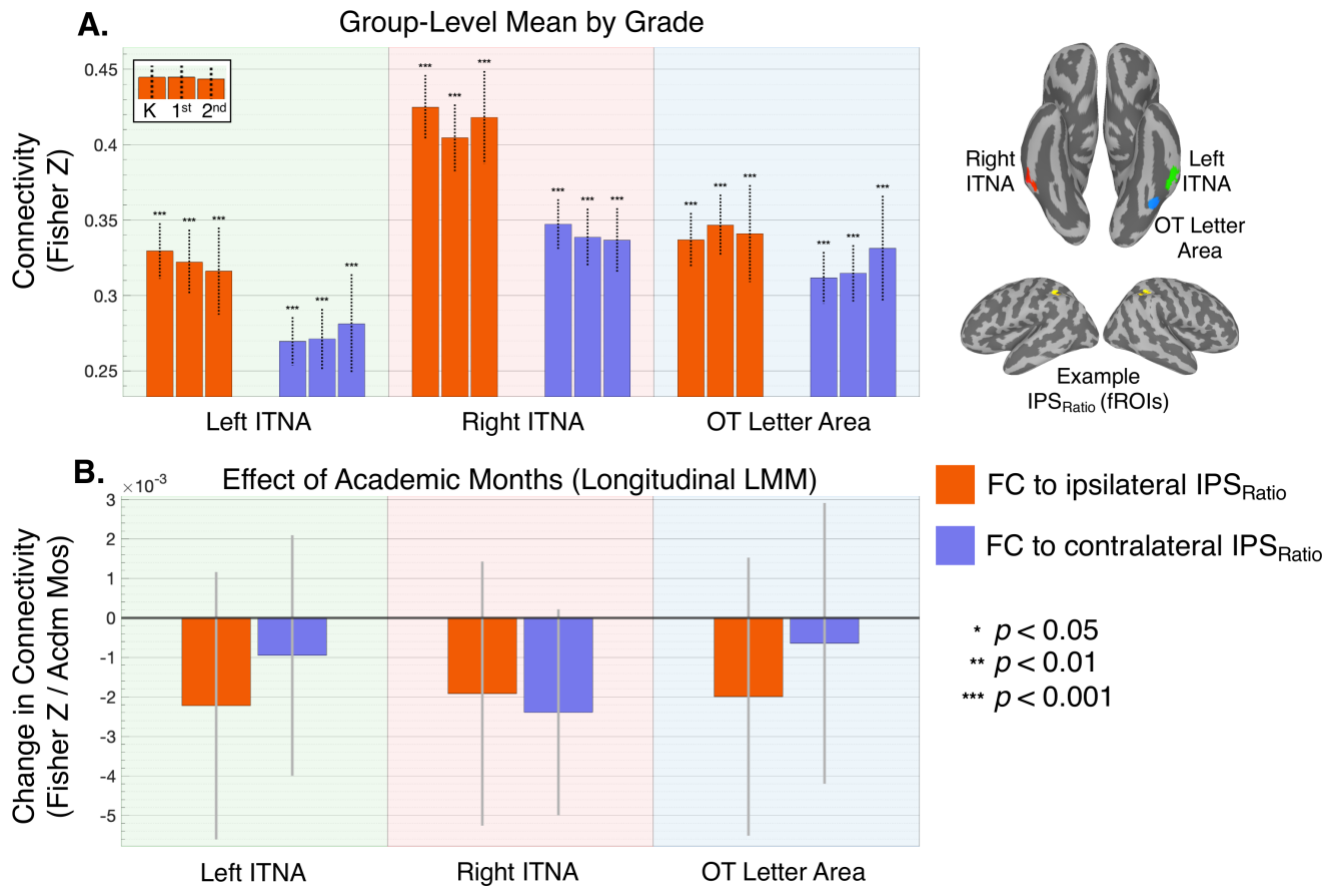
**Figure 20.** Longitudinal change in exemplar decodability

A) Mean exemplar decodability Z-scores are plotted, along with standard error of means (dotted line), by grade level. Asterisks indicate the significance of one-sample t-tests (none surviving). B) Fixed effect of academic months and 95% confidence intervals for each linear mixed-effect model, where the imaging metric was the dependent variable. LMMs included academic months as a fixed effect and subject as a random effect (slope + intercept), along with censor fraction as a time-varying covariate. Full statistical results are provide in Table 1 & 5. Acadm Mos = academic months; Acc. = classification accuracy; ITNA = inferior temporal numeral area; OT = occipitotemporal

### 3.4.8 Longitudinal changes in “background” functional connectivity

In the next set of analyses, we focused on functional connectivity of the ITNAs with parietal fROIs ( $IPS_{Ratio}$ ). First, we assessed the “background” connectivity patterns, i.e., correlation in the residual timeseries after removal of task effects, which capture the degree of spontaneous coupling between ROIs over the scan session. The group-level means were all

significantly above zero (Figure 21A/Table 6) and suggested strong coupling between OT areas and the intraparietal sulci bilaterally. In the LMMs, however, we observed no significant relations between academic months and connectivity levels (Figure 21B, full statistical results provided in Table 1). This indicates that background connectivity was relatively stable over the period studied here. Note that for these analyses, usable data from the symbolic comparison task was required to define the target fROIs. Due to missing and/or unusable comparison task data, we could not define fROIs in 25 of the 145 (17%) scan sessions included in the previous models looking at local function. The present analyses, as well as the task-evoked connectivity analyses below, include the reduced set of 120 observations.



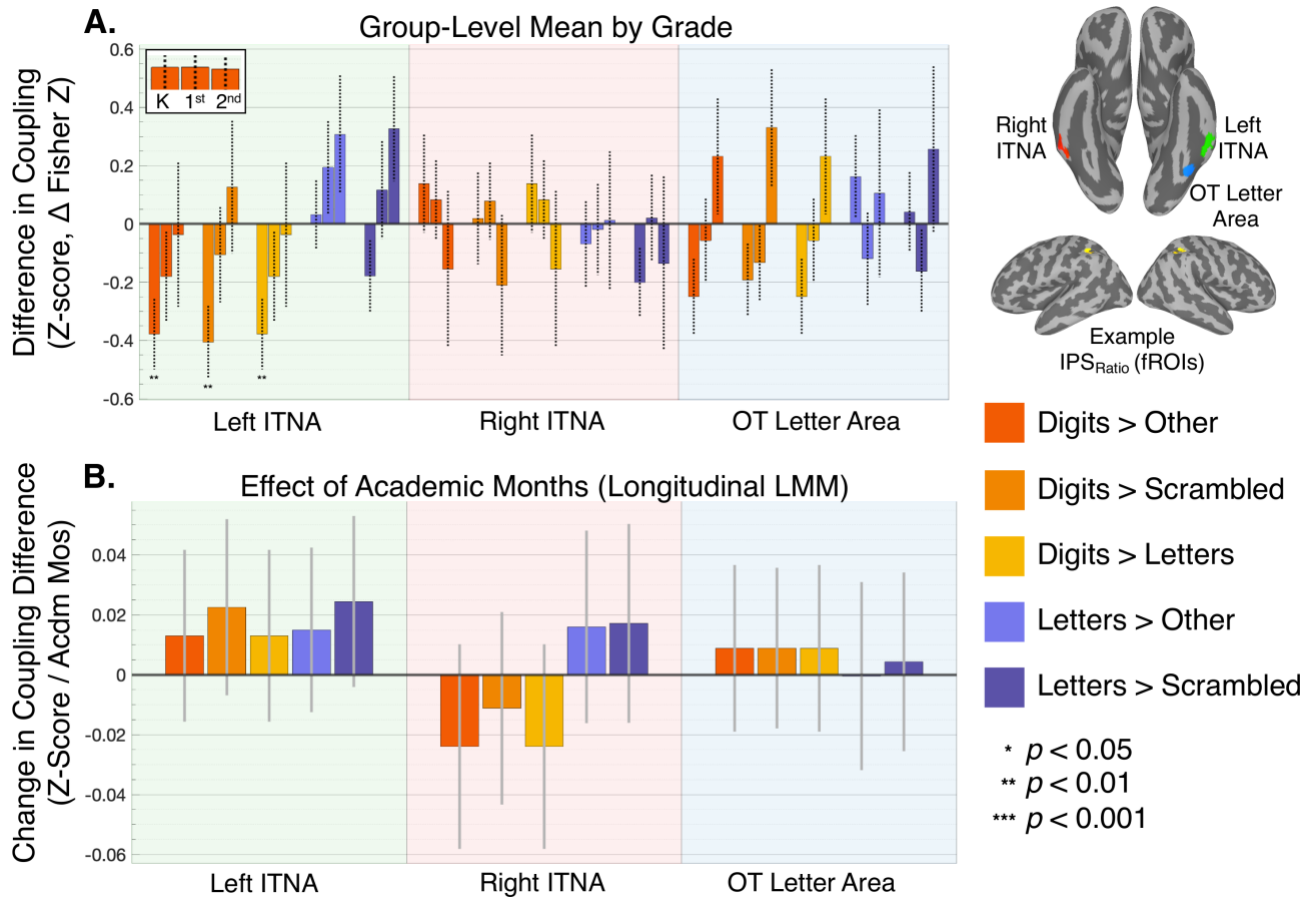
**Figure 21.** Longitudinal change in background functional connectivity with IPS<sub>Ratio</sub> ROIs

A) Mean “background” connectivity (correlation in the residual timeseries across all tasks/runs, after removal of task and nuisance effects), along with standard error of means (dotted line), is plotted by grade level. Asterisks indicate the significance of one-sample t-tests. Example target fROIs in parietal cortex are shown to the right (yellow). B) Fixed effect of academic months and 95% confidence intervals for each linear mixed-effect model, where the imaging metric was the dependent variable. LMMs included academic months as a fixed effect and subject as a random effect (slope + intercept), along with censor fraction as a time-varying covariate. Full statistical results are provide in Table 1 & 6. Acdm Mos = academic months; fROI = functionally-defined region of interest; IPS = intraparietal sulcus; ITNA = inferior temporal numeral area; OT = occipitotemporal

### 3.4.9 Longitudinal changes in task-evoked functional connectivity

Next, we looked at the task-evoked functional connectivity of each ROI with the parietal fROIs, using the beta-series correlation (BSC) method, and whether category-specific coupling changed over schooling. The focus here was on the relative difference in coupling in response to

one category versus another (i.e., a contrast). Thus, a Z-score representing the difference between two Pearson correlation coefficients (BSCs) was the dependent variable. We observed considerable variability in the mean Z-scores across contrasts and grade levels (wide standard error of the means) and few cases where values were significantly different from zero, indicating a general lack of category-specific coupling (Figure 22A/Table 7). An exception was the left ITNA in the kindergarten time period, which showed reduced coupling during the Digit trials compared to Scrambled and Letter trials (Figure 22A, see significant negative values in left panel). In the LMM results, there were no significant relations with academic months for any ROI or contrast (Figure 22, full statistical results provided in Table 1).



**Figure 22.** Longitudinal change in task-evoked connectivity with IPS<sub>Ratio</sub> ROIs

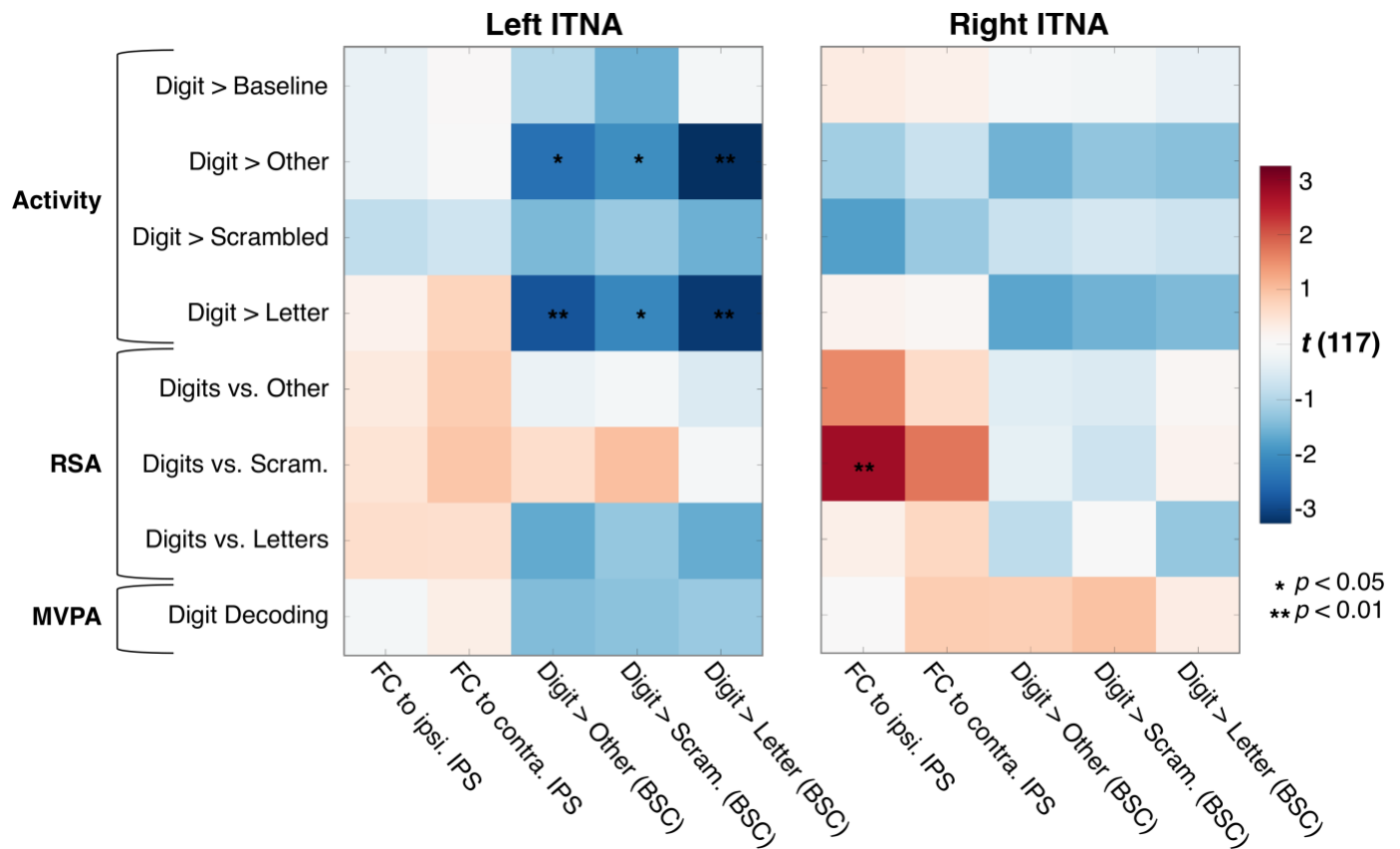
A) Mean task-evoked connectivity differences based on beta-series correlations are plotted by grade level, along with standard error of means (dotted line). Asterisks indicate the significance of one-sample t-tests. Example target fROIs in parietal cortex are shown to the right (yellow). Only ipsilateral connections were analyzed here. B) Fixed effect of academic months and 95% confidence intervals for each linear mixed-effect model, where the imaging metric was the dependent variable. LMMs included academic months as a fixed effect and subject as a random effect (slope + intercept), along with censor fraction as a time-varying covariate. Full statistical results are provide in Table 1 & 7. Acdm Mos = academic months; fROI = functionally-defined region of interest; IPS = intraparietal sulcus; ITNA = inferior temporal numeral area; OT = occipitotemporal

### 3.4.10 Relations between connectivity and local functional metrics

In a final set of analyses, we looked at whether individual differences in the degree of background and category-specific connectivity were related to local measures of ITNA function, including activity levels, representational geometry, and exemplar decodability. As the focus

here was on how different metrics are related, rather than the extent to which digit-specific processing occurs and/or changes within the ITNAs, we included only Digit-specific measures and excluded the OTLA. We used the same LMM structure as before to estimate these relations, except with the connectivity metric as the independent variable instead of academic months. In this case, the model outputs indicate the *overall* association between the two measures across our sample, taking into account repeated measures within individuals. Censor fraction was again included as a covariate of no interest. LMMs were fit for each relation separately and the t-stats for the fixed effect of connectivity are presented in Figure 23. In the left ITNA, the difference in activity between Digits and Letters was *negatively* related to Digit-specific coupling. Though this result is challenging to interpret, it suggests an inverse relation between category-specific activity and coupling in the left hemisphere. Note, that the effect was not observed for Digits > Scrambled (activity), indicating the relation only pertained to familiar symbol processing. For the right ITNA, only one significant effect was observed, involving a positive relation between background functional connectivity and the Digit vs. Scrambled representational geometry. Note that right ITNA and right IPS showed the strongest functional connectivity of any ROI pair (Figure 21A), suggesting this circuit is already well established in children. The present result indicates that, in early school-age children, individual differences in this circuit relate to categorical representations in the right ITNA.





**Figure 23.** Relations between ITNA-IPS<sub>Ratio</sub> connectivity and local functional metrics

Cells represent the significance of the relation ( $t$ -statistic for fixed-effect) between each connectivity measure (x-axis) and local measure (y-axis) across the entire sample ( $n=120$  observations). LMMs included the connectivity measure as a fixed effect and subject as a random effect (slope + intercept), along with censor fraction as a time-varying covariate. Local measures were included as the dependent (predicted) variable. FC = background functional connectivity; IPS = intraparietal sulcus; ITNA = inferior temporal numeral area; BSC = beta-series correlation

		Fixed Effects								Random Effects						
		Inter cept E est (SE)	Inter cept t (p)	Inter cept 2nd Gr d E est (SE)	Inter cept 2nd Gr d t (p)	Censor Frac slope E Est (SE)	Censor Frac slope t (p)	Acdm Mos slope E est (SE)	Acdm Mos slope t (p)	DF	Inter cept Variance	Slope Variance	Residual Variance			
Activity vs. Baseline	Digit > Baseline	ITNA L	0.058(0.0405)	1.421(0.1575)	0.057(0.0352)	1.611(0.1094)	0.258(0.2290)	1.127(0.2616)	-0.000(0.0023)	-0.014(0.9886)	142	0.1777	0.0099	0.1533		
		ITNA R	0.021(0.0418)	0.495(0.6211)	0.078(0.0390)	1.993(0.0482)	0.458(0.2594)	1.768(0.0792)	0.002(0.0024)	0.845(0.3995)	142	0.0776	0.0023	0.1658		
		OTLA	0.231(0.0421)	5.485(0.0000)	0.136(0.0384)	3.554(0.0005)	0.153(0.2617)	0.584(0.5600)	-0.003(0.0024)	-1.437(0.1529)	142	0.1187	0.0021	0.173		
	Letter > Baseline	ITNA L	0.086(0.0427)	2.015(0.0458)	0.063(0.0347)	1.829(0.0695)	-0.331(0.2406)	-1.377(0.1708)	-0.001(0.0024)	-0.341(0.7337)	142	0.198	0.0097	0.1561		
		ITNA R	0.037(0.0382)	0.973(0.3322)	0.061(0.0361)	1.686(0.0941)	0.284(0.2348)	1.208(0.2291)	0.001(0.0022)	0.384(0.7016)	142	0.1154	0.0051	0.1541		
		OTLA	0.277(0.0402)	6.889(0.0000)	0.189(0.0425)	4.461(0.0000)	-0.210(0.2584)	-0.814(0.4170)	-0.003(0.0024)	-1.320(0.1889)	142	0.087	0.0026	0.163		
	Scrambled > Baseline	ITNA L	0.106(0.0481)	2.204(0.0291)	0.078(0.0421)	1.844(0.0672)	0.057(0.2806)	0.203(0.8394)	-0.001(0.0028)	-0.368(0.7133)	142	0.1818	0.0095	0.1919		
		ITNA R	0.165(0.0434)	3.799(0.0002)	0.103(0.0382)	2.681(0.0082)	0.012(0.2672)	0.044(0.9648)	-0.002(0.0024)	-0.941(0.3482)	142	0.145	0.0031	0.1712		
		OTLA	0.498(0.0497)	10.025(0.0000)	0.361(0.0519)	6.952(0.0000)	-0.499(0.3176)	-1.572(0.1182)	-0.005(0.0028)	-1.735(0.0850)	142	0.1501	0.0025	0.1876		
	Activity Contrasts	Digit > Other	ITNA L	-0.034(0.0262)	-1.281(0.2024)	-0.021(0.0252)	-0.826(0.4102)	0.383(0.1650)	2.319(0.0218)	0.000(0.0015)	0.300(0.7644)	142	0.0532	0	0.1119	
			ITNA R	-0.089(0.0254)	-3.490(0.0006)	0.006(0.0277)	0.208(0.8354)	0.314(0.1611)	1.949(0.0533)	0.003(0.0016)	2.119(0.0358)	142	0.0013	0.0034	0.113	
			OTLA	-0.152(0.0271)	-5.624(0.0000)	-0.138(0.0289)	-4.781(0.0000)	0.470(0.1683)	2.794(0.0059)	0.001(0.0017)	0.304(0.7612)	142	0.0661	0.0052	0.1422	
Digit > Scrambled		ITNA L	-0.043(0.0330)	-1.317(0.1900)	-0.028(0.0339)	-0.822(0.4124)	0.214(0.2079)	1.031(0.3043)	0.001(0.0020)	0.277(0.7719)	142	0.0037	0.0029	0.1194		
		ITNA R	-0.155(0.0332)	-4.658(0.0000)	-0.019(0.0336)	-0.553(0.5808)	0.487(0.2111)	2.306(0.0226)	0.005(0.0020)	2.489(0.0140)	142	0.0592	0.0013	0.1408		
		OTLA	-0.260(0.0379)	-6.867(0.0000)	-0.226(0.0375)	-6.032(0.0000)	0.563(0.2290)	2.460(0.0151)	0.001(0.0022)	0.556(0.5791)	142	0.1663	0.0085	0.1263		
Digit > Letter		ITNA L	-0.021(0.0304)	-0.692(0.4900)	-0.014(0.0245)	-0.556(0.5793)	0.548(0.1778)	3.084(0.0025)	0.000(0.0016)	0.164(0.8507)	142	0.1303	0.005	0.1134		
		ITNA R	-0.017(0.0291)	-0.597(0.5518)	0.022(0.0306)	0.730(0.4669)	0.145(0.1776)	0.814(0.4170)	0.001(0.0018)	0.778(0.4392)	142	0.058	0.0058	0.1281		
		OTLA	-0.045(0.0278)	-1.633(0.1047)	-0.053(0.0287)	-1.856(0.0655)	0.381(0.1577)	2.416(0.0170)	-0.000(0.0018)	-0.158(0.8747)	142	0.1106	0.0085	0.1086		
Letter > Other		ITNA L	-0.004(0.0282)	-0.156(0.8760)	-0.002(0.0242)	-0.091(0.9278)	-0.442(0.1616)	-2.738(0.0070)	0.000(0.0016)	0.049(0.9606)	142	0.1194	0.0063	0.1063		
		ITNA R	-0.061(0.0277)	-2.221(0.0279)	-0.024(0.0267)	-0.883(0.3788)	0.063(0.1719)	0.369(0.7125)	0.001(0.0016)	0.826(0.4101)	142	0.0275	0.0019	0.1274		
		OTLA	-0.080(0.0278)	-2.882(0.0046)	-0.057(0.0253)	-2.238(0.0268)	-0.152(0.1522)	-1.000(0.3189)	0.001(0.0017)	0.506(0.6135)	142	0.1417	0.0087	0.0938		
Letter > Scrambled		ITNA L	-0.024(0.0340)	-0.704(0.4828)	-0.017(0.0327)	-0.528(0.5983)	-0.321(0.2077)	-1.547(0.1241)	0.000(0.0020)	0.017(0.9059)	142	0.0708	0.0047	0.1514		
		ITNA R	-0.132(0.0361)	-3.662(0.0004)	-0.038(0.0321)	-1.179(0.2402)	0.278(0.2222)	1.250(0.2133)	0.003(0.0020)	1.682(0.0948)	142	0.1088	0.0028	0.148		
		OTLA	-0.215(0.0389)	-5.523(0.0000)	-0.165(0.0346)	-4.783(0.0000)	0.118(0.2129)	0.552(0.5816)	0.002(0.0022)	0.798(0.4264)	142	0.2247	0.0123	0.1071		
Category-level RSA		Digit vs Other	ITNA L	-0.023(0.0095)	-2.433(0.0162)	0.027(0.0101)	2.639(0.0092)	0.057(0.0602)	0.947(0.3454)	0.002(0.0006)	3.045(0.0288)	142	0.014	0.0012	0.1413	
			ITNA R	0.009(0.0125)	0.749(0.4549)	0.017(0.0145)	1.135(0.2581)	0.084(0.0579)	1.456(0.1477)	0.000(0.0009)	0.301(0.7640)	142	0.0933	0.0065	0.0117	
			OTLA	0.019(0.0124)	1.517(0.1314)	0.054(0.0137)	3.940(0.0001)	-0.046(0.0804)	-0.576(0.5653)	0.001(0.0008)	1.664(0.0983)	142	0.0232	0.0012	0.0508	
		Digit vs Scrambled	ITNA L	-0.008(0.0189)	-0.439(0.6614)	0.073(0.0183)	3.970(0.0001)	0.027(0.1164)	0.229(0.8192)	0.003(0.0011)	2.600(0.0103)	142	0.0537	0.0028	0.0779	
			ITNA R	0.094(0.0246)	3.809(0.0002)	0.067(0.0305)	2.215(0.0283)	-0.201(0.1536)	-1.312(0.1916)	-0.001(0.0017)	-0.564(0.5739)	142	0.0867	0.0076	0.0875	
			OTLA	0.085(0.0230)	3.691(0.0003)	0.159(0.0250)	6.342(0.0000)	-0.281(0.1484)	-1.896(0.0600)	0.003(0.0014)	1.934(0.0550)	142	0.0542	0.0018	0.0908	
		Digit vs Letter	ITNA L	-0.105(0.0170)	-6.152(0.0000)	0.024(0.0208)	1.153(0.2507)	0.212(0.1065)	1.993(0.0482)	0.005(0.0012)	3.974(0.0001)	142	0.026	0.0044	0.0733	
			ITNA R	-0.054(0.0246)	-2.205(0.0291)	0.038(0.0284)	1.340(0.1824)	0.004(0.1427)	0.031(0.9756)	0.003(0.0017)	1.990(0.0485)	142	0.1057	0.0088	0.0874	
			OTLA	-0.007(0.0278)	-0.255(0.7988)	-0.001(0.0340)	-0.022(0.9823)	0.012(0.1600)	0.074(0.9414)	0.000(0.0020)	0.117(0.9073)	142	0.1331	0.0113	0.09	
		Letter vs Other	ITNA L	-0.012(0.0082)	-1.406(0.1618)	0.013(0.0079)	1.653(0.1005)	-0.011(0.0512)	-0.219(0.8273)	0.001(0.0005)	1.817(0.0713)	142	0	0	0.0381	
			ITNA R	0.016(0.0105)	1.542(0.1252)	0.025(0.0113)	2.234(0.0270)	-0.136(0.0653)	-2.088(0.0386)	0.000(0.0007)	0.493(0.6227)	142	0.0116	0.0018	0.0468	
			OTLA	0.034(0.0106)	3.171(0.0019)	0.017(0.0102)	1.661(0.0988)	-0.120(0.0658)	-1.825(0.0701)	-0.001(0.0006)	-0.952(0.3428)	142	0.008	0.0005	0.0489	
		Letter vs Scrambled	ITNA L	0.008(0.0166)	0.500(0.6181)	0.040(0.0160)	2.488(0.0140)	-0.035(0.1039)	-0.335(0.7378)	0.001(0.0010)	1.150(0.2522)	142	0	0	0.0774	
			ITNA R	0.083(0.0209)	3.962(0.0001)	0.075(0.0221)	3.406(0.0009)	-0.386(0.1323)	-2.919(0.0041)	-0.000(0.0013)	-0.214(0.8312)	142	0.0009	0.0024	0.0943	
			OTLA	0.106(0.0214)	4.949(0.0000)	0.104(0.0226)	4.598(0.0000)	-0.346(0.1370)	-2.524(0.0127)	-0.000(0.0013)	-0.054(0.9573)	142	0.029	0.0016	0.0916	
		Exemplar MIPA	Digits	ITNA L	0.227(0.2538)	0.896(0.3717)	-0.251(0.2449)	-1.023(0.3080)	1.684(1.4953)	1.126(0.2621)	-0.017(0.0152)	-1.125(0.2626)	142	1.0036	0.0611	0.9529
				ITNA R	0.284(0.2266)	1.255(0.2116)	0.041(0.2356)	0.175(0.8616)	-3.422(1.3358)	-2.562(0.0114)	-0.009(0.0143)	-0.609(0.5434)	142	0.8233	0.0611	0.8834
				OTLA	0.321(0.1925)	1.669(0.0972)	-0.084(0.1742)	-0.480(0.6316)	-3.540(1.1685)	-3.029(0.0029)	-0.015(0.0111)	-1.313(0.1913)	142	0.5271	0.0239	0.825
			Letters	ITNA L	0.692(0.2202)	3.142(0.0020)	-0.282(0.1929)	-1.463(0.1457)	-2.966(1.3441)	-2.207(0.0289)	-0.035(0.0122)	-2.854(0.0050)	142	0.6972	0.0213	0.8989
				ITNA R	0.108(0.2078)	0.518(0.6050)	-0.548(0.1963)	-2.793(0.0059)	1.639(1.2847)	1.276(0.2042)	-0.024(0.0121)	-1.944(0.0539)	142	0.4812	0.0208	0.8938
				OTLA	0.142(0.1816)	0.783(0.4348)	0.242(0.1996)	1.212(0.2276)	-2.321(1.1720)	-1.981(0.0496)	0.004(0.0111)	0.322(0.7477)	142	0.2984	0.0175	0.7517
	Background FC	Seed to Ipsilateral	ITNA L	0.375(0.0317)	11.841(0.0000)	0.313(0.0288)	10.851(0.0000)	-0.417(0.2120)	-1.969(0.0513)	-0.002(0.0017)	-1.302(0.1956)	117	0.1619	0.0065	0.0773	
			ITNA R	0.452(0.0342)	13.220(0.0000)	0.399(0.0277)	14.413(0.0000)	-0.152(0.2268)	-0.672(0.5028)	-0.002(0.0017)	-1.136(0.2584)	117	0.1756	0.0045	0.0882	
			OTLA	0.367(0.0318)	11.541(0.0000)	0.312(0.0300)	10.392(0.0000)	-0.019(0.2216)	-0.087(0.9311)	-0.002(0.0018)	-1.122(0.2641)	117	0.1404	0.0056	0.0914	
		Seed to Contralateral	ITNA L	0.295(0.0267)	11.064(0.0000)	0.269(0.0285)	9.435(0.0000)	-0.200(0.1939)	-1.029(0.3054)	-0.001(0.0015)	-0.619(0.5371)	117	0.104	0.0039	0.0783	
			ITNA R	0.387(0.0284)	13.633(0.0000)	0.320(0.0200)	16.015(0.0000)	-0.220(0.1819)	-1.212(0.2281)	-0.002(0.0013)	-1.815(0.0720)	117	0.1538	0.0034	0.0733	
			OTLA	0.320(0.0302)	10.590(0.0000)	0.301(0.0314)	9.595(0.0000)	0.102(0.2257)	0.452(0.6518)	-0.001(0.0018)	-0.360(0.7196)	117	0.0648	0.0015	0.1128	
	Condition BSC Contrasts	Digit > Other	ITNA L	-0.394(0.2390)	-1.650(0.1017)	-0.031(0.2404)	-0.128(0.8960)	-0.392(1.7619)	-0.222(0.8243)	0.013(0.0145)	0.900(0.3696)	117	0.0589	0.017	1.0343	
			ITNA R	0.231(0.2900)	0.797(0.4269)	-0.437(0.2692)	-1.623(0.1072)	2.359(1.9790)	1.192(0.2356)	-0.024(0.0172)	-1.390(0.1672)	117	1.023	0.061	1.1034	
			OTLA	-0.094(0.2406)	-0.391(0.6967)	0.153(0.2241)	0.681(0.4973)	-2.782(1.7244)	-1.614(0.1093)	0.009(0.0140)	0.630(0.5302)	117	0.5554	0.0269	0.9526	
		Digit > Scrambled	ITNA L	-0.515(0.2488)	-2.069(0.0408)	0.114(0.2436)	0.469(0.6399)	0.322(1.8310)	0.178(0.8607)	0.023(0.0148)	1.520(0.1313)	117	0.0421	0.0085	1.0883	
			ITNA R	0.035(0.2734)	0.129(0.8977)	-0.277(0.2537)	-1.090(0.2778)	1.678(1.8731)	0.896(0.3723)	-0.011(0.0162)	-0.689(0.4920)	117	0.9425	0.0558	1.0472	
			OTLA	-0.131(0.2241)	-0.587(0.5585)	0.117(0.2220)	0.527(0.5992)	-1.770(1.6314)	-1.085(0.2800)	0.009(0.0135)	0.658(0.5117)	117	0.2853	0.0235	0.9619	
		Digit > Letter	ITNA L	-0.167(0.2289)	-0.729(0.4672)	-0.176(0.2226)	-0.791(0.4303)	-0.847(1.6844)	-0.503(0.6160)	-0.000(0.0136)	-0.024(0.9807)	117	0.0114	0.0012	1.0037	
			ITNA R	0.355(0.2848)	1.245(0.2155)	-0.490(0.2851)	-1.717(0.0886)	2.552(1.9635)	1.300(0.1962)	-0.030(0.0176)	-1.718(0.0888)	117	0.9442	0.0653	1.0825	
			OTLA	-0.012(0.2601)	-0.048(0.9620)	0.145(0.2405)	0.602(0.5485)	-3.139(1.8603)	-1.687(0.0942)	0.006(0.0151)	0.373(0.7100)	117	0.63	0.0295	1.0653	
Letter > Other		ITNA L	-0.131(0.2335)	-0.560(0.5763)	0.287(0.2269)	1.268(0.2080)	1.326(1.7175)	0.773(0.4411)	0.015(0.0139)	1.081(0.2819)	117	0	0	1.0239		
		ITNA R	-0.288(0.2743)	-1.050(0.2960)	0.198(0.2571)											

		F			F			F	
Dig_Coef_LH	3.1172	68	0.0026753	3.23329	54	0.002089	1.9214	18	0.070658
Dig_Coef_RH	3.05247	68	0.003237	2.67226	54	0.0099405	1.9805	18	0.063145
Dig_Coef_OTLA_LH	9.20529	68	1.44E-13	6.44869	54	3.23E-08	4.6666	18	0.00019201
Let_Coef_LH	1.9242	68	0.058516	2.38243	54	0.020749	2.4024	18	0.02729
Let_Coef_RH	3.29316	68	0.0015744	2.08102	54	0.042189	1.9897	18	0.062033
Let_Coef_OTLA_LH	10.474	68	7.95E-16	6.73926	54	1.09E-08	5.9561	18	1.23E-05
Scr_Coef_LH	3.55494	68	0.00069321	3.22012	54	0.0021711	2.4751	18	0.023491
Scr_Coef_RH	6.05281	68	6.87E-08	3.87937	54	0.00028667	4.3293	18	0.00040396
Scr_Coef_OTLA_LH	13.6549	68	3.66E-21	10.1926	54	3.47E-14	8.7618	18	6.55E-08

**Table 2.** One-sample t-test results for activation vs. baseline levels, by grade level.

	Kindergarten			1st grade			2nd grade		
Metric	T-stat	D F	P-value	T-stat	D F	P-value	T-stat	D F	P-value
D_L_S_Coef_LH	-0.036011	68	0.97138	-0.27404	54	0.7851	-0.049688	18	0.96092
D_L_S_Coef_RH	-3.164	68	0.0023274	-0.010849	54	0.99138	-0.99183	18	0.33443
D_L_S_Coef_OTLA_LH	-7.0479	68	1.16E-09	-6.8766	54	6.54E-09	-4.0342	18	0.00077828
D_S_Coef_LH	-1.4611	68	0.1486	-0.96501	54	0.33884	-0.20677	18	0.83851
D_S_Coef_RH	-4.3096	68	5.40E-05	-1.4563	54	0.1511	-1.6428	18	0.11779
D_S_Coef_OTLA_LH	-8.7845	68	8.27E-13	-8.8117	54	4.94E-12	-5.3653	18	4.24E-05
D_L_Coef_LH	1.2656	68	0.20998	0.81188	54	0.42043	0.16827	18	0.86825
D_L_Coef_RH	-0.21809	68	0.82801	1.6052	54	0.11428	0.076369	18	0.93997
D_L_Coef_OTLA_LH	-1.348	68	0.18214	-2.1502	54	0.036037	-0.60819	18	0.55066
L_D_S_Coef_LH	-2.1532	68	0.034851	-1.6762	54	0.099483	-0.31653	18	0.75524
L_D_S_Coef_RH	-2.4499	68	0.016868	-2.7463	54	0.008172	-1.2416	18	0.23033
L_D_S_Coef_OTLA_LH	-5.2857	68	1.43E-06	-4.5067	54	3.57E-05	-3.2605	18	0.0043436
L_S_Coef_LH	-2.5725	68	0.012285	-1.7101	54	0.09298	-0.34067	18	0.7373
L_S_Coef_RH	-3.7678	68	0.00034665	-2.983	54	0.0042779	-1.8711	18	0.077684
L_S_Coef_OTLA_LH	-8.0547	68	1.74E-11	-8.2407	54	4.04E-11	-5.0703	18	7.98E-05

**Table 3.** One-sample t-test results for activation differences, by grade level.

	Kindergarten			1st grade			2nd grade		
Metric	T-stat	D F	P-value	T-stat	D F	P-value	T-stat	D F	P-value
DvO_LH	-1.151	68	0.25378	1.0754	54	0.28696	1.8427	18	0.081911

DvO_RH	2.6444	68	0.010152	2.5324	54	0.014268	1.0703	18	0.29861
DvO_OTLA_LH	3.4747	68	0.00089494	3.3396	54	0.0015263	3.6362	18	0.0018888
DvS_LH	1.2007	68	0.23404	3.8902	54	0.00027687	2.0272	18	0.057717
DvS_RH	5.2748	68	1.49E-06	3.7154	54	0.00048265	2.1583	18	0.044657
DvS_OTLA_LH	6.065	68	6.54E-08	5.9198	54	2.29E-07	5.2894	18	4.98E-05
DvL_LH	-6.0345	68	7.40E-08	-3.3622	54	0.0014266	2.8577	18	0.010457
DvL_RH	-2.2587	68	0.027111	0.020923	54	0.98338	-0.067508	18	0.94692
DvL_OTLA_LH	0.055679	68	0.95576	-0.63035	54	0.53112	0.71844	18	0.48171
LvO_LH	-1.1473	68	0.25528	-0.78174	54	0.43778	2.4073	18	0.027017
LvO_RH	1.2439	68	0.2178	1.8453	54	0.070486	2.0717	18	0.052943
LvO_OTLA_LH	3.556	68	0.00069089	1.9501	54	0.056358	2.1185	18	0.048306
LvS_LH	1.3408	68	0.18445	2.2355	54	0.029542	1.8745	18	0.077185
LvS_RH	4.3679	68	4.39E-05	3.6092	54	0.00067246	3.324	18	0.0037762
LvS_OTLA_LH	6.3984	68	1.69E-08	5.7505	54	4.27E-07	4.0616	18	0.00073217

**Table 4.** One-sample t-test results for category-level representational geometry, by grade level.

Metric	Kindergarten			1st grade			2nd grade		
	T-stat	DF	P-value	T-stat	DF	P-value	T-stat	DF	P-value
SVM_Dig_LH	1.5388	68	0.1285	0.79166	54	0.43202	-1.5197	18	0.14595
SVM_Dig_RH	0.012621	68	0.98997	-0.98126	54	0.33084	1.4046	18	0.17716
SVM_Dig_OTLA_LH	-0.12008	68	0.90477	-1.2445	54	0.2187	-0.8543	18	0.40417
SVM_Let_LH	1.8178	68	0.073502	-1.2775	54	0.20688	0.771	18	0.45071
SVM_Let_RH	0.31934	68	0.75044	-1.2055	54	0.23325	-1.6999	18	0.10637
SVM_Let_OTLA_LH	-0.10457	68	0.91702	1.0736	54	0.2878	-0.39921	18	0.69444

**Table 5.** One-sample t-test results for exemplar decodability, by grade level.

Metric	Kindergarten			1st grade			2nd grade		
	T-stat	DF	P-value	T-stat	DF	P-value	T-stat	DF	P-value
ITNA_lh_Ars17_lh_IFC	15.8236	53	9.96E-22	13.4692	44	3.26E-17	10.9399	18	2.20E-09
ITNA_rh_Ars17_rh_IFC	17.6494	53	7.57E-24	16.5388	44	1.68E-20	13.5696	18	6.81E-11
OTLA_lh_Ars17_lh_IFC	16.69	53	9.39E-23	15.5732	44	1.62E-19	10.6118	18	3.55E-09
ITNA_lh_Ars17_rh_IFC	14.8437	53	1.60E-20	12.271	44	8.45E-16	8.55272	18	9.34E-08
ITNA_rh_Ars17_lh_IFC	18.7055	53	5.28E-25	16.0387	44	5.37E-20	15.797	18	5.40E-12
OTLA_lh_Ars17_rh_IFC	16.054	53	5.27E-22	15.2373	44	3.66E-19	9.51808	18	1.90E-08

**Table 6.** One-sample t-test results for background functional connectivity, by grade level.

Metric	Kindergarten			1st grade			2nd grade		
	T-stat	DF	P-value	T-stat	DF	P-value	T-stat	DF	P-value
ITNA_lh_Ars17_lh_DvLS	-2.7582	53	0.0079586	-1.0647	44	0.29281	-0.14919	18	0.88306
ITNA_rh_Ars17_rh_DvLS	0.72662	53	0.47066	0.55374	44	0.58256	-0.57821	18	0.57029
OTLA_lh_Ars17_lh_DvLS	-1.6933	53	0.096264	-0.35989	44	0.72065	1.1653	18	0.25912
ITNA_lh_Ars17_lh_DvS	-2.8718	53	0.0058565	-0.58647	44	0.56055	0.55553	18	0.58537
ITNA_rh_Ars17_rh_DvS	0.10734	53	0.91492	0.5345	44	0.59569	-0.87351	18	0.39389
OTLA_lh_Ars17_lh_DvS	-1.3633	53	0.17856	-0.93633	44	0.35422	1.6487	18	0.11656
ITNA_lh_Ars17_lh_DvL	-2.7582	53	0.0079586	-1.0647	44	0.29281	-0.14919	18	0.88306
ITNA_rh_Ars17_rh_DvL	0.72662	53	0.47066	0.55374	44	0.58256	-0.57821	18	0.57029
OTLA_lh_Ars17_lh_DvL	-1.6933	53	0.096264	-0.35989	44	0.72065	1.1653	18	0.25912
ITNA_lh_Ars17_lh_LvDS	0.23578	53	0.81451	1.1096	44	0.27322	1.5094	18	0.14856
ITNA_rh_Ars17_rh_LvDS	-0.41574	53	0.67928	-0.11012	44	0.91282	0.051145	18	0.95977
OTLA_lh_Ars17_lh_LvDS	1.0022	53	0.32081	-0.68124	44	0.49929	0.36565	18	0.71889
ITNA_lh_Ars17_lh_LvS	-1.292	53	0.20197	0.62734	44	0.53368	1.8105	18	0.086942
ITNA_rh_Ars17_rh_LvS	-1.5023	53	0.13895	0.1229	44	0.90275	-0.4548	18	0.65469
OTLA_lh_Ars17_lh_LvS	0.25979	53	0.79603	-1.024	44	0.31145	0.90509	18	0.37737

**Table 7.** One-sample t-test results for task-evoked connectivity with  $IPS_{Ratio}$  ROIS, by grade level.

### 3.5 Discussion

#### 3.5.1 Novel symbols elicit strong responses in digit and letter areas

A striking observation from our analyses of mean activation in OTC areas was the strong response to the novel (Scrambled) stimuli. Our modeling suggested that all ROIs showed a significant positive response to these symbols at school entry (Figure 17A). The magnitude of the Scrambled response was approximately twice as large as the response to Digits and Letters in the right ITNA and OTLA (Figure 17A). In direct contrasts, both ROIs show significant negative values at school entry for Digits > Scrambled and Letters > Scrambled (Figure 18A), indicating these OTC areas are more sensitive to novel symbols than familiar symbols in 5-6 year old

children. There are several potential explanations for this finding. Note that we will get to a discussion of how responses change over schooling, but this more general discussion of the task and Scrambled response will help set the stage for later interpretations of the underlying developmental mechanisms.

First, it is possible that a systematic difference in the perceptual features of the scrambled stimuli contributed to increased OTC responses, e.g., through bottom-up visual mechanisms. This is unlikely to be the case as the scrambled set used in the present study was matched to the digits and letter sets in terms of number of pixels and was designed to be equivalent in terms of the number of angles and curves (G. R. Price & Ansari, 2011). Critically, a recent analysis of these same stimuli empirically demonstrated that there were no differences in the perimetric (visual) complexity across symbol categories (D. J. Yeo et al., 2020), corroborating earlier work comparing digits and letter features (Schubert, 2017), and further confirming that the present results were not driven by differing perceptual features between stimuli.

The present result is consistent with a “novelty” effect observed in fMRI studies whereby activity increases in response to unfamiliar versus familiar stimuli (de Chastelaine, Mattson, Wang, Donley, & Rugg, 2017; Diana, Yonelinas, & Ranganath, 2007). In the task used here, participants were instructed to judge whether they “knew the name” of the symbol. However, only a “yes” or “no” button press was required, making the task at its core a decision about stimulus *familiarity*. Attending to this feature may have amplified the “novelty” effect compared to other task settings. Notably, however, in studies using passive and perceptual matching tasks, where stimulus identity is irrelevant, an increased OTC response to novel symbols compared to digits and/or letters has similarly been observed using fMRI and event-related potentials (Park, Chiang, Brannon, & Woldorff, 2014; Park et al., 2012; Vinckier et al., 2007). The differential

response in these studies was instead attributed to a general increase in “attentional engagement” with the unfamiliar symbols. This suggests that the present result is not solely an artifact of task demands, but be explainable via Price & Devlin’s interactive account, where a novelty effect can occur with or without explicit cognitive goals as a function of *prediction errors* (for further discussion, see Introduction section 1.3.4).

### **3.5.2 An increasing preference for digits in the right ITNA**

The interactive account makes a clear prediction about the developmental course of OTC activation over learning, proposing an inverted-U shaped trajectory. In the pre-learning stage, there are no representations associated with a stimulus and thus no top-down predictions or prediction error. The response in OTC at this stage is characterized as a more purely bottom-up response based on the stimulus’ visual features. After some (unspecified) amount of learning, predictions are generated, but they are imprecise, resulting in high prediction error and increased OTC activity. With repeated experience, the distributed representations become more refined and OTC activity declines to an intermediate level (C. J. Price & Devlin, 2011). In light of the previous discussion, it should be noted that the children in the present study had been exposed to the Scrambled stimuli on at least two separate occasions before their first scan, during mock scanner training and the day-of-scan practice session. The brief exposure, coupled with the required task of making an active decision about these symbols, may have been sufficient for participants to already attach “meaning” to the novel shapes, placing our children in the early learning/high prediction error/increased OTC activation part of the curve. More importantly, this proposal predicts that the response to digits and letters in OTC areas should *decrease* over children’s time in school. This model stands in contrast to more traditional “maturational” or “expertise-based” accounts of OTC development, whereby category-preferring areas become

*increasingly* sensitive over learning, responding more strongly to their preferred object domain, albeit emphasizing different underlying mechanisms (L. Cohen & Dehaene, 2004; Gauthier, 2000; Johnson, 2011).

So, what (if any) developmental trajectory do we see in the response levels of three ROIs analyzed here? First, there were no significant effects of academic months on the stimulus versus baseline activity levels for any symbol category or ROI (Figure 17B), suggesting that the raw sensitivities of symbol areas to novel and familiar symbols are (linearly) stable over K-2<sup>nd</sup> grade. To test for potential nonlinear effects, we fit models with a quadratic term (academic months<sup>2</sup>), which could indicate exponential or non-monotonic (e.g., inverted-U) growth. For instance, a recent study found that the *volume* of OTC responses to words first increased and then receded over the same window studied here (Dehaene-Lambertz et al., 2018). Their result was mixed, however, as functionally localized peaks of word-sensitivity (defined retrospectively) showed a reliable *linear increase* in their response to words. In the present case, we found that linear models were superior to quadratic models in all cases, indicating there was insufficient evidence of a more complex trajectory.

Though the category versus baseline responses were relatively stable, there was some evidence that the right ITNA's response to digits *relative* to other symbols increased over schooling. This effect was particularly driven by the Digits > Scrambled contrast (Figure 18B), as there was no evidence for an increasing preference for digits over letters. Relatedly, in Figure 17B, there appears to be a “trade-off” in sensitivity to digits (increasing) versus scrambled symbols (decreasing) in the right ITNA. Though the effect is relatively weak, this finding represents the first evidence that the ITNA's selectivity for digits over novel symbols increases in children. On the other hand, given an increasing preference for digits over letters *was not*



observed, we cannot claim the right ITNA is becoming more specialized for digit processing over this window. The lack of univariate selectivity for digits compared to letters is consistent with prior studies in 4-9 year old children (Cantlon et al., 2011; Dehaene-Lambertz et al., 2018; Nordt et al., 2018, 2020; Park et al., 2018), and taken together, suggests that a “mature” ITNA selectivity for digits must emerge later in development.

Our results may be considered consistent with the *pruning account*, whereby selectivity for one category (Digits) emerges due to a *decreasing* response to non-preferred categories (Scrambled) (Cantlon et al., 2011). However, a strict interpretation of pruning predicts that the sensitivity to all symbols starts out roughly *similar*. In the present case, the responses to Scrambled started out much higher than to Digits, emphasizing the importance of considering task-induced, top-down modulations when interpreting these results. We further did not observe significant changes in the *sensitivity* to any category (i.e., no significant decrease in Scrambled sensitivity) , so the story appears more complex, potentially involving several interacting developmental mechanisms (see General Discussion section 4.3 for more on these findings and their implications).

### **3.5.3 Increasing digit-biased categorical representations in left ITNA**

Representational similarity analysis (RSA) provides a potentially more powerful analytical approach to characterizing the representational content of a region. At the scale of whole ROIs as used here (5-10mm), focusing on a univariate measure of average activity risks missing the fine-grained detail contained in the *spatial pattern* of responses across a region. In the present study, we assessed the extent to which neural representational geometry in symbol areas fit with category-level representational models, and whether fits changed over schooling. Of the three regions, the most significant changes were observed in the left ITNA, which showed

increasing correlation to the Digit vs. Other, Digit vs. Scrambled, and Digit vs. Letter model RDMs over months in school (Figure 19B). We interpret this finding as representing a “digit-biased” developmental trajectory in the left ITNA, as it was only the models involving digits as a distinct category that showed an effect of school. No such effect was observed for the letter-focused models (Letter vs. Other, Letters vs. Scrambled). In the right ITNA, the Digit vs. Letter geometry also positively increased, suggesting some shift towards a category-level representational hierarchy in this region. It is important to note, however, that an effect for the Digit vs. Letter model on its own provides no evidence of a bias for either category – it simply reflects greater within versus between category similarity, i.e., categorical distinction.

As RDM similarity provides evidence for or against a particular representational geometry, it is critical to discuss the aforementioned changes in the context of the raw (Spearman Z) values. As can be appreciated in the mean levels by grade in the left ITNA (Figure 19A), the RDM similarity was first *negative* in K-1<sup>st</sup> grade and then reached relatively strong positive values in our 2<sup>nd</sup> grade sample. Upon closer examination of the neural RDMs (not depicted), we found that the pairwise relationships in exemplar activity patterns were near zero *between* categories (as predicted in the model RDM), indicating that digit and letter representations were unrelated. Critically though, the *negative* RDM similarity was driven by (weakly) anti-correlated responses to exemplars *within* each category. In other words, the model RDM for Digits vs. Letter predicts similar patterns within a category, but in younger children, the opposite was observed. The positive slope (Figure 19B, left ITNA) and positive RDM similarity in 2<sup>nd</sup> graders (Figure 19A, left ITNA), suggests that the left ITNA carried some symbol *identity* information early on, but over schooling, transitioned towards categorical representation. This interpretation is in line with the results of our exemplar-decoding analyses which indicated decreasing

decoding accuracy over schooling for letters ( $p < 0.01$ ) and digits (nonsignificant, negative trend) in the left ITNA (Figure 20A,B). Interestingly, using the adult dataset described in Chapter 1 where participants performed an (active) serial search task, our lab recently found no evidence of exemplar discriminability in the left or right ITNA for either digits or letters (Yeo et al., *in prep*). Both regions instead showed strong discriminability at the category level. Thus, in the present data, we may be observing a developmental shift towards a more “adult-like” state of categorical representation in the left ITNA.

The right ITNA also demonstrated a positive slope for the Digits vs. Letter model and similarly started with a negative fit in kindergartners (Figure 19A). In contrast to the left, RDM similarities in the right ITNA ended up near *zero* in 1<sup>st</sup> and 2<sup>nd</sup> graders, indicating no evidence for representational distinction between digits and letters. This is perhaps puzzling in light of a recent study which found strong evidence for categorical geometries in the right *but not* the left ITNA (D. J. Yeo et al., 2020). That study used data from a passive viewing task so indexed a more “spontaneous” symbol representation process compared to the task used here. It is nevertheless possible that a Digit vs. Letter geometry develops later in the right ITNA, outside of the K-2<sup>nd</sup> grade window, and so was not yet evident in our sample. The right ITNA did, however, demonstrate early and stable fits to the Digit vs. Scrambled and Letter vs. Scrambled models and to a greater extent than observed in the left ITNA (Figure 19A). Our results suggests that category information *is* represented in the right ITNA, but at a supraordinate “familiar vs. novel” level, and that this representational geometry is already present at school entry.

While we have heretofore conceived of a unidirectional, maturational shift in ITNA representations, an important caveat is that, at least in adults, representational content in the ITNAs appears to be *task-specific*. For instance, when access to digit identity and/or numerical

magnitude is required for task performance, there is some evidence that the left ITNA and right OTC can represent digit identity (Lyons & Beilock, 2018; Wilkey et al., 2020). Additionally, in a separate analysis of the visual search task data from Chapter 2, though a group-level mean effect was absent, the *degree* of digit discriminability in the left ITNA related to calculation ability in adults (Yeo et al., *in prep*). It is thus doubtful that the apparent developmental decline in exemplar discriminability we observed here reflects a reduction the ITNA's *capacity* for exemplar representation. Indeed, though it remains open area of investigation, some researchers have postulated that the ITNAs can flexibly shift between category and identity-level representations, depending on task demands (Grotheer et al., 2016; D. J. Yeo et al., 2020, 2017). Here, the children performed a categorization task, which may bias towards categorical geometries at the neural level. The shift towards category discrimination could reflect more strategic modulation of the ITNAs as children progress in school, rather than an fundamental change in how the region processes symbols. Again, the balance of top-down versus bottom-up effects makes interpretation of these data challenging, particularly for a region that interfaces between sensory and associative networks. Studies using a range of task contexts will likely be required to better understand the nature of ITNA representational flexibility, both how it manifests in the mature state and develops in children.

In the OTLA, representational geometries were not significantly related to time in school. However, relatively strong categorical organization was observed in this region as early as kindergarten (Figure 19A), as indicated by the positive RDM similarities for all but the Digits vs. Letters model. The effects were only significant when the Scrambled condition was part of the model, suggesting the OTLA distinguishes familiar from novel symbols but, notably, does not distinguish between digits and letters. The effects for the digit-focused and letter-focused models

were in fact qualitatively similar, providing no evidence for a “letter-bias” in terms of the OTLA’s representational geometry over K-2<sup>nd</sup> grade. In considering these results, it is important to note that the OTLA’s univariate response to all symbol categories was over twofold that of ITNAs (Figure 17A) and the raw difference in the Scrambled versus Digit and Letter responses was similarly scaled (Figure 18A). In our RSA procedure we implemented mean pattern subtraction (also referred to as “cocktail-blanket removal”), which helps avoid artificially inflated correlations by removing the shared component across *all* conditions (Misaki et al., 2010; Walther et al., 2016). This procedure does not explicitly remove differences in response amplitudes *between* conditions – meaning that the univariate difference for the Scrambled condition was still present in the scaled response patterns and may have influenced pattern correlations. On the other hand, the Pearson correlation is invariant to the magnitude and scale of two variables. So, if a *constant* univariate difference was present, i.e., affecting all voxels/nodes to a similar extent, the representational distance between two patterns should be unrelated to their average amplitudes. To verify whether or not Scrambled response amplitudes were associated with representational geometries, we performed a supplementary analysis looking at the simple cross-correlations in these values across all observations included in the primary analyses (n=145). We found that the magnitude of the Scrambled response in the OTLA was not significantly correlated with RDM similarity values (all  $ps > 0.05$ ). However, the univariate contrast results were negatively related to the corresponding RDM similarity scores ([D>S ~ D vs. S],  $r = -0.168$ ,  $p = 0.043$ ; [L>S ~ L vs. S],  $r = -0.174$ ,  $p = 0.037$ ), indicating that a stronger mean response to the Scrambled relative to familiar symbols was associated with greater representational distinction between categories. These results suggest that Scrambled symbols evoked a category-specific pattern of activity across the ROI and that these sets of nodes, in sum,

showed a stronger BOLD signal change than the patterns elicited by familiar symbols.

### **3.5.4 No evidence for symbol identity representations in symbol-preferring ROIs**

Consistent with Yeo et al. (*in prep*) who found no exemplar-level (digit) discriminability at the group level in the ITNAs, we saw no evidence of above-chance exemplar decoding at any age (Figure 20). Yeo et al. did, however, find that individual differences digit discriminability in the left ITNA related to math ability, suggesting spontaneous engagement of identity representations may be related to increased experience/expertise with symbolic number. Further analysis will be required to determine whether differences in exemplar representation are already associated with math ability in this sample. The lack of group-level evidence for exemplar representations in the present study may be due to the task being generally insufficient to engage exemplar-level representations in the ITNAs, or these representations may not emerge until later developmental windows.

### **3.5.5 The ITNAs are functionally connected to number-sensitive IPS by kindergarten**

To test predictions of the interactive specialization hypothesis, we examined the spontaneous (“background”) and task-evoked functional connectivity (FC) of the ITNAs and OTLA with functionally defined target regions in the bilateral intraparietal sulcus, and modeled the developmental trajectory of these measures over K-2<sup>nd</sup> grade. Focusing first on background connectivity, we observed strong coupling of all three ventral stream ROIs with the bilateral parietal ROIs across grade levels (Figure 21A), suggesting these functional circuits are established prior to school entry. Our results are consistent with the study from Nemmi and colleagues (2018), who looked at resting-state connectivity of the right/left ITNA and VWFA, with target clusters in the left and right IPS defined by showing a developmental increase in ITNA connectivity over age (3-21 years old) (Nemmi et al., 2018). Their IPS clusters fell within

the anatomical constraints masks used here (~12mm and 7mm away from our left and right parietal coordinates) and their VWFA was within 4mm of our OTLA coordinate, making for a particularly comparable set of results. From 3 years of age, all three symbol areas showed above zero connectivity (Fisher  $Z \approx 0.2$ ) with the left and right IPS, indicating that spontaneous coupling between OTC areas and the IPS *precedes* the learning of symbolic notations. In fact, recent work looking at resting-state connectivity in human neonates has shown that the lateral OTC is already connected to inferior parietal areas (Barttfeld et al., 2018) and the VWFA already demonstrates adult-like connectivity patterns (J. Li et al., 2020), consistent with observations that the global layout of resting-state networks are largely present *at birth* (Doria et al., 2010; Fransson et al., 2007). Early-developing functional connectivity organization has been taken to support the “proto-map” hypothesis, which posits that a blueprint for functional specialization is laid out in gestation (Arcaro & Livingstone, 2017; Rakic, 1988) and, fits generally within the “maturational” view of brain development.

Though all of our seed ROIs were already significantly connected to the bilateral IPS at kindergarten, there were notable differences between regions (Figure 21A). The ipsilateral connection between the right ITNA and right IPS was considerably stronger than the homologous connections of the left ITNA and OTLA to left IPS. In paired tests, the differences were significant within every grade bin (all  $ps < 0.038$ ). This result is in line with our adult work in Chapter 2, where we found increased functional and structural connectivity of the right ITNA to right IPS compared to the homologous circuit in the left hemisphere. As we discussed there, considerable evidence exists for a rightward asymmetry to number processing, particularly in children (Cantlon et al., 2006; Cantlon & Li, 2013; Hyde et al., 2010; Izard et al., 2008; Kersey & Cantlon, 2017a; Lochy & Schiltz, 2019; S. E. Vogel et al., 2015). The present findings provide

the first direct evidence that asymmetric functional connectivity between the ITNA and IPS is present as early as kindergarten. A fascinating future direction for this work will be to understand whether asymmetry is also present in the white matter pathways connecting these areas, and whether individual differences in structural asymmetry relate to functional connectivity. For instance, in considering the biased connectivity hypothesis, it remains unclear the extent to which functional or structural connectivity is more important in driving cortical specialization, as largescale white matter architecture is also adult-like at birth (Dubois et al., 2014). If structural and functional connectivity are strongly linked over development, it would suggest they mutually guide neural specialization, but a divergence may indicate differing contributions. Another outstanding question is whether asymmetry in this pathway relates to behavior. Some evidence points towards individual differences in *left* hemispheric processing to be specifically related to symbolic number abilities (e.g., Emerson and Cantlon, 2015; Evans et al., 2015; Yeo et al., *in prep*). If IPS-ITNA circuit asymmetry scaffolds lateralized responses to numbers, e.g., through competitive dynamics (Behrmann & Plaut, 2020), early-observable individual differences in asymmetry may prove behaviorally relevant.

### **3.5.6 No parietal bias in left ITNA versus OTLA connectivity**

In comparing the left ITNA and OTLA ROIs, we found they were similarly connected to the left IPS across grade levels (all  $ps > 0.27$ ), indicating no domain-specific *bias* in functional connectivity among left hemisphere symbol areas (Figure 21A). This finding suggests that, at least in terms of functional connectivity, the left ITNA is not preferentially connected to number-sensitive areas of the IPS compared to the nearby OTLA area, contrary to what may be expected based on a strong interpretation of the biased connectivity hypothesis (Hannagan et al., 2015). Our results corroborate those of Nemmi and colleagues (2018), who found that left ITNA and



VWFA connectivity to left IPS did not differentiate until 9.8 years of age, at which point ITNA connectivity steadily increased. Similarly, in their study of neonatal connectivity, Barttfeld and colleagues (2018) noted that no difference was observed between VWFA and the more lateral cortex associated with ITNA in terms of coupling to inferior parietal cortex, speculating that “it is possible such patterns of functional specialization emerge through exposure and learning and that initially only a rough division between mesial and lateral regions is visible” (Barttfeld et al., 2018, p. 3117). Though we will return to this idea in the following discussion of the task-evoked connectivity patterns, our results indicated no change in connectivity to the left IPS over K-2<sup>nd</sup> grade for either the left ITNA or OTLA. It should be noted that the developmental change observed in the study of Nemmi et al. (2018) occurred over 3-21 years of age. The lack of change we observed here (for all three of our ROIs, Figure 21B), despite having a larger sample size in the 5-8 year old range, suggests that developmental increases in spontaneous coupling between the ITNAs and IPS are not robust within this narrower window and rather occurs over a longer timescale.

To the extent that biased connectivity operates *across* hemispheres, we also expected the left ITNA to be more connected than the OTLA to the right IPS. Even if the left IPS undergoes protracted development, the right IPS is known to already be involved in number processing by kindergarten (Cantlon et al., 2006; Holloway et al., 2010; Kersey & Cantlon, 2017a; Libertus et al., 2009), and so may preferentially interact with the left ITNA. Our results argue against this hypothesis, at least in terms of early *functional* connectivity (Figure 21A). Compared to the left ITNA, the OTLA was *more* connected to the contralateral right IPS in K and 1<sup>st</sup> grade ( $t(53) = 2.44, p = 0.018$ ;  $t(44) = 2.26, p = 0.029$ ). This represents the only major divergence from Nemmi et al.’s (2018) results, which found that left ITNA-right IPS connectivity was already stronger

than VWFA-right IPS connectivity by 3.9 years. It is likely that spontaneous interactions between OTC areas and IPS are stronger in background connectivity measured during task performance compared to rest (e.g., due to increased visuo-perceptual processing (Norman-Haignere et al., 2012)), as suggested by the relatively higher Fisher Z values we observed here ( $\approx 0.35$  versus  $0.2$  in Nemmi et al.). This discrepancy may be important for understanding differences in the present results and future studies looking at resting-state connectivity patterns.

### **3.5.7 No digit-selective coupling of the ITNAs with IPS and no change over schooling**

Interactive specialization emphasizes the experientially-driven development of regional networks, which are dynamically engaged based on particular task demands (Anderson, 2015; Johnson, 2011). Based on this model, we predicted that the ITNA would be selectively coupled with number-sensitive IPS regions when recognizing digits compared to other symbols. That is, if the ITNA-IPS circuit facilitates the “mapping” of number symbols to magnitude referents in parietal cortex, over learning it should develop into a number-preferring functional network. A strong Numerical Stroop interference effect (i.e., where number identity interfered with judgements about physical size) was present in our kindergarten sample ( $t(66) = 4.70, p = 1.4e^{-5}$ ), suggesting these children were already *implicitly* and/or *automatically* mapping digits to their semantic representations. In the present categorization task, we thus expected to 1) find evidence of implicit mapping in kindergarten in terms of digit-selective coupling between ITNA-IPS and 2) increasing digit-specific coupling over schooling, as this domain-specific circuit is repeatedly engaged during math instruction. Our results supported neither of these predictions. The digit-specific coupling (Digits > Other, > Scrambled, and > Letters) in the left hemisphere was significantly *negative* in kindergartners and rose to approximately zero by 2<sup>nd</sup> grade (Figure 22A). The fixed effect of academic months, however, was not significant (Figure 22B),

suggesting that the trajectory of change was inconsistent across participants and/or unrelated to time in school. Though the positive trend in the left hemisphere suggests digit-specific coupling may eventually be established later in school, the very same trend was observed for the letter-specific contrasts, which more conclusively argues against an interactive specialization account. Moreover, in the right hemisphere, the letter-specific contrasts showed positive trends, but the digit-specific trends were *negative*, further indicating that this circuit is not *preferentially* engaged by digits. As previously discussed, however, the categorization task employed here required no access to numerical magnitude and so may not sufficiently engage the ITNA-IPS circuit. Finally, even if implicit engagement of number-sensitive populations in IPS occurred in this task, it is plausible this activity is too weak or even undetectable at the spatial resolution acquired here (2.5 x 2.5 x 3.25mm). In monkeys, for instance, it has been shown that only 15-20% of neurons within the number-sensitive VIP region of IPS code for nonsymbolic number (Nieder, 2016). Intracranial recordings in humans suggest this percentage is likely to be even smaller for symbolic numbers (Daitch et al., 2016; Kutter et al., 2018). We therefore must avoid interpreting the present null result as evidence of *absence* of an effect. Future work in a comparative sample of adults will be important to determine whether the ITNA-IPS circuit is selectively engaged within this particular task paradigm in the mature state. It may be that higher-level tasks, such as number comparison or arithmetic, are necessary to evoke this functional circuit.

### **3.6 Limitations**

#### **3.6.1 COVID-19**

We began MRI scanning for the longitudinal study described in early 2018, and the baseline Kindergarten sessions were acquired through the summer of 2019. The subsequent

timepoints thus were scheduled for 2019-2020, and 2020-2021. In early March 2020, all research activities were put on indefinite hold due to the COVID-19 pandemic. The shutdown unfortunately occurred at nearly the midpoint of data collection for the project. This resulted in a reduced sample size for the present analyses, with a particularly limited set of three-timepoint participants from which (within-subject) linear trajectories can be reliably estimated. This guided our statistical approach focused on population-level fixed effects, rather than within-subject trajectories and individual differences in relation to behavior (e.g., how baseline connectivity predicts 2<sup>nd</sup> grade activation or numerical ability). As more data is acquired over the coming months, alternative approaches will be possible.

In mid-August 2020, we did resume scanning, but at a limited capacity and with numerous new safety protocols. Some aspects, e.g., limited exposure to study personnel or required masking during MRI, could have systematically affected these sessions in unexpected ways and impacted our results. Furthermore, the virtual schooling and other environmental factors associated with the pandemic may have unduly influenced our sample. Critically, however, of the 145 scan sessions included in the present analyses, only 16 (11%) occurred after the study resumed, suggesting minimal impact on our results.

### **3.6.2 Assumption of normality and individual differences in trajectories**

Where the fixed effect of academic months was insignificant, it is possible that the assumption of normality was violated. For instance, a bimodal distribution, where subsets of participants showed either strong positive or negative slopes, could lead to a null result (Schielzeth et al., 2020). In this situation, while the null effect is statistically “true,” the conclusion of “stable” response pattern over the developmental window would be invalid. We qualitatively examined histograms of the raw participant-level slopes for each model and found

no notable cases of a bimodal distribution. We further visually inspected residual plots and found no concerns of nonnormality. Nevertheless, significant *variability* in slope estimates was common. Understanding the neural and behavioral relevance of these individual differences will be an important avenue of future investigation, but was outside the scope of the present work.

### **3.6.3 Group-level ROI Definition**

Our use of group-level ITNA and OTLA ROIs was principally motivated based on several factors (see Chapter 3 section 3.3.12). However, this approach is undoubtedly imperfect. The size of these ROIs was relatively small and may have missed the “sensitive” area in some (or many) subjects, due to misalignment of cortical surfaces and/or true anatomical variability in ITNA location. We extracted activation estimates from 6mm smoothed data (with the exception of RSA and MVPA analyses) in an effort to minimize this variability. Though it was not possible here, individually localized fROIs, defined retrospectively, may be the most sensitive approach, such as adopted in similar longitudinal studies (Dehaene-Lambertz et al., 2018; Saygin et al., 2016). A more thorough investigation of individual differences in the location and spatial extent of digit-related activity across the occipitotemporal cortex may be a fruitful next step in the present sample, but again, was outside the scope of this dissertation.

## **3.7 Conclusions**

We present here a series of longitudinal analyses looking at how the functional profile of symbol areas changes over the first three years of formal schooling. Our study improved upon prior work in several ways, including a large sample size, an active symbol processing task, and multiple measures of functional differentiation. Our results provide the first evidence that the ITNAs become increasingly “numeral-biased” in their response profiles and representational

geometries in early school-age children. More generally, our findings provide novel insights into experience-dependent functional plasticity in the ventral visual cortex.

## CHAPTER 4

### GENERAL DISCUSSION

The representation and processing of alphanumeric symbols in the brain provides an appealing model system for probing mechanisms of brain function and development. Humans use abstract signs, such as letters and numbers, to efficiently tap into distributed brain networks involved in language and mathematics. The invention of written symbol systems occurred too recently in human history for dedicated brain circuits to have *evolved* for their use (Dehaene & Cohen, 2007). Remarkably, however, after sufficient learning, numbers and letters are found to engage distinct areas along the ventral visual pathway within the occipitotemporal cortex (OTC), including bilateral regions responsive to numerals and a left-lateralized region responsive to letters (Hannagan et al., 2015). The ventral pathway supports object recognition, housing neural populations that represent “what” an input is (i.e., properties of its identity). In humans and non-human primates, the OTC contains a patchwork of areas whose spatial layout is *consistent* and largely organized around behaviorally-relevant *categories* of experience, including regions preferentially involved in processing faces, bodies, places, and manipulable objects (Tsao et al., 2003). Numbers and letters carve out their respective niches within this pre-existing circuitry but, many outstanding questions remain. For instance, why are symbol areas segregated and consistently localized where they are? How and when do they come to acquire their preference for one set of symbols versus another?

#### 4.1 Digit versus letter area connectivity

An influential class of theories posit that the functional role of any given brain region is dictated by its *connections* to and *communication* with other regions involved in particular

cognitive and behavioral capacities (Hannagan et al., 2015; Johnson, 2011; Mahon & Caramazza, 2011; Riesenhuber, 2007). Such principles may help to explain the differential locations and hemispheric asymmetries of number and letter areas (Behrmann & Plaut, 2020). To test these theories, researchers have turned to increasingly sophisticated approaches for non-invasively measuring axonal wiring and interactivity in the human brain. These methods have provided an unprecedented window into brain architecture and organization, particularly in the OTC. However, only a few studies have examined the connectivity of number and letter areas (Abboud et al., 2015; Barttfeld et al., 2018; Grotheer et al., 2019; Nemmi et al., 2018). In our first empirical chapter (Chapter 2), we used state-of-the-art methods to assess, for the first time, both the structural and functional connectivity of symbol areas in the same group of individuals.

Our analyses revealed marked distinctions in Digit and Letter-area connectivity. As predicted by the biased-connectivity hypothesis, we found that the Digit area had more axonal projections to inferior parietal regions involved in numerical magnitude representation and arithmetic, including the intraparietal sulcus (IPS) (Figure 5E). During the symbol detection task, stimulus-evoked responses of the Digit area and IPS were also more strongly coupled (Figure 6D), implying that these areas more readily communicate in service of behavior. The present findings provide evidence of a brain circuit plausibly involved in mapping symbols to abstract numerical quantities, and one that appears critical to symbolic number abilities and mathematics in humans (Amalric & Dehaene, 2016, 2018). If this circuit is intact *before* symbol learning, it may *constrain* the localization of number processing in the OTC and help explain why the ITNA is consistently localized in the posterior ITG, lateral to letter and word form areas. Of course, observing this domain-specific circuit in adults does not directly address the claim that connectivity is a *causal driver* of functional specification – after all, increased connectivity could



be a *consequence* of numeracy acquisition. Nevertheless, our findings are generally consistent with connectivity-based accounts in terms of what should be observed in the mature state. Together with findings that the ITNA is already functionally connected to the same frontoparietal network we observed here by 3 years of age (Nemmi et al., 2018), and that structural connectivity patterns in pre-reading children can predict the future location of the VWFA (Saygin et al., 2016), our results build on the mounting body of evidence for connectivity-constrained processing of symbols in the OTC.

A important caveat to the above interpretation is that the Digit area *also* showed greater structural connectivity (than the Letter area) to putative *language* regions, including the superior temporal and inferior frontal gyri (Figure 5E), which may be taken as evidence *against* the biased-connectivity hypothesis. One possibility is that it is actually the VWFA, which lies slightly anterior to the Letter area we analyzed here, that is preferentially connected to language areas. In the present study, we used functionally defined locations of digit and letter sensitivity to specifically address why responses to these categories are segregated within the same (asemantic) task context. One may argue, though, that *words* rather than single letters are mapped to language representations, and so, a more apt test of biased-connectivity involves comparison of ITNA and VWFA proper.

While we agree this is an interesting question for future work, we did find, as predicted, that the Letter area was more *functionally* connected to language areas (Figure 6D). This result indicates a significant *dissociation* between structural and functional connectivity measures. The connectivity-based theories we have discussed herein do not explicitly differentiate the roles of structural versus functional connectivity in driving regional selectivity. Often the two modalities have been conflated and/or expected to go in the same direction, even in current discussions of

the topic (Q. Chen, Garcea, Almeida, & Mahon, 2017; Op de Beeck et al., 2019). As we outlined in Chapter 1, functional interactions can occur over *polysynaptic* pathways that are not typically considered (or directly assessable) in tractography analyses. Based on this fact alone, it seems unwise to conflate structural and functional connectivity.

Our results strongly suggest that the assumption of correspondence between connectivity measures is unfounded, at least in consideration of anterior OTC areas. It further highlights the utility of including multiple modalities in one study, where the ROIs and participant sample are consistent between analyses. Going forward, it will be important to clarify the relative contributions of functional and structural connectivity to OTC organization, and further refine existing theoretical frameworks. Directly comparing modalities in future longitudinal studies of OTC development will be particularly helpful in this regard (e.g., *how do structural or functional connectivity patterns uniquely predict future specialization?*).

A final observation to reiterate is that the Digit and Letter areas were members of distinct functional networks (Figure 6D). We found that the Digit area was associated with the putative frontoparietal “control” network (FPN), corroborating previous reports of posterior ITG coupling in studies of resting-state and task-evoked connectivity (Abboud et al., 2015; Cole et al., 2013; Marek & Dosenbach, 2018; Nemmi et al., 2018; Vincent et al., 2008; B. T. Yeo et al., 2011). In contrast, the Letter area was functionally connected to primary visual, superior temporal, dorsal attention, somatomotor, and insular regions, generally consistent with reported connectivity patterns of the VWFA (L. Chen et al., 2019; Nemmi et al., 2018; A. C. Vogel et al., 2012; B. T. Yeo et al., 2011). Thus, despite their close proximity, digit and letter-preferring areas fall on either side of a steep *gradient* in functional connectivity with the rest of the brain. If the tenets of connectivity-based accounts hold, our findings would suggest that digits and letters engage

qualitatively distinct networks.

How these largescale networks map onto *semantic* domains has received recent attention in the literature. Over a series of studies, Amalric & Dehaene have demonstrated that the frontoparietal-inferior temporal network is preferentially involved in processing mathematical versus nonmathematical semantic statements (Amalric & Dehaene, 2016, 2019). The same network was engaged across all levels of numerical tasks, from the recognition of digits to high-level mathematical reflection. The authors have argued for a broad dissociation in the networks supporting math versus linguistic skills (Amalric & Dehaene, 2018). They cite a recent study that further supports their idea in which a brain “atlas” of semantic knowledge was presented (e.g., emotional, social, locational, abstract, numeric, tactile, temporal, visual, etc.) (Huth, De Heer, Griffiths, Theunissen, & Gallant, 2016). A distributed set of regions, similar to the Digit-area network we observed here, was selective for a semantic dimension that included *numeric* words (e.g., “four”, “extra”, “shillings”, “pairs”, “smaller”, “double”, etc.). More medial areas, including the occipitotemporal sulcus and fusiform gyrus, did not show this selectivity (Huth et al., 2016). Together with these studies, our data suggest that the localization of digit processing in the OTC may be due to this area’s involvement in a largescale brain system that is particularly well suited for mathematical thinking. It is possible that this system was originally geared towards the processing of magnitude and space, and in modern humans, is co-opted for usage in symbolic number abilities. However, given the frontoparietal/inferior temporal system has been proposed more generally as “hub” network involved in “adaptive task control” (Cole et al., 2013), or a “multiple-demand” network central to “intelligent thought and action” (J. Duncan, 2010), its particular involvement in (even rudimentary) numerical operations remains mysterious (Amalric & Dehaene, 2018). Future work will be necessary to understand the functional roles of

digit and letter areas within largescale networks. Insights may come through analysis of network-level connectivity across different task contexts (Conrad et al., 2020), but also through more nuanced characterization of the local stimulus preferences and representational content within these areas (D. J. Yeo et al., 2020).

## 4.2 Hemispheric asymmetries in ITNA connectivity

Connectivity is thought to constrain not only the localization of categorical selectivity in the OTC, but also the *hemispheric lateralization* of selectivity (Behrmann & Plaut, 2020). Perhaps the most well documented example of asymmetric selectivity is that of word processing in the left hemisphere and face processing in the right. Though it is unclear whether letter processing is already biased to the left hemisphere in pre-reading children (Cantlon et al., 2011; Maurer, Brem, Bucher, & Brandeis, 2005), what is clear is that a preference for letters and words reliably emerges in the left fusiform gyrus/occipitotemporal sulcus in the earliest stages of reading acquisition (Tracy M. Centanni et al., 2018; Dehaene-Lambertz et al., 2018; Dehaene et al., 2015; Lochy & Schiltz, 2019; Nordt et al., 2018). It is commonly recognized that the left hemisphere's dominance in language processing contributes to VWFA lateralization, but more specifically, *why might this occur?* First, the restriction of language faculties to one hemisphere is thought to afford increased processing efficiency and, though the origins are still debated, it appears to be tied to innate asymmetries in white matter architecture already present at birth (Behrmann & Plaut, 2015; Dehaene-Lambertz, Dehaene, & Hertz-Pannier, 2002; Dubois et al., 2014, 2009). This functional asymmetry is thus in place long before the learning of alphanumeric symbols. An additional pressure at play is the fact that forming and maintaining axons comes at a significant *wiring cost*. Most axonal projections in the mammalian brain are relatively short and few exist *between* hemispheres, aside from connections among homologous regions via the

corpus collosum (Behrmann & Plaut, 2020; Rubinov, Ypma, Watson, Bullmore, & Raichle, 2015). Thus, left hemisphere regions involved in phonological representation and speech production only directly project to areas of the *left* OTC. Even if both hemispheres are suitable for alphanumeric symbol processing, the VWFA naturally emerges in left due to these architectural constraints. Remarkably, the emergence of a *rightward* lateralization for *face* processing appears to coincide with VWFA development. Evidence suggests that the fusiform gyrus is initially bilaterally engaged by faces but, as one learns to read, the left fusiform is increasingly recruited for word recognition (Behrmann & Plaut, 2015, 2020). Words and faces are thought to draw on similar computational resources, e.g., foveal vision and a need for fine discrimination among similar exemplars, so a *competition* for cortical space is thought to play out. Ultimately, the VWFA “wins out” in the left fusiform and the right fusiform is increasingly relied on for face recognition, leading to consistent localization of the FFA in the right hemisphere.

In the case of number processing in the OTC, as we have discussed, *both* hemispheres appear to support digit recognition, depending on the task context. This provides an intriguing opportunity to explore connectivity-based constraints on functional asymmetry in the brain. Based on neuropsychological evidence, Cohen & Dehaene proposed differential contributions of the left and right ITNAs, but empirical investigation into these differences has only recently begun (L. Cohen & Dehaene, 1995; D. J. Yeo et al., 2020). A central question is, if either ITNA is able to process digits, *are their roles redundant or complementary?* We hypothesized that asymmetric connectivity profiles may differentially constrain the function of the ITNAs. In Chapter 2 we aimed characterize and compare, for the first time, the structural and functional connectivity of left and right ITNA.

Based on the triple-code model of number processing (Figure 1), along with evidence that language dominance in the left hemisphere affects OTC organization, we predicted that the left ITNA would show stronger within-hemisphere connectivity to language areas. Conversely, given the well documented rightward dominance for magnitude processing (see Chapter 2 Introduction), based on the same logic we predicted stronger connectivity would be observed within the right ITNA-IPS circuit. Our results agreed with both predictions. Compared to the same pathway in the right hemisphere, the left ITNA had significantly more axonal projections to the opercular IFG, a region involved in speech perception and production (Figure 5F). The left ITNA showed greater functional coupling with areas of middle temporal gyrus and superior temporal sulcus, regions implicated in phonological and lexical processes (Figure 6E). In the right hemisphere, we found stronger structural and functional connectivity of the ITNA with the IPS and inferior parietal lobe. According to the triple-code model, the left “visual number form” area should have privileged access to the language system (i.e., the “verbal code”), and our findings support this idea. Conversely, though the triple-code model did not explicitly predict asymmetry in the ITNA to IPS (i.e., the “magnitude” code) circuit, our results suggest the right ITNA has privileged access to the magnitude system. The present results suggest this access is not simply a matter of *proximity*, but reveal significant *asymmetries* in the connectional architecture within each hemisphere.

Given this was a sample of adults, we cannot speak to the *origins* of asymmetry in these circuits – the observed patterns could predate the learning of number symbols, arise as a consequence, or (most likely) involve a mixture of both. In any case, based on the idea that connectivity *constrains* the function of OTC areas, our findings suggest that the left ITNA should support the mapping of digits to verbal word forms (e.g., during retrieval-based arithmetic

or multi-digit reading), and potentially any higher order numerical or mathematical operation centered on linguistic representations. It was recently shown, for instance, that mathematical formulas and constants selectively activated the left ITNA in mathematicians much more so than in controls, whereas responses were similar between groups in the right ITNA (Amalric & Dehaene, 2016). It is plausible that these (advanced) mathematical “objects” are more *lexicalized* in mathematicians, and so more readily engage verbal systems via the left ITNA (Yeo et al., *in prep*).

The rightward lateralization of the ITNA-IPS (“visual-to-quantity code”) circuit may consequently lead to a biased involvement of the right ITNA in numerical tasks that tap non-verbal and more purely quantitative concepts. For instance, we recently found that during a number comparison task the right ITNA, but not the left, was functionally associated with a network of parietal areas (Conrad et al., 2020). Given an association with quantity is a *categorically* distinct feature of digits, activity in the right ITNA may be more *selective* for digits versus other symbol categories. This may explain why the right ITNA is more robustly observed in tasks that contrast digit versus letter processing, for example (Lochy & Schiltz, 2019; Park et al., 2014, 2018; D. J. Yeo et al., 2017). Additionally corroborating this idea, Yeo et al. recently found digit-biased categorical representations in the right ITNA, but not the left, during passive viewing of symbols (D. J. Yeo et al., 2020). Again, the idea here is that rightward lateralization of this circuit leads to more robust quantity-related (and therefore categorically distinct) information in the right ITNA.

To conclude, our study provides novel evidence that the ITNAs are asymmetrically connected within their respective hemispheres. These findings are consistent with the triple-code model of number processing and may explain a number of functional asymmetries observed in

prior work. Future studies will be required to understand *how* and *in what contexts* the left and right ITNAs leverage their privileged connectivity with language and magnitude systems.

### **4.3 The functional development of symbol areas**

As we have discussed, symbol areas in the OTC have the potential to inform us, not only on how function may be locally constrained within the brain but also, on fundamental mechanisms of brain development and experience-dependent plasticity. In my introduction section 1.3, I introduced several theories of cortical development and how these ideas may apply to symbol processing in the OTC, including: innate proto-maps and the shape hypothesis, biased connectivity, interactive specialization, and the interactive account (Arcaro & Livingstone, 2017; Hannagan et al., 2015; Johnson, 2011; C. J. Price & Devlin, 2011). With these theoretical frameworks providing backdrop, in Chapter 3, we explored how and when the ITNAs develop their functional preferences for digits over children’s first years of formal schooling and compared these trajectories with those of a nearby letter area (OTLA).

#### **4.3.1 The shape hypothesis**

First let us consider the shape hypothesis, which builds off the notion that *proto-maps* of neural specialization emerge innately in the primate OTC as a product of shared visual features and/or computational requirements across object categories (Hannagan et al., 2015). This hypothesis posits that symbol processing rests on the foveal-based recognition of object shapes, or the “adjacency of the component parts of an object,” involving representations that are invariant to the particular physical features of the stimulus. This computational requirement should lead to a rough confinement of symbol selectivity within the OTC, across an area encompassing at least the NFA and VWFA. In line with this idea, we found that symbol areas



were generally responsive to numbers, letters, and scrambled symbols across K-2<sup>nd</sup> grade, with above baseline responses consistently observed for each symbol category and grade level (albeit to a larger extent for scrambled, presumably due to a novelty effect; Figure 17). Mean response levels to digits and letters were also similar within each area (Figure 18). This suggests that similar computational processes may be occurring in these areas, regardless of symbol type, as predicted by the shape hypothesis. Responses were already observed in kindergarteners and did not change over the study, suggesting the mechanisms underlying this activity are both early-developing and stable, at least within the window analyzed here. We cannot say, however, that these computations are *symbol*-specific or even *shape*-based. Responses to other types of stimuli, not included in our paradigm, would need to be examined. Furthermore, given we focused on *a priori* ROIs, we also cannot say whether shared processing of symbols occurred *outside* of the hypothesized shape-sensitive zone. For instance, if similar, above-baseline responses to symbols were observed in medial areas of OTC, traditionally implicated in peripheral vision and place/scene processing, it would argue against a visual feature-specific account such as put forward in the shape hypothesis. Though outside the scope of the present work, this question can be addressed in future analyses of our data (e.g., inclusion of FFA and PPA ROIs and/or whole-brain analyses). In summary, our results point to an early-developing recruitment of the ITNAs and OTLA for symbol processing that is consistent with Hannagan et al.'s shape hypothesis. Other task paradigms and analyses will be required to understand the nature of these (presumably) shared computations, including their spatial distribution and specificity to symbols. Sampling from children's earliest exposure to alphanumeric symbols onward may be necessary to delineate the developmental origins of these processes.

### 4.3.2 The interactive account

Further reflecting on the mean activity levels we observed, a clear finding was the strong response to novel (scrambled) symbols in the ITNAs and OTLA. In section 3.5.1, I discussed at length how Price & Devlin’s interactive account may help to explain the novelty effects observed here and elsewhere. In general, this result highlights an imperative need for studies of OTC function to consider both top-down and bottom-up effects, and how they may interact in different task paradigms. One way researchers have skirted around this problem is the use of passive designs, which are suggested to reduce the confound of top-down effects (Dehaene & Cohen, 2011). However, in their interactive account, Price & Devlin review evidence that top-down signaling occurs *automatically*, challenging the supposed “purity” of passive designs. Perhaps more importantly, the engagement with symbols that we *really care about* involves active, attentional processing, e.g., in the classroom or workplace, at the grocery store, in the car, etc. In this sense, active tasks are more *ecologically valid*, engaging brain systems that support symbol *use* in service of some goal (even if just simple classification). Of course, as we have come up against here, top-down and bottom-up effects make for a more complicated story. It will be important to incorporate into models of OTC selectivity and development both feedforward and feedback inputs, and how each of these sources may differentially change with experience. Furthermore, it will be necessary to not only consider these effects in a theoretical sense, but also in an empirical sense, via measures of effective connectivity such as dynamic causal modelling (Booth, Mehdiratta, Burman, & Bitan, 2008; K J Friston et al., 2017; Zeidman et al., 2019), or high-resolution laminar fMRI methods which can help disentangle input and output-related signals within a cortical area (Yang, Huber, Yu, & Bandettini, 2021).

In an attempt to address the development of top-down signals, the interactive account

does make some predictions about how learning modifies OTC responses (C. J. Price & Devlin, 2011). An inverted U-shaped trajectory was proposed, starting with no activity in “pre-learning”, high activity during early learning, and, as prediction errors are minimized, reduced activity with expertise. Some evidence for such a process exists, suggesting OTC responses to words *peak* sometime in K-2<sup>nd</sup> grade period as children learn to read (Dehaene-Lambertz et al., 2018; Maurer et al., 2006; note that in Dehaene-Lambertz et al., an inverted-U curve was observed in terms of the *volume* of word-selective activation around the VWFA, while responses at the peak voxel of VWFA activity showed a linear increase in selectivity). In the case of single alphanumeric symbols, however, our interpretation of Price & Devlin’s proposal is that the transition from “Stage 1” (pre-learning/no activity) to “Stage 2” (early learning/high activity) would occur *before* kindergarten, when children are first exposed to symbols (and their labels/referents) at home or in preschool. Though speculative, based on this model, we would expect to observe peak responses to single digits and letters sometime around school entry, with a linear *decrease* in activity levels over 1<sup>st</sup> and 2<sup>nd</sup> grade. Whatever the case, in our data, we did not observe either decreasing or inverted U-shaped trajectories at the group level (Figure 18-19; note we tested models with quadratic terms, but these fits were inferior to simpler linear models). It is nevertheless possible that individual variability in the *onset* of this process exists, such that some children are increasing while others are decreasing, leading to a null group effect like we see here. We cannot adequately test this hypothesis in the present dataset, as detecting non-linear trajectories *within* individuals would require more than three timepoints (King et al., 2018). It may be revealing, however, to examine individual or subgroup differences in “increasers” and “decreasers”, and how trajectories relate to concurrent symbol processing abilities. Ultimately, future studies involving repeatedly-sampled individuals will be necessary to characterize

inverted U-shaped plasticity in the OTC. Novel symbol training studies in adults may be necessary to capture the entirety of this process, given the challenges involved in imaging young children.

### 4.3.3 The biased connectivity hypothesis

The two connectivity-focused ideas we outlined in the introduction, biased connectivity and interactive specialization, emphasize roles for axonal projections and co-activation in defining a region's functional selectivity over learning. Several observations from the present developmental results speak to these theories. First, the biased connectivity hypothesis posits that innate connectivity of the ITNA with numerical magnitude-sensitive areas of parietal cortex drive the ITNA towards a preference for numerals (Hannagan et al., 2015). We longitudinally measured “background” functional connectivity in our sample, i.e., the degree to which symbol areas and IPS sites spontaneously co-activated over an entire fMRI session. Both ITNAs, as well as the OTLA, showed positive coupling with the IPS that was significant at school entry and stable over the K-2<sup>nd</sup> grade window (Figure 21). However, the right ITNA-IPS coupling was *particularly* strong, suggesting two features are already present at school entry: 1) *biased* connectivity of the right ITNA with IPS (compared to the OTLA), and 2) a rightward *asymmetry* to the ITNA-IPS pathway. These findings are consistent with prior work looking at resting-state connectivity of the ITNA in young children and adults (Abboud et al., 2015; Nemmi et al., 2018), as well as with our study of adults in Chapter 2 (Figure 5F; Figure 6E). Taken together, it appears that “privileged” connectivity of the right ITNA with IPS is present prior to the learning of alphanumeric symbols, and so may plausibly serve as a pre-existing constraint on *where* numeral preference will ultimately develop in the OTC. There remains a considerable amount of work to be done, however, to fully test the predictions of the biased connectivity hypothesis as it

pertains to number processing. For instance, Hannagan and colleagues originally proposed biases in the *structural* connectivity of symbol areas, despite they and others interpreting measures of *functional* connectivity as a proxy for the same mechanism (Barttfeld et al., 2018; Hannagan et al., 2015; J. Li et al., 2020; Nemmi et al., 2018). One study of VWFA structural connectivity showed that white matter projections in pre-reading predict the future location of word-selectivity, and so suggests that white matter *scaffolds* OTC development (Saygin et al., 2016). It will be important to perform analogous longitudinal analyses for the ITNA, to determine whether a similar scaffolding process is at play within the numeral-selective network. Further, in light of our adult findings showing considerable *discrepancies* between structural and functional connectivity of OTC areas, it seems premature to assume that structure and function contribute to local specialization in the same manner. The inclusion of both modalities in a single developmental study will be helpful in refining the biased connectivity framework into a more precise theory.

#### **4.3.4 Interactive specialization**

Compared to the biased connectivity hypothesis, Johnson's theory of interactive specialization is a more all-encompassing account of neural development, including predictions about how local responses evolve over learning (Johnson, 2001, 2011). One overarching principle adopted in interactive specialization is the idea that "to learn is to eliminate," and our results of ITNA activity levels (and possibly representational geometry) speak to this idea (Changeux & Dehaene, 1989; Johnson & de Haan, 2015). Johnson builds from an assumption that cortical areas are first broadly tuned, responding similarly to stimuli with shared features (e.g., written symbols – note the consistency here with the shape hypothesis). Over experience, as domain- and/or stimulus-specific networks are repeatedly co-activated, activation will become

more *focal*, confined to particular areas such as the ITNA, and *selective*, in that responses to preferred inputs are maintained while responses to non-preferred inputs are reduced. To explain this at the neuronal level, Johnson invokes the idea of “selective stabilization” through synaptic pruning, referring to the process by which a subset of synapses is maintained while others are eliminated (Changeux & Dehaene, 1989; Johnson & de Haan, 2015). In the case of the ITNA, a pruning account predicts a stable response level for digits over learning (similar *sensitivity* over time) with a decreasing response to non-preferred characters (increasing *selectivity* over time). Though this had not yet been demonstrated in the ITNA, some evidence exists for pruning within the VWFA and FFA (Cantlon et al., 2011; Joseph, Gathers, & Bhatt, 2011; Kubota, Joo, Huber, & Yeatman, 2019). In our analysis, we found that the right ITNA’s sensitivity to digits was roughly stable (Figure 17), while selectivity for digits increased over schooling (Digits > Others, Digits > Scrambled; Figure 18). This is consistent with an account of increasing specialization of the right ITNA via synaptic pruning, providing the first evidence that such a process may occur for digits. Critically, however, the effect seemed to be driven by differential responses to digits versus scrambled symbols, and *not* by digits versus letters. If the right ITNA does ultimately “care” more about digits than letters (and not familiar versus novel symbols more generally), our results suggest its development extends beyond the K-2<sup>nd</sup> grade window, or possibly is not directly related to children’s time in school. We have thus demonstrated only partial evidence for pruning in the right ITNA. Given the aforementioned novelty effect involving the scrambled symbols, and how this may also be modulated by experience, it remains difficult to fully square our results with any one particular model. As is the norm in neuroscience, things are more complicated than we may wish!

As we outlined in our Introduction section 1.3.3, a central claim in interactive

specialization is that repeated coactivation of groups of regions in service of some goal leads to increasing selectivity at a network level. Based on this account, we expected to see inter-regional functional connectivity between the ITNA and number-sensitive IPS increase over the study. Not only should this network become more selectively engaged by digits, but also, as a byproduct of increased coactivity during schooling, background connectivity between the ITNA and IPS may also increase. We found no evidence that either form of connectivity was related to children's time in school (Figure 21/Figure 22), which may be taken as evidence against the interactive specialization model. However, for our connectivity analyses, we made assumptions about not only the location (and surface area) of digit selectivity but also the target location in the IPS. The particular *scale* at which interactive specialization should operate (e.g., from synapses to largescale functional regions) is admittedly vague, so it is hard to disprove based on this (or any one) study alone. As a first step, it may be fruitful to assess whether the ITNA's connectivity with *any* region changes over time in a whole-brain analysis.

Alternatively, our null findings could be due to the developmental process extending beyond the K-2<sup>nd</sup> window. For example, Nemmi et al. found that intrinsic connectivity of ITNA and IPS increases from early childhood to at least early adulthood (Nemmi et al., 2018). Future work following task-evoked and stimulus-specific connectivity patterns over longer developmental periods will be informative in this regard. Additionally, it may be important to employ task designs which explicitly engage the number-processing network, as opposed to the low-level categorization task employed here. For instance, evidence *in favor* of interactive specialization was presented in a recent longitudinal study of arithmetic in 8-14 year-olds, where connectivity between the OTC and IPS during an arithmetic task increased over time (Battista et al., 2018). Interestingly, the control task in that study was a number identification task,

suggesting that increasing specialization of the OTC-IPS circuit occurs for higher-order processing of numbers *over and above* simple visual recognition. Though outside the scope of the present work, the symbolic comparison task we acquired here may be a more fruitful paradigm for testing longitudinal predictions of interactive specialization in the K-2<sup>nd</sup> grade window.

#### **4.3.5 Representational similarity**

Though it appears the ITNAs are not yet fully specialized, in the traditional univariate sense, for processing digits over letters by 2<sup>nd</sup> grade, they may already carry information about the distinction between symbol categories. In section 3.2, we reviewed recent empirical work showing representational patterns in OTC are established early in development, potentially before selectivity is first observable (M. A. Cohen et al., 2019; Dehaene-Lambertz et al., 2018; Nordt et al., 2018). Our results indicate that category-level representational geometry is at least *changing* in a consistent manner, particularly in the left ITNA (Figure 19B). Taken together with previous findings, our work suggests that investigations of representational content in the OTC is a potentially fruitful avenue for future developmental studies. To our knowledge, there exist no developmental theories that directly address the emergence of representational geometry, so the implications of our findings are still unclear. For instance, are distributed activity patterns fundamentally different from focal activity? If not, they may be driven by the same causal mechanisms (e.g., synaptic pruning, fine-grained axonal projection patterns, etc.). Our results point to differential trajectories in the left and right ITNA, so the emergence of numeral processing in the OTC may be a particularly useful model for disentangling and/or uniting representational geometry from local selectivity.



#### **4.4 Final Remarks**

In this dissertation, I used symbol processing in the ventral stream as a model system for understanding how human learning interacts with innate brain architecture. Our findings were consistent with the idea that long-range connectivity patterns, in terms of axonal wiring and regional communication, determine the location and lateralization of newly-acquired functions in the brain. We further found that brain areas preferentially engaged by Arabic numerals in adults become increasingly tuned to numerals as children go through school, providing novel evidence of experience-dependent plasticity. Our work speaks to several theories of brain organization and development, but perhaps more importantly, opens the door to a number of future directions.

## REFERENCES

- Abbasi, N., Duncan, J., & Rajimehr, R. (2020). Genetic influence is linked to cortical morphology in category-selective areas of visual cortex. *Nature Communications*, *11*(1). <https://doi.org/10.1038/s41467-020-14610-8>
- Abboud, S., Maidenbaum, S., Dehaene, S., & Amedi, A. (2015). A number-form area in the blind. *Nature Communications*, *6*, 6026. <https://doi.org/10.1038/ncomms7026>
- Allendorfer, J. B., Hernando, K. A., Hossain, S., Nenert, R., Holland, S. K., & Szaflarski, J. P. (2016). Arcuate fasciculus asymmetry has a hand in language function but not handedness. *Human Brain Mapping*, *37*(9), 3297–3309. <https://doi.org/10.1002/hbm.23241>
- Allison, T., McCarthy, G., Nobre, A., Puce, A., & Belger, A. (1994). Human extrastriate visual cortex and the perception of faces, words, numbers, and colors, *4*(5), 544–554. Retrieved from <http://cercor.oxfordjournals.org/cgi/content/abstract/4/5/544>
- Amalric, M., & Dehaene, S. (2016). Origins of the brain networks for advanced mathematics in expert mathematicians. *Proceedings of the National Academy of Sciences*, *113*(18), 4909–4917. <https://doi.org/10.1073/pnas.1603205113>
- Amalric, M., & Dehaene, S. (2018). Cortical circuits for mathematical knowledge: Evidence for a major subdivision within the brain’s semantic networks. *Philosophical Transactions of the Royal Society B: Biological Sciences*, *373*(1740), 20160515. <https://doi.org/10.1098/rstb.2016.0515>
- Amalric, M., & Dehaene, S. (2019). A distinct cortical network for mathematical knowledge in the human brain. *NeuroImage*, *189*, 19–31. <https://doi.org/10.1016/j.neuroimage.2019.01.001>
- Anderson, M. L. (2015). Précis of after Phrenology: Neural Reuse and the Interactive Brain. *Behavioral and Brain Sciences*, *39*(2016). <https://doi.org/10.1017/S0140525X15000631>
- Anderson, M. L., Kinnison, J., & Pessoa, L. (2013). Describing functional diversity of brain regions and brain networks. *NeuroImage*, *73*, 50–58. <https://doi.org/10.1016/j.neuroimage.2013.01.071>
- Andersson, J. L. R., Graham, M. S., Zsoldos, E., & Sotiropoulos, S. N. (2016). Incorporating outlier detection and replacement into a non-parametric framework for movement and distortion correction of diffusion MR images. *NeuroImage*, *141*, 556–572. <https://doi.org/10.1016/j.neuroimage.2016.06.058>
- Andersson, J. L. R., Skare, S., & Ashburner, J. (2003). How to correct susceptibility distortions in spin-echo echo-planar images: Application to diffusion tensor imaging. *NeuroImage*, *20*(2), 870–888. [https://doi.org/10.1016/S1053-8119\(03\)00336-7](https://doi.org/10.1016/S1053-8119(03)00336-7)
- Andersson, J. L. R., & Sotiropoulos, S. N. (2016). An integrated approach to correction for off-resonance effects and subject movement in diffusion MR imaging. *NeuroImage*, *125*, 1063–1078. <https://doi.org/10.1016/j.neuroimage.2015.10.019>
- Ansari, D. (2008). Effects of development and enculturation on number representation in the brain. *Nature Reviews Neuroscience*, *9*(4), 278–291. <https://doi.org/10.1038/nrn2334>
- Anticevic, A., Dierker, D. L., Gillespie, S. K., Repovs, G., Csernansky, J. G., Van Essen, D. C., & Barch, D. M. (2008). Comparing surface-based and volume-based analyses of functional neuroimaging data in patients with schizophrenia. *NeuroImage*, *41*(3), 835–848. <https://doi.org/10.1016/j.neuroimage.2008.02.052>
- Arcaro, M. J., & Livingstone, M. S. (2017). A hierarchical, retinotopic proto-organization of the primate visual system at birth. *ELife*, *6*, 1–24. <https://doi.org/10.7554/eLife.26196>
- Arcaro, M. J., Schade, P. F., Vincent, J. L., Ponce, C. R., & Livingstone, M. S. (2017). Seeing

- faces is necessary for face-domain formation. *Nature Neuroscience*, 20(10), 1404–1412. <https://doi.org/10.1038/nn.4635>
- Arsalidou, M., Pawliw-Levac, M., Sadeghi, M., & Pascual-Leone, J. (2017). Brain areas associated with numbers and calculations in children: Meta-analyses of fMRI studies. *Developmental Cognitive Neuroscience*, 30(July 2017), 239–250. <https://doi.org/10.1016/j.dcn.2017.08.002>
- Arsalidou, M., & Taylor, M. J. (2011). Is  $2+2=4$ ? Meta-analyses of brain areas needed for numbers and calculations. *NeuroImage*, 54(3), 2382–2393. <https://doi.org/10.1016/j.neuroimage.2010.10.009>
- Baker, C. I., Liu, J., Wald, L. L., Kwong, K. K., Benner, T., & Kanwisher, N. (2007). Visual word processing and experiential origins of functional selectivity in human extrastriate cortex. *Proceedings of the National Academy of Sciences of the United States of America*, 104(21), 9087–9092. <https://doi.org/10.1073/pnas.0703300104>
- Barrick, T. R., Lawes, I. N., Mackay, C. E., & Clark, C. A. (2007). White matter pathway asymmetry underlies functional lateralization. *Cerebral Cortex*, 17(3), 591–598. <https://doi.org/10.1093/cercor/bhk004>
- Barttfeld, P., Abboud, S., Lagercrantz, H., Adén, U., Padilla, N., Edwards, A. D., ... Dehaene-Lambertz, G. (2018). A lateral-to-mesial organization of human ventral visual cortex at birth. *Brain Structure and Function*, 223(7), 3107–3119. <https://doi.org/10.1007/s00429-018-1676-3>
- Battista, C., Evans, T. M., Ngoon, T. J., Chen, T., Chen, L., Kochalka, J., & Menon, V. (2018). Mechanisms of interactive specialization and emergence of functional brain circuits supporting cognitive development in children. *Npj Science of Learning*, 3(1), 1. <https://doi.org/10.1038/s41539-017-0017-2>
- Behrmann, M., & Plaut, D. C. (2015). A vision of graded hemispheric specialization. *Annals of the New York Academy of Sciences*, 1359(1), 30–46. <https://doi.org/10.1111/nyas.12833>
- Behrmann, M., & Plaut, D. C. (2020). Hemispheric Organization for Visual Object Recognition: A Theoretical Account and Empirical Evidence\*. *Perception*, 49(4), 373–404. <https://doi.org/10.1177/0301006619899049>
- Behzadi, Y., Restom, K., Liao, J., & Liu, T. T. (2007). A component based noise correction method (CompCor) for BOLD and perfusion based fMRI. *NeuroImage*, 37(1), 90–101. <https://doi.org/10.1016/j.neuroimage.2007.04.042>
- Ben-Shachar, M., Dougherty, R. F., Deutsch, G. K., & Wandell, B. A. (2011). The Development of Cortical Sensitivity to Visual Word Forms. *Journal of Cognitive Neuroscience*, 23(9), 2387–2399. <https://doi.org/10.1162/jocn.2011.21615>
- Berman, M. G., Park, J., Gonzalez, R., Polk, T. A., Gehrke, A., Knaffla, S., & Jonides, J. (2010). Evaluating functional localizers: The case of the FFA. *NeuroImage*, 50(1), 56–71. <https://doi.org/10.1016/j.neuroimage.2009.12.024>
- Binder, J. R. (2015). The Wernicke area: Modern evidence and a reinterpretation. *Neurology*, 85(24), 2170–2175. <https://doi.org/10.1212/WNL.0000000000002219>
- Booth, J. R., Mehdiratta, N., Burman, D. D., & Bitan, T. (2008). Developmental increases in effective connectivity to brain regions involved in phonological processing during tasks with orthographic demands. *Brain Research*, 1189(1), 78–89. <https://doi.org/10.1016/j.brainres.2007.10.080>
- Bouhali, F., Thiebaut de Schotten, M., Pinel, P., Poupon, C., Mangin, J.-F., Dehaene, S., & Cohen, L. (2014). Anatomical Connections of the Visual Word Form Area. *Journal of*

- Neuroscience*, 34(46), 15402–15414. <https://doi.org/10.1523/JNEUROSCI.4918-13.2014>
- Bouhali, Florence, Bézagu, Z., Dehaene, S., & Cohen, L. (2019). A mesial-to-lateral dissociation for orthographic processing in the visual cortex. *Proceedings of the National Academy of Sciences*, 116(43), 201904184. <https://doi.org/10.1073/pnas.1904184116>
- Bracci, S., Cavina-Pratesi, C., Ietswaart, M., Caramazza, A., & Peelen, M. V. (2012). Closely overlapping responses to tools and hands in left lateral occipitotemporal cortex. *Journal of Neurophysiology*, 107(5), 1443–1446. <https://doi.org/10.1152/jn.00619.2011>
- Bracci, S., Ritchie, J. B., & de Beeck, H. O. (2017). On the partnership between neural representations of object categories and visual features in the ventral visual pathway. *Neuropsychologia*, 105(October 2016), 153–164. <https://doi.org/10.1016/j.neuropsychologia.2017.06.010>
- Bray, S., Arnold, A. E. G. F., Iaria, G., & MacQueen, G. (2013). Structural connectivity of visuotopic intraparietal sulcus. *NeuroImage*, 82, 137–145. <https://doi.org/10.1016/j.neuroimage.2013.05.080>
- Brem, S., Bach, S., Kucian, K., Kujala, J. V., Guttorm, T. K., Martin, E., ... Richardson, U. (2010). Brain sensitivity to print emerges when children learn letter–speech sound correspondences. *Proceedings of the National Academy of Sciences*, 107(17), 7939–7944. <https://doi.org/10.1073/pnas.0904402107>
- Brincat, S. L., & Connor, C. E. (2006). Dynamic shape synthesis in posterior inferotemporal cortex. *Neuron*, 49(1), 17–24. <https://doi.org/10.1016/j.neuron.2005.11.026>
- Buchanan, C. R., Bastin, M. E., Ritchie, S. J., Liewald, D. C., Madole, J. W., Tucker-Drob, E. M., ... Cox, S. R. (2020). The effect of network thresholding and weighting on structural brain networks in the UK Biobank. *NeuroImage*, 211(November 2019), 116443. <https://doi.org/10.1016/j.neuroimage.2019.116443>
- Bugden, S., Price, G. R., McLean, D. A., & Ansari, D. (2012). The role of the left intraparietal sulcus in the relationship between symbolic number processing and children’s arithmetic competence. *Developmental Cognitive Neuroscience*, 2(4), 448–457. <https://doi.org/10.1016/j.dcn.2012.04.001>
- Bugden, S., Woldorff, M. G., & Brannon, E. M. (2019). Shared and distinct neural circuitry for nonsymbolic and symbolic double-digit addition. *Human Brain Mapping*, 40(4), 1328–1343. <https://doi.org/10.1002/hbm.24452>
- Caballero-Gaudes, C., & Reynolds, R. C. (2017). Methods for cleaning the BOLD fMRI signal. *NeuroImage*, 154(December 2016), 128–149. <https://doi.org/10.1016/j.neuroimage.2016.12.018>
- Cantlon, J. F., Brannon, E. M., Carter, E. J., & Pelphrey, K. A. (2006). Functional imaging of numerical processing in adults and 4-y-old children. *PLoS Biology*, 4(5), 844–854. <https://doi.org/10.1371/journal.pbio.0040125>
- Cantlon, J. F., & Li, R. (2013). Neural Activity during Natural Viewing of Sesame Street Statistically Predicts Test Scores in Early Childhood. *PLoS Biology*, 11(1). <https://doi.org/10.1371/journal.pbio.1001462>
- Cantlon, J. F., Pinel, P., Dehaene, S., & Pelphrey, K. A. (2011). Cortical representations of symbols, objects, and faces are pruned back during early childhood. *Cerebral Cortex*, 21(1), 191–199. <https://doi.org/10.1093/cercor/bhq078>
- Carreiras, M., Quiñones, I., Hernández-Cabrera, J. A., & Duñabeitia, J. A. (2015). Orthographic coding: Brain activation for letters, symbols, and digits. *Cerebral Cortex*, 25(12), 4748–4760. <https://doi.org/10.1093/cercor/bhu163>

- Castaldi, E., Vignaud, A., & Eger, E. (2020). Mapping subcomponents of numerical cognition in relation to functional and anatomical landmarks of human parietal cortex. *NeuroImage*, 221(March), 117210. <https://doi.org/10.1016/j.neuroimage.2020.117210>
- Catani, M., Allin, M. P. G., Husain, M., Pugliese, L., Mesulam, M. M., Murray, R. M., & Jones, D. K. (2007). Symmetries in human brain language pathways correlate with verbal recall. *Proceedings of the National Academy of Sciences of the United States of America*, 104(43), 17163–17168. <https://doi.org/10.1073/pnas.0702116104>
- Centanni, T. M., Norton, E. S., Ozernov-Palchik, O., Park, A., Beach, S. D., Halverson, K., ... Gabrieli, J. D. E. (2019). Disrupted left fusiform response to print in beginning kindergartners is associated with subsequent reading. *NeuroImage: Clinical*, 22(February), 101715. <https://doi.org/10.1016/j.nicl.2019.101715>
- Centanni, Tracy M., King, L. W., Eddy, M. D., Whitfield-Gabrieli, S., & Gabrieli, J. D. E. (2017). Development of sensitivity versus specificity for print in the visual word form area. *Brain and Language*, 170, 62–70. <https://doi.org/10.1016/j.bandl.2017.03.009>
- Centanni, Tracy M., Norton, E. S., Park, A., Beach, S. D., Halverson, K., Ozernov-Palchik, O., ... Gabrieli, J. D. E. DE. (2018). Early development of letter specialization in left fusiform is associated with better word reading and smaller fusiform face area. *Developmental Science*, 21(5), 1–10. <https://doi.org/10.1111/desc.12658>
- Changeux, J.-P., & Dehaene, S. (1989). Neuronal models of cognitive functions. *Cognition*, 33(1–2), 63–109. [https://doi.org/10.1016/0010-0277\(89\)90006-1](https://doi.org/10.1016/0010-0277(89)90006-1)
- Chen, L., Wassermann, D., Abrams, D. A., Kochalka, J., Gallardo-Diez, G., & Menon, V. (2019). The visual word form area (VWFA) is part of both language and attention circuitry. *Nature Communications*, 10(1), 5601. <https://doi.org/10.1038/s41467-019-13634-z>
- Chen, Q., Garcea, F. E., Almeida, J., & Mahon, B. Z. (2017). Connectivity-based constraints on category-specificity in the ventral object processing pathway. *Neuropsychologia*, 105(July 2016), 184–196. <https://doi.org/10.1016/j.neuropsychologia.2016.11.014>
- Chochon, F., Cohen, L., Moortele, P. F. van de, & Dehaene, S. (1999). Differential Contributions of the Left and Right Inferior Parietal Lobules to Number Processing. *Journal of Cognitive Neuroscience*, 11(6), 617–630. <https://doi.org/10.1162/089892999563689>
- Chochon, F., Cohen, L., Van De Moortele, P. F., Dehaene, S., Moortele, P. F. van de, & Dehaene, S. (1999). Differential Contributions of the Left and Right Inferior Parietal Lobules to Number Processing. *Journal of Cognitive Neuroscience*, 11(6), 617–630. <https://doi.org/10.1162/089892999563689>
- Ciric, R., Wolf, D. H., Power, J. D., Roalf, D. R., Baum, G. L., Ruparel, K., ... Satterthwaite, T. D. (2017). Benchmarking of participant-level confound regression strategies for the control of motion artifact in studies of functional connectivity. *NeuroImage*, 154(March), 174–187. <https://doi.org/10.1016/j.neuroimage.2017.03.020>
- Cisler, J. M., Bush, K., & Steele, J. S. (2014). A comparison of statistical methods for detecting context-modulated functional connectivity in fMRI. *NeuroImage*, 84, 1042–1052. <https://doi.org/10.1016/j.neuroimage.2013.09.018>
- Coalson, T. S., Van Essen, D. C., & Glasser, M. F. (2018). The impact of traditional neuroimaging methods on the spatial localization of cortical areas. *Proceedings of the National Academy of Sciences of the United States of America*, 115(27), E6356–E6365. <https://doi.org/10.1073/pnas.1801582115>
- Cohen, L., & Dehaene, S. (1995). Number processing in pure alexia: The effect of hemispheric asymmetries and task demands. *Neurocase*, 1(2), 121–137.

- <https://doi.org/10.1080/13554799508402356>
- Cohen, L., & Dehaene, S. (2004). Specialization within the ventral stream: The case for the visual word form area. *NeuroImage*, 22(1), 466–476.  
<https://doi.org/10.1016/j.neuroimage.2003.12.049>
- Cohen, L., Lehericy, S., Chochon, F., Lemer, C., Rivaud, S., & Dehaene, S. (2002). Language-specific tuning of visual cortex? Functional properties of the Visual Word Form Area. *Brain*, 125(5), 1054–1069. <https://doi.org/10.1093/brain/awf094>
- Cohen, M. A., Dilks, D. D., Koldewyn, K., Weigelt, S., Feather, J., Kell, A. J., ... Kanwisher, N. (2019). Representational similarity precedes category selectivity in the developing ventral visual pathway. *NeuroImage*, 197(September 2018), 565–574.  
<https://doi.org/10.1016/j.neuroimage.2019.05.010>
- Cole, M. W., Bassett, D. S., Power, J. D., Braver, T. S., & Petersen, S. E. (2014). Intrinsic and task-evoked network architectures of the human brain. *Neuron*, 83(1), 238–251.  
<https://doi.org/10.1016/j.neuron.2014.05.014>
- Cole, M. W., Ito, T., Schultz, D., Mill, R., Chen, R., & Cocuzza, C. (2019). Task activations produce spurious but systematic inflation of task functional connectivity estimates. *NeuroImage*, 189(August 2018), 1–18. <https://doi.org/10.1016/j.neuroimage.2018.12.054>
- Cole, M. W., Repovš, G., & Anticevic, A. (2014). The frontoparietal control system: A central role in mental health. *Neuroscientist*, 20(6), 652–664.  
<https://doi.org/10.1177/1073858414525995>
- Cole, M. W., Reynolds, J. R., Power, J. D., Repovš, G., Anticevic, A., & Braver, T. S. (2013). Multi-task connectivity reveals flexible hubs for adaptive task control. *Nature Neuroscience*, 16(9), 1348–1355. <https://doi.org/10.1038/nn.3470>
- Conrad, B. N., Wilkey, E. D., Yeo, D. J., & Price, G. R. (2020). Network topology of symbolic and nonsymbolic number comparison. *Network Neuroscience*, 1–32.  
[https://doi.org/10.1162/netn\\_a\\_00144](https://doi.org/10.1162/netn_a_00144)
- Corbetta, M., & Shulman, G. L. (2002). Control of goal-directed and stimulus-driven attention in the brain. *Nature Reviews Neuroscience*, 3(3), 201–215. <https://doi.org/10.1038/nrn755>
- Cordero-Grande, L., Christiaens, D., Hutter, J., Price, A. N., & Hajnal, J. V. (2019). Complex diffusion-weighted image estimation via matrix recovery under general noise models. *NeuroImage*, 200(March), 391–404. <https://doi.org/10.1016/j.neuroimage.2019.06.039>
- Cox, R. W. (1996). AFNI: software for analysis and visualization of functional magnetic resonance neuroimages. *Computers and Biomedical Research*, 29(29), 162–173.  
<https://doi.org/10.1006/cbmr.1996.0014>
- D’Errico, F., Backwell, L., Villa, P., Degano, I., Lucejko, J. J., Bamford, M. K., ... Beaumont, P. B. (2012). Early evidence of San material culture represented by organic artifacts from Border Cave, South Africa. *Proceedings of the National Academy of Sciences of the United States of America*, 109(33), 13214–13219. <https://doi.org/10.1073/pnas.1204213109>
- Daitch, A. L., Foster, B. L., Schrouff, J., Rangarajan, V., Kaşikçi, I., Gattas, S., & Parvizi, J. (2016). Mapping human temporal and parietal neuronal population activity and functional coupling during mathematical cognition. *Proceedings of the National Academy of Sciences*, 113(46), E7277–E7286. <https://doi.org/10.1073/pnas.1608434113>
- de Chastelaine, M., Mattson, J. T., Wang, T. H., Donley, B. E., & Rugg, M. D. (2017). Independent contributions of fMRI familiarity and novelty effects to recognition memory and their stability across the adult lifespan. *NeuroImage*, 156(May), 340–351.  
<https://doi.org/10.1016/j.neuroimage.2017.05.039>

- Deen, B., Richardson, H., Dilks, D. D., Takahashi, A., Keil, B., Wald, L. L., ... Saxe, R. (2017). Organization of high-level visual cortex in human infants. *Nature Communications*, 8, 1–10. <https://doi.org/10.1038/ncomms13995>
- Dehaene-Lambertz, G., Dehaene, S., & Hertz-Pannier, L. (2002). Functional neuroimaging of speech perception in infants. *Science*, 298(5600), 2013–2015. <https://doi.org/10.1126/science.1077066>
- Dehaene-Lambertz, G., Monzalvo, K., & Dehaene, S. (2018). The emergence of the visual word form: Longitudinal evolution of category-specific ventral visual areas during reading acquisition. *PLOS Biology*, 16(3), e2004103. <https://doi.org/10.1371/journal.pbio.2004103>
- Dehaene, S. (1992). Varieties of numerical abilities. *Cognition*, 44(1–2), 1–42. [https://doi.org/10.1016/0010-0277\(92\)90049-N](https://doi.org/10.1016/0010-0277(92)90049-N)
- Dehaene, S. (2007). Symbols and quantities in parietal cortex: Elements of a mathematical theory of number representation and manipulation. *Attention & Performance XXII. Sensori-Motor ...*, 527–574. <https://doi.org/10.1093/acprof:oso/9780199231447.003.0024>
- Dehaene, S., & Akhavein, R. (1995). Attention, automaticity, and levels of representation in number processing. *Journal of Experimental Psychology: Learning, Memory, and Cognition*, 21(2), 314–326. <https://doi.org/10.1037/0278-7393.21.2.314>
- Dehaene, S., & Cohen, L. (1995). Towards an Anatomical and Functional Model of Number Processing. *Mathematical Cognition*, 1, 83–120.
- Dehaene, S., & Cohen, L. (2007). Cultural recycling of cortical maps. *Neuron*, 56(2), 384–398. <https://doi.org/10.1016/j.neuron.2007.10.004>
- Dehaene, S., & Cohen, L. (2011). The unique role of the visual word form area in reading. *Trends in Cognitive Sciences*, 15(6), 254–262. <https://doi.org/10.1016/j.tics.2011.04.003>
- Dehaene, S., Cohen, L., Morais, J., & Kolinsky, R. (2015). Illiterate to literate: behavioural and cerebral changes induced by reading acquisition. *Nature Reviews Neuroscience*, 16(4), 234–244. <https://doi.org/10.1038/nrn3924>
- Dehaene, S., Pegado, F., Braga, L. W., Ventura, P., Filho, G. N., Jobert, A., ... Cohen, L. (2010). How Learning to Read Changes the Cortical Networks for Vision and Language. *Science*, 330(6009), 1359–1364. <https://doi.org/10.1126/science.1194140>
- Dehaene, S., Piazza, M., Pinel, P., & Cohen, L. (2003). Three parietal circuits for number processing. *Cognitive Neuropsychology*, 20(3–6), 487–506. <https://doi.org/10.1080/02643290244000239>
- Destrieux, C., Fischl, B., Dale, A., & Halgren, E. (2010). Automatic parcellation of human cortical gyri and sulci using standard anatomical nomenclature. *NeuroImage*, 53(1), 1–15. <https://doi.org/10.1016/j.neuroimage.2010.06.010>
- Dhollander, T., & Connelly, A. (2016). A novel iterative approach to reap the benefits of multi-tissue CSD from just single-shell ( + b = 0 ) diffusion MRI data A novel iterative approach to reap the benefits of multi-tissue CSD. *Proc. Intl. Soc. Mag. Reson. Med*, (May).
- Dhollander, T., Mito, R., Raffelt, D., & Connelly, A. (2019). Improved white matter response function estimation for 3-tissue constrained spherical deconvolution. *Proc. Intl. Soc. Mag. Reson. Med*, (May 11-16), 555.
- Di, X., Reynolds, R. C., & Biswal, B. B. (2017). Imperfect (De)convolution may introduce spurious psychophysiological interactions and how to avoid it. *Human Brain Mapping*, 38(4), 1723–1740. <https://doi.org/10.1002/hbm.23413>
- Di, X., Zhang, Z., & Biswal, B. B. (2020). Understanding psychophysiological interaction and its relations to beta series correlation. *Brain Imaging and Behavior*.

- <https://doi.org/10.1007/s11682-020-00304-8>
- Diana, R. A., Yonelinas, A. P., & Ranganath, C. (2007). Imaging recollection and familiarity in the medial temporal lobe: a three-component model. *Trends in Cognitive Sciences*, *11*(9), 379–386. <https://doi.org/10.1016/j.tics.2007.08.001>
- Diedrichsen, J., & Kriegeskorte, N. (2017). *Representational models: A common framework for understanding encoding*. *PLoS Computational Biology* (Vol. 13). Retrieved from <https://journals.plos.org/ploscompbiol/article/file?id=10.1371/journal.pcbi.1005508&type=printable>
- Doria, V., Beckmann, C. F., Arichi, T., Merchant, N., Groppo, M., Turkheimer, F. E., ... Edwards, A. D. (2010). Emergence of resting state networks in the preterm human brain. *Proceedings of the National Academy of Sciences of the United States of America*, *107*(46), 20015–20020. <https://doi.org/10.1073/pnas.1007921107>
- Dotan, D., & Friedmann, N. (2019). Separate mechanisms for number reading and word reading: Evidence from selective impairments. *Cortex*, *114*, 176–192. <https://doi.org/10.1016/j.cortex.2018.05.010>
- Downing, P. E., Chan, A. W. Y., Peelen, M. V., Dodds, C. M., & Kanwisher, N. (2006). Domain specificity in visual cortex. *Cerebral Cortex*, *16*(10), 1453–1461. <https://doi.org/10.1093/cercor/bhj086>
- Dubois, J., Dehaene-Lambertz, G., Kulikova, S., Poupon, C., Hüppi, P. S., & Hertz-Pannier, L. (2014). The early development of brain white matter: A review of imaging studies in fetuses, newborns and infants. *Neuroscience*, *276*, 48–71. <https://doi.org/10.1016/j.neuroscience.2013.12.044>
- Dubois, J., Hertz-Pannier, L., Cachia, A., Mangin, J. F., Le Bihan, D., & Dehaene-Lambertz, G. (2009). Structural asymmetries in the infant language and sensori-motor networks. *Cerebral Cortex*, *19*(2), 414–423. <https://doi.org/10.1093/cercor/bhn097>
- Duncan, G. J., Dowsett, C. J., Claessens, A., Magnuson, K., Huston, A. C., Klebanov, P., ... Japel, C. (2007). School readiness and later achievement. *Developmental Psychology*, *43*(6), 1428–1446. <https://doi.org/10.1037/0012-1649.43.6.1428>
- Duncan, J. (2010). The multiple-demand (MD) system of the primate brain: mental programs for intelligent behaviour. *Trends in Cognitive Sciences*, *14*(4), 172–179. <https://doi.org/10.1016/j.tics.2010.01.004>
- Durnez, J., Blair, R., & Poldrack, R. A. (2017). Neurodesign: Optimal Experimental Designs for Task fMRI. *BioRxiv*. <https://doi.org/10.1101/119594>
- Eger, E., Sterzer, P., Russ, M. O., Giraud, A.-L., & Kleinschmidt, A. (2003). A supramodal number representation in human intraparietal cortex. *Neuron*, *37*(4), 719–725. Retrieved from <http://www.ncbi.nlm.nih.gov/pubmed/12597867>
- Emerson, R. W., & Cantlon, J. F. (2015). Continuity and change in children’s longitudinal neural responses to numbers. *Developmental Science*, *18*(2), 314–326. <https://doi.org/10.1111/desc.12215>
- Engelhardt, L. E., Roe, M. A., Juranek, J., DeMaster, D., Harden, K. P., Tucker-Drob, E. M., & Church, J. A. (2017). Children’s head motion during fMRI tasks is heritable and stable over time. *Developmental Cognitive Neuroscience*, *25*, 58–68. <https://doi.org/10.1016/j.dcn.2017.01.011>
- Evans, T. M., Kochalka, J., Ngoon, T. J., Wu, S. S., Qin, S., Battista, C., & Menon, V. (2015). Brain Structural Integrity and Intrinsic Functional Connectivity Forecast 6 Year Longitudinal Growth in Children’s Numerical Abilities. *Journal of Neuroscience*, *35*(33),



- 11743–11750. <https://doi.org/10.1523/JNEUROSCI.0216-15.2015>
- Fair, D. A., Schlaggar, B. L., Cohen, A. L., Miezin, F. M., Dosenbach, N. U. F. F., Wenger, K. K., ... Petersen, S. E. (2007). A method for using blocked and event-related fMRI data to study “resting state” functional connectivity. *NeuroImage*, 35(1), 396–405. <https://doi.org/10.1016/j.neuroimage.2006.11.051>
- Faye, A., Jacquin-Courtois, S., Reynaud, E., Lesourd, M., Besnard, J., & Osiurak, F. (2019). Numerical cognition: A meta-analysis of neuroimaging, transcranial magnetic stimulation and brain-damaged patients studies. *NeuroImage: Clinical*, 24(October), 102053. <https://doi.org/10.1016/j.nicl.2019.102053>
- Fedorenko, E., & Blank, I. (2020). Broca’s area is not a natural kind. *Submitted*, 1–15. <https://doi.org/10.1016/j.tics.2020.01.001>
- Fisher, R. A. (1915). Frequency Distribution of the Values of the Correlation Coefficient in Samples from an Indefinitely Large Population. *Biometrika*, 10(4), 507. <https://doi.org/10.2307/2331838>
- Flinker, A., Korzeniewska, A., Shestyuk, A. Y., Franszczuk, P. J., Dronkers, N. F., Knight, R. T., & Crone, N. E. (2015). Redefining the role of broca’s area in speech. *Proceedings of the National Academy of Sciences of the United States of America*, 112(9), 2871–2875. <https://doi.org/10.1073/pnas.1414491112>
- Flowers, D. L., Jones, K., Noble, K., VanMeter, J., Zeffiro, T. A., Wood, F. B., & Eden, G. F. (2004). Attention to single letters activates left extrastriate cortex. *NeuroImage*, 21(3), 829–839. <https://doi.org/10.1016/j.neuroimage.2003.10.002>
- Fornito, A., Yoon, J., Zalesky, A., Bullmore, E. T., & Carter, C. S. (2011). General and specific functional connectivity disturbances in first-episode schizophrenia during cognitive control performance. *Biological Psychiatry*, 70(1), 64–72. <https://doi.org/10.1016/j.biopsych.2011.02.019>
- Fransson, P., Skiold, B., Horsch, S., Nordell, A., Blennow, M., Lagercrantz, H., & Aden, U. (2007). Resting-state networks in the infant brain. *Proceedings of the National Academy of Sciences*, 104(39), 15531–15536. <https://doi.org/10.1073/pnas.0704380104>
- Friederici, A. D. (2009). Pathways to language: fiber tracts in the human brain. *Trends in Cognitive Sciences*, 13(4), 175–181. <https://doi.org/10.1016/j.tics.2009.01.001>
- Friston, K. (2010). The free-energy principle: A unified brain theory? *Nature Reviews Neuroscience*, 11(2), 127–138. <https://doi.org/10.1038/nrn2787>
- Friston, K J, Preller, K. H., Mathys, C., Cagnan, H., Heinzle, J., Razi, A., & Zeidman, P. (2017). Dynamic causal modelling revisited. *NeuroImage*, (February), 0–1. <https://doi.org/10.1016/j.neuroimage.2017.02.045>
- Friston, Karl J., & Price, C. J. (2011). Modules and brain mapping. *Cognitive Neuropsychology*, 28(3–4), 241–250. <https://doi.org/10.1080/02643294.2011.558835>
- Gauthier, I. (2000). What constrains the organization of the ventral temporal cortex? *Trends in Cognitive Sciences*, 4(1), 1–2. [https://doi.org/10.1016/S1364-6613\(99\)01416-3](https://doi.org/10.1016/S1364-6613(99)01416-3)
- Gauthier, I., Tarr, M. J., Anderson, A. W., Skudlarski, P., & Gore, J. C. (1999). Activation of the middle fusiform “face area” increases with expertise in recognizing novel objects. *Nature Neuroscience*, 2(6), 568–573. <https://doi.org/10.1038/9224>
- Geary, D. C. (2011). Consequences, Characteristics, and Causes of Mathematical Learning Disabilities and Persistent Low Achievement in Mathematics. *Journal of Developmental & Behavioral Pediatrics*, 32(3), 250–263. <https://doi.org/10.1097/DBP.0b013e318209edef>
- Geib, B. R., Stanley, M. L., Dennis, N. A., Woldorff, M. G., & Cabeza, R. (2017). From

- Hippocampus to Whole-Brain : The Role of Integrative Processing in Episodic Memory Retrieval, 2259, 2242–2259. <https://doi.org/10.1002/hbm.23518>
- Genon, S., Reid, A., Langner, R., Amunts, K., & Eickhoff, S. B. (2018). How to Characterize the Function of a Brain Region. *Trends in Cognitive Sciences*, 22(4), 350–364. <https://doi.org/10.1016/j.tics.2018.01.010>
- Glasser, M. F., & Rilling, J. K. (2008). DTI tractography of the human brain’s language pathways. *Cerebral Cortex*, 18(11), 2471–2482. <https://doi.org/10.1093/cercor/bhn011>
- Glezer, L. S., Jiang, X., & Riesenhuber, M. (2009). Evidence for Highly Selective Neuronal Tuning to Whole Words in the “Visual Word Form Area.” *Neuron*, 62(2), 199–204. <https://doi.org/10.1016/j.neuron.2009.03.017>
- Glezer, L. S., & Riesenhuber, M. (2013). Individual variability in location impacts orthographic selectivity in the “visual word form area.” *Journal of Neuroscience*, 33(27), 11221–11226. <https://doi.org/10.1523/JNEUROSCI.5002-12.2013>
- Göbel, S., Walsh, V., & Rushworth, M. F. S. (2001). The mental number line and the human angular gyrus. *NeuroImage*, 14(6), 1278–1289. <https://doi.org/10.1006/nimg.2001.0927>
- Golarai, G., Ghahremani, D. G., Whitfield-Gabrieli, S., Reiss, A., Eberhardt, J. L., Gabrieli, J. D. E., & Grill-Spector, K. (2007). Differential development of high-level visual cortex correlates with category-specific recognition memory. *Nature Neuroscience*, 10(4), 512–522. <https://doi.org/10.1038/nn1865>
- Golarai, G., Liberman, A., & Grill-Spector, K. (2017). Experience Shapes the Development of Neural Substrates of Face Processing in Human Ventral Temporal Cortex. *Cerebral Cortex (New York, N.Y. : 1991)*, 27(2), 1229–1244. <https://doi.org/10.1093/cercor/bhv314>
- Golarai, G., Liberman, A., Yoon, J. M. D., & Grill-Spector, K. (2010). Differential development of the ventral visual cortex extends through adolescence. *Frontiers in Human Neuroscience*, 3(FEB), 1–19. <https://doi.org/10.3389/neuro.09.080.2009>
- Goltz, D., Gundlach, C., Nierhaus, T., Villringer, A., Müller, M., & Pleger, B. (2015). Connections between Intraparietal Sulcus and a Sensorimotor Network Underpin Sustained Tactile Attention. *The Journal of Neuroscience*, 35(20), 7938–7949. <https://doi.org/10.1523/jneurosci.3421-14.2015>
- Gomez, J., Pestilli, F., Witthoft, N., Golarai, G., Liberman, A., Poltoratski, S., ... Grill-Spector, K. (2015). Functionally Defined White Matter Reveals Segregated Pathways in Human Ventral Temporal Cortex Associated with Category-Specific Processing. *Neuron*, 85(1), 216–227. <https://doi.org/10.1016/j.neuron.2014.12.027>
- Göttlich, M., Beyer, F., & Krämer, U. M. (2015). BASCO : a toolbox for task-related functional connectivity, 9(September), 1–10. <https://doi.org/10.3389/fnsys.2015.00126>
- Grabner, R. H., Ischebeck, A., Reishofer, G., Koschutnig, K., Delazer, M., Ebner, F., & Neuper, C. (2009). Fact learning in complex arithmetic and figural-spatial tasks: The role of the angular gyrus and its relation to mathematical competence. *Human Brain Mapping*, 30(9), 2936–2952. <https://doi.org/10.1002/hbm.20720>
- Graves, W. W., Desai, R., Humphries, C., Seidenberg, M. S., & Binder, J. R. (2010). Neural systems for reading aloud: A multiparametric approach. *Cerebral Cortex*, 20(8), 1799–1815. <https://doi.org/10.1093/cercor/bhp245>
- Greene, D. J., Koller, J. M., Hampton, J. M., Wesevich, V., Van, A. N., Nguyen, A. L., ... Dosenbach, N. U. F. (2018). Behavioral interventions for reducing head motion during MRI scans in children. *NeuroImage*, 171(September 2017), 234–245. <https://doi.org/10.1016/j.neuroimage.2018.01.023>

- Grill-Spector, K., & Weiner, K. S. (2014). The functional architecture of the ventral temporal cortex and its role in categorization. *Nature Reviews Neuroscience*, *15*(8), 536–548. <https://doi.org/10.1038/nrn3747>
- Grimaldi, P., Saleem, K. S., & Tsao, D. (2016). Anatomical Connections of the Functionally Defined “Face Patches” in the Macaque Monkey. *Neuron*, *90*(6), 1325–1342. <https://doi.org/10.1016/j.neuron.2016.05.009>
- Grotheer, M., Herrmann, K.-H., & Kovacs, G. (2016). Neuroimaging Evidence of a Bilateral Representation for Visually Presented Numbers. *Journal of Neuroscience*, *36*(1), 88–97. <https://doi.org/10.1523/JNEUROSCI.2129-15.2016>
- Grotheer, M., Jeska, B., & Grill-Spector, K. (2018). A preference for mathematical processing outweighs the selectivity for Arabic numbers in the inferior temporal gyrus. *NeuroImage*, *175*(March), 188–200. <https://doi.org/10.1016/j.neuroimage.2018.03.064>
- Grotheer, M., Zhen, Z., Lerma-Usabiaga, G., & Grill-Spector, K. (2019). Separate lanes for adding and reading in the white matter highways of the human brain. *Nature Communications*, *10*(1), 3675. <https://doi.org/10.1038/s41467-019-11424-1>
- Gschwind, M., Pourtois, G., Schwartz, S., Van De Ville, D., & Vuilleumier, P. (2012). White-matter connectivity between face-responsive regions in the human brain. *Cerebral Cortex*, *22*(7), 1564–1576. <https://doi.org/10.1093/cercor/bhr226>
- Gullick, M. M., Sprute, L. A., & Temple, E. (2011). Individual differences in working memory, nonverbal IQ, and mathematics achievement and brain mechanisms associated with symbolic and nonsymbolic number processing. *Learning and Individual Differences*, *21*(6), 644–654. <https://doi.org/10.1016/j.lindif.2010.10.003>
- Hagmann, P., Cammoun, L., Martuzzi, R., Maeder, P., Clarke, S., Thiran, J. P., & Meuli, R. (2006). Hand preference and sex shape the architecture of language networks. *Human Brain Mapping*, *27*(10), 828–835. <https://doi.org/10.1002/hbm.20224>
- Haller, S. P. W., Mills, K. L., Hartwright, C. E., David, A. S., & Cohen Kadosh, K. (2018). When change is the only constant: The promise of longitudinal neuroimaging in understanding social anxiety disorder. *Developmental Cognitive Neuroscience*, *33*(May), 73–82. <https://doi.org/10.1016/j.dcn.2018.05.005>
- Hannagan, T., Amedi, A., Cohen, L., Dehaene-Lambertz, G., & Dehaene, S. (2015). Origins of the specialization for letters and numbers in ventral occipitotemporal cortex. *Trends in Cognitive Sciences*, *19*(7), 374–382. <https://doi.org/10.1016/j.tics.2015.05.006>
- Hansen, C. B., Yang, Q., Lyu, I., Rheault, F., Kerley, C., Chandio, B. Q., ... Schilling, K. G. (2021). Pandora: 4-D White Matter Bundle Population-Based Atlases Derived from Diffusion MRI Fiber Tractography. *Neuroinformatics*, *19*(3), 447–460. <https://doi.org/10.1007/s12021-020-09497-1>
- Harel, A. (2016). What is special about expertise? Visual expertise reveals the interactive nature of real-world object recognition. *Neuropsychologia*, *83*, 88–99. <https://doi.org/10.1016/j.neuropsychologia.2015.06.004>
- Harmand, S., Lewis, J. E., Feibel, C. S., Lepre, C. J., Prat, S., Lenoble, A., ... Roche, H. (2015). 3.3-million-year-old stone tools from Lomekwi 3, West Turkana, Kenya. *Nature*, *521*(7552), 310–315. <https://doi.org/10.1038/nature14464>
- Harrigan, R. L. R. L., Yvernault, B. C. B. C., Boyd, B. D. B. D., Damon, S. M. S. M., Gibney, K. D. K. D., Conrad, B. N., ... Landman, B. A. B. A. (2016). Vanderbilt University Institute of Imaging Science Center for Computational Imaging XNAT: A multimodal data archive and processing environment. *NeuroImage*, *124*, 1097–1101.

- <https://doi.org/10.1016/j.neuroimage.2015.05.021>
- Harvey, B. M., Ferri, S., & Orban, G. A. (2017). Comparing Parietal Quantity-Processing Mechanisms between Humans and Macaques. *Trends in Cognitive Sciences*, 21(10), 779–793. <https://doi.org/10.1016/j.tics.2017.07.002>
- Hauser, M. D., Chomsky, N., & Fitch, W. T. (2010). The faculty of language: What is it, who has it, and how did it evolve? *The Evolution of Human Language: Biolinguistic Perspectives*, 298(November), 14–42. <https://doi.org/10.1017/CBO9780511817755.002>
- Henik, A., & Tzelgov, J. (1982). Is three greater than five: The relation between physical and semantic size in comparison tasks. *Memory & Cognition*, 10(4), 389–395. <https://doi.org/10.3758/BF03202431>
- Hermes, D., Rangarajan, V., Foster, B. L., King, J. R., Kasikci, I., Miller, K. J., & Parvizi, J. (2017). Electrophysiological Responses in the Ventral Temporal Cortex During Reading of Numerals and Calculation. *Cerebral Cortex (New York, N.Y. : 1991)*, 27(1), 567–575. <https://doi.org/10.1093/cercor/bhv250>
- Holloway, I. D., Price, G. R., & Ansari, D. (2010). Common and segregated neural pathways for the processing of symbolic and nonsymbolic numerical magnitude: An fMRI study. *NeuroImage*, 49(1), 1006–1017. <https://doi.org/10.1016/j.neuroimage.2009.07.071>
- Hurka, J. Vanden, Baelena, M. Van, & Beecka, H. P. O. (2017). Development of visual category selectivity in ventral visual cortex does not require visual experience. *Proceedings of the National Academy of Sciences of the United States of America*, 114(22), E4501–E4510. <https://doi.org/10.1073/pnas.1612862114>
- Huth, A. G., De Heer, W. A., Griffiths, T. L., Theunissen, F. E., & Gallant, J. L. (2016). Natural speech reveals the semantic maps that tile human cerebral cortex. *Nature*, 532(7600), 453–458. <https://doi.org/10.1038/nature17637>
- Hyde, D. C., Boas, D. A., Blair, C., & Carey, S. (2010). Near-infrared spectroscopy shows right parietal specialization for number in pre-verbal infants. *NeuroImage*, 53(2), 647–652. <https://doi.org/10.1016/j.neuroimage.2010.06.030>
- Izard, V., Dehaene-Lambertz, G., & Dehaene, S. (2008). Distinct cerebral pathways for object identity and number in human infants. *PLoS Biology*, 6(2), 0275–0285. <https://doi.org/10.1371/journal.pbio.0060011>
- James, K. H., James, T. W., Jobard, G., Wong, A. C.-N., & Gauthier, I. (2005). Letter processing in the visual system: Different activation patterns for single letters and strings. *Cognitive, Affective, & Behavioral Neuroscience*, 5(4), 452–466. <https://doi.org/10.3758/CABN.5.4.452>
- Jeurissen, B., Tournier, J. D., Dhollander, T., Connelly, A., & Sijbers, J. (2014). Multi-tissue constrained spherical deconvolution for improved analysis of multi-shell diffusion MRI data. *NeuroImage*, 103, 411–426. <https://doi.org/10.1016/j.neuroimage.2014.07.061>
- Jo, H. J., Saad, Z. S., Gotts, S. J., Martin, A., & Cox, R. W. (2012). Quantifying Agreement between Anatomical and Functional Interhemispheric Correspondences in the Resting Brain. *PLoS ONE*, 7(11), e48847. <https://doi.org/10.1371/journal.pone.0048847>
- Johnson, M. H. (2001). Functional brain development in humans. *Nature Reviews Neuroscience*, 2(7), 475–483. <https://doi.org/10.1038/35081509>
- Johnson, M. H. (2011). Interactive Specialization: A domain-general framework for human functional brain development? *Developmental Cognitive Neuroscience*, 1(1), 7–21. <https://doi.org/10.1016/j.dcn.2010.07.003>
- Johnson, M. H., & de Haan, M. (2015). Interactive Specialization. In *Developmental Cognitive*

- Neuroscience* (4th ed., pp. 222–239). John Wiley & Sons, Incorporated.
- Jones, M. N., & Mewhort, D. J. K. (2004). Case-sensitive letter and bigram frequency counts from large-scale English corpora. *Behavior Research Methods, Instruments, and Computers*, *36*(3), 388–396. <https://doi.org/10.3758/BF03195586>
- Joseph, J. E., Gathers, A. D., & Bhatt, R. S. (2011). Progressive and regressive developmental changes in neural substrates for face processing: Testing specific predictions of the Interactive Specialization account. *Developmental Science*, *14*(2), 227–241. <https://doi.org/10.1111/j.1467-7687.2010.00963.x>
- Kanwisher, N. (2010). Functional specificity in the human brain: A window into the functional architecture of the mind. *Proceedings of the National Academy of Sciences of the United States of America*, *107*(25), 11163–11170. <https://doi.org/10.1073/pnas.1005062107>
- Kay, K. N., & Yeatman, J. D. (2017). Bottom-up and top-down computations in word- and face-selective cortex. *ELife*, *6*, 1–29. <https://doi.org/10.7554/elife.22341>
- Keller, S. S., Crow, T., Foundas, A., Amunts, K., & Roberts, N. (2009). Broca’s area: Nomenclature, anatomy, typology and asymmetry. *Brain and Language*, *109*(1), 29–48. <https://doi.org/10.1016/j.bandl.2008.11.005>
- Kersey, A. J., & Cantlon, J. F. (2017a). Neural tuning to numerosity relates to perceptual tuning in 3–6-year-old children. *Journal of Neuroscience*, *37*(3), 512–522. <https://doi.org/10.1523/JNEUROSCI.0065-16.2016>
- Kersey, A. J., & Cantlon, J. F. (2017b). Primitive Concepts of Number and the Developing Human Brain. *Language Learning and Development*, *13*(2), 191–214. <https://doi.org/10.1080/15475441.2016.1264878>
- Kherif, F., Josse, G., & Price, C. J. (2011). Automatic top-down processing explains common left occipito-temporal responses to visual words and objects. *Cerebral Cortex*, *21*(1), 103–114. <https://doi.org/10.1093/cercor/bhq063>
- King, K. M., Littlefield, A. K., McCabe, C. J., Mills, K. L., Flournoy, J., & Chassin, L. (2018). Longitudinal modeling in developmental neuroimaging research: Common challenges, and solutions from developmental psychology. *Developmental Cognitive Neuroscience*, *33*(November 2017), 54–72. <https://doi.org/10.1016/j.dcn.2017.11.009>
- Klein, E., Moeller, K., Glauche, V., Weiller, C., & Willmes, K. (2013). Processing Pathways in Mental Arithmetic—Evidence from Probabilistic Fiber Tracking. *PLoS ONE*, *8*(1). <https://doi.org/10.1371/journal.pone.0055455>
- Krause, F., Benjamins, C., Eck, J., Lührs, M., van Hoof, R., & Goebel, R. (2019). Active head motion reduction in magnetic resonance imaging using tactile feedback. *Human Brain Mapping*, *40*(14), 4026–4037. <https://doi.org/10.1002/hbm.24683>
- Kriegeskorte, N., Goebel, R., & Bandettini, P. (2006). Information-based functional brain mapping. *Proceedings of the National Academy of Sciences*, *103*(10), 3863–3868. <https://doi.org/10.1073/pnas.0600244103>
- Kriegeskorte, N., Mur, M., & Bandettini, P. A. (2008). Representational similarity analysis – connecting the branches of systems neuroscience. *Frontiers in Systems Neuroscience*, *2*(November), 1–28. <https://doi.org/10.3389/neuro.06.004.2008>
- Kriegeskorte, N., Mur, M., Ruff, D. A., Kiani, R., Bodurka, J., Esteky, H., ... Bandettini, P. A. (2008). Matching Categorical Object Representations in Inferior Temporal Cortex of Man and Monkey. *Neuron*, *60*(6), 1126–1141. <https://doi.org/10.1016/j.neuron.2008.10.043>
- Kronbichler, M., Hutzler, F., Wimmer, H., Mair, A., Staffen, W., & Ladurner, G. (2004). The visual word form area and the frequency with which words are encountered: Evidence from

- a parametric fMRI study. *NeuroImage*, *21*(3), 946–953.  
<https://doi.org/10.1016/j.neuroimage.2003.10.021>
- Kubota, E. C., Joo, S. J., Huber, E., & Yeatman, J. D. (2019). Word selectivity in high-level visual cortex and reading skill. *Developmental Cognitive Neuroscience*, *36*(June 2018), 100593. <https://doi.org/10.1016/j.dcn.2018.09.003>
- Kutter, E. F., Bostroem, J., Elger, C. E., Mormann, F., Correspondence, A. N., & Nieder, A. (2018). Single Neurons in the Human Brain Encode Numbers Article Single Neurons in the Human Brain Encode Numbers. *Neuron*, *100*, 1–9.  
<https://doi.org/10.1016/j.neuron.2018.08.036>
- Lancaster, J. L., Tordesillas-Gutiérrez, D., Martínez, M., Salinas, F., Evans, A., Zilles, K., ... Fox, P. T. (2007). Bias between MNI and talairach coordinates analyzed using the ICBM-152 brain template. *Human Brain Mapping*, *28*(11), 1194–1205.  
<https://doi.org/10.1002/hbm.20345>
- Lewis, C. M., Baldassarre, A., Committeri, G., Romani, G. L., & Corbetta, M. (2009). Learning sculpts the spontaneous activity of the resting human brain. *Proceedings of the National Academy of Sciences*, *106*(41), 17558–17563. <https://doi.org/10.1073/pnas.0902455106>
- Li, J., Osher, D. E., Hansen, H. A., & Saygin, Z. M. (2020). Innate connectivity patterns drive the development of the visual word form area. *Scientific Reports*, 1–12.  
<https://doi.org/10.1038/s41598-020-75015-7>
- Li, X., Morgan, P. S., Ashburner, J., Smith, J., & Rorden, C. (2016). The first step for neuroimaging data analysis: DICOM to NIfTI conversion. *Journal of Neuroscience Methods*, *264*, 47–56. <https://doi.org/10.1016/j.jneumeth.2016.03.001>
- Libertus, M. E., Brannon, E. M., & Pelphrey, K. A. (2009). Developmental changes in category-specific brain responses to numbers and letters in a working memory task. *NeuroImage*, *44*(4), 1404–1414. <https://doi.org/10.1016/j.neuroimage.2008.10.027>
- Lochy, A., & Schiltz, C. (2019). Lateralized Neural Responses to Letters and Digits in First Graders. *Child Development*, *90*(6), 1866–1874. <https://doi.org/10.1111/cdev.13337>
- Lussier, C. A., & Cantlon, J. F. (2017). Developmental bias for number words in the intraparietal sulcus. *Developmental Science*, *20*(3), 1–18. <https://doi.org/10.1111/desc.12385>
- Lyons, I. M., Ansari, D., & Beilock, S. L. (2012). Symbolic estrangement: Evidence against a strong association between numerical symbols and the quantities they represent. *Journal of Experimental Psychology: General*, *141*(4), 635–641. <https://doi.org/10.1037/a0027248>
- Lyons, I. M., & Beilock, S. L. (2018). Characterizing the neural coding of symbolic quantities. *NeuroImage*, *178*(May), 503–518. <https://doi.org/10.1016/j.neuroimage.2018.05.062>
- Mahon, B. Z., Anzellotti, S., Schwarzbach, J., Zampini, M., & Caramazza, A. (2009). Category-Specific Organization in the Human Brain Does Not Require Visual Experience. *Neuron*, *63*(3), 397–405. <https://doi.org/10.1016/j.neuron.2009.07.012>
- Mahon, B. Z., & Caramazza, A. (2009). Concepts and categories: A cognitive neuropsychological perspective. *Annual Review of Psychology*, *60*, 27–51.  
<https://doi.org/10.1146/annurev.psych.60.110707.163532>
- Mahon, B. Z., & Caramazza, A. (2011). What drives the organization of object knowledge in the brain? *Trends in Cognitive Sciences*, *15*(3), 97–103.  
<https://doi.org/10.1016/j.tics.2011.01.004>
- Marek, S., & Dosenbach, N. U. F. (2018). The frontoparietal network: function, electrophysiology, and importance of individual precision mapping. *Dialogues Clin Neurosci*, *20*, 133–140. Retrieved from [www.dialogues-cns.org](http://www.dialogues-cns.org)

- Martin, A. (2007). The representation of object concepts in the brain. *Annual Review of Psychology*, 58(1), 25–45. <https://doi.org/10.1146/annurev.psych.57.102904.190143>
- Matejko, A. A., & Ansari, D. (2016). Trajectories of symbolic and nonsymbolic magnitude processing in the first year of formal schooling. *PLoS ONE*, 11(3), 1–15. <https://doi.org/10.1371/journal.pone.0149863>
- Maurer, U., Brem, S., Bucher, K., & Brandeis, D. (2005). Emerging neurophysiological specialization for letter strings. *Journal of Cognitive Neuroscience*, 17(10), 1532–1552. <https://doi.org/10.1162/089892905774597218>
- Maurer, U., Brem, S., Kranz, F., Bucher, K., Benz, R., Halder, P., ... Brandeis, D. (2006). Coarse neural tuning for print peaks when children learn to read. *NeuroImage*, 33(2), 749–758. <https://doi.org/10.1016/j.neuroimage.2006.06.025>
- McCandliss, B. D., Cohen, L., & Dehaene, S. (2003). The visual word form area: Expertise for reading in the fusiform gyrus. *Trends in Cognitive Sciences*, 7(7), 293–299. [https://doi.org/10.1016/S1364-6613\(03\)00134-7](https://doi.org/10.1016/S1364-6613(03)00134-7)
- McCloskey, M. (1992). Cognitive mechanisms in numerical processing: Evidence from acquired dyscalculia. *Cognition*, 44(1–2), 107–157. [https://doi.org/10.1016/0010-0277\(92\)90052-J](https://doi.org/10.1016/0010-0277(92)90052-J)
- McGugin, R. W., Gatenby, J. C., Gore, J. C., & Gauthier, I. (2012). High-resolution imaging of expertise reveals reliable object selectivity in the fusiform face area related to perceptual performance. *Proceedings of the National Academy of Sciences of the United States of America*, 109(42), 17063–17068. <https://doi.org/10.1073/pnas.1116333109>
- Meissner, T. W., Walbrin, J., Nordt, M., Koldewyn, K., & Weigelt, S. (2020). Head motion during fMRI tasks is reduced in children and adults if participants take breaks. *Developmental Cognitive Neuroscience*, 44, 100803. <https://doi.org/10.1016/j.dcn.2020.100803>
- Merkley, R., Conrad, B., Price, G., & Ansari, D. (2019). Investigating the visual number form area: A replication study. *Royal Society Open Science*, 6(10). <https://doi.org/10.1098/rsos.182067>
- Mills, K. L., Goddings, A. L., Herting, M. M., Meuwese, R., Blakemore, S. J., Crone, E. A., ... Tamnes, C. K. (2016). Structural brain development between childhood and adulthood: Convergence across four longitudinal samples. *NeuroImage*, 141, 273–281. <https://doi.org/10.1016/j.neuroimage.2016.07.044>
- Milner, A. D., & Goodale, M. A. (2008). Two visual systems re-viewed. *Neuropsychologia*, 46(3), 774–785. <https://doi.org/10.1016/j.neuropsychologia.2007.10.005>
- Misaki, M., Kim, Y., Bandettini, P. A., & Kriegeskorte, N. (2010). Comparison of multivariate classifiers and response normalizations for pattern-information fMRI. *NeuroImage*, 53(1), 103–118. <https://doi.org/10.1016/j.neuroimage.2010.05.051>
- Mishkin, M., Ungerleider, L. G., & Macko, K. A. (1983). Object vision and spatial vision: two cortical pathways. *Trends in Neurosciences*, 6(C), 414–417. [https://doi.org/10.1016/0166-2236\(83\)90190-X](https://doi.org/10.1016/0166-2236(83)90190-X)
- Molenberghs, P., Mesulam, M. M., Peeters, R., & Vandenberghe, R. R. C. (2007). Remapping attentional priorities: Differential contribution of superior parietal lobule and intraparietal sulcus. *Cerebral Cortex*, 17(11), 2703–2712. <https://doi.org/10.1093/cercor/bhl179>
- Monge, Z. A., Geib, B. R., Siciliano, R. E., Packard, L. E., Tallman, C. W., & Madden, D. J. (2017). Functional modular architecture underlying attentional control in aging. *NeuroImage*, 155(May), 257–270. <https://doi.org/10.1016/j.neuroimage.2017.05.002>
- Mumford, J. A., Turner, B. O., Ashby, F. G., & Poldrack, R. A. (2012). Deconvolving BOLD

- activation in event-related designs for multivoxel pattern classification analyses. *NeuroImage*, 59(3), 2636–2643. <https://doi.org/10.1016/j.neuroimage.2011.08.076>
- Mur, M., Bandettini, P. A., & Kriegeskorte, N. (2009). Revealing representational content with pattern-information fMRI - An introductory guide. *Social Cognitive and Affective Neuroscience*, 4(1), 101–109. <https://doi.org/10.1093/scan/nsn044>
- Muschelli, J., Nebel, M. B., Caffo, B. S., Barber, A. D., Pekar, J. J., & Mostofsky, S. H. (2014). Reduction of motion-related artifacts in resting state fMRI using aCompCor. *NeuroImage*, 96(2), 22–35. <https://doi.org/10.1016/j.neuroimage.2014.03.028>
- Nath, V., Schilling, K. G., Parvathaneni, P., Huo, Y., Blaber, J. A., Hainline, A. E., ... Landman, B. A. (2019). Tractography reproducibility challenge with empirical data (TraCED): The 2017 ISMRM diffusion study group challenge. *Journal of Magnetic Resonance Imaging*, 1–16. <https://doi.org/10.1002/jmri.26794>
- Nemmi, F., Schel, M. A., & Klingberg, T. (2018). Connectivity of the Human Number Form Area Reveals Development of a Cortical Network for Mathematics. *Frontiers in Human Neuroscience*, 12(November), 1–15. <https://doi.org/10.3389/fnhum.2018.00465>
- Nieder, A. (2016). The neuronal code for number. *Nature Reviews Neuroscience*, advance on(6), 366–382. <https://doi.org/10.1038/nrn.2016.40>
- Nieder, A., & Dehaene, S. (2009). Representation of Number in the Brain. *Annual Review of Neuroscience*, 32(1), 185–208. <https://doi.org/10.1146/annurev.neuro.051508.135550>
- Nieto-Castañón, A., & Fedorenko, E. (2012). Subject-specific functional localizers increase sensitivity and functional resolution of multi-subject analyses. *NeuroImage*, 63(3), 1646–1669. <https://doi.org/10.1016/j.neuroimage.2012.06.065>
- Nissen, H. J. (1986). The archaic texts from Uruk. *World Archaeology*, 17(3), 317–334. <https://doi.org/10.1080/00438243.1986.9979973>
- Nordt, M., Gomez, J., Natu, V., Jeska, B., Barnett, M., & Grill-Spector, K. (2018). Learning to Read Increases the Informativeness of Distributed Ventral Temporal Responses. *Cerebral Cortex*, 1–16. <https://doi.org/10.1093/cercor/bhy178>
- Nordt, M., Gomez, J., Natu, V., Rezai, A. A., Finzi, D., Kular, H., & Grill-Spector, K. (2020). Cortical recycling in high-level visual cortex during childhood development. *BioRxiv*, 1–35. <https://doi.org/10.1101/2020.07.18.209783>
- Norman-Haignere, S. V., McCarthy, G., Chun, M. M., & Turk-Browne, N. B. (2012). Category-selective background connectivity in ventral visual cortex. *Cerebral Cortex*, 22(2), 391–402. <https://doi.org/10.1093/cercor/bhr118>
- Norman, K. A., Polyn, S. M., Detre, G. J., & Haxby, J. V. (2006). Beyond mind-reading: multi-voxel pattern analysis of fMRI data. *Trends in Cognitive Sciences*, 10(9), 424–430. <https://doi.org/10.1016/j.tics.2006.07.005>
- Norton, E. S., Beach, S. D., & Gabrieli, J. D. E. (2015). Neurobiology of dyslexia. *Current Opinion in Neurobiology*, 30, 73–78. <https://doi.org/10.1016/j.conb.2014.09.007>
- Nucifora, P. G. P., Verma, R., Melhem, E. R., Gur, R. E., & Gur, R. C. (2005). Leftward asymmetry in relative fiber density of the arcuate fasciculus. *NeuroReport*, 16(8), 791–794. <https://doi.org/10.1097/00001756-200505310-00002>
- OECD. (2016). Proficiency in Key Information-Processing Skills among Working-Age Adults, 55–100. <https://doi.org/http://dx.doi.org/10.1787/9789264204256-en>
- Oh, S. W., Harris, J. A., Ng, L., Winslow, B., Cain, N., Mihalas, S., ... Zeng, H. (2014). A mesoscale connectome of the mouse brain. *Nature*, 508(7495), 207–214. <https://doi.org/10.1038/nature13186>



- Oosterhof, N. N., Connolly, A. C., & Haxby, J. V. (2016). CoSMoMVPA: Multi-Modal Multivariate Pattern Analysis of Neuroimaging Data in Matlab/GNU Octave. *Frontiers in Neuroinformatics*, *10*(July), 1–27. <https://doi.org/10.3389/fninf.2016.00027>
- Op de Beeck, H. P., Pillot, I., & Ritchie, J. B. (2019). Factors Determining Where Category-Selective Areas Emerge in Visual Cortex. *Trends in Cognitive Sciences*, 1–14. <https://doi.org/10.1016/j.tics.2019.06.006>
- Osher, D. E., Saxe, R. R., Koldewyn, K., Gabrieli, J. D. E., Kanwisher, N., & Saygin, Z. M. (2016). Structural Connectivity Fingerprints Predict Cortical Selectivity for Multiple Visual Categories across Cortex. *Cerebral Cortex*, *26*(4), 1668–1683. <https://doi.org/10.1093/cercor/bhu303>
- Owen, A. M., McMillan, K. M., Laird, A. R., & Bullmore, E. (2005). N-back working memory paradigm: A meta-analysis of normative functional neuroimaging studies. *Human Brain Mapping*, *25*(1), 46–59. <https://doi.org/10.1002/hbm.20131>
- Park, J., Chiang, C., Brannon, E. M., & Woldorff, M. G. (2014). Experience-dependent Hemispheric Specialization of Letters and Numbers Is Revealed in Early Visual Processing. *Journal of Cognitive Neuroscience*, *26*(10), 2239–2249. [https://doi.org/10.1162/jocn\\_a\\_00621](https://doi.org/10.1162/jocn_a_00621)
- Park, J., Hebrank, A., Polk, T. A., & Park, D. C. (2012). Neural dissociation of number from letter recognition and its relationship to parietal numerical processing. *Journal of Cognitive Neuroscience*, *24*(1), 39–50. [https://doi.org/10.1162/jocn\\_a\\_00085](https://doi.org/10.1162/jocn_a_00085)
- Park, J., van den Berg, B., Chiang, C., Woldorff, M. G., & Brannon, E. M. (2018). Developmental trajectory of neural specialization for letter and number visual processing. *Developmental Science*, *21*(3), 1–14. <https://doi.org/10.1111/desc.12578>
- Parsons, S., & Bynner, J. (2005). *Does Numeracy Matter More? National Research and Development Centre for Adult Literacy and Numeracy*. London, UK.
- Peelen, M. V., & Downing, P. E. (2017). Category selectivity in human visual cortex: Beyond visual object recognition. *Neuropsychologia*, *105*(April), 177–183. <https://doi.org/10.1016/j.neuropsychologia.2017.03.033>
- Pernet, C., Celsis, P., & Démonet, J. F. (2005). Selective response to letter categorization within the left fusiform gyrus. *NeuroImage*, *28*(3), 738–744. <https://doi.org/10.1016/j.neuroimage.2005.06.046>
- Piazza, M. (2011). Neurocognitive Start-Up Tools for Symbolic Number Representations. *Space, Time and Number in the Brain*, *14*(12), 267–285. <https://doi.org/10.1016/B978-0-12-385948-8.00017-7>
- Piazza, M., Izard, V., Pinel, P., Le Bihan, D., & Dehaene, S. (2004). Tuning Curves for Approximate Numerosity in the Human Intraparietal Sulcus. *Neuron*, *44*(3), 547–555. <https://doi.org/10.1016/j.neuron.2004.10.014>
- Piazza, M., Pinel, P., Le Bihan, D., & Dehaene, S. (2007). A Magnitude Code Common to Numerosities and Number Symbols in Human Intraparietal Cortex. *Neuron*, *53*(2), 293–305. <https://doi.org/10.1016/j.neuron.2006.11.022>
- Pinel, P., & Dehaene, S. (2013). Genetic and environmental contributions to brain activation during calculation. *NeuroImage*, *81*, 306–316. <https://doi.org/10.1016/j.neuroimage.2013.04.118>
- Pinel, P., Piazza, M., Le Bihan, D., & Dehaene, S. (2004). Distributed and overlapping cerebral representations of number, size, and luminance during comparative judgments. *Neuron*, *41*(6), 983–993. [https://doi.org/10.1016/S0896-6273\(04\)00107-2](https://doi.org/10.1016/S0896-6273(04)00107-2)

- Pinheiro-Chagas, P., Daitch, A., Parvizi, J., & Dehaene, S. (2018). Brain Mechanisms of Arithmetic: A Crucial Role for Ventral Temporal Cortex. *Journal of Cognitive Neuroscience*, *30*(12), 1757–1772. [https://doi.org/10.1162/jocn\\_a\\_01319](https://doi.org/10.1162/jocn_a_01319)
- Polk, T. A., Stallcup, M., Aguirre, G. K., Alsop, D. C., D’Esposito, M., Detre, J. A., & Farah, M. J. (2002). Neural specialization for letter recognition. *Journal of Cognitive Neuroscience*, *14*(2), 145–159. <https://doi.org/10.1162/089892902317236803>
- Pollack, C., Luk, G., & Christodoulou, J. A. (2015). A meta-analysis of functional reading systems in typically developing and struggling readers across different alphabetic languages. *Frontiers in Psychology*, *6*(MAR), 1–10. <https://doi.org/10.3389/fpsyg.2015.00191>
- Pollack, C., & Price, G. R. (2019). Neurocognitive mechanisms of digit processing and their relationship with mathematics competence. *NeuroImage*, *185*(May 2018), 245–254. <https://doi.org/10.1016/j.neuroimage.2018.10.047>
- Powell, H. W. R., Parker, G. J. M., Alexander, D. C., Symms, M. R., Boulby, P. A., Wheeler-Kingshott, C. A. M., ... Duncan, J. S. (2006). Hemispheric asymmetries in language-related pathways: A combined functional MRI and tractography study. *NeuroImage*, *32*(1), 388–399. <https://doi.org/10.1016/j.neuroimage.2006.03.011>
- Practices, N. G. A. C. for B., & Officers, C. of C. S. S. (2010). Common Core State Standards. *National Governors Association Center for Best Practices, Council of Chief State School Officers, Washington D.C.*
- Price, C. J. (2012). A review and synthesis of the first 20 years of PET and fMRI studies of heard speech, spoken language and reading. *NeuroImage*, *62*(2), 816–847. <https://doi.org/10.1016/j.neuroimage.2012.04.062>
- Price, C. J., & Devlin, J. T. (2011). The Interactive Account of ventral occipitotemporal contributions to reading. *Trends in Cognitive Sciences*, *15*(6), 246–253. <https://doi.org/10.1016/j.tics.2011.04.001>
- Price, C. J., & Friston, K. J. (2005). Functional ontologies for cognition: The systematic definition of structure and function. *Cognitive Neuropsychology*, *22*(3–4), 262–275. <https://doi.org/10.1080/02643290442000095>
- Price, G. R., & Ansari, D. (2011). Symbol processing in the left angular gyrus: Evidence from passive perception of digits. *NeuroImage*, *57*(3), 1205–1211. <https://doi.org/10.1016/j.neuroimage.2011.05.035>
- Price, G. R., Holloway, I., Räsänen, P., Vesterinen, M., & Ansari, D. (2007). Impaired parietal magnitude processing in developmental dyscalculia. *Current Biology*, *17*(24), 1042–1043. <https://doi.org/10.1016/j.cub.2007.10.013>
- Price, G. R., Yeo, D. J., Wilkey, E. D., & Cutting, L. E. (2017). Prospective Relations between Resting-State Connectivity of Parietal Subdivisions and Arithmetic Competence. *Developmental Cognitive Neuroscience*. <https://doi.org/10.1016/j.dcn.2017.02.006>
- Puce, A., Allison, T., Asgari, M., Gore, J. C., & McCarthy, G. (1996). Differential sensitivity of human visual cortex to faces, letterstrings, and textures: A functional magnetic resonance imaging study. *Journal of Neuroscience*, *16*(16), 5205–5215. <https://doi.org/10.1523/jneurosci.16-16-05205.1996>
- Raffelt, D., Dhollander, T., Tournier, J. D., Tabbara, R., Smith, R. E., Pierre, E., & Connelly, A. (2017). Bias field correction and intensity normalisation for quantitative analysis of apparent fiber density. *Proc Intl Soc Mag Reson Med*, *25*(April), 3541. Retrieved from <https://www.researchgate.net/publication/315836355>

- Rajimehr, R., Young, J. C., & Tootell, R. B. H. (2009). An anterior temporal face patch in human cortex, predicted by macaque maps. *Proceedings of the National Academy of Sciences of the United States of America*, *106*(6), 1995–2000. <https://doi.org/10.1073/pnas.0807304106>
- Rakic, P. (1988). Specification of cerebral cortical areas. *Science*, *241*(4862), 170–176. <https://doi.org/10.1126/science.3291116>
- Rakic, P. (2009). Evolution of the neocortex: A perspective from developmental biology. *Nature Reviews Neuroscience*, *10*(10), 724–735. <https://doi.org/10.1038/nrn2719>
- Ray, K. L., Lesh, T. A., Howell, A. M., Salo, T. P., Ragland, J. D., MacDonald, A. W., ... Carter, C. S. (2017). Functional network changes and cognitive control in schizophrenia. *NeuroImage: Clinical*, *15*(May), 161–170. <https://doi.org/10.1016/j.nicl.2017.05.001>
- Reich, L., Szwed, M., Cohen, L., & Amedi, A. (2011). A ventral visual stream reading center independent of visual experience. *Current Biology*, *21*(5), 363–368. <https://doi.org/10.1016/j.cub.2011.01.040>
- Riesenhuber, M. (2007). Appearance Isn't Everything: News on Object Representation in Cortex. *Neuron*, *55*(3), 341–344. <https://doi.org/10.1016/j.neuron.2007.07.017>
- Rissman, J., Gazzaley, A., & D'Esposito, M. (2004). Measuring functional connectivity during distinct stages of a cognitive task. *NeuroImage*, *23*(2), 752–763. <https://doi.org/10.1016/j.neuroimage.2004.06.035>
- Rivera, S. M., Reiss, A. L., Eckert, M. A., & Menon, V. (2005). Developmental changes in mental arithmetic: Evidence for increased functional specialization in the left inferior parietal cortex. *Cerebral Cortex*, *15*(11), 1779–1790. <https://doi.org/10.1093/cercor/bhi055>
- Roberts, J. A., Perry, A., Roberts, G., Mitchell, P. B., & Breakspear, M. (2017). Consistency-based thresholding of the human connectome. *NeuroImage*, *145*(September 2016), 118–129. <https://doi.org/10.1016/j.neuroimage.2016.09.053>
- Rothlein, D., & Rapp, B. (2014). The similarity structure of distributed neural responses reveals the multiple representations of letters. *NeuroImage*, *89*, 331–344. <https://doi.org/10.1016/j.neuroimage.2013.11.054>
- Roux, F. E., Lubrano, V., Lauwers-Cances, V., Giussani, C., & Démonet, J. F. (2008). Cortical areas involved in Arabic number reading. *Neurology*, *70*(3), 210–217. <https://doi.org/10.1212/01.wnl.0000297194.14452.a0>
- Rubinov, M., Ypma, R. J. F., Watson, C., Bullmore, E. T., & Raichle, M. E. (2015). Wiring cost and topological participation of the mouse brain connectome. *Proceedings of the National Academy of Sciences of the United States of America*, *112*(32), 10032–10037. <https://doi.org/10.1073/pnas.1420315112>
- Rubinsten, O., Henik, A., Berger, A., & Shahar-Shalev, S. (2002). The Development of Internal Representations of Magnitude and Their Association with Arabic Numerals. *Journal of Experimental Child Psychology*, *81*(1), 74–92. <https://doi.org/10.1006/jecp.2001.2645>
- Saad, Z. S., & Reynolds, R. C. (2012). SUMA. *NeuroImage*, *62*(2), 768–773. <https://doi.org/10.1016/j.neuroimage.2011.09.016>
- Saad, Z. S., Reynolds, R. C., Argall, B., Japee, S., & Cox, R. W. (2005). SUMA: An interface for surface-based intra- and inter-subject analysis with AFNI. In *2004 2nd IEEE International Symposium on Biomedical Imaging: Macro to Nano (IEEE Cat No. 04EX821)* (Vol. 2, pp. 1510–1513). IEEE. <https://doi.org/10.1109/ISBI.2004.1398837>
- Saalman, Y. B., & Kastner, S. (2011). Cognitive and Perceptual Functions of the Visual Thalamus. *Neuron*, *71*(2), 209–223. <https://doi.org/10.1016/j.neuron.2011.06.027>

- Satterthwaite, T. D., Wolf, D. H., Loughhead, J., Ruparel, K., Elliott, M. A., Hakonarson, H., ... Gur, R. E. (2012). Impact of in-scanner head motion on multiple measures of functional connectivity: Relevance for studies of neurodevelopment in youth. *NeuroImage*, *60*(1), 623–632. <https://doi.org/10.1016/j.neuroimage.2011.12.063>
- Saygin, Z. M., Osher, D. E., Koldewyn, K., Reynolds, G., Gabrieli, J. D. E., & Saxe, R. R. (2012). Anatomical connectivity patterns predict face selectivity in the fusiform gyrus. *Nature Neuroscience*, *15*(2), 321–327. <https://doi.org/10.1038/nn.3001>
- Saygin, Z. M., Osher, D. E., Norton, E. S., Youssoufian, D. A., Beach, S. D., Feather, J., ... Kanwisher, N. (2016). Connectivity precedes function in the development of the visual word form area. *Nature Neuroscience*, *19*(9), 1250–1255. <https://doi.org/10.1038/nn.4354>
- Schedlbauer, A. M., Copara, M. S., Watrous, A. J., & Ekstrom, A. D. (2014). Multiple interacting brain areas underlie successful spatiotemporal memory retrieval in humans. *Scientific Reports*, *4*, 1–9. <https://doi.org/10.1038/srep06431>
- Scherf, K. S., Behrmann, M., Humphreys, K., & Luna, B. (2007). Visual category-selectivity for faces, places and objects emerges along different developmental trajectories. *Developmental Science*, *10*(4). <https://doi.org/10.1111/j.1467-7687.2007.00595.x>
- Schielzeth, H., Dingemans, N. J., Nakagawa, S., Westneat, D. F., Allogue, H., Teplitsky, C., ... Araya-Ajoy, Y. G. (2020). Robustness of linear mixed-effects models to violations of distributional assumptions. *Methods in Ecology and Evolution*, *11*(9), 1141–1152. <https://doi.org/10.1111/2041-210X.13434>
- Schilling, K. G., Blaber, J., Hansen, C., Rogers, B., Anderson, A., Smith, S., ... Landman, B. (2020). Registration-free Distortion Correction of Diffusion Weighted MRI. *PLOS ONE*, *15*(7), e0236418. <https://doi.org/10.1101/2020.01.19.911784>
- Schilling, K. G., Blaber, J., Huo, Y., Newton, A., Hansen, C., Nath, V., ... Landman, B. A. (2019). Synthesized b0 for diffusion distortion correction (Synb0-DisCo). *Magnetic Resonance Imaging*, *64*(December 2018), 62–70. <https://doi.org/10.1016/j.mri.2019.05.008>
- Schubert, T. M. (2017). Why are digits easier to identify than letters? *Neuropsychologia*, *95*(November 2016), 136–155. <https://doi.org/10.1016/j.neuropsychologia.2016.12.016>
- Seghier, M. L. (2013). The angular gyrus: Multiple functions and multiple subdivisions. *Neuroscientist*, *19*(1), 43–61. <https://doi.org/10.1177/1073858412440596>
- Seltzer, B., & Pandya, D. N. (1984). Further observations on parieto-temporal connections in the rhesus monkey. *Experimental Brain Research*, *55*(2), 301–312. <https://doi.org/10.1007/BF00237280>
- Shaywitz, B. A., Shaywitz, S. E., Blachman, B. A., Pugh, K. R., Fulbright, R. K., Skudlarski, P., ... Gore, J. C. (2004). Development of left occipitotemporal systems for skilled reading in children after a phonologically-based intervention. *Biological Psychiatry*, *55*(9), 926–933. <https://doi.org/10.1016/j.biopsych.2003.12.019>
- Shaywitz, B. A., Shaywitz, S. E., Pugh, K. R., Constable, R. T., Skudlarski, P., Fulbright, R. K., ... Gore, J. C. (1995). Sex differences in the functional organization of the brain for language. *Nature*, *373*(6515), 607–609. <https://doi.org/10.1038/373607a0>
- Shum, J., Hermes, D., Foster, B. L., Dastjerdi, M., Rangarajan, V., Winawer, J., ... Parvizi, J. (2013). A Brain Area for Visual Numerals. *Journal of Neuroscience*, *33*(16), 6709–6715. <https://doi.org/10.1523/JNEUROSCI.4558-12.2013>
- Smith, R. E., Raffelt, D., Tournier, J., & Connelly, A. (2020). Quantitative streamlines tractography : methods and inter-subject normalisation, (c), 1–27.
- Smith, R. E., Tournier, J.-D., Calamante, F., & Connelly, A. (2012). Anatomically-constrained

- tractography: Improved diffusion MRI streamlines tractography through effective use of anatomical information. *NeuroImage*, *62*(3), 1924–1938. <https://doi.org/10.1016/j.neuroimage.2012.06.005>
- Smith, R. E., Tournier, J. D., Calamante, F., & Connelly, A. (2013). SIFT: Spherical-deconvolution informed filtering of tractograms. *NeuroImage*, *67*, 298–312. <https://doi.org/10.1016/j.neuroimage.2012.11.049>
- Smith, R. E., Tournier, J. D., Calamante, F., & Connelly, A. (2015a). SIFT2: Enabling dense quantitative assessment of brain white matter connectivity using streamlines tractography. *NeuroImage*, *119*, 338–351. <https://doi.org/10.1016/j.neuroimage.2015.06.092>
- Smith, R. E., Tournier, J. D., Calamante, F., & Connelly, A. (2015b). The effects of SIFT on the reproducibility and biological accuracy of the structural connectome. *NeuroImage*, *104*, 253–265. <https://doi.org/10.1016/j.neuroimage.2014.10.004>
- Smith, S. M., Jenkinson, M., Woolrich, M. W., Beckmann, C. F., Behrens, T. E. J., Johansen-Berg, H., ... Matthews, P. M. (2004). Advances in functional and structural MR image analysis and implementation as FSL. *NeuroImage*, *23*(SUPPL. 1), S208–S219. <https://doi.org/10.1016/j.neuroimage.2004.07.051>
- Smith, S. M., & Nichols, T. E. (2009). Threshold-free cluster enhancement: Addressing problems of smoothing, threshold dependence and localisation in cluster inference. *NeuroImage*, *44*(1), 83–98. <https://doi.org/10.1016/j.neuroimage.2008.03.061>
- Song, Y., Hu, S., Li, X., Li, W., & Liu, J. (2010). The role of top-down task context in learning to perceive objects. *Journal of Neuroscience*, *30*(29), 9869–9876. <https://doi.org/10.1523/JNEUROSCI.0140-10.2010>
- Srihasam, K., Mandeville, J. B., Morocz, I. A., Sullivan, K. J., & Livingstone, M. S. (2012). Behavioral and anatomical consequences of early versus late symbol training in macaques. *Neuron*, *73*(3), 608–619. <https://doi.org/10.1016/j.neuron.2011.12.022>
- Srihasam, K., Vincent, J. L., & Livingstone, M. S. (2014). Novel domain formation reveals proto-architecture in inferotemporal cortex. *Nature Neuroscience*, *17*(12), 1776–1783. <https://doi.org/10.1038/nn.3855>
- Stevens, W. D., Kravitz, D. J., Peng, C. S., Tessler, M. H., & Martin, A. (2017). Privileged Functional Connectivity between the Visual Word Form Area and the Language System. *The Journal of Neuroscience*, *37*(21), 5288–5297. <https://doi.org/10.1523/JNEUROSCI.0138-17.2017>
- Stigliani, A., Weiner, K. S., & Grill-Spector, K. (2015). Temporal Processing Capacity in High-Level Visual Cortex Is Domain Specific. *Journal of Neuroscience*, *35*(36), 12412–12424. <https://doi.org/10.1523/JNEUROSCI.4822-14.2015>
- Takaya, S., Kuperberg, G. R., Liu, H., Greve, D. N., Makris, N., & Stufflebeam, S. M. (2015). Asymmetric projections of the arcuate fasciculus to the temporal cortex underlie lateralized language function in the human brain. *Frontiers in Neuroanatomy*, *9*(September), 1–12. <https://doi.org/10.3389/fnana.2015.00119>
- Tate, M. C., Herbet, G., Moritz-Gasser, S., Tate, J. E., & Duffau, H. (2014). Probabilistic map of critical functional regions of the human cerebral cortex: Broca's area revisited. *Brain*, *137*(10), 2773–2782. <https://doi.org/10.1093/brain/awu168>
- Thesen, T., McDonald, C. R., Carlson, C., Doyle, W., Cash, S., Sherfey, J., ... Halgren, E. (2012). Sequential then interactive processing of letters and words in the left fusiform gyrus. *Nature Communications*, *3*, 1–8. <https://doi.org/10.1038/ncomms2220>
- Tournier, J-D., & , F. Calamante, and a. C. (2010). Improved probabilistic streamlines

- tractography by 2 nd order integration over fibre orientation distributions. *Ismrm*, 88(2003), 2010.
- Tournier, J-Donald, Smith, R., Raffelt, D., Tabbara, R., Dhollander, T., Pietsch, M., ... Connelly, A. (2019). MRtrix3: A fast, flexible and open software framework for medical image processing and visualisation. *NeuroImage*, 202(January), 116137. <https://doi.org/10.1016/j.neuroimage.2019.116137>
- Tsao, D. Y., Freiwald, W. A., Knutsen, T. A., Mandeville, J. B., & Tootell, R. B. H. (2003). Faces and objects in macaque cerebral cortex. *Nature Neuroscience*, 6(9), 989–995. <https://doi.org/10.1038/nn1111>
- Tustison, N. J., Avants, B. B., Cook, P. A., & Gee, J. C. (2010). N4ITK: Improved N3 bias correction with robust B-spline approximation, 29(6), 708–711. <https://doi.org/10.1109/isbi.2010.5490078>
- Twomey, T., Kawabata Duncan, K. J., Price, C. J., & Devlin, J. T. (2011). Top-down modulation of ventral occipito-temporal responses during visual word recognition. *NeuroImage*, 55(3), 1242–1251. <https://doi.org/10.1016/j.neuroimage.2011.01.001>
- Uddin, L. Q., Supekar, K., Amin, H., Rykhlevskaia, E., Nguyen, D. A., Greicius, M. D., & Menon, V. (2010). Dissociable connectivity within human angular gyrus and intraparietal sulcus: Evidence from functional and structural connectivity. *Cerebral Cortex*, 20(11), 2636–2646. <https://doi.org/10.1093/cercor/bhq011>
- Undheim, A. M. (2003). Dyslexia and psychosocial factors. A follow-up study of young Norwegian adults with a history of dyslexia in childhood. *Nordic Journal of Psychiatry*, 57(3), 221–226. <https://doi.org/10.1080/08039480310001391>
- Uyeda, J. C., Hansen, T. F., Arnold, S. J., & Pienaar, J. (2011). The million-year wait for macroevolutionary bursts. *Proceedings of the National Academy of Sciences of the United States of America*, 108(38), 15908–15913. <https://doi.org/10.1073/pnas.1014503108>
- van den Heuvel, M. P., Scholtens, L. H., & de Reus, M. A. (2016). Topological organization of connectivity strength in the rat connectome. *Brain Structure and Function*, 221(3), 1719–1736. <https://doi.org/10.1007/s00429-015-0999-6>
- Veraart, J., Novikov, D. S., Christiaens, D., Ades-aron, B., Sijbers, J., & Fieremans, E. (2016). Denoising of diffusion MRI using random matrix theory. *NeuroImage*, 142, 394–406. <https://doi.org/10.1016/j.neuroimage.2016.08.016>
- Verguts, T., & Fias, W. (2004). Representation of Number in Animals and Humans: A Neural Model. *Journal of Cognitive Neuroscience*, 16(9), 1493–1504. <https://doi.org/10.1162/0898929042568497>
- Vernooij, M. W., Smits, M., Wielopolski, P. A., Houston, G. C., Krestin, G. P., & van der Lugt, A. (2007). Fiber density asymmetry of the arcuate fasciculus in relation to functional hemispheric language lateralization in both right- and left-handed healthy subjects: A combined fMRI and DTI study. *NeuroImage*, 35(3), 1064–1076. <https://doi.org/10.1016/j.neuroimage.2006.12.041>
- Vijayakumar, N., Mills, K. L., Alexander-Bloch, A., Tamnes, C. K., & Whittle, S. (2018). Structural brain development: A review of methodological approaches and best practices. *Developmental Cognitive Neuroscience*, 33(June 2017), 129–148. <https://doi.org/10.1016/j.dcn.2017.11.008>
- Vincent, J. L., Kahn, I., Snyder, A. Z., Raichle, M. E., & Buckner, R. L. (2008). Evidence for a frontoparietal control system revealed by intrinsic functional connectivity. *Journal of Neurophysiology*, 100(6), 3328–3342. <https://doi.org/10.1152/jn.90355.2008>

- Vinckier, F., Dehaene, S., Jobert, A., Dubus, J. P., Sigman, M., & Cohen, L. (2007). Hierarchical Coding of Letter Strings in the Ventral Stream: Dissecting the Inner Organization of the Visual Word-Form System. *Neuron*, *55*(1), 143–156. <https://doi.org/10.1016/j.neuron.2007.05.031>
- Vogel, A. C., Miezin, F. M., Petersen, S. E., & Schlaggar, B. L. (2012). The Putative Visual Word Form Area Is Functionally Connected to the Dorsal Attention Network. *Cerebral Cortex*, *22*(3), 537–549. <https://doi.org/10.1093/cercor/bhr100>
- Vogel, A. C., Petersen, S. E., & Schlaggar, B. L. (2014). The VWFA: it's not just for words anymore. *Frontiers in Human Neuroscience*, *8*(March), 1–10. <https://doi.org/10.3389/fnhum.2014.00088>
- Vogel, S. E., Goffin, C., & Ansari, D. (2015). Developmental specialization of the left parietal cortex for the semantic representation of Arabic numerals: An fMR-adaptation study. *Developmental Cognitive Neuroscience*, *12*(1), 61–73. <https://doi.org/10.1016/j.dcn.2014.12.001>
- Vossel, S., Geng, J. J., & Fink, G. R. (2014). Dorsal and ventral attention systems: Distinct neural circuits but collaborative roles. *Neuroscientist*, *20*(2), 150–159. <https://doi.org/10.1177/1073858413494269>
- Walther, A., Nili, H., Ejaz, N., Alink, A., Kriegeskorte, N., & Diedrichsen, J. (2016). Reliability of dissimilarity measures for multi-voxel pattern analysis. *NeuroImage*, *137*, 188–200. <https://doi.org/10.1016/j.neuroimage.2015.12.012>
- Wandell, B. A., Rauschecker, A. M., & Yeatman, J. D. (2012). Learning to See Words. *Annual Review of Psychology*, *63*(1), 31–53. <https://doi.org/10.1146/annurev-psych-120710-100434>
- Warrington, S., Bryant, K. L., Khrapitchev, A. A., Sallet, J., Charquero-Ballester, M., Douaud, G., ... Sotiropoulos, S. N. (2020). XTRACT - Standardised protocols for automated tractography in the human and macaque brain. *NeuroImage*, *217*(March), 1–15. <https://doi.org/10.1016/j.neuroimage.2020.116923>
- Wendelken, C., Ferrer, E., Ghetti, S., Bailey, S. K., Cutting, L., & Bunge, S. A. (2017). Frontoparietal Structural Connectivity in Childhood Predicts Development of Functional Connectivity and Reasoning Ability: A Large-Scale Longitudinal Investigation. *The Journal of Neuroscience*, *37*(35), 8549–8558. <https://doi.org/10.1523/JNEUROSCI.3726-16.2017>
- Whitfield-Gabrieli, S., & Nieto-Castanon, A. (2012). Conn : A Functional Connectivity Toolbox for Correlated and Anticorrelated Brain Networks. *Brain Connectivity*, *2*(3), 125–141. <https://doi.org/10.1089/brain.2012.0073>
- Wierenga, L. M., Langen, M., Oranje, B., & Durston, S. (2014). Unique developmental trajectories of cortical thickness and surface area. *NeuroImage*, *87*, 120–126. <https://doi.org/10.1016/j.neuroimage.2013.11.010>
- Wilkey, E. D., & Ansari, D. (2020). Challenging the neurobiological link between number sense and symbolic numerical abilities. *Annals of the New York Academy of Sciences*, *1464*(1), 76–98. <https://doi.org/10.1111/nyas.14225>
- Wilkey, E. D., Barone, J. C., Mazzocco, M. M. M., Vogel, S. E., & Price, G. R. (2017). The effect of visual parameters on neural activation during nonsymbolic number comparison and its relation to math competency. *NeuroImage*, *159*(August), 430–442. <https://doi.org/10.1016/j.neuroimage.2017.08.023>
- Wilkey, E. D., Conrad, B. N., Yeo, D. J., & Price, G. R. (2020). Shared Numerosity Representations Across Formats and Tasks Revealed with 7 Tesla fMRI: Decoding, Generalization, and Individual Differences in Behavior. *Cerebral Cortex Communications*,

- I*(1), 1–19. <https://doi.org/10.1093/texcom/tgaa038>
- Wright, D. B. (2017). Some Limits Using Random Slope Models to Measure Academic Growth. *Frontiers in Education*, 2(November). <https://doi.org/10.3389/feduc.2017.00058>
- Yang, J., Huber, L., Yu, Y., & Bandettini, P. A. (2021). Linking cortical circuit models to human cognition with laminar fMRI. *Neuroscience & Biobehavioral Reviews*, 128, 467–478. <https://doi.org/10.1016/j.neubiorev.2021.07.005>
- Yeatman, J. D., Rauschecker, A. M., & Wandell, B. A. (2013). Anatomy of the visual word form area: Adjacent cortical circuits and long-range white matter connections. *Brain and Language*, 125(2), 146–155. <https://doi.org/10.1016/j.bandl.2012.04.010>
- Yeatman, J. D., Weiner, K. S., Pestilli, F., Rokem, A., Mezer, A., & Wandell, B. A. (2014). The vertical occipital fasciculus: A century of controversy resolved by in vivo measurements. *Proceedings of the National Academy of Sciences*, 111(48), E5214–E5223. <https://doi.org/10.1073/pnas.1418503111>
- Yeh, C. H., Smith, R. E., Liang, X., Calamante, F., & Connelly, A. (2016). Correction for diffusion MRI fibre tracking biases: The consequences for structural connectomic metrics. *NeuroImage*, 142, 150–162. <https://doi.org/10.1016/j.neuroimage.2016.05.047>
- Yeo, B. T., Krienen, F. M., Sepulcre, J., Sabuncu, M. R., Lashkari, D., Hollinshead, M., ... Buckner, R. L. (2011). The organization of the human cerebral cortex estimated by intrinsic functional connectivity. *Journal of Neurophysiology*, 106(3), 1125–1165. <https://doi.org/10.1152/jn.00338.2011>
- Yeo, D. J., Pollack, C., Merkley, R., Ansari, D., & Price, G. R. (2020). The “Inferior Temporal Numeral Area” distinguishes numerals from other character categories during passive viewing: A representational similarity analysis. *NeuroImage*, 214(October 2019), 116716. <https://doi.org/10.1016/j.neuroimage.2020.116716>
- Yeo, D. J., Wilkey, E. D., & Price, G. R. (2017). The search for the number form area: A functional neuroimaging meta-analysis. *Neuroscience & Biobehavioral Reviews*, 78(April), 145–160. <https://doi.org/10.1016/j.neubiorev.2017.04.027>
- Zeidman, P., Jafarian, A., Corbin, N., Seghier, M. L., Razi, A., Price, C. J., & Friston, K. J. (2019). A guide to group effective connectivity analysis, part 1: First level analysis with DCM for fMRI. *NeuroImage*, 200(May), 174–190. <https://doi.org/10.1016/j.neuroimage.2019.06.031>